THE
PHYSICAL REVIEW

*A journal of experimental and theoretical physics established by E. L. Nichols in 1893*

SECOND SERIES, VOL. 74, NO. 3 AUGUST 1, 1948

# On Closed Shells in Nuclei*

MARIA G. MAYER
*Argonne National Laboratory and Institute for Nuclear Studies, University of Chicago, Chicago, Illinois*

(Received April 16, 1948)

Experimental facts are summarized to show that nuclei with 20, 50, 82, or 126 neutrons or protons are particularly stable.

IT has been suggested in the past that special numbers of neutrons or protons in the nucleus form a particularly stable configuration.[1] The complete evidence for this has never been summarized, nor is it generally recognized how convincing this evidence is. That twenty neutrons or protons ($Ca^{40}$) form a closed shell is predicted by the Hartree model. A number of calculations support this fact.[2] These considerations will not be repeated here. In this paper, the experimental facts indicating a particular stability of shells of 50 and 82 protons and of 50, 82, and 126 neutrons will be listed.

## I. ISOTOPIC ABUNDANCES

The discussion in this section will be mostly confined to the heavy elements, which for this purpose may be defined as those with atomic number greater than 33; selenium would be the first "heavy" element. For these elements, the isotopic abundances show a number of striking regularities which are violated in very few cases.

(a) For elements with even $Z$, the relative abundance of a single isotope is not greater than 60 percent. This becomes more pronounced with increasing $Z$; for $Z>40$, relative abundances greater than 35 percent are not encountered. The exceptions to this rule are given in Table I.

(b) The isotopic abundances are not symmetrically distributed around the center, but the light, neutron-poor isotopes have low abundances. The concentration of the lightest isotope is, as a rule, less than 2 percent. The exceptions to this rule are listed in Table II.

It is seen that the violations of these two regularities occur practically only at neutron numbers 50 and 82. Only the case of ruthenium in Table II, which is not a very pronounced exception, does not fall into one of these groups.

The case of samarium, where the lightest isotope has an isotopic abundance of 3 percent, is only a bare violation of the rule and may not seem striking. However, what is extraordinary, the next heavier even isotope of samarium, $Sm^{146}$ with 84 neutrons, which one would expect to find in greater concentration, does not exist at all.

## II. NUMBER OF ISOTONES

Figures 1 and 2 reproduce the parts of the table by Segrè in the region of nuclei with 50

* This document is based on work performed under Contract Number W-31-109-eng-38 for the Atomic Energy Commission at the Argonne National Laboratory. Submitted for declassification on February 13th, 1948.

[1] W. Elsasser, J. de phys. et rad. 5, 625 (1934).

[2] E. Wigner, Phys. Rev. 51, 947 (1937); W. H. Barkas, Phys. Rev. 55, 691 (1939).

TABLE I. Even nuclei with $Z>32$ with isotopic abundance greater than 60 percent.

| Element | Abundance in percent | Number of neutrons |
|---|---|---|
| $Sr^{88}$ | 82 | 50 |
| $Ba^{138}$ | 71.66 | 82 |
| $Ce^{140}$ | 90 | 82 |

TABLE II. Lightest isotopes of elements with even $Z>32$ with isotopic abundance greater than 2 percent.

| Element | Abundance in percent | Number of neutrons |
|---|---|---|
| $Zr^{96}$ | 48 | 50 |
| $Mo^{92}$ | 15.5 | 50 |
| $Ru^{96}$ | 5 | 52 |
| $Nd^{142}$ | 25.95 | 82 |
| $Sm^{144}$ | 3 | 82 |

and 82 neutrons, respectively. For 82 neutrons, there exist seven stable nuclei, which, for convenience, shall be called isotones. For neutron number 50 there exist six naturally occurring isotones, of which one, $Rb^{87}$, is $\beta$-active, however, with a lifetime of $10^{11}$ years and a maximum $\beta$-energy of 0.25 Mev. The average number of isotones for odd neutrons number is somewhat less than one; the same number for even $N$ varies as a rule between three and four. The greatest number of isotones, attained only once in the periodic table, is seven for neutron number 82; six isotones are encountered once only, and for neutron number 50. Five isotones are found five times, namely, for $N=20$, 28, 58, 74, and 78. The frequency of $N=28$ is probably due to the stability of $Ca^{48}$, with 20 protons, that of $N=74$ to the stability of $Sn^{124}$, with 50 protons. As few as two isotones for even $N$ are found only three times for heavy nuclei, namely, for neutron numbers 84, 86, and 120.

### III. THE SLOPE OF THE CENTER AND THE EDGES OF THE STABILITY CURVE

In the case of neutron number $N=82$ two isotones of odd $Z$ are found, La and Pr. The same is the case for $N=50$, where the unstable but long-lived $Rb^{87}$ and $Y^{89}$ differ only in proton number. Only one other case where nuclei of different odd $Z$ have the same number of neutrons is encountered in the periodic table, namely, that of $Cl^{37}$ (abundance 24.6 percent) and $K^{39}$ (abundance 93.3 percent); this is the case of 20 neutrons. The case of 82 neutrons is most pronounced, since the La and Pr isotopes in question have isotopic abundances of 100 percent.

As Fig. 2 shows, the isotones $Nd^{142}$ and $Sm^{144}$ are both the lightest isotopes of their respective elements. Here, the limit of the stability for neutron-poor isotopes stays at constant neutron number. Exactly the same is true for $N=50$ (Fig. 1). This situation does not occur anywhere else in the periodic table.

The limit of stability for neutron-rich isotopes also stays at constant neutron number for $N=50$ and $N=82$, namely, the pairs of isotones, $Kr^{86}$, $Sr^{88}$ and $Xe^{136}$, $Ba^{138}$ are the heaviest isotopes of their elements. Such a case is encountered once more in the periodic table: $Ca^{48}$ and $Ti^{50}$ are the heaviest isotopes of their respective elements and have the same neutron number $N=28$.

### IV. THE CASE OF 20 AND 50 PROTONS

Ca, with 20 protons, has five isotopes, which is not too unusual for this region of the periodic table. The difference in mass number between its heaviest and lightest isotope is eight mass numbers, which is quite outstanding, since this difference does not exceed four for elements in this neighborhood.

Sn, $Z=50$, has without exception the greatest number of isotopes of any element, namely, 10. Its heaviest and lightest nuclei differ by 12 neutrons. Such a spread of isotopes is encountered in only one other case, namely, at Xe, where it may be attributed to the stability of $Xe^{136}$ with 82 neutrons.

Incidentally, the next largest difference, 10, in mass number between heaviest and lightest isotope of an element, is encountered once only, in samarium, and may be attributed to the unusual stability of $Sm^{144}$ with 82 neutrons.

### V. THE CASE OF 82 PROTONS AND 126 NEUTRONS

Lead, $Z=82$, is the end of all radioactive chains. It has only four stable isotopes, of which the heaviest one, $Pb^{208}$, has 126 neutrons.

Evidence for the stability of 82 protons and 126 neutrons can be obtained from the energies of radioactive decay. If, for constant value of the charge of the resultant nucleus the energies of $\alpha$-decay are plotted against the neutron num-

| | | | | | | | | | | | | |
|---|---|---|---|---|---|---|---|---|---|---|---|---|
| | | | | | | | | | | $Gd^{152}$ 0.2 | | $Gd^{154}$ 1.5 |
| | | | | | | | | | | $Eu^{151}$ 49 | | $Eu^{153}$ 50.9 |
| | | | | $Sm^{144}$ 3 | | | $Sm^{147}$ 17 | $Sm^{148}$ 14 | $Sm^{149}$ 15 | $Sm^{150}$ 5 | | $Sm^{152}$ 26 |
| | | | | | | | | | | | | |
| | | | | $Nd^{142}$ 25.95 | $Nd^{143}$ 13 | $Nd^{144}$ 22.6 | $Nd^{145}$ 9.2 | $Nd^{146}$ 16.5 | | $Nd^{148}$ 6.8 | | $Nd^{150}$ 5.95 |
| | | | | $Pr^{141}$ 100 | | | | | | | | |
| $Ce^{136}$ <1 | | $Ce^{138}$ <1 | | $Ce^{140}$ 90 | | $Ce^{142}$ 10 | | | | | | |
| | | | | $La^{139}$ 100 | | | | | | | | |
| $Ba^{134}$ 2.43 | $Ba^{135}$ 6.59 | $Ba^{136}$ 7.81 | $Ba^{137}$ 11.32 | $Ba^{138}$ 71.66 | | | | | | | | |
| $Cs^{133}$ 100 | | | | | | | | | | | | |
| $Xe^{132}$ 26.96 | | $Xe^{134}$ 10.54 | | $Xe^{136}$ 8.95 | | | | | | | | |
| | | | | | | | | | | | | |
| $Te^{130}$ 33.1 | | | | | | | | | | | | |
| $N=78$ | 79 | 80 | 81 | 82 | 83 | 84 | 85 | 86 | 87 | 88 | 89 | 90 |

FIG. 1.

ber of the resultant nucleus, a sharp dip in energy is encountered when $N$ drops below 126, indicating a larger binding energy for the 126th neutron. From these considerations, Elsasser[1] estimates the discontinuity in neutron binding energy at 126 neutrons to be 2.2 Mev or larger, the discontinuity in proton binding energy at $Z=82$ to be 1.6 Mev. These relations have been studied in detail by A. Berthelot.[2a]

## VI. ABSOLUTE ABUNDANCE

Absolute abundances are notoriously uncertain. The best estimates are probably contained in the book by Goldschmidt.[3] For the light elements, the abundances vary erratically; for heavy elements, from about Se on, they remain roughly constant. In the region of heavy elements, the following abundance peaks are apparent. At Zr (50 neutrons), at Sn (50 protons); at Ba (82 neutrons), at W and at lead (82 protons or 126 neutrons). In Goldschmidt's plot of abundance against neutron number, page 127, the Zr and Ba peaks are seen to be at neutron number 50 and 82 and become much more pronounced and narrow, whereas the peak at Sn, $Z=50$, as well as the peak at W, become much broader than in the plot against $Z$.

Most trustworthy among absolute abundances is probably the relative abundance of the rare earths, since these are not likely to have been appreciably fractionated in the earth's crust. The case of 82 neutrons falls just on the edge of this region. According to Goldschmidt's data on the abundance of rare earths in eruptive rocks (which are probably more reliable chemical analyses than the abundance in meteorites), the

[2a] A. Berthelot, J. de phys. et rad. (8) 3, 17, 52 (1942).
[3] V. M. Goldschmidt, *Geochemische Verteilungsgesetze der Elemente* (Norske Videnskaps Akademi, Oslo, 1938), Fig. 1, page 117, or Fig. 2, page 118.

| | | | | | | | | | | | | |
|---|---|---|---|---|---|---|---|---|---|---|---|---|
| | | | | | | $Ru^{96}$ 5 | | $Ru^{98}$ 2.2 | $Ru^{99}$ 12 | $Ru^{100}$ 14 | $Ru^{101}$ 22 | $Ru^{102}$ 30 |
| | | | | | | | | | | | | |
| | | | | $Mo^{92}$ 15.5 | | $Mo^{94}$ 8.7 | $Mo^{95}$ 16.3 | $Mo^{96}$ 16.8 | $Mo^{97}$ 8.7 | $Mo^{98}$ 25.4 | | $Mo^{100}$ 8.6 |
| | | | | | | $Cb^{93}$ 100 | | | | | | |
| | | | | $Zr^{90}$ 48 | $Zr^{91}$ 11.5 | $Zr^{92}$ 22 | | $Zr^{94}$ 17 | | $Zr^{96}$ 1.5 | | |
| | | | | $Y^{89}$ 100 | | | | | | | | |
| $Sr^{84}$ 0.56 | | $Sr^{86}$ 9.86 | $Sr^{87}$ 7.02 | $Sr^{88}$ 82.56 | | | | | | | | |
| | | $Rb^{85}$ 72.3 | | $Rb^{87}$ 27.7 | | | | | | | | |
| $Kr^{82}$ 11.53 | $Kr^{83}$ 11.53 | $Kr^{84}$ 57.1 | | $Kr^{86}$ 17.47 | | | | | | | | |
| $Br^{81}$ 49.4 | | | | | | | | | | | | |
| $Se^{80}$ 48.0 | | $Se^{82}$ 9.3 | | | | | | | | | | |
| $N=46$ | 47 | 48 | 49 | 50 | 51 | 52 | 53 | 54 | 55 | 56 | 57 | 58 |

FIG. 2.

abundances of rare earths heavier than samarium are reasonably constant, except that the elements with even $Z$ are about 5.7 times as abundant as those with odd $Z$. Of the lighter rare earths, however, praesodymium ($N=82$) is about 8 times and lanthanum ($N=82$) about 27 times as abundant as the average of the odd rare earth with greater $Z$. Nd, with a 26 percent isotopic composition of isotopes with $N=82$, is about five times as abundant; cerium, with 90 percent composition of isotopes with $N=82$, is about twelve times as abundant as the average of the heavier even rare earths. In the composition of meteors the differences are not quite as striking, but still very pronounced.

## VII. DELAYED NEUTRON EMITTERS

If 50 or 82 neutrons form a closed shell, and the 51st and 83rd neutrons have less than average binding energy, one would expect especially low binding energies for the last neutron in $Kr^{87}$ and $Xe^{137}$, which have 51 and 83 neutrons, respectively, and the smallest charge compatible with a stable nucleus with 50 or 82 neutrons, respectively. It so happens that the only two delayed neutron emitters identified are these two nuclei.[4]

The fission products $Br^{87}$ ($N=52$), as well as $I^{137}$ ($N=84$), have not enough energy to evaporate a neutron, and undergo $\beta$-decay; in the resultant nuclei, $Kr^{87}$ and $Xe^{137}$, the binding energy of the last neutron is small enough to allow neutron evaporation.

## VIII. ABSORPTION CROSS SECTIONS[5]

The neutron absorption cross sections for nuclei containing 50, 82, or 126 neutrons seem all to be unusually low. This is seen very clearly in the measurements of Griffiths[6] with Ra $\gamma$-Be neutrons, and those of Mescheryakov[7] with neutrons from $a(d,d)$ reaction. These measurements extend from mass number 51 to 209. In general,

[4] A. H. Snell, Y. S. Levinger, E. D. Meiners, Jr., M. B. Sampson, and R. G. Wilkinson, Phys. Rev. 72, 545 (1947).

[5] The author is indebted to Dr. Katherine Way, who pointed out the connection of the closed shells with neutron absorption cross sections.

[6] J. H. E. Griffiths, Proc. Roy. Soc. 170, 513 (1939).

[7] C. R. Mescheryakov, C. R. U.S.S.R. 48, 555 (1945).

the cross sections increase with increasing mass number. Griffiths investigates, of the nuclei in question, yttrium (89) with 50 neutrons and lanthanum and praesodymium with 82 neutrons. The activation cross section for yttrium is the smallest he observes for any element; it is about 20 to 30 times smaller than the cross sections in that region of mass number. There is a very pronounced dip of cross sections for lanthanum and praesodymium; the cross section of $Pr^{141}$ is about one-seventh of the average of this region, and that of $La^{139}$ is still smaller by a factor 3. Mescheryakov investigates, among others, La, Pr, barium (138), and bismuth (209). He finds a similar dip at La and Pr, and finds that the cross section of $Ba^{138}$ with 82 neutrons is even lower, namely, less than 0.03 of that of lanthanum. The cross section of bismuth with 126 neutrons is even smaller. The only other unusually small cross section which Griffiths finds is that of thallium (122 or 124 neutrons), which is about the same as that for praesodymium.

Recent experiments by Hughes[8] with fission neutrons have shown exceptionally low neutron absorption cross sections for $Pb^{208}$, $Bi^{209}$ (126 neutrons) and for $Ba^{136}$ (82 neutrons).

## IX. ASYMMETRIC FISSION

It is somewhat tempting to associate the existence of the closed shells of 50 and 82 neutrons with the dissymmetry of masses encountered in the fission process. $U^{235}$ contains $143=82+50+11$ neutrons. It appears that the probable fissions are such that one fragment has at least 82, one other at least 50, neutrons.

## X. THEORETICAL ESTIMATE OF THE DISCONTINUITY IN BINDING ENERGIES

It is possible to make an estimate of the change in neutron binding energy at, for instance, 82 neutrons. There exists the semi-empirical formula for the mass of an atom[9] with mass number $A$ and charge $Z$.

$$M_{A,Z}=A-0.00081Z-0.00611A+0.014A^{\frac{2}{3}}+0.083(A/2-Z)^2A^{-1}-0.000627Z^2A^{-\frac{1}{3}}+\delta; \quad (1)$$

with $\delta=0$ for $A$ odd, $\delta=-0.036A^{-\frac{1}{2}}$ for $A$ even, $Z$ even, $\delta=+0.036A^{-\frac{1}{2}}$ for $A$ odd, $Z$ odd. For odd $A$, this formula permits the calculation of the value of $Z$ for which the energy is a minimum. For $Z$ less than 50 and for neutron numbers greater than 82, the calculated curve is in good agreement with the position of, for instance, the nuclei of odd $Z$. Between $Z=50$ and $N=82$, however, the experimental values of $Z$ seem to be below the theoretical curve. The disagreement can be explained by a definite shift of the stability line at 82 neutrons. This shift of the stability line can be explained by a change in binding energy of about 2 Mev. Also, according to the formula (1), xenon (136), with 82 neutrons, should be unstable by about 2 Mev, whereas it is undoubtedly stable; $Sm^{144}$ should be unstable against $K$-capture by 0.6 Mev, whereas $Ba^{140}$, with 84 neutrons, which is unstable, would be just stable according to formula (1).

Whereas these calculations are undoubtedly very uncertain, they may serve as an estimate of the order of magnitude of the discontinuity in the binding energies. Since the average neutron binding energy in this region of the periodic table is about 6 Mev, the discontinuities represent only a variation of the order of 30 percent. This situation is very different from that encountered at the closed shells of electrons in atoms where the ionization energy varies by several hundred percent. Nevertheless, the effect of closed shells in the nuclei seems very pronounced.

[8] D. J. Hughes, private communication.

[9] N. Bohr and J. A. Wheeler, Phys. Rev. 56, 426 (1939); G. B. von Albada, Astrophys. J. 105, 393 (1947).

# Neutron Induced Radioactivity in Certain Rare-Earth Elements

J. M. CORK, R. G. SHREFFLER, AND C. M. FOWLER
*Department of Physics, University of Michigan, Ann Arbor, Michigan*

(Received April 16, 1948)

By activating specimens of lanthanum, neodymium, samarium, europium, gadolinium, and terbium in the Oak Ridge pile for a particularly long exposure, several hitherto unobserved radioactivities are found. Determinations are made of the half-lives and of the beta- and gamma-energies by absorption and spectrometric methods. Lanthanum and neodymium were the only elements showing no internal conversion lines. Terbium appears as a contaminant in its neighboring elements by virtue of its very large cross section for neutron capture. Terbium and europium show complex beta-spectra, and each has many conversion electron lines.

## I. INTRODUCTION

OXIDE specimens of the elements; lanthanum, neodymium, samarium, europium, gadolinium, and terbium were irradiated in the Oak Ridge pile for exposures of 2 months' duration. These are the lighter rare-earth elements with atomic numbers ranging from 57 to 65. The reaction expected in the pile is usually the neutron capture process, but it also appears possible to produce the excited state of stable isotopes where such long-lived activities exist. Short-lived activities are not observed in this investigation as observational study did not begin until three days after the end of the bombardments. By virtue of the very long intense neutron bombardment, many activities not previously observed have been found to exist.

Each specimen was divided into parts, for its half-life determination and for the evaluation of beta- and gamma-energies by absorption methods and by magnetic spectrometers. The results obtained with europium and with terbium have been, in part, reported[1] previously.

## II. TERBIUM

Terbium exists in nature as a single isotope of mass 159. By neutron capture the radioactive isotope of mass 160 should be made. Previous studies[2–4] had assigned half-lives of 3.9 hours and 72 days to this isomeric activity. The longer half-life is in this investigation found to be 77.3 days. The gamma-radiation emitted is found by the photographic spectrometer to give, in all, about nine electron lines by internal conversion. These lines are shown collectively in Fig. 1 along with the *K–L–M–N* energy levels in the next heavier element dysprosium, plotted to the same scale. It is thus apparent that certain groups of the observed lines combine to represent a single gamma-ray. The energies of the observed lines together with the interpretation and the energy of the resulting four gamma-rays are shown in Table I.

In one combination a line due to converted '*N*' electrons is observed for the first time. This portion of the photographic plate is shown enlarged in Fig. 2. The ratio of the *L*, *M*, and *N* conversion intensities can be judged from this photogram.

By absorption methods a gamma-ray of energy 1.15 Mev is found to be present. There is evidence of the existence of other gamma-rays of intermediate energy which are only slightly converted.

The beta-spectrum of terbium is found to be complex, that is, there are two overlapping spectra whose upper limits of energy are 546 and 882 kev, respectively. This activity was studied on a thick electron lens spectrometer. The observed electron distribution with momentum was converted so as to represent graphically the Fermi function *versus* energy as shown in Fig. 3. It is apparent that at higher energy a very straight line curve is obtained except for some photoelectrons due to the energetic gamma-radiation. By the proper subtraction of this projected curve at lower energies a second

[1] J. M. Cork, R. G. Shreffler, and C. M. Fowler, Phys. Rev. **72**, 1209 (1947); **73**, 78 (1948).
[2] W. Bothe, Naturwiss. **31**, 551 (1943).
[3] M. Poole, L. Quill, and J. Kurbatov, Phys. Rev. **53**, 437 (1938).
[4] G. Hevesy and G. Levi, Nature **137**, 185 (1936).

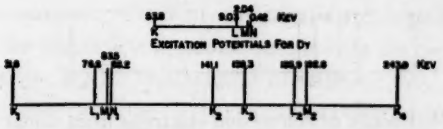


FIG. 1. Energy of conversion lines from terbium (160).

Fermi curve is obtained as shown, whose intercept with the energy axis is not quite as exact as that of the high energy intercept.

Terbium is of interest since it has a very large cross section for neutron capture. If present in only a slight amount as an impurity in another element its spectrum is disturbingly prominent.

### III. LANTHANUM

Lanthanum consists of a single stable isotope of mass 139. By neutron capture it converts to radioactive lanthanum of mass 140. Previous investigations[5] had ascribed to this isotope a half-life of 40 hours with the emission of beta-radiation and gamma-radiation each characterized by several distinct energies. The analysis of the decay curve of this strongly irradiated sample shows clearly two half-lives, namely 43.4 hours and another about three years, not yet accurately determined. In the photographic spectrometer no conversion lines due to low energy gamma-radiation were observed in a reasonable exposure of five days.

A strong gamma-ray of 1.6 Mev was observed in connection with the shorter half-life by absorption methods. In the long-lived activity a gamma-ray of 0.79 Mev was found by absorption, and an upper limit of the beta-spectrum of approximately 0.9 Mev.

It is possible that the longer half-life here observed is really in an excited state of cerium 140 produced by beta-emission from lanthanum 140. This activity had previously been reported as having a half-life of 140 days.

### IV. NEODYMIUM

Neodymium has several stable isotopes ranging in mass from 142 to 150. Previous investigations[6] had indicated the existence of radioactive isotopes of mass 141 and 147 whose half-lives were 2.5 hours and 47 hours, respectively. The present investigation shows the presence of three half-lives, whose values are 50 hours, 11.8 days, and 1.7 years. Absorption methods reveal a gamma-ray of energy 0.72 Mev and by the Feather rule beta-radiation with an upper limit of 0.74 Mev. This radiation seems to be associated with the very long-lived activity. No conversion electrons due to gamma-radiation could be observed in the spectrometers.

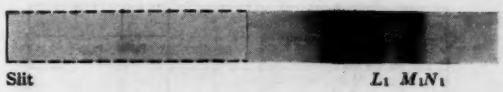


FIG. 2. Enlarged low energy spectrum of terbium (160) showing an '$N$' electron group.

### V. SAMARIUM

Several stable isotopes of samarium with masses ranging from 144 to 154 exist in nature. Samarium 148 exhibits natural radioactivity with a half-life of $1.6\times10^{11}$ years. Previous researches[6,7] had revealed an induced radioactivity of 47-hour half-life ascribed to isotope of mass 153, and other activities in samarium derived from fission ascribed to isotopic masses greater than 154.

An exposure of the irradiated samarium in the beta-ray spectrometer showed several electron lines due to gamma-conversion. These lines are shown collectively in Fig. 4. One group of such lines had energy differences identical with the differences in the levels characteristic of the next heavier element, europium, as expected if the gamma-emission follows beta-radiation. The en-

TABLE I. Conversion electron spectrum of terbium.

| Observed energy | Identification | Gamma-energy |
|---|---|---|
| 31.6 kev | $K_1$ | 85.4 kev |
| 76.6 | $L_1$ | 85.6 |
| 83.5 | $M_1$ | 85.5 |
| 85.2 | $N_1$ | 85.6 |
| 141.1 | $K_2$ | 194.9 |
| 158.3 | $K_3$ | 212.1 |
| 185.9 | $L_2$ | 194.9 |
| 192.6 | $M_2$ | 194.6 |
| 242.7 | $K_4$ | 296.5 |

[5] P. Weimar, M. Poole, and J. Kurbatov, Phys. Rev. 63, 67 (1943); R. Osborne and W. Peacock, Phys. Rev. 69, 679 (1946); C. Mandeville and W. Scherb, Phys. Rev. 73, 1437 (1948).

[6] J. Kurbatov, D. MacDonald, M. Poole, and L. Quill, Phys. Rev. 61, 106 (1942); C. S. Wu and E. Segré, Phys. Rev. 61, 203 (1942).

[7] B. Inghram, R. Hayden, and D. Hess, Phys. Rev. 71, 643, 743 (1947).

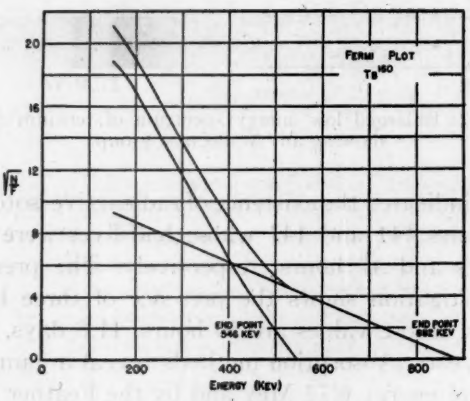


FIG. 3. Fermi plot of the beta-radiation from terbium (160).

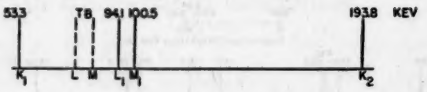


FIG. 4. Energy of conversion electrons from samarium, immediately after bombardment.

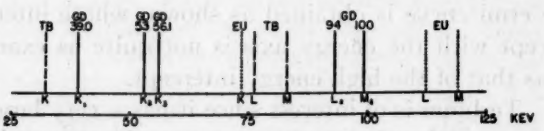


FIG. 5. Energy of conversion electrons observed from a gadolinium source, showing europium and terbium impurities.

ergy of this gamma-ray is 102.1 kev and it was found to die out with the half-life of 50 hours.

It was noted that certain of the lines agreed exactly with those observed in radioactive terbium, thus indicating the presence of this element as an impurity in the samarium. One additional line interpreted as a '*K*' conversion line indicates a gamma-energy of 242.4 kev in samarium associated with a long half-life.

The decay curve of samarium showed in addition to the 50-hour half-life and the 77.3-day terbium period, some activity of half-life greater than 150 days.

## VI. GADOLINIUM

Several stable isotopes of gadolinium exist in nature. The strongly irradiated specimen of supposedly chemically pure gadolinium, yielded a spectrogram of many conversion lines in the magnetic spectrometer. These lines, 12 in number, are shown graphically in Fig. 5. From the information gained in the study of other elements it was at once apparent that both terbium and europium existed as impurities in the gadolinium. To show the ease of identifying such impurities the spectra of the three elements are shown together in Fig. 6. On subtracting the known lines due to terbium and europium, it is presumed that those that remain are really due to gadolinium. Peculiarly, however, one group of three lines has a *K–L–M* relationship exactly like that observed for the 50-hour samarium activity of energy 102 kev yet here the half-life is long. This is as would be expected if the activity in

TABLE II. Collected data on the radioactivity of the rare-earth elements.

| Atomic number | Element | Half-life | Beta-radiation (Mev) | Gamma-radiation | | Probable active isotope |
|---|---|---|---|---|---|---|
| | | | | Absorption (Mev) | Spectrometer (kev) | |
| 57 | Lanthanum | 43.4 hr. | | 1.60 | | 140 |
| | | ~3 yr. | .90 | 0.79 | | 140 |
| 60 | Neodymium | 50 hr. | | | | |
| | | 11.8 da. | | 0.72 | | 147 |
| | | 1.7 yr. | 0.74 | | | |
| 62 | Samarium | 50 hr. | 1.23 | | 102.1 | 153 |
| | | >150 da. | | .95 | 242.4 | 155 |
| 63 | Europium | ~6 yr. | 0.751, 1.57 | 1.23 | 39.9, 122.1, 247.3, 286.0, 342.8, 407.8 | 154 or 152 |
| 64 | Gadolinium | 76 hr. | | 2.10 | | |
| | | — | | | {102 | 153 |
| | | Long | | | {91.0, 108.1 | 159 or 161 |
| 65 | Terbium | 77.3 da. | 0.546, 0.882 | 1.15 | 85.6, 194.8, 212.1, 296.5 | 160 |

gadolinium is positron emission from mass 153, and the short-lived samarium is due to electron emission from samarium of mass 153, both transitions ending in the same excited levels of europium 153. The impurities revealed by this method may be present in only slight traces, yet by virtue of their large capture cross section for neutrons, they introduce a disturbingly large radioactivity with certainty, but a half-life of 110 days is indicated.

Two electron groups of energy 39.0 and 56.1 kev, when interpreted as $K$-conversion lines in gadolinium, indicate gamma-rays of energy 91.0 and 108.1 kev. Because of the interference of impurities such as europium with a six-year half-life, it is impossible to fix the periods of the gadolinium activities.

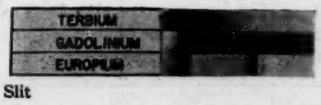


FIG. 6. Spectrograms showing the presence of terbium and europium as impurities in gadolinium.

The new information pertaining to this group of elements is assembled together in Table II.

The beta-spectrum of terbium was observed on the spectrometer by Mr. E. Salmi and that of europium by Mr. F. Shull. This investigation was made possible by the support of the Office of Naval Research.

---

PHYSICAL REVIEW VOLUME 74, NUMBER 3 AUGUST 1, 1948

# Microwave Determination of the Molecular Structures and Nuclear Couplings of the Methyl Halides*

WALTER GORDY, JAMES W. SIMMONS, AND A. G. SMITH
*Department of Physics, Duke University, Durham, North Carolina*

(Received April 19, 1948)

Accurate measurements on the pure rotation spectra of methyl chloride, bromide and iodide have been made with multiples of a 10 mc/sec. frequency monitored by station WWV. The measurements, with existing infra-red data, allow a complete determination of the structures of these molecules. The $I_B$ values in g/cm$^2\times10^{-40}$ are: $63.11_{38}$ for $C^{12}H_3Cl^{35}$, $64.10_{09}$ for $C^{12}H_3Cl^{37}$, $87.68_{36}$ for $C^{12}H_3Br^{79}$, $88.01_{80}$ for $C^{12}H_3Br^{81}$, $111.8_{43}$ for $C^{12}H_3I^{127}$ and $117.8_{48}$ for $C^{13}H_3I^{127}$. The molecular dimensions obtained are: for methyl chloride, $d_{CH}=1.109$A, $d_{CCl}=1.779$A, $<HCH=110°\,0'$; for methyl bromide, $d_{CH}=1.104$A, $d_{CBr}=1.936$A, $<HCH=110°\,15'$; for methyl iodide, $d_{CH}=1.100$A, $d_{CI}=2.139$A, $<HCH=110°\,58'$. The nuclear quadrupole couplings, $eQ(\partial^2V/\partial z^2)$, are: for $Cl^{35}$, $-75.13$ mc/sec.; for $Cl^{37}$, $-59.03$ mc/sec.; for $Br^{79}$, 577.0 mc/sec.; for $Br^{81}$, 482.0 mc/sec.; and for $I^{127}$, $-1934$ mc/sec. Second-order effects in the hyperfine structure were observed for methyl bromide and methyl iodide.

## I. INTRODUCTION

PRELIMINARY results on the microwave absorption of $CH_3Cl$, $CH_3Br$, and $CH_3I$ have been reported.[1] In the earlier work the measurements were made with cavity wave meters and were accurate to four places only. Since that time an instrument has been constructed in our laboratory for multiplying to the millimeter region 10 mc/sec. frequencies monitored by WWV, the station of the Bureau of Standards. With it the lines of methyl chloride, bromide, and iodide occurring in the region of 8 to 11.5 mm have been measured to seven significant figures. Some improvement has also been made in the measurements of relative intensities, although we are not yet able to measure these with a high degree of accuracy.

As pointed out in the previous notes, the rotational levels of the above molecules have

* The research described in this report was supported by Contract No. W-28-099-ac-125 with the Army Air Forces, Watson Laboratories, Air Materiel Command, and is based on a thesis submitted by J. W. Simmons to the Graduate School of Arts and Sciences of Duke University in partial fulfillment of the requirements for the degree of Doctor of Philosophy.

[1] W. Gordy, J. W. Simmons, and A. G. Smith, Phys. Rev. 72, 249, 344 (1947).

TABLE I. Hyperfine structure of the $J=0$ to $J=1$, $K=0$ to $K=0$ rotational transition of $CH_3Cl$ in the ground vibrational state.

| $F$ transition | Frequency Observed | Frequency Calculated* | Relative intensity Observed | Relative intensity Theoretical |
|---|---|---|---|---|
| | For $C^{13}H_3Cl^{35}$ | | | |
| 3/2→1/2 | 26604.57 mc/sec. | 26604.55 mc/sec. | 25 | 33.3 |
| 3/2→3/2 | 26570.77 | 26570.74 | 78 | 66.7 |
| 3/2→5/2 | 26589.49 | 26589.53 | 100 | 100.0 |
| | For $C^{13}H_3Cl^{37}$ | | | |
| 3/2→1/2 | 26191.13 | 26191.13 | 6 | 11.1 |
| 3/2→3/2 | 26164.57 | 26164.56 | 22 | 22.2 |
| 3/2→5/2 | 26179.30 | 26179.32 | 34 | 33.3 |

Probable error ±0.07 mc/sec.

* Using $eQ(\partial^2V/\partial z^2) = -75.13$ mc/sec. for $CH_3Cl^{35}$ and $-59.03$ mc/sec. for $CH_3Cl^{37}$.

hyperfine structure caused by the interaction of the nuclear quadrupole moment of the halogen. More recently anomalies have been reported[2] in this hyperfine structure for the $J=2\rightarrow3$ transition of methyl iodide. The more accurate measurements have revealed second-order effects in the hyperfine spectra of $CH_3Br$ and $CH_3I$ reported here. Prior to our detection of the rotational spectra and its hyperfine structure for these molecules Hershberger[3] has made microwave measurements of the attenuation at high pressures in non-resonant regions of methyl chloride and methyl bromide.

The first rotational transition of methyl fluoride has been observed at 5.87-mm wave-length by Edwards, Gilliam, and Gordy.[3a] No nuclear quadrupole splitting of the line was observed. This is in agreement with the value of 1/2 for the nuclear spin of fluorine.

TABLE II Hyperfine structure of the $J=1$ to $J=2$ rotational transition of $CH_3Br$ in the ground vibrational state.

| $F$ transition | Frequency Observed | Frequency Calculated* | Relative intensity Observed | Relative intensity Theoretical** |
|---|---|---|---|---|
| | For $C^{13}H_3Br^{79}$ | | | |
| | $K=0\rightarrow K=0$ | | | |
| 1/2→1/2 | 38272.40 mc/sec. | 38272.38 mc/sec. | 14 | 13.6 |
| 1/2→3/2 | 38417.09 | 38417.01 | 14 | 13.6 |
| 3/2→3/2 | 38157.30 | 38157.34 | 21 | 17.5 |
| 3/2→5/2 | 38260.10 | 38260.05 | 100 | 100.0 |
| 5/2→7/2 | 38260.10 | 38260.10 | | |
| 5/2→5/2 | 38404.49 | 38404.43 | 21 | 14.8 |
| | $K=1\rightarrow K=1$ | | | |
| 1/2→1/2 | 38128.40 | 38128.38 | 7 | 10.2 |
| 1/2→3/2 | 38200.52 | 38200.50 | 7 | 10.2 |
| 3/2→3/2 | 38330.25 | 38330.30 | 10 | 13.2 |
| 3/2→5/2 | 38381.70 | 38381.73 | 27 | 25.8 |
| 5/2→5/2 | 38309.45 | 38309.55 | 10 | 11.1 |
| 5/2→7/2 | 38237.14 | 38237.15 | 51 | 49.2 |
| | For $C^{13}H_3Br^{81}$ | | | |
| | $K=0\rightarrow K=0$ | | | |
| 1/2→1/2 | 38126.97 | 38126.98 | 14 | 13.6 |
| 1/2→3/2 | 38247.77 | 38247.68 | 27 | 13.6 |
| 3/2→3/2 | 38030.77 | 38030.84 | 14 | 17.5 |
| 3/2→5/2 | 38116.65 | 38116.61 | 100 | 100.0 |
| 5/2→7/2 | 38116.65 | 38116.65 | | |
| 5/2→5/2 | 38237.14 | 38237.20 | 25 | 14.8 |
| | $K=1\rightarrow K=1$ | | | |
| 1/2→1/2 | 38006.47 | 38006.48 | 10 | 10.2 |
| 1/2→3/2 | 38066.72 | 38066.73 | 7 | 10.2 |
| 3/2→3/2 | 38175.08 | 38175.16 | 14 | 13.2 |
| 3/2→5/2 | 38218.21 | 38218.13 | 27 | 25.8 |
| 5/2→5/2 | 38157.70 | 38157.85 | 10 | 11.1 |
| 5/2→7/2 | 38057.45 | 38097.50 | 55 | 49.2 |

Probable error ±0.08 mc/sec.

* This calculation includes both first- and second-order nuclear effects and a centrifugal stretching term $-D_{J,K}J(J+1)K^2$. The values of $eQ(\partial^2V/\partial z^2)$ used are 577.0 mc/sec. and 482.0 mc/sec. for $CH_3Br^{79}$ and $CH_3Br^{81}$, respectively. The value of $D_{J,K}$ is 90 kc/sec. The $F\rightarrow F-1$ transitions are omitted because of their low intensity.

** The factor $\nu e^{-(E_r/kT)}$ is neglected in the calculations.

## II. EXPERIMENTAL PROCEDURE

The observations were made with the gas at low pressure, $\approx10^{-3}$ mm of Hg, in a silver wave guide cell 60 feet in length. The single crystal detecting system[4] was used, employing video filtering to eliminate the r-f reflections and mode contour. The system for frequency measurement was constructed in this laboratory by Mr. R. Unterberger. It employs a conventional electronic multiplier to convert the signal of a 10-mc/sec. crystal oscillator monitored by the standard 10-mc/sec. broadcast by WWV to a frequency of 270 mc/sec., then a klystron multiplier and a crystal converter to obtain standard markers in the desired region. A tuneable receiver, also calibrated with WWV, is used to interpolate between the standard markers, which are 90 mc/sec. apart. Relative intensities of the components of the hyperfine structure were observed by comparing the heights of the different lines on the oscilloscope with the detector crystal tuned to each line and with the power adjusted as nearly as possible to the same level. The millimeter wave oscillators used as sources, QK-140, QK-141, and QK-142, were obtained from the Raytheon Manufacturing Company.

## III. THEORY

### Frequencies

The pure rotational energy levels of the non-rigid symmetric top molecules as derived

[2] O. R. Gilliam, H. D. Edwards, and W. Gordy, Phys. Rev. 73, 635 (1948).

[3] W. D. Hershberger, J. App. Phys. 17, 495 (1946).

[3a] H. D. Edwards, O. R. Gilliam, and W. Gordy, to be published.

[4] W. Gordy and M. Kessler, Phys. Rev. 71, 640 (1947); 72, 664 (1947).

by Slawsky and Dennison are given by the formula:[5,6]

$$E_r=\frac{h}{8\pi^2c}\left[\frac{J(J+1)}{I_B}+\left(\frac{1}{I_A}-\frac{1}{I_B}\right)K^2\right]$$
$$-D_JJ^2(J+1)^2-D_{J,K}J(J+1)K^2-D_KK^4, \quad (1)$$

where the selection rules for the pure rotation absorption spectra are:

$$\Delta J=+1, \quad \Delta K=0.$$

Here $I_A$ is the moment of inertia about the axis of symmetry and $I_B$ that about the axis perpendicular to the symmetry axis. The last three terms in this expression are corrections for nonrigidity. The constants $D_J$, $D_{J,K}$, and $D_K$ are extremely small, and the last terms do not contribute significantly to the energy when $J$ and $K$ are small. The present work indicates that $D_{J,K}$ for the methyl halides is $\approx 90$ kc/sec. or $3\times 01^{-6}$ cm$^{-1}$. No evaluation of $D_J$ and $D_K$ can be made from the present data.

For the methyl halides considered here, there must be added to the rotational energy $E_r$ the energy of the nuclear interactions of the halogen, which is given to the first order of approximation by the formula:

$$E_Q=eQ\frac{\partial^2V}{\partial z^2}\left(\frac{3K^2}{J(J+1)}-1\right)$$
$$\times\left(\frac{3/4C(C+1)-I(I+1)J(J+1)}{2(2J+3)(2J-1)I(2I-1)}\right), \quad (2)$$

where $C=F(F+1)-I(I+1)-J(J+1)$

$$F=J+I,\ J+I-1,\ \cdots|J-I|,$$

and where the selection rules require that $\Delta F=0$, $\pm 1$. The quadrupole coupling $eQ(\partial^2V/\partial z^2)$ is constant for a given molecule. $Q$ is the quadrupole moment of the halogen nucleus, and $\partial^2V/\partial z^2$ is the measure of the rate of variation of the electrical field at the halogen nucleus in the direction of the molecular axis. A summary of the development of this formula is given elsewhere.[7]

TABLE III. Hyperfine structure of the $J=1$ to $J=2$ rotational transition for $CH_3I$ in the ground vibrational state.

| $F$ transition | Frequency Observed | Frequency Calculated* | Relative intensity Observed | Relative intensity Theoretical** |
|---|---|---|---|---|
| | $C^{13}H_3I^{127}$ (98.9% $C^{12}$) | | | |
| | For $K=0\rightarrow K=0$ | | | |
| 3/2→1/2 | 30121.32 mc/sec. | 30021.31 mc/sec. | 26 | 20.0 |
| 3/2→3/2 | 29872.52 | 29872.56 | 36 | 28.0 |
| 3/2→5/2 | 29598.95 | 29598.83 | 17 | 18.7 |
| 5/2→3/2 | 30453.46 | 30453.53 | 7 | 12.0 |
| 5/2→5/2 | 30179.71 | 30179.79 | 39 | 36.6 |
| 5/2→7/2 | 30079.72 | 30079.75 | 66 | 51.4 |
| 7/2→5/2 | 29773.95 | 29774.05 | 4 | 4.7 |
| 7/2→7/2 | 29673.95 | 29674.00 | 25 | 28.6 |
| 7/2→9/2 | 30046.99 | 30046.99 | 100 | 100.0 |
| | For $K=1\rightarrow K=1$ | | | |
| 3/2→1/2 | | 30331.48 | 7 | 15.0 |
| 3/2→3/2 | 30215.95 | 30216.01 | 28 | 21.0 |
| 3/2→5/2 | 30075.08 | 30075.04 | 12 | 14.0 |
| 5/2→3/2 | 29923.50 | 29923.63 | 5 | 9.0 |
| 5/2→5/2 | 29782.71 | 29782.66 | 20 | 27.4 |
| 5/2→7/2 | 29735.71 | 29735.61 | 29 | 38.5 |
| 7/2→5/2 | 29986.84 | 29986.98 | 4 | 3.5 |
| 7/2→7/2 | 29939.87 | 29939.93 | 20 | 21.4 |
| 7/2→9/2 | 30123.64 | 30123.55 | 80 | 75.0 |
| | $C^{13}H_3I^{127}$ (49% $C^{13}$) | | | |
| | For $K=0\rightarrow K=0$ | | | |
| 3/2→3/2 | 28343.64 | 28343.71 | 17 | 13.9 |
| 3/2→5/2 | 28069.99 | 28069.98 | 9 | 9.3 |
| 5/2→5/2 | 28650.91 | 28650.94 | 17 | 18.1 |
| 5/2→7/2 | 28550.86 | 28550.90 | 29 | 25.5 |
| 7/2→7/2 | 28145.01 | 28145.15 | 17 | 14.2 |
| 7/2→9/2 | 28518.14 | 28518.14 | 48 | 49.6 |
| | For $K=1\rightarrow K=1$ | | | |
| 3/2→3/2 | 28687.21 | 28687.16 | 9 | 10.4 |
| 5/2→5/2 | 28253.84 | 28253.81 | 11 | 13.6 |
| 5/2→7/2 | 28206.90 | 28206.76 | 17 | 19.1 |
| 7/2→7/2 | 28411.19 | 28411.08 | 11 | 10.6 |
| 7/2→9/2 | 28594.74 | 28594.70 | 40 | 37.2 |

Probable error ±0.08 mc/sec.

* This calculation includes both first- and second-order nuclear effects and a centrifugal stretching term $-D_{J,K}J(J+1)K^2$. The value −1934 mc/sec. was used for $eQ(\partial^2V/\partial z^2)$ and 95 kc/sec. for $D_{J,K}$.
** The factor $\nu e^{-(E_r/kT)}$ is neglected in the calculations.

The second order theory of the interactions between levels of different $J$ but of the same $F$ and $M_F$ has been derived for linear and symmetric top molecules by Bardeen and Townes.[8] The displacement of the levels caused by this type of interaction is of the form

$$E_Q=\sum_{J'}\frac{(IJFM_F|H_Q|IJ'FM_F)^2}{E_r-E_r'} \quad (3)$$

where $J'$ can differ from $J$ by 1 or 2. These authors have advised us of some typographical errors in their formulae for evaluating the

[5] G. Herzberg, *Infrared and Raman Spectra of Polyatomic Molecules* (D. Van Nostrand Company, Inc., New York, 1945), p. 26.
[6] Z. I. Slawsky and D. M. Dennison, J. Chem. Phys. **7**, 509 (1939).
[7] J. Bardeen and C. H. Townes, Phys. Rev. **73**, 97 (1948).
[8] J. Bardeen and C. H. Townes, Phys. Rev. **73**, 627 (1948).

squared matrix element in the numerator. The corrected forms are:

$$(IJFM_F|H_Q|IJ+1FM_F)^2$$

$$=\left[\frac{(3eqQK)}{(8I(2I-1)J(J+2)}\right]^2\left[1-\frac{K^2}{(J+1)^2}\right]$$

$$\times\frac{[F(F+1)-I(I+1)-J(J+2)]^2}{(2J+1)(2J+3)}$$

$$\times(I+J+F+2)(J+F-I+1)$$

$$\times(I+F-J)(J+I-F+1), \quad (4)$$

$$(IJFM_F|H_Q|IJ+2FM_F)^2$$

$$=\left[\frac{3eqQ}{16I(2I-1)(2J+3)}\right]^2\left[1-\frac{K^2}{(J+1)^2}\right]$$

$$\times\left[1-\frac{K^2}{(J+2)^2}\right]\frac{1}{(2J+1)(2J+5)}$$

$$\times(F+I+J+3)(F+I+J+2)$$

$$\times(J+I-F+2)(J+I-F+1)$$

$$\times(J+F-I+2)(J+F-I+1)$$

$$\times(I+F-J)(I+F-J-1). \quad (5)$$

Here $q$ is used to represent the form $\partial^2V/\partial z^2$.

### Intensities

The intensities of the lines exclusive of nuclear effects are given by the expression:[9]

$$Int(J,K)=C\nu\frac{(J+1)^2-K^2}{(J+1)(2J+1)}g_{JK}$$

$$\times\exp\left[\frac{-E(J,K)}{kT}\right], \quad (6)$$

where $g_{JK}=2(2J+1)$ for $K\neq 0$ and

$$2J+1 \text{ for } K=0.$$

Here $J$ and $K$ are for the lower state. In addition, nuclear effects must be taken into account. In general, for molecules having the symmetry of the methyl halides the weight factors caused by the nuclear spin $I$ of the three identical corner atoms are:[10]

$$1/3(2I+1)(4I^2+4I+3) \text{ for } K=0, 3, 6\cdots$$

and (7)

$$1/3(2I+1)(4I^2+4I) \text{ for } K \text{ not divisible by } 3.$$

For the particular cases here the spin of the hydrogen $I=1/2$, and the ratio of these two factors becomes 2:1. After the over-all intensities (neglecting the halogen nuclear quadrupole splitting of the lines) are calculated as indicated above, the relative intensities of the different hyperfine components of a given rotational transition are determined by the weights $(2F+1)$ of both the upper and lower hyperfine levels with the methods used in atomic spectra to determine the relative intensities of the fine structure or the hyperfine structure. For the transitions studied here, indeed for most cases needed in microwave investigations, the numerical values are already

TABLE IV. Second-order effects in the hyperfine structure of the $J=1$ to $J=2$ line of $C^{12}H_3I$ in the ground vibrational state. Frequencies are given in mc/sec. relative to the strongest line, $F=7/2$ to $F=9/2$, $K=0\rightarrow 0$. $eQ$ $(\partial^2V/\partial z^2)$ $=-1934$ mc/sec.

| $F$ transition | Experimental $\Delta\nu$ | First-order theory $\Delta\nu$ | Experiment minus first-order theory | Second-order theory |
|---|---|---|---|---|
| | For $K=0\rightarrow K=0$ | | | |
| 3/2→1/2 | +74.33 | +74.59 | −0.26 | −0.27 |
| 3/2→3/2 | −174.47 | −174.06 | −0.41 | −0.37 |
| 3/2→5/2 | −448.04 | −450.35 | +2.31 | +2.19 |
| 5/2→3/2 | +406.47 | +406.14 | +0.33 | +0.40 |
| 5/2→5/2 | +132.72 | +129.85 | +2.87 | +2.95 |
| 5/2→7/2 | +32.73 | +33.15 | −0.42 | −0.39 |
| 7/2→5/2 | −273.04 | −276.29 | +3.25 | +3.35 |
| 7/2→7/2 | −373.04 | −372.99 | −0.05 | 0 |
| 7/2→9/2 | 0 | — | — | — |
| | For $K=1\rightarrow K=1$* | | | |
| 3/2→1/2 | — | +281.73 | — | +2.76 |
| 3/2→3/2 | +168.96 | +163.02 | +5.94 | +6.00 |
| 3/2→5/2 | +28.09 | +24.85 | +3.24 | +3.20 |
| 5/2→3/2 | −123.49 | −127.08 | +3.59 | +3.72 |
| 5/2→5/2 | −264.28 | −265.25 | +0.97 | +0.92 |
| 5/2→7/2 | −311.28 | −313.60 | +2.32 | +2.22 |
| 7/2→5/2 | −60.15 | −62.18 | +2.03 | +2.17 |
| 7/2→7/2 | −107.12 | −110.53 | +3.41 | +3.47 |
| 7/2→9/2 | +76.65 | +75.99 | +0.66 | +0.57 |

* Because the reference line is a $K=0$ line the second-order corrections for $K=1$ lines include, in addition to the second-order energy predicted by Eq. (3), a constant −0.38 mc/sec. to correct for term $-D_{J,K}J(J+1)K^2$ in the rotational energy, Eq. (1).

[9] See reference 5, p. 32.

[10] D. M. Dennison, Rev. Mod. Phys. 3, 280 (1931).

compiled in tables which may be found in standard texts on atomic spectra.[11]

## IV. RESULTS

### Nuclear Effects

Because of the interaction of the nuclear quadrupole moment of the halogen, the pure rotational lines of the molecules considered here are split into a number of components. Table I gives the observed and calculated hyperfine structure of the $J=0\rightarrow1$ transition of $CH_3Cl^{35}$ and $CH_3Cl^{37}$. The relative intensities and separations of the components were calculated by the methods described above. Equation (2) is in substantial agreement with observation for methyl chloride: that is, in this molecule the second-order effects are negligible, as is predicted by Eq. (3).

In Table II are given the calculated and observed hyperfine structures of the $J=1\rightarrow2$ transition of $CH_3Br^{79}$ and $CH_3Br^{81}$. For these cases the second-order effects are outside the range of experimental error. The theory of Bardeen and Townes is found to account for the deviations from the first-order theory.

In methyl iodide, where the nuclear quadrupole coupling is large, the deviations from first-order theory are considerable, in some cases as great as 5 mc/sec. Table III gives the observed and calculated spectrum. From examination of Table IV it may be seen that Eq. (3) accounts well for the deviations from first-order theory.

TABLE V. The nuclear quadrupole coupling coefficients in mc/sec. for Cl, Br, and I in methyl chloride, bromide, and iodide compared with values found in other compounds.

| Atom | Spin | Molecule $CH_3Cl$ | ClCN | ICl | $CH_3Br$ | BrCN | $CH_3I$ | ICN |
|---|---|---|---|---|---|---|---|---|
| $Cl^{35}$ | 3/2 | −75.13 | −84[a]<br>−83.5[c] | −82.5[b] | | | | |
| $Cl^{37}$ | 3/2 | −59.03 | −64[a]<br>−65.0[c] | | | | | |
| $Br^{79}$ | 3/2 | | | | 577.0 | 686[c] | | |
| $Br^{81}$ | 3/2 | | | | 482.0 | 573[c] | | |
| $I^{127}$ | 5/2 | | | −2930[b] | | | −1934 | −2420[d]<br>−2420[c] |

[a] C. H. Townes, A. N. Holden, J. Bardeen, and F. R. Merritt, Phys. Rev. 71, 644 (1947).
[b] C. H. Townes, F. R. Merritt, and B. D. Wright, privately communicated.
[c] A. G. Smith, H. Ring, W. V. Smith, and W. Gordy, Phys. Rev. (to be published).
[d] See reference 8.

TABLE VI. Frequencies of hypothetical unsplit rotational lines, $\nu_0$, and resulting moments of inertia for methyl chloride, bromide, and iodide.

| Molecule | $J$ transition | $\nu_0$ (mc/sec.) | $I_B$ ($10^{-40}$ g-cm$^2$) | $I_A$ ($10^{-40}$ g-cm$^2$) |
|---|---|---|---|---|
| $C^{12}H_3Cl^{35}$ | 0→1 | 26585.77 | $63.11_{38}$ | 5.52 |
| $C^{13}H_3Cl^{37}$ | 0→1 | 26176.37 | $64.10_{09}$ | 5.52 |
| $C^{12}H_3Br^{79}$ | 1→2 | 38272.40 | $87.68_{35}$ | 5.50 |
| $C^{12}H_3Br^{81}$ | 1→2 | 38126.97 | $88.01_{80}$ | 5.50 |
| $C^{12}H_3I^{127}$ | 1→2 | 30005.00 | $111.8_{48}$ | 5.50 |
| $C^{13}H_3I^{127}$ | 1→2 | 28476.16 | $117.8_{48}$ | 5.50 |

Table V lists the quadrupole coupling $eQ(\partial^2V/\partial z^2)$ obtained for the different halide nuclei. In this table are given for comparison the coupling factors of these nuclei in certain other molecules. Since the nuclear quadrupole moment $Q$ does not change, it is apparent that the factor $\partial^2V/\partial z^2$, which measures the rate of change of the electric field of the molecule at the position of the halogen nucleus, varies appreciably from molecule to molecule. This factor must be evaluated from other sources before microwave data can be used to calculate $Q$. No method has been evolved for determining the absolute value of $\partial^2V/\partial z^2$ in molecules of this type, though Townes[12] has suggested a method by which its order of magnitude may be obtained. With the atomic beam method, Davis, Feld, Zabel, and Zacharias[13] have recently measured the hyperfine splitting of $^2P_{3/2}$ ground states for $Cl^{35}$ and $Cl^{37}$. From this experiment they evaluated the nuclear quadrupole moment of $Cl^{35}$ as $-(7.921\pm0.05)\times10^{-26}$ cm$^2$ and that of $Cl^{37}$ as $-(6.189\pm0.05)\times10^{-26}$ cm$^2$. Using their value of $Q$ with the value of $eQ(\partial^2V/\partial z^2)$ listed in Table V, the $\partial^2V/\partial z^2$ at the chlorine nucleus in methyl chloride is found to be $13\times10^{15}$ e.s.u. Our measurements give the ratio of $Q$ for $Cl^{35}$ to that for $Cl^{37}$ as 1.273, in satisfactory agreement with the ratio 1.280 determined by the atomic beam method. Our measurements yield a ratio of 1.197 for the nuclear quadrupole moment of $Br^{79}$ to that of $Br^{81}$.

[11] For example: H. E. White, *Introduction to Atomic Spectra* (McGraw-Hill Book Company, Inc., New York, 1934), p. 439; E. U. Condon and G. H. Shortley, *The Theory of Atomic Spectra* (The Cambridge University Press, New York, 1935).

[12] C. H. Townes, Phys. Rev. 71, 909 (1947).

[13] L. Davis, B. T. Feld, C. W. Zabel, and J. R. Zacharias, Phys. Rev. 73, 525 (1948); also, L. Davis and C. W. Zabel, private communication.

TABLE VII. Molecular dimensions of the methyl halides.

| Molecule | C–X distance ($10^{-8}$ cm) | C–H distance ($10^{-8}$ cm) | ∠HCH | Ref. |
|---|---|---|---|---|
| $CH_3F$ | $1.38_4$ | $1.11_2$ | 110° 0′ (assumed) | a, e, 21 |
| $CH_3Cl$ | 1.779 | 1.109 | 110° 0′ | b, e |
| $CH_3Br$ | 1.936 | 1.104 | 110° 15′ | c, e |
| $CH_3I$ | 2.139 | 1.100 | 110° 58′ | d, e |

[a] Using $M_X$ for $F^{19}$ = 19.00452 a.m.u. as given by M. S. Livingston and H. A. Bethe, Rev. Mod. Phys. 9, 373 (1937).
[b] Using $M_X$ for $Cl^{35}$ = 34.98107 a.m.u. and $M_X$ for $Cl^{37}$ = 36.97829 a.m.u. as given by E. Pollard, Phys. Rev. 57, 1186 (1940).
[c] Using $M_X$ for $Br^{79}$ = 78.9417 a.m.u. and $M_X$ for $Br^{81}$ = 80.9400 a.m.u. as given by F. W. Aston, Nature, 141, 1096 (1938).
[d] Using $M_X$ for $I^{127}$ = 126.932 a.m.u. as given by F. W. Aston, Proc. Roy. Soc. A115, 487 (1927), and $M_C$ for $C^{12}$ = 13.00761 a.m.u. as given by M. S. Livingston and H. A. Bethe, Rev. Mod. Phys. 9, 370 (1937).
[e] Other constants used: $h = 6.624_2 \times 10^{-27}$ erg-sec., $M_H$ for $H^1$ = 1.00813 a.m.u., $M_C$ for $C^{12}$ = 12.00386 a.m.u. and mass of atom of unit atomic mass = $1.6599_0 \times 10^{-24}$ g, all as given by R. T. Birge, Rev. Mod. Phys. 13, 233 (1941).

## Molecular Structures

By combining the microwave results obtained here with existing infra-red data it is possible for the first time to determine unambiguously the structure of these molecules. Though the carbon-halogen distances have been determined by electron diffraction[14] to an accuracy of about 3 percent, because of the low electron scattering power of the hydrogens it is not possible to determine either the bond angles or the CH bond lengths by this method.

From the analysis of the microwave hyperfine spectra above, the $\nu_0$, or the frequency of the rotational line which would be observed if no nuclear quadrupole interaction existed, has been determined for each of the $J$ transitions studied. These frequencies, with the $I_B$ values determined from them by Eq. (1), are listed in Table VI. Though the frequency measurements here are accurate to better than four parts in a million, the moments of inertia depend upon Planck's constant, which has not been determined to the same accuracy. Hence, the last two figures in the $I_B$ values have only relative significance.

From infra-red rotation-vibration spectra alone it is not possible to obtain very accurate values for either $I_A$, the moment of inertia about the symmetry axis, or $I_B$, that about an axis perpendicular to the symmetry axis. Now that $I_B$ is known, however, it is possible to obtain fairly accurate values of $I_A$ from previously measured separations of certain lines in the fundamental rotation-vibration spectra, which depend on $I_A$ and $I_B$ together. Johnston and Dennison[15] have shown that

$$\sum \Delta\nu_i = \left(\frac{6}{I_A} - \frac{7}{I_B}\right)\frac{h}{8\pi^2 c} \tag{8}$$

where the summation refers to the sums of the average line separations of zero branch lines in the three fundamental perpendicular type vibration bands. The summed values are: for methyl chloride[16] 27.31; for methyl bromide[16] 28.32; and for methyl iodide[16,17] 28.78 $cm^{-1}$. These, together with the $I_B$ values determined in this work, were used to compute the $I_A$ values listed in Table VI. As pointed out by Herzberg,[18] the accuracy of $I_A$ determined by this equation is limited, because the dependence of $I_A$ and $I_B$ on the vibrational frequency has been neglected and because the sum rule holds exactly for strictly harmonic vibrations only. It is also limited by the accuracy of measurement of the separations of the lines in the vibrational bands. Fortunately, the bond distances can be determined somewhat more accurately since they depend upon the square root of the moment of inertia. Furthermore, the carbon-halogen distance depends primarily upon the $I_B$ value, which is accurately known.

In Table VII are given the molecular dimensions evaluated from the moments of inertia with the following equations, which are readily obtained from the geometry of the molecules:

$$d_{CX}^2\left[M_X - \frac{M_X^2}{3M_H+M_C+M_X}\right] + d_{CX}a\left[2M_X - \frac{2M_X(M_C+M_X)}{3M_H+M_C+M_X}\right] + a^2\left[(M_C+M_X) - \frac{(M_C+M_X)^2}{3M_H+M_C+M_X}\right] = I_B - I_A/2, \tag{9}$$

where

$$a \equiv \left(d_{CH}^2 - \frac{I_A}{3M_H}\right)^{\frac{1}{2}} = d_{CH}\cos\beta, \tag{10}$$

[14] L. R. Maxwell, J. Opt. Soc. Am. 30, 388 (1940).
[15] M. Johnston and D. M. Dennison, Phys. Rev. 48, 868 (1935).
[16] W. H. Bennett and C. F. Meyer, Phys. Rev. 32, 888 (1928).
[17] R. T. Lagemann and H. H. Nielsen, J. Chem. Phys. 10, 668 (1942).
[18] See reference 5, p. 436.

and where $X$ designates halogen and $\beta$, the angle of CH with the symmetry axis, is related to $\angle$HCH by

$$\sin\beta = \frac{2}{\sqrt{3}} \sin(1/2 \angle \mathrm{HCH}). \qquad (11)$$

With regard to the microwave data, the accuracy of the molecular structure determinations depends upon the accuracy of the measurement of the separations of the corresponding lines for the different isotopes. For methyl chloride this difference has been measured to an accuracy of about 0.04 percent, for methyl bromide to an accuracy of about 0.12 percent, and for methyl iodide about 0.01 percent. The structure determinations are also rather sensitive to the ratios of the atomic weights of the isotopes. The atomic weights used are listed in the table. In these calculations it is assumed that the carbon-halogen distances of the ground vibrational state are the same for the two isotopes. Though this is not exactly true, the error introduced by this assumption is probably not as great as that caused by the $I_A$ values. Though the probable limits of error in the values given are not definitely known, in each case the last figure is uncertain.

The *C*-halogen bonds of methyl chloride, bromide, and iodide are somewhat longer than had been anticipated. They are significantly longer than the sum of the covalent radii (1.76, 1.91, and 2.10A) if the value[19] 0.77A is used as the single bond covalent radius of carbon, but they agree fairly well with the sum of the radii if the revised value[20] 0.79A is used for the carbon radius. Resonance with ionic structures of the type $H_3{\equiv}C^+X^-$ would be expected to shorten rather than lengthen the C−X bonds and so would contributions of double bonded structures of the type $H_3^-{=}C{=}X^+$. Small contributions of hyperconjugated structures of the type $H_3^+{=}C\,X^-$ would lengthen both the CH and CX bonds, but significant contributions from such unstable structures does not seem probable. In contrast, the C-halogen interatomic distance in methyl fluoride is appreciably shorter than the sum of the single bond covalent radii (either 1.49A or 1.51A). Microwave measurement in this laboratory[3a] yields a value for the C−F distance (see Table VII) which is in good agreement with the latest electron diffraction value[21] 1.39A.

Though bond lengths shorter than the sum of the single bond covalent radii are of wide occurrence, there are only a few instances known of bonds which are significantly longer than this sum. Carbon to halogen bonds of abnormal length (1.83A, 1.95A, and 2.13A for CCl, CBr, and CI, respectively) have, however, been found in $H-C{\equiv}C-CH_2$ (Hal) by electron diffraction measurements.[22]

The CH bond-stretching force constants calculated by Linnett[23] for $CH_3I$, $CH_3Br$, $CH_3Cl$ and $CH_3F$ are 5.00, 4.95, 4.90, and $4.71\times10^{-5}$ dyne/cm, respectively. The bond lengths, 1.100A, 1.104A, 1.109A, and 1.112A are in accord with this sequence, since the longer bond would have the weaker force constant.

We wish to thank Dr. H. Lyons, of the National Bureau of Standards, for the calibration of a wave meter used in the preliminary work; also Drs. Bardeen and Townes for sending us a prepublication copy of their paper on second order effects. We are indebted to Mr. H. Ring for preparing some of the compounds and to Mr. R. Unterberger for assisting with some of the measurements.

[19] L. Pauling, *The Nature of the Chemical Bond* (Cornell University Press, Ithaca, New York, 1940), p. 164.
[20] W. Gordy, J. Chem. Phys. 15, 81 (1947).
[21] V. Schomaker and D. P. Stevenson, J. Am. Chem. Soc. 63, 37 (1941).
[22] L. Pauling, W. Gordy, and J. H. Saylor, J. Am. Chem. Soc. 64, 1753 (1942).
[23] J. W. Linnett, J. Chem. Phys. 8, 91 (1940).

# The Magnetic Moment of the Electron†

P. KUSCH AND H. M. FOLEY
*Department of Physics, Columbia University, New York, New York*

(Received April 19, 1948)

A comparison of the $g_J$ values of Ga in the $^2P_{3/2}$ and $^2P_{\frac{1}{2}}$ states, In in the $^2P_{\frac{1}{2}}$ state, and Na in the $^2S_{\frac{1}{2}}$ state has been made by a measurement of the frequencies of lines in the *hfs* spectra in a constant magnetic field. The ratios of the $g_J$ values depart from the values obtained on the basis of the assumption that the electron spin gyromagnetic ratio is 2 and that the orbital electron gyromagnetic ratio is 1. Except for small residual effects, the results can be described by the statement that $g_L=1$ and $g_S=2(1.00119\pm0.00005)$. The possibility that the observed effects may be explained by perturbations is precluded by the consistency of the result as obtained by various comparisons and also on the basis of theoretical considerations.

## 1. INTRODUCTION

ONE of the important conclusions derived from the relativistic Dirac theory of the electron is that the electron possesses an angular momentum of $\frac{1}{2}$ measured in units of $h/2\pi$ and that with this angular momentum is associated a magnetic moment of one Bohr magneton. This conclusion substantiates earlier conclusions based on an analysis of the experimental data on the anomalous Zeeman effect. Indeed, all relevant experimental data have been in substantial agreement with this conclusion.

A direct measurement of the electron moment can most easily be made by a measurement of the $g$ value of an atomic energy state. Direct determinations of the $g$ values of atomic states from measurements of the frequencies of Zeeman lines in known magnetic fields, as, for example, in the work of Kinsler and Houston,[1] have yielded no significant differences between the measured atomic gyromagnetic ratios and the values consequent from the Dirac theory.* Millman and Kusch[2] have measured the magnetic moments of various nuclei, in particular that of the proton, in terms of the magnetic moment of the electron, assumed to be one Bohr magneton. The magnetic moments so found agree with those dependent on a measurement of a magnetic field in terms of classical standards to within about 0.14 percent $\pm0.5$ percent. This again indicates that the $g$ value of the electron is 2, to within the stated precision. It seems certain that any discrepancy with the theoretical value will be small.

The growth of various techniques of microwave and r-f spectroscopy makes available a series of new tools for the investigation of the detailed structure of atomic spectra. These techniques make it possible to resolve extremely minute details of structure and to determine the relative positions of energy levels to a very high degree of precision. The recent experiments of Lamb and Retherford[3] on the fine structure of hydrogen indicate that the Dirac theory does not adequately describe the hydrogen atom and that all the detailed conclusions of the Dirac theory are, therefore, presumably suspect to some degree.

In the recent measurements of Nafe, Nelson, and Rabi[4] of the hyperfine spectrum of the ground states of atomic hydrogen and deuterium, deviations of the zero field level splittings from the values predicted from theory were found. The theoretical values depend on a knowledge of the nuclear magnetic moment of the nucleus (known only in terms of an assumed value of the electron moment) as well as on the assumption that the magnetic moment of the electron is one Bohr magneton. Breit[5] has suggested that the discrepancy may be removed by the assumption that the electron possesses an "intrinsic" mag-

† Publication assisted by the Ernest Kempton Adams Fund for physical research at Columbia University.

[1] L. E. Kinsler and W. V. Houston, Phys. Rev. **45**, 104 (1934); **46**, 533 (1934).

* See, however, a consideration of these measurements in Section 6.

[2] S. Millman and P. Kusch, Phys. Rev. **60**, 91 (1941).

[3] W. E. Lamb, Jr. and R. C. Retherford, Phys. Rev. **72**, 241 (1947).

[4] J. E. Nafe, E. B. Nelson, and I. I. Rabi, Phys. Rev. **71**, 914 (1947). J. E. Nafe and E. B. Nelson, Phys. Rev. **73**, 718 (1948).

[5] G. Breit, Phys. Rev. **72**, 984 (1947).

netic moment, i.e., a magnetic moment over and above that deduced from the Dirac theory.

The present experiments were undertaken to utilize the power of the atomic beam magnetic resonance method to provide an accurate determination of the electron moment. Preliminary results of the present experiments were given in two Letters to the Editor.[6] Subsequent to the publication of preliminary results of our experiments, Schwinger[7] has published results of theoretical investigation which indicate that the magnetic moment of the electron is, indeed, to be modified as the result of the interaction of the electron with the radiation field.

A deviation of the magnetic moment of the electron from the accepted value of one Bohr magneton could be detected by a precise measurement of the magnetic moment of an atom in a state in which the coupling of the electron spin with the orbital angular momentum is sufficiently well known. An absolute measurement of the magnetic moment requires a measurement of the Zeeman splitting of the zero field energy level in a known magnetic field. At the present time it is difficult to produce magnetic fields which are accurately known in terms of absolute standards and of sufficient magnitude to be useful in atomic beam determinations of the Zeeman splittings of energy levels. However, the frequencies of lines in the Zeeman spectrum of atoms (that is, the differences between atomic energy levels) may be determined by use of readily available techniques to within one part in ten or twenty thousand, and where precision is limited by statistical errors, as, for example, those arising from the least count of an instrument, a considerable improvement in precision may be obtained by a suitable repetition of observations. From measurements of the frequencies of Zeeman lines in two atomic states arising in either the same or different atoms but in the same constant magnetic fields, it is possible to deduce the ratio of the values of the atomic gyromagnetic ratios of these two states. If the spin and orbit vectors are coupled in the same way in the two states, the measured ratio yields no information about the fundamental $g$ values of the electron. If the spin orbit coupling in the two states is different, however, the electron spin $g$ value may be determined in terms of the orbital $g$ value, provided only that suitable information is available, either on experimental or theoretical grounds, as to the validity of the assumed coupling. The principal limitations on such an experimental determination of the electron spin $g$ value are the accuracy in the determination of the line frequencies (limitations imposed by a frequency meter and by the line widths) and the stability and homogeneity of the magnetic field.

In actual practice the single atomic level described above is split into two or more h.f.s. levels because of the presence of the nuclear angular momentum. In such a case the interpretation of data on line frequencies becomes considerably more complicated.

## 2. THEORY OF THE EXPERIMENT

In this and the following section is developed the elementary theory on the basis of which the experimental data have actually been reduced. Corrections to the results of these sections are considered in Section 6.

The Hamiltonian of the interaction of the electrons in an atom with a constant applied magnetic field $H$ may be written as:

$$\mathcal{H}=g_L\mu_0 L_z H_z+g_S\mu_0 S_z H_z, \tag{1}$$

in which $g_L$ and $g_S$ are the orbital and electron spin gyromagnetic ratios, $\mu_0$ is the Bohr magneton, and $L_z$ and $S_z$ are the operators of the $z$ components of orbital and spin angular momentum. The diamagnetic energy is negligible at the fields employed in this experiment ($H<500$ gauss). For the calculation of matrix elements diagonal in the total atomic angular momentum $J$, i.e., neglecting atomic Paschen-Back effects, this Hamiltonian may be written:

$$\begin{aligned}\mathcal{H}&=g_L\mu_0 H_z(J|L_z|J)J_z+g_S\mu_0 H_z(J|S_z|J)J_z\\&=g_L\mu_0 H_z\alpha_L J_z+g_S\mu_0 H_z\alpha_S J_z\\&=g_J\mu_0 H_z J_z.\end{aligned} \tag{2}$$

The constants $\alpha_L$ and $\alpha_S$ are determined by the electronic wave functions. For Russell-Saunders coupling:

$$\alpha_S=[J(J+1)+S(S+1)-L(L+1)]/2J(J+1), \tag{3}$$

[6] P. Kusch and H. M. Foley, Phys. Rev. 72, 1256 (1947); H. M. Foley and P. Kusch, Phys. Rev. 73, 412 (1948).
[7] J. Schwinger, Phys. Rev. 73, 416 (1948).

TABLE I. The hyperfine structure separations and the nuclear $g$ values of the atoms whose spectra have been observed.

| | $(\Delta W/h)\times10^{-6}$ sec.$^{-1}$ | $I$ | $g_I$ |
|---|---|---|---|
| $Na^{23}$ | 1771.75 | 3/2 | −0.0008039 |
| $Ga^{69}$ | 2677.56 | 3/2 | −0.0007239 |
| $Ga^{71}$ | 3402.09 | 3/2 | −0.0009218 |
| $In^{115}$ | 11413 | 9/2 | −0.000664 |

and

$$\alpha_L=[J(J+1)+L(L+1)-S(S+1)]/2J(J+1).$$

The ratio of the $g_J$ values of two atomic states in the same or different atoms is:

$$g_{J_1}/g_{J_2}=[(g_L\alpha_{L_1}+g_S\alpha_{S_1})/(g_L\alpha_{L_2}+g_S\alpha_{S_2})], \quad (4)$$

in which it is assumed that the values of $g_L$ and $g_S$ are independent of the atomic state. If the fundamental gyromagnetic ratios differ from the conventional values by small amounts, then

$$g_S=2(1+\delta_S),$$
$$g_L=1+\delta_L,$$

and

$$g_{J_1}/g_{J_2}=[(2\alpha_{S_1}+\alpha_{L_1})/(2\alpha_{S_2}+\alpha_{L_2})]+2[(\alpha_{S_1}\alpha_{L_1}-\alpha_{L_1}\alpha_{S_2})/(2\alpha_{S_2}+\alpha_{L_2})^2]\times\{\delta_S-\delta_L\}. \quad (5)$$

Thus if the constants $\alpha_{S_1}$, $\alpha_{L_1}$, $\alpha_{S_2}$, $\alpha_{L_2}$ are known from the state of coupling of the atomic levels, the quantity $\{\delta_S-\delta_L\}$ can be determined from the ratio of the atomic $g_J$ values. Clearly, no experiment of this type can distinguish between an effect produced by a small change from the previously accepted values of the spin or the orbital gyromagnetic ratios.

The measurement of the $g$ values of two different atomic energy states in an experiment in which the magnetic field is known in terms of classical standards would, in principle, yield the absolute values of $g_S$ and of $g_L$ separately. However, such a determination would depend on a precisely known value of $e/m$. Of the experimental methods which have been used to evaluate $e/m$, the determination from the Zeeman splitting of singlet states assumes that $g_L=1$, and the magnetic deflection results make use of the corresponding assumption of the Lorentz force law. Other determinations of $e/m$ appear either to be of intrinsically low accuracy or to have a rather doubtful theoretical background. In the remainder of the present paper we shall adopt the convention $g_L=1$, and we shall express the experimentally determined quantity $(\delta_S-\delta_L)$ as $\delta_S$.

If hyperfine interactions were absent or entirely negligible the ratio of the frequencies of the Zeeman lines of two atomic states would give directly the ratio of the atomic $g_J$ values. By Zeeman lines we mean here lines resulting from transitions between the magnetic levels of a single atomic energy state. In the atomic states which were studied in the present experiments and at the values of the magnetic field at which lines were observed, the splitting of the energy levels into a hyperfine structure must be taken into account. The existence of this hyperfine structure complicates the analysis of the data from which the ratio of the $g_J$ values is obtained; at the same time the possibility of observing a number of lines of different frequency resulting from hyperfine transitions within each atomic level gives a means of checking the self-consistency of data and improving the accuracy of the results.

### 3. DESCRIPTION OF THE ENERGY LEVELS

For the energy levels with $J=\frac{1}{2}$ the relevant part of the Hamiltonian is taken to be:

$$\mathcal{H}=a\mathbf{I}\cdot\mathbf{J}+g_I\mu_0I_zH_z+g_J\mu_0J_zH_z, \quad (6)$$

in which $\mathbf{I}$ is the nuclear spin operator and $\mathbf{J}$ is the operator of the total electronic angular momentum. The solutions of the secular equations for the energy eigenvalues are:[8]

$$W_{I\pm\frac{1}{2},m_F}=-[\Delta W/2(2I+1)]+g_I\mu_0H_zm_F\pm(\Delta W/2)[1+(4/(2I+1))m_Fx+x^2]^{\frac{1}{2}}. \quad (7)$$

The "weak field" quantum numbers $F=I\pm\frac{1}{2}$, $m_F$ are used to designate the levels. The parameter, $x$, is defined by

$$x=(g_J-g_I)(\mu_0H/\Delta W), \quad (8)$$

and $\Delta W=2a$ is the zero field hyperfine separation.

The constants in the energy expression which are given in Table I have been determined with

[8] S. Millman, I. I. Rabi, and J. R. Zacharias, Phys. Rev. 53, 384 (1938).

precision, by Kusch, Millman, and Rabi[9,10] for sodium, by Becker and Kusch[11] for gallium, and by Hardy and Millman[12] for indium. The results of this paper demand some modification of the values of $g_I$ as given in Table I. However, $g_I$ enters into the expression for the energies of the states only as a correction term, and hence reasonable changes in $g_I$ do not affect our results.[13]

For the $^2P_{3/2}$ level of gallium it is necessary to include in the energy expression a term corresponding to a nuclear electric quadrupole interaction. In this case the Hamiltonian becomes

$$\mathcal{H}=a\mathbf{I}\cdot\mathbf{J}+2b\mathbf{I}\cdot\mathbf{J}(2\mathbf{I}\cdot\mathbf{J}+1)+\mu_0H_z(g_JJ_z+g_II_z). \quad (9)$$

Terms due to moments of a higher order than the quadrupole moment are not included. The resulting secular determinant of sixteen rows and columns factors according to the total magnetic quantum number; thus there are two secular equations of the first, second, and third degrees, and one quartic equation. The expressions from which the energy levels may be determined are given below for the case in which $I=\frac{3}{2}$. The complexity of the expressions becomes much greater for $I>\frac{3}{2}$. To simplify the equations we have written:

$$x=(g_J-g_I)(\mu_0H/a), \quad (10a)$$

an expression reminiscent of that employed in describing the energy levels of the states for which $J=\frac{1}{2}$,

$$y=(g_J+g_I)(\mu_0H/a) \quad (10b)$$

and

$$r=b/a.$$

For

$$\begin{aligned}&F=3,\ m_F=\pm3,\ W/a=(9/4)(1+11r)\pm\tfrac{3}{2}y,\\&F=3,\ m_F=\pm2,\ W/a=\tfrac{3}{4}(1+17r)\pm y\\&\qquad+\tfrac{1}{2}[x^2+9(1+8r)^2]^{\frac{1}{2}},\\&F=2,\ m_F=\pm2,\ W/a=\tfrac{3}{4}(1+17r)\pm y\\&\qquad-\tfrac{1}{2}[x^2+9(1+8r)^2]^{\frac{1}{2}}. \quad (11)\end{aligned}$$

The cubic equations may be simplified by use of the substitution

$$W/a=(W_0/a)+(\delta W/a), \quad (12)$$

where $W_0/a$ is the weak field, first-order approximation to the energy of the level. For $F=3$, $m_F=\pm1$

$$W_0/a=(9/4)(1+11r)\pm\tfrac{1}{2}y \quad (13a)$$

and

$$(\delta W/a)^3+8(1+3r)(\delta W/a)^2-(x^2-15-120r)(\delta W/a)-2x^2=0. \quad (13b)$$

The value of $\delta W/a$ is the same for $m_F=\pm1$. For $F=2$, $m_F=\pm1$,

$$W_0/a=-\tfrac{3}{4}(1-r)\pm\tfrac{1}{2}y \quad (14a)$$

and

$$(\delta W/a)^3-(1+48r)(\delta W/a)^2-(x^2-24r-576r^2+6)(\delta W/a)+(1+24r)x^2=0. \quad (14b)$$

For $F=1$, $m_F=\pm1$,

$$W_0/a=-(11/4)(1-9r)\pm\tfrac{1}{2}y \quad (15a)$$

and

$$(\delta W/a)^3-(7-24r)(\delta W/a)^2-(x^2-10+120r)(\delta W/a)-3x^2=0. \quad (15b)$$

The quartic equation, whose roots determine the energies of the states for which $m_F=0$, is:

$$\begin{aligned}&(W/a)^4+(5-99r)(W/a)^3+[(9/8)(2755r^2\\&\quad-266r-1)-(5/2)x^2](W/a)^2\\&\quad-[(9/16)(57123r^3-9487r^2\\&\quad-163r+47)+(9/4)(1-55r)x^2](W/a)\\&\quad+(4455/256)(1287r^4-1412r^3\\&\quad+114r^2+12r-1)-(135/32)\\&\qquad\times(363r^2-26r-1)x^2+(9/16)x^4=0. \quad (16)\end{aligned}$$

A graph showing the energies of the levels as a function of field has been given by BK. The interaction constants, $a$ and $b$, have been deter-

[9] P. Kusch, S. Millman, and I. I. Rabi, Phys. Rev. **57**, 765 (1940).
[10] S. Millman and P. Kusch, Phys. Rev. **58**, 438 (1940).
[11] G. E. Becker and P. Kusch, Phys. Rev. **73**, 584 (1948). (This reference is hereinafter referred to as BK.)
[12] T. C. Hardy and S. Millman, Phys. Rev. **61**, 459 (1942).
[13] All the nuclear $g$ values, with the exception of those of the gallium and indium isotopes, depend on the assumption that the $g_J$ value for the $^2S_{\frac{1}{2}}$ state of Rb and Cs is 2. The $g_I$ values given for the isotopes of gallium and indium depend on the assumption that the $g_J$ value for the $^2P_{\frac{1}{2}}$ states of these atoms is $\frac{2}{3}$. Not only are these assumptions subject to correction, but they are inconsistent as well. To place the $g_I$ values of Ga and In on the scale used for all other nuclei, a reduction of 0.25 percent is required. An arithmetical error made by Becker and Kusch just compensates for the required reduction of 0.25 percent in the case of $Ga^{69}$. The $g_I$ values of $Ga^{69}$, $Ga^{71}$, $In^{115}$ on the same scale as that used in all other cases are $-0.0007239$, $-0.0009195$, and $-0.0006616$. These changes have no effect at all on the results presented in this paper.

mined to be

for $Ga^{69}$:

$$a=190.790\times10^6 \text{ sec.}^{-1}, \quad b=2.6049\times10^6 \text{ sec.}^{-1};$$

and for $Ga^{71}$:

$$a=242.424\times10^6 \text{ sec.}^{-1}, \quad b=1.6416\times10^6 \text{ sec.}^{-1}.$$

It is to be noted that all expressions for the levels determine the energy of a level in the same units in which $\Delta W$, $a$, and $b$ are known. Experimentally, these quantities have been determined in sec.$^{-1}$ and observations of line frequencies, of course, lead to separations of energy levels expressed in terms of sec.$^{-1}$. The quantities $x$ and $y$ always contain the factor $\mu_0 H/a$ (or $\mu_0 H/\Delta W$) where $a$ and $\Delta W$ are expressed in ergs. If we express all frequency measurements in terms of megacycles per second, then the quantity above becomes:

$$(\mu_0 H/ha)\times10^{-6}=(eH/4\pi ma)\times10^{-6}=H'/a \quad (17)$$

or

$$H'=1.3998H.$$

In all subsequent discussion we use the quantity $H'$ as a measure of the field.

It should be pointed out that in previous experiments with lithium and potassium in the $J=\frac{1}{2}$ states, observations made at very low fields and at high fields yielded self-consistent values of the interaction constants. This fact indicates that the Hamiltonian function given above is adequate to describe the hyperfine structure of alkali atoms in the $^2S_{\frac{1}{2}}$ state within experimental error. Thus it was unnecessary in the present experiment to carry out observations of all the possible transitions and over a range of values of the absolute magnetic field. For the $^2P_{3/2}$ state of gallium the self-consistency of the frequencies of four lines at a field strength of 380 gauss, under which conditions there is intermediate decoupling of the nuclear spin and the atomic angular momentum, was regarded as a confirmation of the adequacy of the Hamiltonian. Moreover, from a study of the h.f.s. pattern of gallium in the $^2P_{3/2}$ state at very low magnetic fields, BK conclude that no moments of a higher order than the quadrupole need to be included in the Hamiltonian to describe the energy levels.

For the accuracy required in these experiments, perturbation approximations to the energies of the levels were inadequate and, in all cases, accurate solutions to the secular equations were found.

In the present series of experiments the direction of the oscillating magnetic field was perpendicular to the constant magnetic field. Thus the allowed transitions are given, in weak field notation, by $\Delta F=\pm1, 0$, and $\Delta m_F=\pm1$. Under very strong magnetic field conditions the nuclear and atomic angular momenta are decoupled, and the transitions may be classified according to $\Delta m_J=\pm1$, $\Delta m_I=0$ or $\Delta m_J=0$, $\Delta m_I=\pm1$. Whether or not a particular field is "weak" or "strong" for a particular atomic state depends on the value of $x$ (or $y$) which corresponds to that field. This, in turn, depends on the value of $\Delta W$ or $a$.

The decisions as to what magnetic field strength should be employed and which lines should be observed were made on the basis of the following considerations. Since the present experiments are directed toward the measurement of an atomic magnetic moment the lines to be observed should be selected to possess the greatest possible field sensitivity. Under very strong field conditions the field sensitivity of the transitions $\Delta m_I=\pm1$ is so small that these lines are not useful for the purpose of this experiment. The transitions $\Delta m_J=\pm1$ show adequate field sensitivity, but in most cases these lines occur at frequencies which are difficult to obtain experimentally. Under very weak field conditions the transitions $\Delta F=0$ are the most suitable for this experiment, as the frequencies of these lines are very nearly proportional to the field strength and are sufficiently field sensitive. Very weak fields ($H<100$ gauss) could not be employed in this experiment because of the residual inhomogeneity of the field.

The value of the magnetic field used in most of these experiments ($\sim$400 gauss) represents very weak field conditions for $^2P_{\frac{1}{2}}(In^{115})$, $^2P_{\frac{1}{2}}(Ga^{69})$; for $^2S_{\frac{1}{2}}(Na^{23})$ a considerable departure from weak field conditions appears, and for gallium in the $^2P_{3/2}$ state the field is very strong. Only a few lines in the spectrum of $^2P_{3/2}(Ga)$ of frequency less than $10^9$ sec.$^{-1}$ permit a satisfactory determination of $g_J$.

In practice the large field sensitivity of some

lines, particularly in the $^2S_{\frac{1}{2}}$(Na) spectrum, did not bring about a proportional increase in the precision of measurement of the field because of the lack of complete homogeneity in the constant field.

In principle it is possible, from the observed frequencies of lines in the spectra of atoms in two different states, to calculate directly the ratio $g_{J_1}/g_{J_2}$. However, such a procedure is extremely laborious. We have, instead, calculated the quantity $H'$ for each observed line. If a discrepancy in the value of $H'$ occurs for atoms in two different states and under conditions for which $H'$ is known to be identical, the discrepancy may be removed by an adjustment of the $g_J$ values. This is evident since in the expressions for the energies of the levels, $H'$ always occurs in the product $g_J H'$.[14] Suppose the assumed values of $g_J$ are $g_{J_1}{}^0$ and $g_{J_2}{}^0$ for two different states. The corresponding values of $H'$ are $H_1'$ and $H_2'$. $\Delta H' = H_1' - H_2'$. Then:

$$g_{J_1}/g_{J_2} = (g_{J_1}{}^0/g_{J_2}{}^0)[1+(\Delta H'/H')]. \quad (18)$$

#### 4. APPARATUS AND PROCEDURE

The general procedures and instrumental requirements for the observation of lines in the radio frequency spectra of atoms have been discussed in a number of papers. The molecular beam apparatus used in the experiments described in this paper was originally designed as an apparatus for the study of the radio frequency spectra of molecules in very high magnetic fields. Accordingly, the deflecting fields are long and may be operated at high flux densities in order to deflect molecules with a total moment of the order of one nuclear magneton. The magnetic field in which transitions occur is 48 cm long and can operate at fields as high as twenty thousand gauss. Unfortunately, the field is not entirely homogeneous, and the use of a large fraction of the length of the transition field for the observation of extremely field sensitive atomic lines broadens the lines excessively. In all of the present experiments, the effective length of the transition field was reduced to 2 cm by the expedient of reducing the length of the r-f field through which the beam passes. The deflecting fields were operated at a very low level of flux density to permit refocussing of atoms whose moment is of the order of one Bohr magneton.

For the purpose of consecutive measurement of lines in the radio frequency spectra of two different atomic species, such as gallium and sodium, a special oven chamber was constructed in which an oven containing gallium and another containing sodium were mounted on a platform attached to a ground joint which could be rotated from the outside of the apparatus. This arrangement permitted rapid interchange and adjustment of the two ovens.

All frequency measurements were made on a General Radio heterodyne frequency meter, model 620A. The meter may be used to determine frequencies to about one part in twenty thousand, but the precision in reading may be somewhat greater or less than this, depending on the linearity of the scale at a particular reading, on the thermal stability of the meter and other factors. Because of the limit of accuracy in the location of the centers of the resonance curves imposed by their width, it was not worth while to use more accurate frequency measuring equipment. The uncertainties in frequency measurement imposed by the meter and by the line widths are statistical in character and the precision is improved by judicious repetition of observations. Readings on the wave meter are determined in terms of a crystal within the wave meter. The frequency of the crystal in the wave meter which we used differed from its nominal value by 0.0045 percent, as determined by comparison with signals from WWV. The correction is of no importance in the measurements of the frequencies of the lines of gallium, since BK used the identical meter in determining the constants of gallium. The correction has been applied to all cases, however.

All experimental data considered in the experiments discussed in this paper are measurements of the frequencies of spectral lines. No knowledge

[14] It is true that a term $g_I H'$ also occurs. However, in the cases of $Li^7$, $Na^{23}$, $Ga^{69}$, $Ga^{71}$, and $In^{115}$ the value of $g_I$ has been determined in each case in terms of $g_J$ of the ground state of the atom in which the nucleus occurs. The term $g_I H'$ may then be written as $(g_I/g_J)g_J H'$ where the ratio $g_I/g_J$ is a quantity independent of any assumption as to $g_J$. The only case in which $g_I H'$ is an independent term is that of the $^2P_{3/2}$ state of gallium, where $g_I$ is known in terms of $g_J(^3P_1)$ and not in terms of $g_J(^3P_{3/2})$. However the term is so small that uncertainties in $g_I$ have no appreciable effect on our results.

TABLE II. Observations of lines in the spectrum of the $^2P_{\frac{1}{2}}$ state of gallium.

| Isotope | Line | Obs. $f\times10^{-6}$ sec.$^{-1}$ | Calc. $f\times10^{-6}$ sec.$^{-1}$ |
|---|---|---|---|
| 71 | $(2, 0)\leftrightarrow(2, -1)$ | 89.434 | 89.422 |
| 69 | $(2, 0)\leftrightarrow(2, -1)$ | 89.867 | 89.870 |
| 71 | $(1, 0)\leftrightarrow(1, -1)$ | 90.389 | 90.395 |
| 69 | $(1, 0)\leftrightarrow(1, -1)$ | 90.637 | 90.634 |
| 71 | $(2, -1)\leftrightarrow(2, -2)$ | 94.716 | 94.714 |
| 69 | $(2, -1)\leftrightarrow(2, -2)$ | 96.848 | 96.848 |

of the magnetic field in which transitions occur is required, though it is necessary that transitions resulting in lines whose frequencies are to be compared, occur in the same magnetic field. In practice, a magnetic field is not entirely constant, and the rate of drift of the field depends upon a number of factors, of which the principal two are the condition of the storage cells which supply the exciting current to the magnet and the temperature stability of the d.c. circuit and the magnet. A drift is observed by noting a change in the frequency of a line with time and a very good correction for drift of field may be made by alternately measuring the frequencies of each of two lines to be compared and then, by suitable graphical or other methods, determining the frequencies of each of the lines at any arbitrary instant of time.

To reduce the time interval between observations on successive lines, and hence minimize the effects of a drifting field, all observations were made on the basis of a single frequency reading for each line. That is, no detailed plot was made of the reduction of beam intensity as a function of frequency; rather, the observer noted the frequency at which the maximum reduction of beam intensity occurred, the mean of the frequencies at which one-half the maximum reduction occurred or the mean frequency of any other pair of symmetrical points. On the basis of several of these observations of a single line,

TABLE III. The comparison of the apparent values of $H'$ in the $^2P_{\frac{1}{2}}$ and $^2P_{3/2}$ states of gallium.

| $I(^2P_{\frac{1}{2}})$ $f\times10^{-6}$ sec.$^{-1}$ | $II(^2P_{\frac{1}{2}})$ $H'$ | $III(^2P_{3/2})$ isotope | $IV(^2P_{3/2})$ transition | $V(^2P_{3/2})$ $f\times10^{-6}$ sec.$^{-1}$ | $VI(^2P_{3/2})$ $H'$ | $VII$ $\Delta H'$ |
|---|---|---|---|---|---|---|
| 96.832 | 527.24 | 69 | $(3, 0)\leftrightarrow(2, -1)$ | 492.33 | 528.27 | 1.03 |
| 96.751 | 526.84 | 71 | $(3, -1)\leftrightarrow(3, -2)$ | 459.77 | 527.63 | 0.79 |
| 96.620 | 526.19 | 69 | $(3, 0)\leftrightarrow(3, -1)$ | 443.92 | 527.08 | 0.89 |
| | | | | | Mean | 0.90 |

TABLE IV. The comparison of the apparent values of $H'$ in the $^2P_{\frac{1}{2}}$ and $^2P_{3/2}$ states of gallium.

| $I(^2P_{\frac{1}{2}})$ $f\times10^{-6}$ sec.$^{-1}$ | $II(^2P_{\frac{1}{2}})$ $H'$ | $III$ isotope | $IV(^2P_{3/2})$ transition | $V(^2P_{3/2})$ $f\times10^{-6}$ sec.$^{-1}$ | $VI(^2P_{3/2})$ $H'$ | $VII$ $\Delta H'$ | $VIII$ |
|---|---|---|---|---|---|---|---|
| 90.909 | 528.92 | 69 | $(3, 0)\leftrightarrow(3, -1)$ | 447.06 | 529.79 | 0.87 | 3 |
| 90.910 | 528.93 | 69 | $(3, -1)\leftrightarrow(3, -2)$ | 486.90 | 529.85 | 0.92 | 3 |
| 90.913 | 528.94 | 71 | $(3, -3)\leftrightarrow(3, -2)$ | 491.14 | 529.90 | 0.96 | 2 |
| 90.921 | 528.99 | 71 | $(3, -1)\leftrightarrow(3, -2)$ | 462.23 | 529.91 | 0.92 | 1 |
| | | | | | Mean | 0.91 | |

the observer recorded a single reading on a wave meter.

## 5. EXPERIMENTAL RESULTS

### a. The Determination of the Ratio of the $g_J$ Value of Gallium in the $^2P_{3/2}$ State and in the $^2P_{\frac{1}{2}}$ State

To estimate the precision with which the frequency of a line may be determined, six lines in the spectrum of gallium in the $^2P_{\frac{1}{2}}$ state were measured in rapid succession. Preliminary observation had indicated that the field did not drift at a rapid rate just prior to the observations. Each line frequency is, therefore, the result of a single observation. By use of constants given by BK the frequencies of all lines were calculated, where the $(2, -1)\leftrightarrow(2, -2)$ line of $Ga^{69}$ was used to determine the value of the magnetic field. The results are shown in Table II. The agreement between calculated and observed frequencies is very good. The results indicate, in general, that line frequencies are, indeed, measurable to within one part in twenty thousand. The constants given by BK and used in the calculations are consistent for the two isotopes of gallium and the relationships which determine the frequencies of the lines are valid to within the error in measurement of the line frequencies.

It should be pointed out, however, that all the lines recorded in Table II lie in the same frequency range and have very nearly the same frequency dependence on field. This means that inhomogeneities in the magnetic field, will affect all lines in a similar way and that similar agreement may not occur when two lines in a spectrum have a markedly different frequency dependence on field. In fact, for the case of $Na^{23}$, to be discussed later, a small systematic discrepancy occurs between the magnetic field as calculated from two lines with markedly different field dependence.

Three lines in the $^2P_{3/2}$ state of gallium were observed alternately with the $(2, -1)\leftrightarrow(2, -2)$ line of $Ga^{69}$ in the $^2P_{\frac{1}{2}}$ state. The results are shown in Table III. Column I gives the frequency of the $(2, -1)\leftrightarrow(2, -2)$ line of $Ga^{69}$ in the $^2P_{\frac{1}{2}}$ state in megacycles per second. Column II gives the value of $H'$ as previously defined and calculated on the basis of the assumption that $g_J(^2P_{\frac{1}{2}})=\frac{2}{3}$. Column III indicates the isotope of gallium in the spectrum of which the line tabulated in column IV has been measured. The lines in column IV are in the spectrum of the $^2P_{3/2}$ state. Column V lists the observed frequency in megacycles per second, and column VI the corresponding value of $H'$ calculated on the basis of the assumption that $g_J(^2P_{3/2})=4/3$. Column VII lists the difference between the values of $H'$ for the $^2P_{3/2}$ and the $^2P_{\frac{1}{2}}$ states. The data and results in Table III are to be considered as the result of an exploratory experiment. The rather large variation between the values of $\Delta H'$ can be ascribed to an insufficient number of successive observations of each line in the face of a drifting magnetic field and to insufficient care in locating the resonance minima. The rapid drift of field is apparent from an observation of the successive values of $H'$ in columns II and VI. The deviation of the values of $\Delta H'$ from the mean can be explained by uncertainties, for the first line, of one part in ten thousand in frequency measurement, and for the second line of only slightly more than this.

In a repetition of the previous experiment, the frequencies of four lines in the spectrum of Ga in the $^2P_{3/2}$ state were measured alternately with the frequency of the $(1, 0)\leftrightarrow(1, -1)$ line of $Ga^{69}$ in the $^2P_{\frac{1}{2}}$ state. The results are shown in Table IV. Column I gives the frequency of the $(1, 0)\leftrightarrow(1, -1)$ line of $Ga^{69}$ in the $^2P_{\frac{1}{2}}$ state. The other columns are exactly as in Table III. Column VIII gives a weight assigned to each observation, based on an evaluation of experimental factors. It should be noted that the rate of drift of field for these observations is very much less than in the case of the data recorded in Table III. The particular lines in the spectrum of gallium in the $^2P_{3/2}$ state which have been measured are rather arbitrary; the lines themselves were not identified until rather elaborate reductions of data had been made. That is to say, observations were made at a field and within a frequency range known to contain lines with suitable frequency dependence on field. The assignment was subsequently made by use of the criterion that all lines in the spectrum of gallium in the $^2P_{3/2}$ state should determine substantially the same field. The assignment is unique. All the lines in the spectrum of gallium in the $^2P_{3/2}$ state which are recorded in the two tables have about the same frequency dependence on field with the exception of the first line in Table III, where the frequency dependence on field is about half as great as for the other lines. In all cases measurements have been made against a single line in the spectrum of gallium in the $^2P_{\frac{1}{2}}$ state, but auxiliary data were taken to make the assignment of the line definite.

TABLE V. Notation used in describing lines in the spectra of sodium, and of gallium in the $^2P_{\frac{1}{2}}$ state.

| Line | | | Symbol |
|---|---|---|---|
| $(2, -2)\leftrightarrow(2, -1)$ | | | Na*I* |
| $(1, 0)\leftrightarrow(1, -1)$ | | | Na*II* |
| $(2, 0)\leftrightarrow(2, -1)$ | | | Na*III* |
| $(1, 1)\leftrightarrow(1, 0)$ | | | Na*IV* |
| $(2, 1)\leftrightarrow(2, 0)$ | | | Na*V* |
| $(2, 2)\leftrightarrow(2, 1)$ | | | Na*VI* |
| $(1, 0)\leftrightarrow(1, -1)$ | 69 | | Ga*I* |
| $(2, 0)\leftrightarrow(2, -1)$ | 69 | | Ga*II* |

TABLE VI. The observed frequencies and apparent values of $H'$ for several lines in the spectrum of sodium.

| Time | Na*I* | Na*II* | Na*III* | Na*IV* | Na*V* | Na*VI* |
|---|---|---|---|---|---|---|
| 3:10 | 418.10 (531.84) | | | | | |
| 3:25 | | | | | | 176.85 (531.77) |
| 3:35 | 418.06 (531.80) | | | | | |
| 3:45 | 418.00 (531.75) | | | | | |
| 3:50 | 417.99 (531.74) | | | | | |
| 3:55 | | | | | | 176.83 (531.67) |
| 4:15 | | | 260.51 (531.63) | | | |
| 4:15 | | | 260.50 (531.60) | | | |
| 4:30 | | 261.34 (531.56) | | | | |
| 4:30 | | 261.34 (531.56) | | | | |
| 4:35 | | | | | | 176.81 (531.59) |
| 4:40 | | | | | 206.77 (531.59) | |
| 4:45 | | | | 207.61 (531.53) | | |
| 4:50 | | | | | | 176.78 (531.47) |
| 5:00 | 417.72 (531.50) | | | | | |

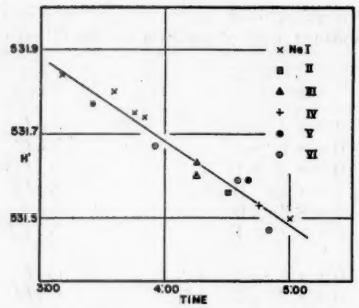


FIG. 1. Values of $H'$ calculated from the observed frequencies of several lines in the spectrum of Na.

An uncertainty in the measurement of the frequency of the $(1, 0)\leftrightarrow(1, -1)$ line of $Ga^{69}$ in the $^2P_{\frac{1}{2}}$ state of one part in twenty thousand gives rise to an uncertainty in the corresponding $H'$ of 0.03. The same fractional uncertainty in the measurement of the frequencies of the lines in the spectrum of the $^2P_{3/2}$ state gives rise to an uncertainty in the corresponding value of $H'$ of 0.02. Thus the maximum variation among the values of $\Delta H'$ can be ascribed entirely to the limitation of frequency determination. In our experimental arrangement, a better frequency meter could not be expected to increase the precision of the result to a significant extent, since the width of the resonance curves rendered a significant measurement of frequency to a higher precision impossible.

The variation among the values of $\Delta H'$ shown in Table IV are statistical in character. We conclude that for these observations $\Delta H'=0.91 \pm 0.03$. The agreement of this value with the mean obtained from Table III indicates that the large scatter of values obtained in the first performance of the experiment is statistical.

On the basis of the assumption that $g_J(^2P_{3/2}) = 4/3$ and that $g_J(^2P_{\frac{1}{2}})=\frac{2}{3}$, the ratio of the apparent field as calculated from lines in the spectrum of the $^2P_{3/2}$ state to that calculated from lines in the spectrum of the $^2P_{\frac{1}{2}}$ state is $1.00172\pm0.00006$. Evidently the field is independent of the mechanism of measurement. To satisfy this requirement we must make

$$g_J(^2P_{3/2}\text{Ga})/g_J(^2P_{\frac{1}{2}}\text{Ga}) = 2(1.00172\pm0.00006)$$

where it is assumed that the deviation of the $g_J$ values from their nominal values is small.

### b. The Determination of the Ratio of the $g_J$ Value of Sodium in the $^2S_{\frac{1}{2}}$ State and That of Gallium in the $^2P_{\frac{1}{2}}$ State

Six lines of the spectrum of sodium and two lines of the spectrum of gallium were used in the determination of the ratio of the $g_J$ values. To assist in the discussion of the observations, the notation given in Table V is used. All lines of sodium are those of the $^2S_{\frac{1}{2}}$ state and the lines of gallium are of the $^2P_{\frac{1}{2}}$ state.

As in the previous experiment, a test was made to determine the consistency of frequency measurements. In Table VI are given the observed frequencies of the six lines of sodium and the time at which each frequency was measured. Directly beneath each frequency in megacycles per second is given, in parentheses. the value of $H'$ corresponding to the observed frequency and calculated on the basis of the assumption that $g_J(^2S_{\frac{1}{2}})=2$. The data of Table VI are plotted in Fig. 1, where the calculated values of $H'$ are plotted against the time. A straight line is drawn through the points and the average deviation of the points from the mean line is less than 0.03 units of $H'$. The maximum deviation is 0.04.

TABLE VII. The observed frequencies and values of $H'$ of several lines in the spectrum of sodium and gallium.

| Time | Na*I* | Na*II* | Na*III* | Ga*I* | Ga*II* |
|---|---|---|---|---|---|
| 6:30 | | | | 91.093<br>(529.97)+0.00 | |
| 6:40 | | | | | 90.319<br>(529.93)−0.01 |
| 6:50 | | | | 91.087<br>(529.93)+0.01 | |
| 7:05 | | | 260.32<br>(531.16)+0.00 | | |
| 7:05 | | 261.17<br>(531.14)−0.02 | | | |
| 7:15 | 417.33<br>(531.15)+0.02 | | | | |
| 7:40 | | | | 91.060<br>(529.78)−0.01 | |
| 7:40 | | | | | 90.295<br>(529.79)+0.00 |
| 7:58 | | | 260.27<br>(531.02)−0.01 | | |
| 8:02 | | 261.12<br>(531.01)−0.01 | | | |
| 8:14 | 417.17<br>(531.00)+0.01 | | | | |
| 8:28 | | | | 91.038<br>(539.65)−0.02 | |
| 8:35 | | | | | 90.275<br>(529.68)+0.02 |
| 8:45 | | | 260.21<br>(530.89)+0.00 | | |
| 8:49 | | 261.05<br>(530.85)−0.05 | | | |
| 9:10 | 417.04<br>(530.88)+0.03 | | | | |
| 9:10 | 417.05<br>(530.89)+0.04 | | | | |
| 9:26 | | | | 91.014<br>(529.52)−0.01 | |
| 9:26 | | | | | 90.248<br>(529.52)−0.01 |

That is, the maximum deviation of the magnetic field as calculated from the separate lines is one part in thirteen thousand from the average as determined from all observations.

From the frequencies of the Na*I* and Na*VI* lines, at the same instant of time, we have found for $\Delta\nu$ of Na the value $1771.60\times10^6$ sec.$^{-1}$. A change in the assumed frequency of either line of one part in twenty thousand will alter the $\Delta\nu$ by about $0.25\times10^6$ sec.$^{-1}$. The agreement of the result with the value of $1771.75\times10^6$ sec.$^{-1}$ given by Millman and Kusch is therefore very good. It is to be noted that the value of the magnetic field employed in these experiments is poorly chosen for the determination of $\Delta\nu$ as compared to the fields used by Millman and Kusch. The widths of the sodium lines was roughly proportional to the rate of variation of line frequency with magnetic field and are presumably due to inhomogeneities in the magnetic field. The observed width of the Na*I* line was about $0.280\times10^6$ sec.$^{-1}$, that of the Na*II* and Na*III* lines about $0.150\times10^6$ sec.$^{-1}$ and that of the Na*VI* line about $0.070\times10^6$ sec.$^{-1}$. The very good internal consistency noted above indicates that the measured center of the resonance curve is, indeed, the center of the line and that all line frequencies determine the same mean magnetic field.

Three lines in the sodium spectrum which have the greatest sensitivity to field were measured alternately with two lines in the spectrum of gallium. The data are given in Table VII. The time of observation is indicated in the first column, and in the other columns are given the observed line frequencies in megacycles per second. Directly below the observed frequency is recorded, in parentheses, the value of $H'$ calculated on the basis of the assumption that $g_J(^2S_{\frac{1}{2}})=2$ and $g_J(^2P_{\frac{1}{2}})=\frac{2}{3}$. The quantity which appears directly after the value of $H'$ is the difference between the observed $H'$ and that calculated from a least squares solution of the data.

The data are graphically presented in Fig. 2. An independent least squares solution of the variation of $H'$ with time for sodium and for gallium gives very nearly the same rate of drift of field in both cases, as expected. A combined least squares solution for both sets of lines, where the rate of drift of field is the same in both cases, yields the result

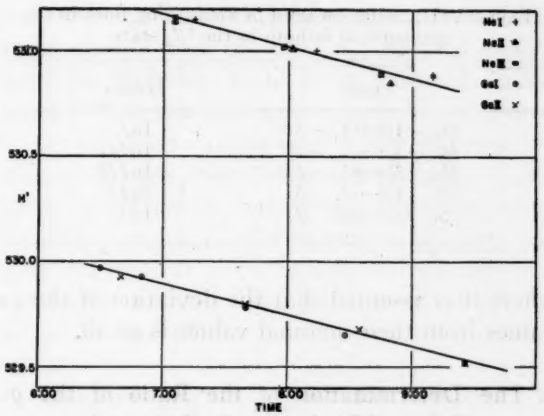


FIG. 2. Values of $H'$ calculated from the observed frequencies of several lines in the spectra of Na and of Ga in the $^2P_{\frac{1}{2}}$ state.

$$\begin{aligned}\text{for Na: } H'&=531.319-0.002475t,\\ \text{for Ga: } H'&=530.036-0.002475t,\end{aligned}\qquad(19)$$

where the time, $t$, is measured in minutes from 6:00. The difference between the observed and calculated values is indicated in the table. It is to be noted that the differences are all positive for the Na*I* line and negative or zero for the Na*II* and Na*III* lines. The effect probably represents a slightly unsymmetrical broadening of the lines by the inhomogeneities of the field. The difference in the value of $H'$ for Na and that for Ga is $531.319-530.036=1.283$. To this value we assign the arbitrary precision value of $\pm0.030$, which is the sum of the mean deviation of the values of $H'$ yielded by Eq. (19) from those calculated for the individually observed Na lines and of the corresponding quantity for Ga. This uncertainty is obviously somewhat greater than the probable error calculated from the internal consistency of the data and is given in view of the fact that a systematic error may occur.

On the basis of the assumption that $g_J(^2S_{\frac{1}{2}})=2$ and that $g_J(^2P_{\frac{1}{2}})=\frac{2}{3}$, the ratio of the apparent field as calculated from Na to that as calculated from Ga is $1.00242\pm0.00006$. Other data has given the value for the same quantity of $1.00247\pm0.00020$. To satisfy the condition that the magnetic field is the same for a measurement of the frequencies of the gallium and sodium lines, we must set:

$$g_J(^2S_{\frac{1}{2}}\text{ Na})/g_J(^2P_{\frac{1}{2}}\text{ Ga})=3(1.00242\pm0.00006),$$

TABLE VIII. Notation used in identifying lines in the spectrum of indium in the $^2P_{\frac{1}{2}}$ state.

| Line | Symbol |
|---|---|
| $(4, -4)\leftrightarrow(4, -3)$ | In*I* |
| $(4, -3)\leftrightarrow(4, -2)$ | In*II* |
| $(5, 5)\leftrightarrow(5, 4)$ | In*III* |
| $(5, 4)\leftrightarrow(5, 3)$ | In*IV* |
| $(5, 3)\leftrightarrow(5, 2)$ | In*V* |

where it is assumed that the deviation of the $g_J$ values from their nominal values is small.

### c. The Determination of the Ratio of the $g_J$ Value of Na in the $^2S_{\frac{1}{2}}$ State and That of In in the $^2P_{\frac{1}{2}}$ State

The $\Delta\nu$ of $In^{115}$ and its $g_I$ have been determined by Hardy and Millman.[12] The low abundance of $In^{113}$ together with the fact that its $\Delta\nu$ is almost identical to that of $In^{115}$ makes it impossible to observe lines in the spectrum of $In^{113}$ in our experiments. In fact, the frequencies of the In lines which we observe are predominantly due to the term $g_F\mu_0 H/h$, and higher order terms, involving $\Delta\nu$, contribute at most about 3 percent to the frequencies of the lines. Under these conditions the small variation of the $\Delta\nu$ between the two isotopes of indium would not permit the independent observation of lines in the spectrum of both isotopes in our apparatus.

For the purposes of the comparison of the $g_J$ values, we have used three lines in the spectrum of sodium, previously identified as Na*I*, Na*II* and Na*III*. Five lines in the spectrum of indium have been used, identified as indicated in Table VIII. The data were observed in exactly the same way as in the case of the comparison of the $g_J$ values of gallium and sodium and the arrangement of Table IX, wherein are recorded the observations on sodium and indium, is identical to the arrangement of Table VII.

It can be seen from the table that the rate of drift of magnetic field during the experiment was very small. In making a least squares reduction of the data, the observations on the Na*II* line

TABLE IX. The observed frequencies and values of $H'$ for several lines in the spectrum of indium and sodium.

| Time | In*I* | In*II* | In*III* | In*IV* | In*V* | Na*I* | Na*III* | Na*IV* |
|---|---|---|---|---|---|---|---|---|
| 3:45 | 35.4104 (514.56) −0.03 | | | | | | | |
| 3:47 | | 35.1936 (514.58) −0.02 | | | | | | |
| 3:53 | | | 33.0891 (514.57) −0.03 | | | | | |
| 3:54 | | | | 33.2855 (514.64) +0.04 | | | | |
| 3:55 | | | | | 33.4769 (514.57) −0.04 | | | |
| 4:08 | | | | | | 254.210 (515.90) +0.03 | | |
| 4:35 | | | | | | | 254.989 (515.88) −0.01 | |
| 4:40 | | | | | | 254.166 (515.92) +0.03 | | |
| 5:00 | | | | | | | 254.980 (515.84) −0.07 | |
| 5:10 | 35.4194 (514.69) +0.02 | | | | | | | |
| 5:12 | | 35.1982 (514.64) −0.03 | | | | | | |
| 5:20 | | | 33.0973 (514.70) +0.02 | | | | | |
| 5:22 | | | | 33.2909 (514.72) +0.04 | | | | |
| 5:24 | | | | | 33.4855 (514.70) +0.02 | | | |
| 5:47 | | | | | | 254.181 (515.96) +0.01 | | |
| 5:52 | | | | | | | 255.00 (515.91) −0.05 | |
| 5:54 | | | | | | 254.186 (515.97) +0.01 | | |
| 6:02 | | | | | | | | 203.323 (515.944) −0.02 |
| 6:16 | 35.4228 (514.74) +0.02 | | | | | | | |
| 6:30 | | 35.2032 (514.72) −0.02 | | | | | | |
| 6:40 | | | | 33.2929 (514.76) −0.01 | | | | |
| 6:45 | | | | | 33.4879 (514.74) −0.04 | | | |

have been weighted by two because of experimental factors which made it very much easier to locate this line than the other two lines in the spectrum of sodium. The data may be adequately represented by assuming a linear drift of field. If $t$ is the time in minutes from 3:45, we can express the result

$$\begin{aligned} &\text{for In: } H' = 514.594 + 0.000861t; \\ &\text{for Na: } H' = 515.846 + 0.000861t. \end{aligned} \tag{20}$$

The difference in the value of $H'$ for Na and In is 1.252. If all the sodium lines are weighted equally, this difference becomes 1.243. The first of these two values is believed to be the better one. The data are clearly inferior to those obtained in the case of gallium. To the value of 1.252 we assign the arbitrary precision value of $\pm 0.050$, obtained as in the previous experiment. This uncertainty is obviously somewhat greater than the probable error calculated from the internal consistency of the data.

On the basis of the assumption that $g_J(^2S_{\frac{1}{2}}) = 2$ and that $g_J(^2P_{\frac{1}{2}}) = \frac{2}{3}$, the ratio of the apparent field as calculated from Na to that as calculated from In is $1.00243 \pm 0.00010$. To satisfy the condition that the magnetic field is the same for a measurement of the lines in each of the two spectra, we must set:

$$g_J(^2S_{\frac{1}{2}}\ \text{Na})/g_J(^2P_{\frac{1}{2}}\ \text{In}) = 3(1.00243 \pm 0.00010).$$

### 6. DISCUSSION OF RESULTS

The observed deviations of the ratios of the atomic $g_J$ values from those calculated under the assumptions that pure $LS$ coupling obtains and that the fundamental gyromagnetic ratios of spin and orbit have the values 2 and 1, respectively, may be attributed, in any particular case, to a deviation of the spin or orbit $g$ values from their accepted values. It was shown in Section 2 that $\delta_S$, defined by $g_S = 2(1+\delta_S)$, can be computed from the observed ratio of the $g$ values of two atomic states of different spectral term classifications. This quantity has been evaluated from the results of the three relevant experiments. The results appear in Table X. The error assigned to $\delta_S$ in each case follows directly from the error assigned to the corresponding ratio of the $g$ values. Thus from the experimental results, the difference between the value of $\delta_S$ which results from the $^2P_{3/2}(\text{Ga}) - {}^2P_{\frac{1}{2}}(\text{Ga})$ experiment and that which results from the $^2P_{\frac{1}{2}}(\text{Ga}) - {}^2S_{\frac{1}{2}}(\text{Na})$ experiment is probably real. It is, however, quite possible that this discrepancy may be accounted for by small deviations of the properties of the atomic systems from the simple description implicit in the theory underlying the calculations by means of which the experimental data has been reduced. It is to be emphasized that the numerical results are independent of the precise values of any of the fundamental atomic constants.

The agreement of the values of $\delta_S$ in Table X is very strong evidence in support of the hypothesis that the fundamental spin gyromagnetic ratio does, in fact, differ from the accepted integral value by an amount of very nearly the magnitude of the quantities given in Table X. An alternative explanation of these results in terms of perturbations (e.g., configuration interactions) of the individual atomic states would require that the perturbations on the $g$ values of the four states should have just such magnitudes as to give the agreement noted above. Aside from the question of the possible magnitude of such perturbations (discussed below) it should be pointed out that three different atomic species and three states of different spectral classification are involved in these experiments. It is very unlikely that under these conditions there should occur the systematic effect shown in these results. Schwinger[7] has reported the results of a theoretical study of the interaction of an electron with the quantized electromagnetic field. By a canonical transformation of the Hamiltonian the infinite interaction terms are separated from the rest of the Hamiltonian and are shown to be properly included in the experimental mass of the electron. The evaluation of the remaining finite terms in the case of an applied magnetic field leads to an interaction energy term corresponding to a spin moment of the electron increased from the accepted value of one Bohr magneton by a factor $(1+\alpha/2\pi) = 1.00116$. This value is in very good agreement with our experimental results. The possible reasons for the small remaining discrepancies are discussed below.

The result of this experiment, that the electron spin $g$ value differs from 2 by about 12 parts in ten thousand, may be compared with previous

TABLE X. Observed ratios of atomic $g$ values and the corresponding values of $\delta g$.

| Experimental ratio | $\delta g$ |
|---|---|
| $g_J(^2P_{3/2}\text{Ga})/g_J(^2P_{\frac{1}{2}}\text{Ga}) = 2(1.00172 \pm 0.00006)$ | $0.00114 \pm 0.00004$ |
| $g_J(^2S_{\frac{1}{2}}\text{Na})/g_J(^2P_{\frac{1}{2}}\text{Ga}) = 3(1.00242 \pm 0.00006)$ | $0.00121 \pm 0.00003$ |
| $g_J(^2S_{\frac{1}{2}}\text{Na})/g_J(^2P_{\frac{1}{2}}\text{In}) = 3(1.00243 \pm 0.00010)$ | $0.00121 \pm 0.00005$ |

measurements of atomic $g$ values in the Zeeman effect. In the classic work of Back[15] the uncertainty in the measured atomic $g$ values is not less than one part in a thousand, and thus the effect would escape detection. In the somewhat more accurate work of Kinsler and Houston[1] on the determination of $e/m$ from the Zeeman pattern in standard magnetic fields, singlet states were studied in almost all cases, so that no discrepancy corresponding to the effect described in the present paper could be found. However, in one experiment of this series, Kinsler[16] measured the $g$ values of the two states $2p^5 3s\,^1P_1$(Ne) and $2p^5 3s\,^3P_1$(Ne). These two states arise from the same configuration and are the only states of this configuration with $J=1$. Application of the $g$ sum rule to the experimental values yields $2.5017 \pm 0.0016$ for the sum of the atomic $g$ values. In view of the assigned experimental uncertainty this value was considered by Kinsler to be in sufficiently good agreement with the value 2.5000 predicted on the basis of the accepted integral $g$ values of the electron. Introduction of the spin moment $g$ value reported in the present work gives a predicted value of the $g$ sum of 2.5012.

There are several perturbations of the electronic states involved in the present experiments which in principle could bring about deviations of the atomic $g$ values from the values given by the Russell-Saunders coupling formula. Estimates of the magnitude of these effects will be given in the following paragraphs.

In all of the atomic states employed in this experiment the configuration corresponds to a single valence electron outside of closed shells. Thus, the term classification is unique, and the question of the type of coupling does not arise for these states.

By far the largest configuration perturbation is the electrostatic interaction. If the excited configurations of the atomic system be described in first approximation by Russell-Saunders coupling it is well known that the electrostatic coupling will mix states only of the same values of total $L$ and $S$. Thus the electrostatic coupling among pure $LS$ states does not change the atomic $g$ value in any approximation.

The effect on the $g_J$ values of gallium and indium of the magnetic interactions with the excited configurations of the outer group of three electrons is small. The ordinary spin-orbit interaction with these configurations vanishes. A magnetic interaction with a $^4P$ state of magnitude 100 cm$^{-1}$ would increase the $g_J(^2P_{\frac{1}{2}}\text{Ga})$ by about $1\times10^{-5}$. The effects in indium might be somewhat larger than in gallium. The $g_J(^2P_{3/2}\text{Ga})$ is affected by a still smaller amount than is the $g_J(^2P_{\frac{1}{2}}\text{Ga})$, as the $g_J$ of all the $J=\frac{3}{2}$ terms of the interacting configurations differ very little from $g_J(^2P_{3/2})$. Spin-orbit interactions with excited states of the core will produce effects no larger than those described above, because of the high excitation of these levels.

It appears that an important perturbation of the $g_J$ values of gallium or of indium would occur only if in the lower excited configurations, i.e., those of the outer three electrons in each case, there is a very considerable departure from Russell-Saunders coupling. In this case the electrostatic configuration mixing could bring about an appreciable alteration from the Russell-Saunders values of the $g_J$ values of the states employed in the present experiment. The evidence as to the character of the coupling in the excited states of gallium and of indium is meager. In the $4s4p^2\ ^4P$ term of gallium the interval rule appears to be obeyed accurately, while in the corresponding term $5s5p^2\ ^4P$ of indium the fine structure interval ratio differs by 17 percent from the Landé rule. The relative positions of the terms arising from the $5s5p^2$ configuration of Sb*III* seem to be accounted for by $LS$ coupling with the addition of electrostatic interaction with other configurations.[17]

The effect of configuration interactions on the $g_J$ values of the ground states of the alkali metal

[15] E. Back and A. Landé, *Zeemaneffekt* (Verlag Julius Springer, Berlin, 1925). See also, R. Bacher and S. Goudsmit, *Atomic Energy States* (McGraw-Hill Book Company, Inc., New York, 1932).

[16] L. E. Kinsler, Phys. Rev. **46**, 533 (1934).

[17] E. U. Condon and G. H. Shortley, *Theory of Atomic Spectra* (University Press, Cambridge, 1935).

atoms were investigated by Phillips,[18] who indicated that these effects are negligible.

Relativistic effects on the $g_J$ values of a Dirac electron have been considered by Margenau[19] who showed that the atomic $g_J$ value of a single electron is decreased by a factor $1-[(2J+1)/2(J+1)][\bar{T}/mc^2]$ for $J=L+\frac{1}{2}$ and $1-[(2J+1)/2J][\bar{T}/mc^2]$ for $J=L-\frac{1}{2}$. $\bar{T}$ is the mean kinetic energy. For the alkali metals the reduction in the $g_J$ value is about 1 part in $10^5$. For gallium and indium the effect is somewhat larger because of penetration of the core and because of the larger numerical factor in the relativistic expression for the $^2P_{\frac{1}{2}}$ state. When approximate account is taken of the penetration the $g_J$ values of the $^2P_{\frac{1}{2}}$ states of gallium and indium are reduced by four parts in $10^5$, and the $^2P_{3/2}$(Ga)$g_J$ value is reduced by about two parts in $10^5$.

The magnitude of the orientation dependence of the diamagnetic susceptibility, which in principle could affect the spectrum of the $^2P_{3/2}$(Ga) state, is negligible (less than one part in $10^5$) at the fields employed in this experiment.

Incipient electronic Paschen-Back effect produces a perturbation in the line frequencies of the $^2P_{3/2}$(Ga) spectrum of about one part in $10^5$.

The interaction of the valence electron spin with the diamagnetically induced moment of the core electrons reduces the $g_J$ value of the atom. The calculation of this effect requires fairly accurate core and valence electron charge distributions. Such a calculation has been carried out for $^2S_{\frac{1}{2}}$(Na) with Hartree fields and a corresponding optical electron wave function. The decrease in the $g_J$ value is less than one part in $10^5$. It is believed that this effect is also negligible for the other atomic states.

The application of the corrections estimated in this section to the experimental values of the $g_J$ ratios of Table X affects the calculated values of $\delta_S$ by about one percent. This magnitude is well within the experimental uncertainty and these corrections have not been applied in Table X.

We write $g_S=2(1.00119\pm0.00005)$ as the best value of the spin gyromagnetic ratio obtainable from the present experiments. The discrepancy between individual values of $\delta_S$ indicates the existence of small residual systematic effects and further analysis might indicate that $g_S$ differs somewhat from the value given here.

The original motivation for these experiments came from the suggestion of G. Breit with regard to the intrinsic magnetic moment of the electron. The actual method of testing Breit's hypothesis by comparing the $g$ values of atomic states was suggested to us by I. I. Rabi. We wish to express our thanks to both Dr. Breit and Dr. Rabi for many helpful discussions and to Miss Zelda Marblestone who performed a considerable fraction of the rather extensive calculations involved in this work.

[18] M. Phillips, Phys. Rev. 60, 100 (1941).
[19] H. Margenau, Phys. Rev. 57, 383 (1940).

# The Isotopes $Os^{185}$ and $Os^{193}$

LEONARD I. KATZIN AND M. POBERESKIN
*Chemistry Division, Argonne National Laboratory, Chicago, Illinois*

(Received April 19, 1948)

The half-life of $Os^{193}$ is shown to be 15.0 days, decay being by emission of a beta-particle with range less than 35 milligrams per square centimeter of aluminum (energy not more than 0.165 Mev). A highly converted gamma-ray of about 0.13-Mev energy is probably emitted at each disintegration, producing x-rays in large abundance. $Os^{185}$ decays by orbital capture with a half-life of 97 days. A gamma-ray of 0.75 Mev is probably emitted at each event. The relative cross sections for pile (slow) neutron capture of the isotopes $Os^{184}$, $Os^{190}$, and $Os^{192}$ have been estimated as 80:3.5:1, on the basis of measurements on the daughter activities.

## I. INTRODUCTION

ZINGG[1] has reported an osmium activity, obtained with neutrons from a radium-beryllium source, of the order of 10-days half-life, in addition to an activity of about 30-hours half-life known from earlier work. Seaborg and Friedlander[2] identified the 32-hour activity they found with cyclotron neutrons as $Os^{191}$, and reported $Os^{193}$ to emit 0.35-Mev beta-particles with a half-life of 17 days. Goodman and Pool,[3] also using cyclotron neutrons, failed to find the 17-day activity.

The basic fact is that the beta-radiation of $Os^{193}$ is actually very soft. Its aluminum range by the Feather method is not more than 35 milligrams of aluminum, corresponding to a maximum energy of 165 kev. The beta-radiation is accompanied by a soft gamma-ray, and x-rays caused by the internal conversion of the gamma-ray. In all but the thinnest-walled measuring instruments, a significant portion of the activity registered is due to the quantum radiation. The error in the energy assignment by Seaborg and Friedlander is therefore probably due to the influence of the *L* x-rays. Presumably Goodman and Pool failed to find the activity because of low intensity and heavy-walled measuring equipment.

The nature of the radiation from $Os^{193}$ also misled Seaborg and Friedlander as to its half-life, since together with it we find a long-lived *K*-capture isotope, whose radiations, blending with those of the 15.0-day isotope, can produce a fictitious 17-day period. Goodman and Pool have described a long-lived isotope from deuterons on rhenium,[3] whose identity with the product of neutron capture we have confirmed, so it is undoubtedly $Os^{185}$.

[1] E. Zingg, Helv. Phys. Acta 13, 219 (1940).
[2] G. T. Seaborg and G. Friedlander, Phys. Rev. 59, 400 (1941).
[3] L. J. Goodman and M. L. Pool, Phys. Rev. 71, 288 (1947).

## II. EXPERIMENTAL

Osmium was activated by several irradiations in the heavy-water moderated chain reactor of the Argonne Laboratory, for 7, 21, and 35 days, respectively. Osmium metal was treated with nitric acid in a distillation apparatus and distilled into an air-cooled condenser. A bubbler trap with concentrated ammonia solution was used as a safety trap, but most of the material was found in the air condensate. This distillation was usually repeated twice more. The osmium was then precipitated by hydrogen sulfide gas, dried, and sealed into a quartz irradiation vessel. At termination of the irradiation the capsule was broken and the osmium distilled again. These purification procedures eliminated small iridium activities. Samples of the final material were precipitated as the sulfide and mounted on mica approximately 3 milligrams per square centimeter surface density. After drying, the samples were made permanent with the aid of a film of zapon approximately 15 micrograms per square centimeter. Experience showed that a post-irradiation decay period of perhaps three weeks had to be allowed to avoid interference by the hard beta-radiation of the 32-hour $Os^{191}$ activity.

With exceptions to be noted below, the activity measurements were made with Geiger counters of the mica end-window type. Windows were usually about 3 milligrams per square centimeter, and

the air path was 1.8 centimeters. The usual counter filling was the standard 9 centimeters pressure of argon, 1 centimeter of alcohol. In the case of absorption curves in which the primary aim was the determination of energies of the quantum components of the radiation, xenon was substituted for the argon. This increased the counting efficiency of the quanta other than the hardest by a factor averaging 3.5.

Preliminary absorption and decay measurements showed that the radiation of the mixed isotopes consisted of four main components: soft beta-radiation, quantum radiation corresponding to $L$ x-rays of elements in the vicinity of osmium, quantum radiation corresponding to $K$ x-rays of the same region, and a gamma-ray of somewhat less than 1-Mev energy. Differential decay measurements showed the beta-radiation to decay most rapidly, the gamma-ray to decay least rapidly, and the intermediate quantum radiation to decay with intermediate rates. This preliminary information immediately gave the picture of a beta-emitter also emitting $L$ x-rays and either a soft gamma with $K$ x-rays or a gamma-ray just too soft to convert in the $K$ shell, and a second isotope emitting a hard gamma-ray together with $K$ and $L$ x-rays. If the long-lived isotope were due to an impurity, such as ruthenium, a harder beta-particle and softer gamma-ray would be found,[4] but a more direct reason for considering the activity due to a $K$-capture with gamma-radiation is the high ratio of soft quantum to hard quantum counts. Since $Os^{185}$ would be expected to be either a positron emitter or $K$-capture isotope, it seemed probable that we were not dealing with an impurity.

The decay rate of the soft beta-activity was determined differentially, using an ionization chamber fitted with an FP-54 electrometer and sealed with a window of mica of 5-mg/cm² surface density. A pair of measurements was made at each observation, one of the bare sample and one with 30 mg/cm² of polythene sheet interposed. The difference between the two readings represents the ionization contribution of the soft particles alone. Absorption experiments with additional polythene showed essentially zero absorption of the quantum radiation by the material. The results of these measurements, illustrated in Fig. 1, give a half-life of 15.0 days for $Os^{193}$. The slight tailing at the end is due to soft particles, conversion electrons, or secondary radiation accompanying the longer-lived isotope.

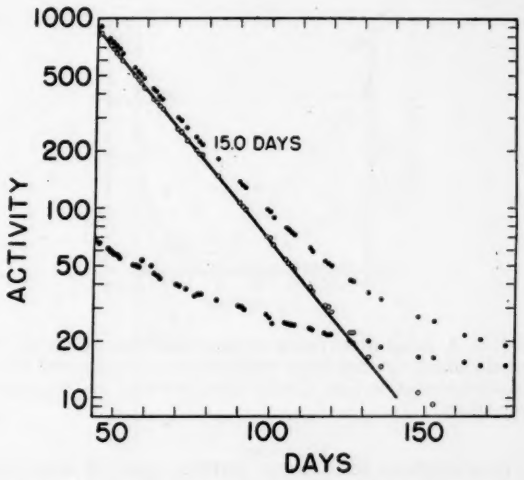


FIG. 1. Half-life determination of $Os^{193}$. Upper full points, FP-54 values with no added absorber; lower full points, FP-54 values with 30 mg/cm² of polythene over sample; open points, difference values.

Coincidence absorption measurements were also made with a sample of the 7-day irradiation material. These measurements showed a quantum of half-thickness 25–30 mg Al per cm² to be in coincidence with the beta-particle. The half-thickness value corresponds well with that to be expected from the prominent $L$ x-rays of iridium.[5]

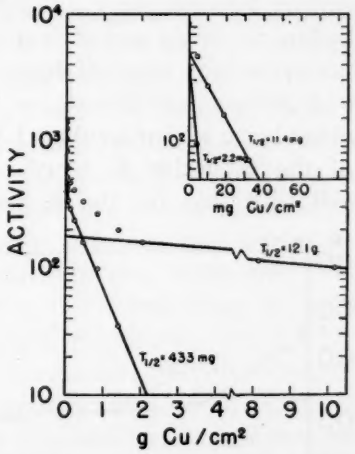


FIG. 2. Copper absorption curve, radiations of $Os^{185}$. Inset—$L$ x-ray components. Curve taken through 470 mg/cm² of beryllium.

[4] Plutonium Project, J. Am. Chem. Soc. 68, 2411 (1946).

[5] A. H. Compton and S. K. Allison, *X-Rays in Theory and Experiment* (D. Van Nostrand and Company, Inc., New York, 1935).

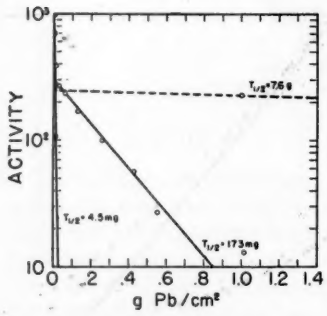


FIG. 3. Lead absorption curve, radiations of $Os^{185}$. The hard gamma-ray has been resolved out, as indicated by the dashed resolution line. Curve taken through 470 mg/cm² of beryllium.

Coincidences with some harder quanta were also observed, as well as some quantum-quantum coincidences.

A sample of osmium irradiated for 21 days was followed differentially with the Geiger counter. The gamma-radiation decayed with a half-life of 100 days, and the other radiations approached a similar slope. The gross decay and differential decay approximated each other after some 12 half-lives of the $Os^{193}$; a good average of the slopes is given by a half-life of 97 days. Absorption curves for the material when the short-lived isotope had died out are shown in Figs. 2 and 3. The resolution of the $L$ x-ray components into two by the copper is expected for x-rays of rhenium, with the absorption edge of copper at 1.377A cutting between the $L_\alpha$ and $L_\beta$ components.[5] Failure to obtain any such resolution of significance in the early stages of decay, when the $L$ x-rays of iridium predominate, is consistent with the rays being all harder than 1.377A. The energy of the ostensible $K$ x-ray component agrees well with that for the $K$ radiation of rhenium. The gamma-ray energies obtained from copper and lead absorption curves do not agree, an anomalously low absorption being found for the copper. Since this type of behavior seems usual, reliance is placed on the value with lead. The gamma-ray absorption half-thickness of 7.6 g/cm² obtained from the lead absorption curves corresponds to an energy value of about 0.75 Mev.[6] The counting ratios (argon) are 1:0.34:1.3 at zero absorber for the gamma, $K$ x-rays, and $L$ x-rays, respectively.

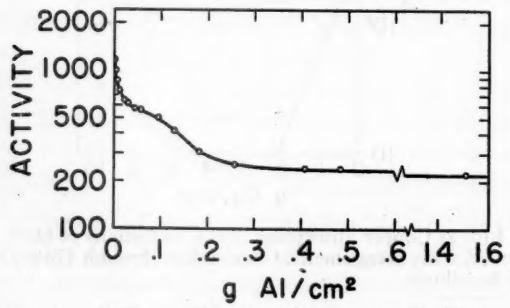


FIG. 4. Aluminum absorption curve of $Os^{185}$. The change of curvature due to secondary particles is clearly shown.

The meaning of the aluminum curve in the soft region (beryllium gives similar results) is not completely clear (Fig. 4). It seems fairly certain that the flat portion of the particle curve represents coming into equilibrium with secondary radiation due to passage of the gamma-ray through the absorber.[7] The initial rapidly dropping portion of the curve may represent secondary radiation of the softer quanta. The range corresponds to energies too high for auger electrons, and not high enough for conversion electrons of the gamma-ray. The possibility that an impurity such as $Ru^{103}$ might be involved was eliminated by producing $Os^{185}$ through cyclotron bombardment of rhenium with deuterons, using the Washington University cyclotron. The $Os^{185}$ activity so produced was apparently identical with that from pile-irradiated material. Measurements with a Geiger counter in a magnetic field make it certain that the soft radiation in question is particulate.

A picture of the radiations of $Os^{193}$ alone can be obtained by subtracting from an absorption curve for the mixed radiations a profile of the absorption curve for the $Os^{185}$, with zero-absorber count appropriate to the time the absorption curve of the mixed radiation is taken. This procedure is most accurate in the early stages of the decay, where $Os^{193}$ is most abundant. A curve of this type is illustrated in Fig. 5. Resolution of this curve shows clearly the soft beta-ray, $L$ x-ray component of 28 mg/cm², and hard component. The half-thickness of the hard component (210 mg lead) is equivalent to either 72 kev or 130 kev,[5] since it cuts across an absorption edge. It was not possible to demonstrate critical absorp-

[6] W. Heitler, *The Quantum Theory of Radiation* (Clarendon Press, Oxford, England, 1936).
[7] L. Meitner, Phys. Rev. 63, 73 (1943).

tion with tantalum, platinum, or gold absorbers (edges from 67.5–81 kev), so the radiation is either not more energetic than 67.5 kev, or falls in the 130-kev range. If the latter is true, there may also be some $K$ x-rays of iridium, *ca.* 65 kev. The difficulty is in theory resolvable by absorption measurements with copper. The behavior of the $Os^{185}$ gamma-ray in copper mentioned above, however, makes copper subtraction curves analogous to Fig. 5 of low usefulness. There does seem to be in these curves a tendency for a considerable hardening of the "tail" as compared to the expected 0.6-gram half-thickness, slopes corresponding to 1–2 grams per square centimeter half-thicknesses being obtained (130 kev should have a 2.5-gram half-thickness), but the reliability is uncertain. An indication may be furnished by the high ratio of $L$ x-ray counts to hard counts, 4:1. This is comparable to that found for the $K$-capture isotope, and might be evidence of a gamma-ray converting to a high degree in the $K$ shell.[8]

Analysis of the range of the beta-particle by the method of Feather[9] is not satisfactory, due perhaps to conversion electrons; it is possible only to set an upper limit of 35-mg aluminum (168 kev). The apparent relative abundances of the beta-particles, $L$ x-rays, and hard quanta are approximately 150:4:1 in terms of counting rates at zero absorber. No greater precision than 15 percent can be claimed for these values, with the beta-particle abundance being probably least reliable.

Gratitude is expressed to Professor F. N. D. Kurie of Washington University for arranging the cyclotron bombardment of rhenium, and to Mrs. Elaine Novey for technical assistance with some of the FP-54 measurements. Thanks are also due the pile operating crew for their cooperation in the osmium activations. Mr. Frank Wagner assisted with the magnetic measurements.

## III. DISCUSSION

From the counting rates of the beta-particles and hard quanta for $Os^{193}$ and the approximate efficiencies of the counting tubes involved, there is roughly one $K$ x-ray quantum or gamma-quantum emitted at each disintegration. From the failure of the copper curves to give any clear resolution of a gamma-ray of the proper energy, it must be presumed that the ray is largely converted in the $K$ shell. A low conversion would also fail to explain readily the high ratio of $L$ to $K$ x-ray counts, which is essentially the same as found for the $K$-capture isotope, $Os^{185}$. The total disintegration energy of $Os^{193}$, taking the beta-energy as 0.16 Mev, and the energy of the gamma-ray as 0.13 Mev, is 0.29 Mev.

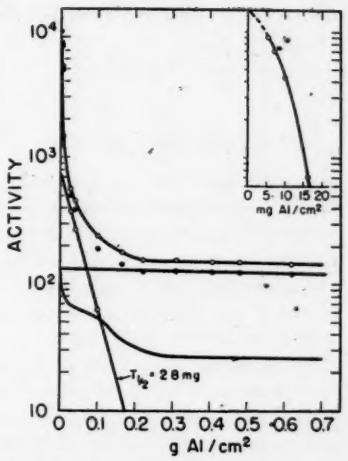


FIG. 5. Aluminum absorption curve of mixed $Os^{185}$ and $Os^{193}$ (upper open points), aluminum absorption curve due to $Os^{185}$ content (bottom curve), and resolution of the $Os^{193}$ curve obtained by difference (full points). Inset—curve for beta-particle component, extrapolated to zero air and counter window absorption.

Similarly, from the counting ratios for $Os^{185}$ there seems to be emission of a gamma-ray of 0.75-Mev energy with each capture of an orbital electron, following a 97-day half-life.

The relative neutron capture cross sections of the parental isotopes, $Os^{184}$, $Os^{190}$, and $Os^{192}$, estimated from the intensities of the daughter activities, are, respectively, 80:3.5:1. The assumption was made of 100 percent counting yield for the beta-particles entering the sensitive volume of the counter, and 1 percent for the 0.75-Mev gamma-ray. The isotopic abundance data of Nier were used.[10]

[8] Since this report was prepared, Cork, Shreffler, and Fowler (Phys. Rev. **72**, 1209 (1947)) have given evidence for conversion electrons from a 129-kev gamma-ray in irradiated osmium.

[9] N. Feather, Proc. Camb. Phil. Soc. **34**, 599 (1938).

[10] A. O. Nier, Phys. Rev. **52**, 887 (1937).

# Non-Product Wave Function for a Negative Ion

ESTHER CONWELL*
*University of Chicago, Chicago, Illinois*
(Received March 19, 1948)

A departure from the Hartree type wave function was attempted along lines found successful for $H^-$. The basic $\psi$ taken was a product of the nine Hartree one-electron functions for $O^-$ multiplied by a term including $r_{ij}$ terms representing what were considered the most important electron interactions—those between four of the $2p$ electrons and a fifth, arbitrarily considered the added one. Since there are six possible configurations for five equivalent $2p$ electrons, the actual $\Psi$ was taken as a linear combination of the six possible $\psi$'s of the type described. Minimizing the energy with respect to the coefficients in this linear combination leads to the same type of secular equation as is obtained in perturbation theory. It is shown that only the diagonal elements of the determinant are non-vanishing, and one of these is chosen for the evaluation of the energy. The electron affinity to be obtained using this wave function is considerably greater than the value gotten by Hartree, Hartree, and Swirles, perhaps twice as much.

THE wave functions available for negative ions other than that of hydrogen are mainly those obtained by Hartree and coworkers by the method of the self-consistent field.[1] Although the Hartree method probably gives a close approximation to the charge distribution of a negative ion it does not give a good value for the electron affinity. For the ground state of $O^-$, for example, the electron affinity obtained by Hartree, Hartree and Swirles[1] is 0.5 volts, as contrasted with experimental values of 2.2 volts, obtained by Lozier,[2] and 3.07 volts, obtained by Vier and Mayer.[3] It is apparent that it would be useful to study other methods of representing negative ions. Since these results are available for comparison, $O^-$ was chosen for this purpose.

According to Hartree,[4] the main defects of the Hartree-Fock approximation are: neglect of spin and relativity effects, and choice of a basic wave function made up of a product of one-electron functions. The second of these is undoubtedly more serious than the first which, in any case, is not important for light atoms.

Investigation of negative ions indicates that the stability of a negative ion is partly due to polarization of the atom by the added electron. In the light of this, the Hartree approximation would seem perhaps worse for a negative ion than it is for an atomic system.[5] A simple product wave function, or linear combination of such functions, cannot adequately show polarization. For such a function the probability distribution of the coordinates of each electron is independent of the *actual* coordinates of all the others. A wave function which does take polarization into account, if we take $H^-$ as an example, is one which includes, apart from the one-electron functions for electrons 1 and 2, a term with $r_{12}$ such that the probability for realizing a particular configuration is large for $r_{12}$ large, or for the two electrons staying away from each other.

Another feature of the Hartree approximation which is perhaps not good for representing a negative ion is the fact that the last or added electron has the same radial function as the others in the same shell. The functions which are most successful for the simplest negative ion $H^-$ treat this last electron differently and specifically have it further from the nucleus than the other electron although each is in a $1s$ state.

A simple wave function for $O^-$ which contains

* Now at Brooklyn College, Brooklyn, New York.

[1] $Cl^-$: D. R. Hartree and W. Hartree, Proc. Roy. Soc. A156, 45 (1936); $O^-$: D. Hartree, W. Hartree, and B. Swirles, Phil. Trans. A238, 229 (1939); D. Bates and H. Massey, Phil. Trans. A239, 269 (1943); $F^-$: F. Brown, Phys. Rev. 44, 214 (1933); D. Hartree, Proc. Roy. Soc. A151, 96 (1935).

[2] W. Lozier, Phys. Rev. 46, 268 (1934).

[3] D. Vier and J. Mayer, J. Chem. Phys. 12, 28 (1944).

[4] D. R. Hartree, and W. Hartree, Proc. Roy. Soc. A150, 9 (1935).

[5] It seems to be the case that the Hartree approximation gets progressively worse as one goes from positive ion to atomic system to negative ion. See Hartree and Black, Proc. Roy. Soc. A139, 311 (1933) and Hartree, Hartree, and Swirles, reference 1.

these features is the following:

$$\psi = u(n_a/x_1)u(n_b/x_2)\cdots u(n_i/x_9)\left[1+c\sum_{\alpha=1}^{8} r_{\alpha 9}\right], \quad (1)$$

where the $u$'s are the one-electron functions, $n_a$, $n_b$, $\cdots n_i$, representing the nine sets of quantum numbers, $x_1$, $x_2$, $\cdots x_9$, the coordinates of the electrons. For specificity, let $n_a$ and $n_b$ represent the $1s$ orbitals, $n_c$ and $n_d$ the $2s$, and $n_e$ through $n_i$ the occupied $2p$ orbitals. To decrease somewhat the excessive amount of calculation, only what were considered the most important electron interactions—those between electrons in the $2p$ shell—were finally included. This limits the values $\alpha$ can take in the summation above to $\alpha=5, \cdots, 8$.

In principle, the way to proceed with this wave function would be to minimize the energy with respect to each of the one-electron functions and $c$. This would lead to a set of equations similar to but worse than the Hartree equations for the system, or the Fock equations if $\psi$ is antisymmetrized. It was decided that it was advisable to use the Hartree-Fock determined one-electron functions and ascertain what change in the electron affinity results from using (1) as the wave function, treating $c$ as an adjustable parameter.

Since there are six different configurations for five equivalent $p$ electrons outside closed shells, this wave function should be modified by replacing the simple product of one-electron functions with a linear combination of these six, as follows:

$$\Psi = \sum_{i=1}^{6} a_i\psi_i\left[1+c\sum_{\alpha=5}^{8} r_{\alpha 9}\right], \quad (2)$$

where the $a_i$ are constant coefficients, also to be determined by the principle of minimum energy.

The abbreviation:

$$x = 1+c\sum_{\alpha=5}^{8} r_{\alpha 9}$$

will be used.

With (2) for $\Psi$ we get for the energy

$$E = \sum_{n=1}^{6}\sum_{n'=1}^{6} a_n a_{n'} H_{nn'} \Big/ \sum_{n=1}^{6}\sum_{n'=1}^{6} a_n a_{n'} \Delta_{nn'},$$

where

$$H_{nn'} = \int x^*\psi_{n'}{}^* H x \psi_n d\tau,$$

$$\Delta_{nn'} = \int x^*\psi_{n'}{}^* x \psi_n d\tau. \quad (3)$$

From the condition that $E$ is to be a minimum with respect to the $a$'s, we derive a set of homogeneous linear equations in the $a$'s. For this set to have a non-trivial solution it is necessary that the determinant of the coefficients vanish, or:

$$\begin{vmatrix} H_{11}-\Delta_{11}E & H_{12}-\Delta_{12}E\cdots H_{16}-\Delta_{16}E \\ H_{21}-\Delta_{21}E & \cdot\ \cdot\ \cdot\ \cdot\ \cdot\ \cdot\ \cdot \\ \cdot\ \cdot\ \cdot\ \cdot\ \cdot\ \cdot\ \cdot\ \cdot\ \cdot & \\ \cdot\ \cdot\ \cdot\ \cdot\ \cdot\ \cdot\ \cdot\ \cdot\ \cdot & \\ H_{61}-\Delta_{61}E & \cdot\ \cdot\ \cdot\ \cdot\ H_{66}-\Delta_{66}E \end{vmatrix} = 0. \quad (4)$$

It is to be expected that the six roots of this equation will be identical since there is only one multiplet level, $^2P$, for this configuration.

Since $x$ contains the parameter $c$, each element of the determinant is of the form $\alpha+\beta c+\gamma c^2$, where $\alpha$, $\beta$, $\gamma$ are functions of $E$. The secular equation would therefore be of twelfth order in $c$. It will be seen that it is nevertheless feasible to obtain $E$ explicitly in terms of $c$. Because of the difficulty in evaluating the radial integrals, however, the coefficients $\gamma$ were not evaluated and the value obtained for $E$ is, as a result, approximate.

Reduction of the diagonal elements of the determinant to angular and radial integrals will be undertaken first. The normalized one-electron functions are given by

$$u(n_\kappa/x_i) = \frac{1}{r_i}P(n_\kappa l_\kappa/r_i)\Theta(l_\kappa m_\kappa/\theta_i)\Phi(m_\kappa/\varphi_i)\delta(m_{s\kappa}/m_{si}),$$

where

$$\Theta(lm/\theta) = \left[\frac{(2l+1)(l-|m|)!}{2(l+|m|)!}\right]^{\frac{1}{2}}\frac{1}{2^l l!}\sin^{|m|}\theta\frac{d^{l+|m|}}{d(\cos\theta)^{l+|m|}}(-\sin^2\theta)^l,$$

$$\Phi(m/\varphi) = \exp(im\varphi)/(2\pi)^{\frac{1}{2}},$$

and $\delta$ is the spin function, $P(nl/r)$ the Hartree determined radial function. Integration over the spin coordinates yields a factor 1 for all diagonal elements since each electron has necessarily the same spin coordinate in $\psi_n$ and $\psi_n^*$, and there are no terms involving spin in the Hamiltonian.

To evaluate these integrals, an expansion of $r_{\alpha\vartheta}$ in Legendre polynomials is needed. This can be written:[6]

$$r_{\alpha\vartheta}=\sum_{k=0}^{\infty}\sum_{m=-k}^{+k}\frac{2}{2k+1}A_k(r_\alpha,r_\vartheta)\Theta(km/\theta_\alpha)\Theta(km/\theta_\vartheta)\exp(im(\varphi_\alpha-\varphi_\vartheta)),$$

where

$$\begin{aligned}A_k(r_\alpha,r_\vartheta)&=r_\alpha(r_\vartheta/r_\alpha)^k\left[\frac{1}{2k+3}\left(\frac{r_\vartheta}{r_\alpha}\right)^2-\frac{1}{2k-1}\right], \quad r_\alpha>r_\vartheta,\\ A_k(r_\alpha,r_\vartheta)&=r_\vartheta(r_\alpha/r_\vartheta)^k\left[\frac{1}{2k+3}\left(\frac{r_\alpha}{r_\vartheta}\right)^2-\frac{1}{2k-1}\right], \quad r_\vartheta>r_\alpha.\end{aligned} \tag{6}$$

For the $\Delta_{nn}$ integrals it can be seen by consideration of the integral over $\varphi$ that this reduces to a single summation over $k$ for all the terms included. $\psi_n$ contributes a factor $\exp(im_\alpha\varphi_\alpha)$, $\psi_n^*$ a factor $\exp(-im_\alpha\varphi_\alpha)$ and $r_{\alpha\vartheta}$ the factor $\exp(\pm im\varphi_\alpha)$. But the integral vanishes unless the exponent of $\varphi_\alpha$ vanishes, and so only the $m=0$ term of the summation over $m$ is non-vanishing.

With all obvious integrations performed we get for $\Delta_{nn}$ to terms in $c$:

$$\Delta_{nn}=1+2c\sum_{\alpha=5}^{8}\sum_{k=0}^{\infty}\frac{2}{2k+1}\xi_k(l_\alpha m_\alpha)\xi_k(l_\vartheta m_\vartheta)\int_{r_\vartheta=0}^{\infty}\int_{r_\alpha=0}^{\infty}P^2(21/r_\alpha)A_k(r_\alpha r_\vartheta)P^2(21/r_\vartheta)dr_\alpha dr_\vartheta,$$

where

$$\xi_k(lm)=\int_{\theta=0}^{\pi}[\Theta(lm/\theta)]^2\Theta(k\theta/\theta)\sin\theta d\theta. \tag{7}$$

Integration of the angular and radial integrals will be taken up later.

In atomic units we have for the Hamiltonian:

$$H=-\frac{1}{2}\sum_{\kappa=1}^{N+1}\left[\nabla_\kappa^2+\frac{2N}{r_\kappa}\right]+\sum_{\kappa=1}^{N+1}\sum_{\substack{\eta=1\\ \eta>\kappa}}^{N+1}\frac{1}{r_{\kappa\eta}}, \tag{8}$$

$N$ being the nuclear charge. The expansion of $1/r_{\kappa\eta}$ differs from the one previously given for $r_{\alpha\vartheta}$ only in the radial factor, which is $r_\eta^k/r_\kappa^{k+1}$ for $r_\kappa>r_\eta$, $r_\kappa^k/r_\eta^{k+1}$ for $r_\eta>r_\kappa$. The radial factor for this case will be denoted by $B_k(r_\kappa,r_\eta)$. The terms of $H_{nn}$ not multiplied by a factor $c$ or $c^2$ must, in view of the original approximation, add up to the Hartree energy, to be denoted here by $E_H$. There are two terms multiplied by $c$ in this integral, differing in that one has $r_{\alpha\vartheta}$ before the Hamiltonian operator; the other has it after. These two are, however, equal, as can be proved by using the Hermitian property of the Hamiltonian and the fact that the integrals are real. We get then for $H_{nn}$, to terms in $c$:

$$\begin{aligned}H_{nn}=E_H+2c\sum_{\alpha=5}^{8}\sum_{k=0}^{\infty}\frac{2}{2k+1}\xi_k(l_\alpha m_\alpha)\xi_k(l_\vartheta m_\vartheta)\int_0^\infty\int_0^\infty P^2(21/r_\alpha)A_k(r_\alpha,r_\vartheta)P^2(21/r_\vartheta)dr_\alpha dr_\vartheta\\ \times\sum_{\substack{\kappa=1\\ \kappa\neq\alpha}}^{8}-\frac{1}{2}\int_0^\infty P(n_\kappa l_\kappa/r_\kappa)\left\{\frac{\partial^2}{\partial r_\kappa^2}+\frac{2N}{r_\kappa}-\frac{l_\kappa(l_\kappa+1)}{r_\kappa^2}\right\}P(n_\kappa l_\kappa/r_\kappa)dr_\kappa\end{aligned}$$

[6] A method for deriving this expression is suggested by R. Williamson, Astrophys. J. 96, 438 (1942).

$$+4c\sum_{\alpha=5}^{8}\sum_{k=0}^{\infty}\frac{2}{2k+1}\xi_k(l_\alpha m_\alpha)\xi_k(l_9 m_9)$$
$$\times -\frac{1}{2}\int_0^\infty\int_0^\infty P^2(21/r_9)A_k(r_\alpha,r_9)P(21/r_\alpha)\left\{\frac{\partial^2}{\partial r_\alpha{}^2}+\frac{2N}{r_\alpha}-\frac{l_\alpha(l_\alpha+1)}{r_\alpha{}^2}\right\}P(21/r_\alpha)dr_\alpha dr_9$$

$$+2c\sum_{\alpha=5}^{8}\sum_{k=0}^{\infty}\frac{2}{2k+1}\xi_k(l_\alpha m_\alpha)\xi_k(l_9 m_9)\int_0^\infty\int_0^\infty P^2(21/r_\alpha)A_k(r_\alpha,r_9)P^2(21/r_9)dr_\alpha dr_9$$
$$\times\sum_{\substack{\kappa=1\\ \kappa\neq\alpha}}^{8}\sum_{\substack{\eta=1\\ \eta\neq\alpha\neq\beta}}^{8}\sum_{j=0}^{\infty}\frac{2}{2j+1}\xi_j(l_\kappa m_\kappa)\xi_j(l_\eta m_\eta)\int_0^\infty\int_0^\infty P^2(n_\kappa l_\kappa/r_\kappa)B_j(r_\kappa r_\eta)P^2(n_\eta l_\eta/r_\eta)dr_\kappa dr_\eta$$

$$+2c\sum_{\alpha=5}^{8}\sum_{\substack{\kappa=1\\ \kappa\neq\alpha}}^{8}\sum_{j=0}^{\infty}\sum_{k=0}^{\infty}\frac{2}{2j+1}\frac{2}{2k+1}\xi_j(l_\kappa m_\kappa)\xi_k(l_9 m_9)\xi_{jk}(l_\alpha m_\alpha)$$
$$\times\int_0^\infty\int_0^\infty\int_0^\infty P^2(21/r_9)A_k(r_\alpha,r_9)P^2(21/r_\alpha)B_j(r_\alpha,r_\kappa)P^2(n_\kappa l_\kappa/r_\kappa)dr_\alpha dr_9 dr_\kappa$$

$$+2c\sum_{\alpha=5}^{8}\sum_{\substack{\kappa=1\\ \kappa\neq\alpha}}^{8}\sum_{j=0}^{\infty}\sum_{k=0}^{\infty}\frac{2}{2j+1}\frac{2}{2k+1}\xi_j(l_\kappa m_\kappa)\xi_k(l_\alpha m_\alpha)\xi_{jk}(l_9 m_9)$$
$$\times\int_0^\infty\int_0^\infty\int_0^\infty P^2(21/r_\alpha)A_k(r_\alpha,r_9)P^2(21/r_9)B_j(r_\kappa,r_9)P^2(n_\kappa l_\kappa/r_\kappa)dr_\alpha dr_\kappa dr_9$$

$$+8c,$$

where

$$\xi_{jk}(lm)=\int_{\theta=0}^{\pi}[\Theta(lm/\theta)]^2\Theta(j0/\theta)\Theta(k0/\theta)\sin\theta d\theta. \tag{9}$$

It can be shown that due to orthogonality of the spin functions and the spherical harmonics all of the off-diagonal elements of the determinant vanish. It is convenient to think that each of the six configurations possible for this case is formed by leaving out a different one of the six possible one-electron functions for the equivalent $p$ electrons. In half of these configurations three of the $p$ electrons have spin $\frac{1}{2}$ and the other two spin $-\frac{1}{2}$, whereas the opposite situation exists in the other half. Matrix elements between configurations of the first kind and those of the second kind must vanish because in no permutation of the electrons among the one-electron functions can all electron spins be matched.

With regard to the orthogonality of the spherical harmonics, Slater[7] develops a theorem which can be shown to apply in this case also. The theorem states that matrix elements between $\psi_n$ and $\psi_{n'}$ vanish unless $\Sigma m$ is the same for both. For the terms of $\Delta_{nn'}$ and $H_{nn'}$ which do not contain any factors of the type $r_{ij}$ or $1/r_{ij}$ the truth of the theorem is a trivial consequence of the fact that the $m$ quantum number of each electron must be identical in $\psi_n$ and $\psi_{n'}$ for the integral to be non-vanishing. Consider now an integral where we have as a factor $r_{\alpha 9}$. Certainly the seven electrons apart from the $\alpha$'th and ninth must have identical one-electron functions in $\psi_n$ and $\psi_{n'}$ for the integral to be non-vanishing. This leaves at most two unmatched functions for the remaining electrons. (Actually only one unless we bring in exchange, but it is as convenient to work with the more general case.) If we indicate by $Pm_i$ the value of the $m$ quantum number of the $i$'th electron in $\psi_n$ and $m_i$ its value in $\psi_{n'}$, then the integral vanishes unless:

$$Pm_\alpha - m_\alpha + m = 0,$$
$$Pm_9 - m_9 - m = 0.$$

[7] J. C. Slater, Phys. Rev. 34, 1293 (1929).

Adding these two we get the condition for the integral to be non-vanishing in the form:

$$Pm_a+Pm_9=m_a+m_9.$$

This condition, coupled with the fact that the other seven electrons must have identical $m$ quantum numbers in $\psi_n$ and $\psi_{n'}$ completes the proof of the theorem for this type of integral. It is clear that there is no need to consider all further cases in detail. In whatever complicated fashion the $r_{ij}$ and $1/r_{ij}$ terms enter into the integrals, when the conditions for the various integrals over $\varphi$ to be non-vanishing are written down and added up, as above, the contribution of these terms must vanish, and the above theorem remains valid.

For the configuration of five equivalent $p$ electrons outside closed shells, $\Sigma m$ is equal to zero minus the $m$ quantum number of the missing one-electron function. Two $\psi$'s with $\Sigma m$ the same must have the $m$ quantum number of the missing function the same. They cannot, therefore, have the spin quantum number of the missing function the same, i.e., they cannot have spins matched, unless they are identical functions. Thus all but the diagonal elements of the determinant vanish.

An attempt was made to introduce exchange for the diagonal elements. The wave function used does not lend itself to antisymmetrizing since the electron coordinates do not appear in it in a symmetrical way; interchange of the coordinates of the second and fifth electron, for example, results in a different factor $x$. A function in which the coordinates of all the electrons do enter in symmetrical fashion is

$$\psi=u(n_a/x_1)u(n_b/x_2)\cdots \times u(n_i/x_9)\left[1+\frac{c}{2}\sum_{i=1}^{9}\sum_{j=1}^{9}r_{ij}\right]. \quad (10)$$

A wave function based on this which does satisfy the Pauli principle is

$$\psi=\sum_P(-1)^P Pu(n_a/x_1)u(n_b/x_2)\cdots \times u(n_i/x_9)\left[1+\frac{c}{2}\sum_{i=1}^{9}\sum_{j=1}^{9}r_{ij}\right], \quad (11)$$

where $P$ represents a particular permutation of the electron coordinates among the one-electron functions, and the summation is to be taken over all possible permutations. The calculation of the energy could be carried through reasonably with this wave function, neglecting the same terms as previously, if it were not for the fact that the terms with $r_{a9}/r_{x\eta}$ give rise to a great number of new radial integrals, and these were particularly tedious to evaluate.

We turn now to the evaluation of the angular integrals. It will first be established that $\xi_k$'s of odd $k$ vanish. Apart from constants, $\Theta(lm/\mu)$ is given by $(1-\mu^2)^{|m|/2}d^{|m|}/d\mu^{|m|}P_l(\mu)$. $P_l(\mu)$ is a polynomial in $\mu$ which is even or odd according as $l$ is even or odd. The square of this, multiplied by $(1-\mu^2)^{|m|}$, will always be even. But $\Theta(k0/\mu)$ is odd for $k$ odd and consequently the integrand is odd in $\mu$ for $k$ odd. The integral will vanish for $k$ odd since it has the same value at the upper and lower limits.

It can also be established that $\xi_k$ vanishes for $k\geq 2l+1$. This is done most conveniently by use of the theorem that the $k$'th Legendre polynomial, $P_k(\mu)$, is orthogonal to $1, \mu, \mu^2\cdots\mu^{k-1}$ in the interval $\mu=-1$ to $+1$. The stated property follows immediately from this and the fact that $[\Theta(lm/\mu)]^2$ is a polynomial in $\mu$ with highest degree term $\mu^{2l}$.

As a result of these two properties of the $\xi$'s the only non-vanishing terms of the summations over $j$, $k$ are those with $j=0,2$, $k=0,2$. The integral $\xi_0$, apart from the factor $\Theta(00/\mu)$ which is $(\frac{1}{2})^{\frac{1}{2}}$, is just the normalization integral and will therefore have the value $(\frac{1}{2})^{\frac{1}{2}}$ for any set of $l,m$. The $\xi_2$ values required are tabulated in Table I. Also tabulated are $\xi_{jk}$'s required. To

TABLE I. Angular integrals.

| | |
|---|---|
| $\xi_0(lm)=\left(\frac{1}{2}\right)^{\frac{1}{2}}$ | |
| $\xi_2(1\pm1)=-\left(\frac{1}{10}\right)^{\frac{1}{2}}$ | $\xi_2(10)=2\left(\frac{1}{10}\right)^{\frac{1}{2}}$ |
| $\xi_{00}(lm)=\frac{1}{2}$ | |
| $\xi_{20}(1\pm1)=-\frac{1}{2}\left(\frac{2}{10}\right)^{\frac{1}{2}}$ | $\xi_{20}(10)=\left(\frac{2}{10}\right)^{\frac{1}{2}}$ |
| $\xi_{22}(1\pm1)=\frac{5}{14}$ | $\xi_{22}(10)=\frac{11}{14}$ |

TABLE II. Radial integrals.

$$\int_0^\infty\int_0^\infty P^2(21/r_\alpha)A_0(r_\alpha,r_9)P^2(21/r_9)dr_\alpha dr_9=+2.066,$$

$$\int_0^\infty\int_0^\infty P^2(21/r_\alpha)A_2(r_\alpha,r_9)P^2(21/r_9)dr_\alpha dr_9=-0.154,$$

$$-\frac{1}{2}\int_0^\infty\int_0^\infty P^2(21/r_9)A_0(r_\alpha,r_9)P(21/r_\alpha)\left\{\frac{\partial^2}{\partial r_\alpha^2}+\frac{2N}{r_\alpha}-\frac{l_\alpha(l_\alpha+1)}{r_\alpha^2}\right\}P(21/r_\alpha)dr_\alpha dr_9=-10.919,$$

$$-\frac{1}{2}\int_0^\infty\int_0^\infty P^2(21/r_9)A_2(r_\alpha,r_9)P(21/r_\alpha)\left\{\frac{\partial^2}{\partial r_\alpha^2}+\frac{2N}{r_\alpha}-\frac{l_\alpha(l_\alpha+1)}{r_\alpha^2}\right\}P(21/r_\alpha)dr_\alpha dr_9=+0.784,$$

$$\int_0^\infty\int_0^\infty\int_0^\infty P^2(21/r_9)A_0(r_\alpha,r_9)P^2(21/r_\alpha)B_0(r_\alpha,r_\kappa)P^2(10/r_\kappa)dr_\alpha dr_\kappa dr_9=+1.787,$$

$$\int_0^\infty\int_0^\infty\int_0^\infty P^2(21/r_9)A_2(r_9,r_\alpha)P^2(21/r_\alpha)B_0(r_\alpha,r_\kappa)P^2(10/r_\kappa)dr_\alpha dr_\kappa dr_9=-0.121,$$

$$\int_0^\infty\int_0^\infty\int_0^\infty P^2(21/r_9)A_0(r_9,r_\alpha)P^2(21/r_\alpha)B_0(r_\alpha,r_\kappa)P^2(20/r_\kappa)dr_\alpha dr_\kappa dr_9=+1.350,$$

$$\int_0^\infty\int_0^\infty\int_0^\infty P^2(21/r_9)A_2(r_9,r_\alpha)P^2(21/r_\alpha)B_0(r_\alpha,r_\kappa)P^2(20/r_\kappa)dr_\alpha dr_\kappa dr_9=-0.0998,$$

$$\int_0^\infty\int_0^\infty\int_0^\infty P^2(21/r_9)A_0(r_9,r_\alpha)P^2(21/r_\alpha)B_0(r_\alpha,r_\kappa)P^2(21/r_\kappa)dr_\alpha dr_\kappa dr_9=+1.227,$$

$$\int_0^\infty\int_0^\infty\int_0^\infty P^2(21/r_9)A_2(r_9,r_\alpha)P^2(21/r_\alpha)B_0(r_\alpha,r_\kappa)P^2(21/r_\kappa)dr_\alpha dr_\kappa dr_9=-0.0905,$$

$$\int_0^\infty\int_0^\infty\int_0^\infty P^2(21/r_9)A_0(r_9,r_\alpha)P^2(21/r_\alpha)B_2(r_\alpha,r_\kappa)P^2(21/r_\kappa)dr_\alpha dr_\kappa dr_9=+0.520,$$

$$^*\int_0^\infty\int_0^\infty P^2(21/r_\alpha)B_0(r_\alpha,r_9)P^2(21/r_9)dr_\alpha dr_9=+0.651,$$

$$^*\int_0^\infty\int_0^\infty P^2(21/r_\alpha)B_2(r_\alpha,r_9)P^2(21/r_9)dr_\alpha dr_9=+0.278,$$

$$\int_0^\infty\int_0^\infty P(10/r_\alpha)P(21/r_9)B_1(r_\alpha,r_9)P(21/r_\alpha)P(10/r_9)dr_\alpha dr_9=+0.078,$$

$$^*\int_0^\infty\int_0^\infty P(20/r_\alpha)P(21/r_9)B_1(r_\alpha,r_9)P(21/r_\alpha)P(20/r_9)dr_\alpha dr_9=+0.421,$$

$$^{**}\ \epsilon_{2p,2p}=+0.259.$$

* Taken from Hartree, Hartree, and Swirles, see reference 1.
** A parameter used by Hartree, Hartree, and Swirles, the value of which is needed for the final energy determination.

terms in $c$, these always occur in conjunction with $\xi_j$ and $\xi_k$, so their special properties need not be investigated.

Integration of the radial integrals required was carried out by using analytic approximations for Hartree's $P(1s)$, $P(2s)$, and $P(2p)$. The analytic approximations used were set up along the lines of Slater's work.[8] Essentially, he uses hydrogen-like functions with a number of adjustable parameters. For example, Slater takes $P(1s)$ and $P(2s)$ as

$$P(1s)=fr\exp(-gr),$$
$$P(2s)=kr\exp(-pr)-sr^2\exp(-tr), \quad (12)$$

where $f$, $k$, $s$, $g$, $p$, $t$ are adjustable parameters.

[8] J. C. Slater, Phys. Rev. 42, 33 (1932).

In order to reproduce the general shape of Hartree's $P(2p)$, however, it was found necessary to use more than one term of the hydrogen type, the separate terms having different exponential dependence to account for the fact that the screening constant, or the effective nuclear charge, is different for different parts of the atom. The form found good by Slater for $P(2p)$ is:

$$P(2p)=r^2(a_1\exp(-b_1r)+a_2\exp(-b_2r)), \quad (13)$$

where $a_1$, $b_1$, $a_2$, $b_2$ are adjustable parameters, the former pair being larger than the latter pair.

The procedure for determining the parameters will be outlined briefly. The numerical values for $P(1s)$, $P(2s)$, $P(2p)$ were taken from Hartree, Hartree, and Swirles.[1] In the case of $P(1s)$ the

constant $g$ is gotten directly as the slope of the graph of $\log_e P(1s)/r$ *vs.* $r$. To fit $P(2p)$, $\log_e P(2p)/r^2$ is plotted. Since $b_1$ is considerably larger than $b_2$, the function from about $r=3$ on is, closely, a straight line from which it is possible to determine $a_2$ and $b_2$. Once these constants have been obtained, the other two can be gotten from the graph of $\log_e(P(2p)-r^2a_2\exp(-b_2r))/r^2$ in the usual way. $P(2s)$ was the most difficult to fit for the two terms are not sufficiently different in magnitude to enable the separate fitting of either part. A method of successive approximations was used. An estimate of $s$ and $t$ can be gotten from the large $r$ part of a graph of $\log_e P(2s)/r^2$, for the second term is predominant at large $r$. Using this, an estimate of the constants for the first term can be gotten, and with that, in turn, a better estimate of the second term, etc. Also, in the case of $P(2s)$ there is the necessity of choosing the constants so that $P(2s)$ is orthogonal to $P(1s)$. The Hartree-determined radial functions are not mutually orthogonal because the Hartree equations have the different electrons moving in different fields. In evaluating integrals previously, we have eliminated a large number of terms by the assumption that the one-electron functions are orthogonal. Now the functions for $1s$ and $2s$ states are orthogonal to the $2p$ functions by virtue of the properties of the spherical harmonics, but this is obviously not the case for $1s$ and $2s$. These one-electron functions can, however, be made orthogonal by suitable choice of the constants $k$ and $s$ in $P(2s)$. The condition that the integral over all configuration space of the product $P(1s/r)P(2s/r)$ must vanish gives rise to a condition on $k$ and $s$ which, as it turns out, could be satisfied to the precision required here. The functions finally chosen were

$$\begin{aligned}P(1s)&=42.4r\exp(-7.62r),\\ P(2s)&=7.05r\exp(-5.53r)\\ &\qquad -10.0r^2\exp(-2.30r),\\ P(2p)&=r^2(9.20\exp(-3.07r)\\ &\qquad +1.17\exp(-1.21r).\end{aligned}\tag{14}$$

The fit to the Hartree functions was quite good. The normalization integrals, evaluated using these analytic approximations, were all within 1.5 percent of 1. The function for $P(2p)$, which is the most important of these for this work, gave excellent fit out to $r=4$ atomic units, but was a little low from here on out. This resulted in making the normalization integral small by about 1 percent, and would tend to make most of the radial integrals small, perhaps by a few percent since most of them have $P^2(21/r_9)$ and $P^2(21/r_\alpha)$ and furthermore are weighted to large $r$ by $A_k(r_\alpha,r_9)$.

With these analytic approximations, integration of the radial integrals is a straightforward, if tedious, procedure. To systematize it somewhat, general formulae were worked out. Almost all of the terms of the radial integrals can be put in the form:

$$\int_{r_9=0}^{\infty}\int_{r_\alpha=0}^{r_9}P^2(21/r_9)r_\alpha{}^n r_9{}^m P^2(21/r_\alpha)dr_\alpha dr_9+\int_{r_9=0}^{\infty}\int_{r_\alpha=r_9}^{\infty}P^2(21/r_9)r_\alpha{}^{n'}r_9{}^{m'}P^2(21/r_\alpha)dr_\alpha dr_9.\tag{15}$$

This applies also the triple integrals which occur for they can be put in this form after integration over $r_s$ is performed. If we use the abbreviations:

$$b_k+b_l=b_{kl},\qquad b_i+b_j+b_k+b_l=b_{ijkl},$$

we can write

$$\begin{aligned}\int_{r_9=0}^{\infty}\int_{r_\alpha=0}^{r_9}P^2(21/r_9)r_\alpha{}^n r_9{}^m P^2(21/r_\alpha)dr_\alpha dr_9=\sum_{i=1}^{2}\sum_{j=1}^{2}\sum_{k=1}^{2}\sum_{l=1}^{2}a_ia_ja_ka_l\Bigg[&\frac{-(n+m+8)!}{b_{kl}b_{ijkl}^{n+m+9}}\\ -\sum_{\kappa=2}^{n+5}&\frac{(n+4)(n+3)\cdots(n+6-\kappa)(n+m+9-\kappa)!}{b_{kl}{}^\kappa b_{ijkl}^{n+m+10-\kappa}}+\frac{(n+4)!(m+4)!}{b_{kl}{}^{n+5}b_{ij}{}^{m+5}}\Bigg],\\ \int_{r_9=0}^{\infty}\int_{r_\alpha=r_9}^{\infty}P^2(21/r_9)r_\alpha{}^{n'}r_9{}^{m'}P^2(21/r_\alpha)dr_\alpha dr_9=\sum_{i=1}^{2}\sum_{j=1}^{2}\sum_{k=1}^{2}\sum_{l=1}^{2}a_ia_ja_ka_l\Bigg[&+\frac{(n'+m'+8)!}{b_{kl}b_{ijkl}^{n'+m'+9}}\\ +\sum_{\kappa=2}^{n'+5}&\frac{(n'+4)(n'+3)\cdots(n'+6-\kappa)(n'+m'+9-\kappa)!}{b_{kl}{}^\kappa b_{ijkl}^{n'+m'+10-\kappa}}\Bigg].\end{aligned}\tag{16}$$

The only difficulty which this type of integral presents is that, especially in the case of triple integrations, it runs into a huge number of terms. The final numerical values for the required integrals are given in Table II. Also given in this table, and indicated by an asterisk, are the values of some radial integrals calculated by Hartree, Hartree, and Swirles which were needed in the final calculation of energy. The integral

$$\int_0^\infty\int_0^\infty\int_0^\infty P^2(21/r_\vartheta)A_2(r_\vartheta,r_\alpha)$$
$$P^2(21/r_\alpha)B_2(r_\alpha,r_\varepsilon)P^2(21/r_\varepsilon)dr_\alpha dr_\vartheta dr_\varepsilon$$

was not evaluated for it is certainly small, about 0.05 probably, and its coefficient is so small that it has no effect on the energy in the third decimal place. Compared with somewhat similar, though less complicated, integrals evaluated by Hartree, Hartree, and Swirles, the values in the table appear quite reasonable.

It is now possible to obtain the numerical value of one of the diagonal matrix elements to terms in $c$. For this it is necessary to choose one of the elements, e.g., one of the configurations. The following set of one-electron functions, listed in the order in which they were assigned to the nine electrons, was chosen: $(100\frac{1}{2})$, $(100{-}\frac{1}{2})$, $(200\frac{1}{2})$, $(200{-}\frac{1}{2})$, $(211\frac{1}{2})$, $(211{-}\frac{1}{2})$, $(210\frac{1}{2})$, $(210{-}\frac{1}{2})$, $(21{-}1\frac{1}{2})$. The effect on the energy of choosing a different configuration or a different orbital for the ninth electron was not investigated. On theoretical grounds, of course, no difference is expected.

In the expression $H_{nn}$ it is to be noted that in the cases where integration over $r_\varepsilon$, or over $r_\varepsilon$ and $r_\eta$, is separable from the integrations over $r_\alpha$ and $r_\vartheta$, the integrals over $r_\varepsilon$ or over $r_\varepsilon$, $r_\eta$ are ones which were for the most part evaluated for $O^-$ by Hartree, Hartree, and Swirles. Unfortunately for the present purposes, however, they did not evaluate all of the integrals needed here, but used two relationships derived from the Hartree-Fock differential equations for the system to eliminate a number of them. To avoid the necessity of calculating all of these integrals, these relationships were used here also. Without exchange, the Hartree expression for the energy is

$$E_H=2I(1s)+2I(2s)+5I(2p)+F_0(1s,1s)+4F_0(1s,2s)+10F_0(1s,2p)$$
$$+F_0(2s,2s)+10F_0(2s,2p)+10F_0(2p,2p)-\tfrac{1}{5}F_2(2p,2p), \quad (17)$$

where

$$I(nl)=-\frac{1}{2}\int_0^\infty P(nl/r)\left\{\frac{\partial^2}{\partial r^2}+\frac{2N}{r}-\frac{l(l+1)}{r^2}\right\}P(nl/r)dr,$$

$$F_k(nl,n'l')=\int_0^\infty\int_0^\infty P^2(nl/r)B_k(r,r')P^2(n'l'/r')drdr'. \quad (18)$$

If we carry out the summations over $\alpha$ and $k$ in $H_{nn}$ for the terms where the $r_\alpha,r_\vartheta$ integrations are separable from the $r_\varepsilon,r_\eta$ ones, putting in the values of the angular integrals for the configuration chosen, we have:

$$2c\left\{4\int_0^\infty\int_0^\infty P^2(21/r_\vartheta)A_0(r_\vartheta r_\alpha)P^2(21/r_\alpha)dr_\alpha dr_\vartheta-\frac{2}{25}\int_0^\infty\int_0^\infty P^2(21/r_\vartheta)A_2(r_\vartheta r_\alpha)P^2(21/r_\alpha)dr_\alpha dr_\vartheta\right\}$$
$$\times[2I(1s)+2I(2s)+3I(2p)+F_0(1s,1s)+4F_0(1s,2s)$$
$$+F_0(2s,2s)+6F_0(1s,2p)+6F_0(2s,2p)+3F_0(2p,2p)]. \quad (19)$$

The terms in the angular bracket could also have been written:

$$[E_H-2I(2p)-4F_0(1s,2p)-4F_0(2s,2p)$$
$$-7F_0(2p,2p)+\tfrac{1}{5}F_2(2p,2p)], \quad (20)$$

using the previous expression for $E_H$. One of the Hartree relationships used to eliminate some of these integrals was

$$-2I(2p)=4F_0(1s,2p)+4F_0(2s,2p)$$
$$+8F_0(2p,2p)-(16/25)F_2(2p,2p)$$
$$+\epsilon_{2p,2p}-\tfrac{2}{3}G_1(1s,2p)$$
$$-\tfrac{2}{3}G_1(2s,2p), \quad (21)$$

where $\epsilon_{2p,2p}$ is a parameter which occurs in the Hartree-Fock equations and the general formula for the $G$ integrals is

$$G_k(nl,n'l')=\int_0^\infty\int_0^\infty P(nl/r)P(n'l'/r')$$
$$B_k(r,r')P(n'l'/r)P(nl/r')drdr'. \quad (22)$$

If we use this relationship to eliminate $I(2p)$ in the expression (20), we get

$$[E_H+F_0(2p,2p)-(11/25)F_2(2p,2p)$$
$$+\epsilon_{2p,2p}-\tfrac{2}{3}G_1(1s,2p)-\tfrac{2}{3}G_1(2s,2p)]. \quad (23)$$

This has the advantage over the previous expression in that it involves only one integral not numerically evaluated by Hartree, that being $G_1(1s,2p)$. In the other form for the expression there were two integrals not evaluated by Hartree, $I(2p)$ and $F_0(1s,2p)$, both of which are much larger than $G_1(1s,2p)$. The value of the latter was obtained by using the analytic approximations for $P(1s)$ and $P(2p)$ in the previous formula for $G_k$.

The final numerical result for the energy to terms in $c$ is:

$$E=\{E_H+16.6c(E_H-0.041)\}/1+16.6c. \quad (24)$$

Of somewhat greater interest is the difference between this energy and the Hartree energy, which to this approximation is given by:

$$E-E_H=-16.6c\times0.041/1+16.6c. \quad (25)$$

A graph of $E-E_H$ *vs.* $c$ shows a rapid, sharp descent. Even for $c=0.1$ an improvement in the electron affinity of about six-tenths of the 0.041 atomic unit results. For $c$ of the order of 0.5, which experience with $H^-$ might suggest as a reasonable value, the improvement with this formula would be about 8/9 of the 0.041 atomic unit. The Hartree electron affinity is 0.019 atomic unit. In view of the steep descent mentioned, it seems quite safe to say that even with $c^2$ terms included the electron affinity to be obtained with this wave function is considerably greater than the Hartree value, perhaps more than twice as large. Similar expectations for the case with exchange, when that can be worked out, seem warranted. The fact that most of the radial integrals are a few percent small will not affect the extent of the improvement of the electron affinity materially because what is of importance is the ratio of the coefficient of $c$ in the numerator to that in the denominator. It is certainly demonstrated that this type of wave function is worth further investigation and use, and offers considerable promise as a direction for departure from the pure product wave functions for heavy ions or atomic systems.

It is a pleasure to acknowledge my debt to Professor S. Chandrasekhar for many valuable discussions and suggestions.

# Wave Functions for $H^-$ Obtained by Variation Method

ESTHER CONWELL*
*University of Chicago, Chicago, Illinois*
(Received March 19, 1948)

A wave function for $H^-$ of the form $\psi=f_1(r_1)f_2(r_2)(1+cr_{12})$ was set up. For a given value of the parameter $c$, determination of the functions $f_1$ and $f_2$ which will make the energy a minimum leads to a pair of simultaneous integro-differential equations for $f_1$ and $f_2$ with the energy as a parameter. Numerical integration of these for different values of the energy and $c$ was carried out for the cases: (1) $f_1$ identical with $f_2$, and (2) $f_1$ taken as the function $e^{-r}$, the ground state of a neutral hydrogen. Neither of these gave as good a value of the electron affinity as has been obtained with previously investigated analytic functions.

EXTENSIVE work has been done on wave functions for the simplest negative ion, $H^-$.[1] In general, the wave function has been represented by an analytic function with a number of adjustable parameters and these parameters then determined to give minimum energy. In all of this work there has been a term with exponential $r$-dependence for each of the electrons, this in some cases multiplied by a series of terms including powers of $r_{12}$, $r_1+r_2$, $r_1-r_2$, and cross-products. An eleven parameter function of this type has led to an energy of $-0.52756$ atomic units, the lowest obtained. It was therefore considered important to investigate wave functions in which the form of the $r$-dependence is determined by the variation method, to find specifically whether these lead to a much changed $r$-dependence or any significant improvement in energy.

Since the variation problem in which no specific form or limitation is specified for $\psi$ (beyond the normalization condition) leads just to the Schrodinger equation, some definite form had to be specified for $\psi$. The analytic functions which have been found most successful, i.e., led to the lowest energy values, have been those which have treated the two electrons differently, specifically providing for different amounts of screening, and those which have included correlation terms, this allowing for the polarization of the atom by the added electron. These two features are about equally important in accounting for the stability. With these points in mind, a function of the form:

$$\psi=f_1(r_1)f_2(r_2)(1+cr_{12}) \tag{1}$$

was assumed, $c$ being a parameter to be determined also to give minimum energy. A wave function of the form (1) has been tried before for neutral helium by Hasse and Baber[2] who have derived the necessary variational equations. In their notation we can write

$$f_1''(r_1)+\left(\frac{2}{r_1}+\frac{D(r_1)}{r_1A(r_1)}\right)f_1'(r_1)$$
$$+\left(\frac{2}{r_1}+E+\frac{B(r_1)+2C(r_1)+G(r_1)}{A(r_1)}\right)f_1(r_1)=0, \tag{2}$$

where $A$, $B$ etc., have meanings similar to the analogous expressions in Hasse and Baber's paper.

In the context of $H^-$ Eq. (2) has now been investigated for two special cases: first, $f_1$ assumed identical with $f_2$, and second $f_1$ taken as the function $e^{-r_1}$. The former case will be taken up first. It can be seen that in this case we have a rather complicated integro-differential equation for $f$. The method of solution attempted was one of successive approximations. An analytic approximation for $f$ is set up so that the integrals $A(r)$, $B(r)$, etc. can be evaluated. The resulting differential equation can then be integrated by ordinary numerical methods. With this solution a better approximation for the coefficients can be obtained and the equation re-

* Now at Brooklyn College, Brooklyn, New York.

[1] For references see article by S. Chandrasekhar, Rev. Mod. Phys. 16, 301 (1944).

[2] For derivation of these equations for the case of helium see H. R. Hasse and T. D. H. Baber, Proc. Camb. Phil. Soc. 33, 253 (1937). The equations for $H^-$ are of course slightly different because the expressions for the potential energy are.

integrated. The iterative process can be continued until successive $f$'s agree within the limits of accuracy desired. Also, each time a new $f$ is obtained the value of the parameter $c$ must be redetermined to give minimum energy with this $f$. The procedure to be adopted is described in greater detail in Hasse and Baber's paper. In this manner the energy was estimated to lie between $-0.509$ and $-0.515$ atomic units after one iteration starting with the function[3]

$$\psi=(1+0.4933507r_{12})\exp(-0.8257257)r \times(E=-0.509), \quad (3)$$

derived from the variational principle. It is not certain how much this energy would be improved by further iteration. In the case of Hasse and Baber, who worked out a function of this type for helium, the energy improvement on iteration was less than 0.01 atomic units. Of course, the process would be expected to converge more rapidly for helium since the starting wave function is a better approximation in that case. Still, it does not seem likely that the energy value would be enough bettered on iteration to make the additional numerical work on this function worthwhile. It would seem to be the case, from the lack of significant energy improvement, that the radial dependence of the one-electron functions cannot be greatly different from $e^{-r}$.

The second function tried was:

$$\psi=e^{-r_1}f(r_2)(1+cr_{12}). \quad (4)$$

This form was considered of particular interest because it has the function representing the ground state of the hydrogen atom multiplied by a function representing the added electron only and a correlation term. But the results were disappointing, the energy being lower than even $-0.507$ atomic units. Since a wave function of the form

$$\psi=(\exp(-ar_1-br_2) +\exp(-ar_2-br_1))(1+cr_{12}), \quad (5)$$

gives an energy $E=-0.5259$ atomic units, it is apparent that exchange is quite important in the binding of the ion. It is therefore to be expected that a function which does include exchange, e.g.:

$$\psi=\{f_1(r_1)f_2(r_2)+f_2(r_1)f_1(r_2)\}(1+cr_{12}) \quad (6)$$

will be more successful than either of the functions tried. This, however, leads to a more complicated integro-differential equation.

I am grateful to Mr. Tracy Kinyon for doing a great deal of numerical work connected with these calculations.

[3] R. E. Williamson, Astrophysical Journal 96, 438 (1942).

# The Radioactive Decay Constants of $K^{40}$ as Determined from the Accumulation of $Ca^{40}$ in Ancient Minerals

L. H. AHRENS AND ROBLEY D. EVANS
*Departments of Geology and of Physics, Massachusetts Institute of Technology, Cambridge, Massachusetts**

(Received April 15, 1948)

New measurements of the rate of emission of gamma-ray energy by $K^{40}$ give $4.9\pm0.1$ Mev/sec. g K, in agreement with Gleditsch and Gráf. Thus the minimum value of the probability of electron capture in $K^{40}$ is $\lambda_e=0.062\times10^{-9}$ yr.$^{-1}$. Spectrochemical analysis of 4 samples of lepidolite known to be $2.1\times10^9$ years old, as well as 22 younger lepidolites, gives a maximum value of 22, and a most probable value of 11 for the ratio of radiogenic $Ca^{40}$ to residual $K^{40}$ in the $2.1\times10^9$ year old minerals. In such an ancient mineral, the $Ca^{40}/K^{40}$ ratio is a function not only of the probability of $\beta$-ray decay, $\lambda_\beta$, of $K^{40}$ into $Ca^{40}$, but also the probability of transformation by electron capture, $\lambda_e$, of $K^{40}$ into $A^{40}$. This is because the electron capture process may significantly deplete the $K^{40}$, thus tending to produce larger $Ca^{40}/K^{40}$ ratios than would result from $\beta$-decay alone. The decay constants $\lambda_\beta$ and $\lambda_e$ reported by Bleuler and Gabriel predict $Ca^{40}/K^{40}=152$, while Mühlhoff's $\lambda_\beta$ predicts $Ca^{40}/K^{40}=1.48$ for a $2.1\times10^9$ year old mineral. We have therefore suggested approximate corrections for the effects of $\beta$-ray scattering in the observations by Mühlhoff and by Bleuler and Gabriel on the absolute rate of emission of $\beta$-rays by K. These corrections lead to a mean value of 34 $\beta$-rays/sec. g K, or $\lambda_\beta=(0.65\pm0.1)\times10^{-9}$ yr.$^{-1}$. The observed value of $C^{40}/K^{40}=11$ then leads to $\lambda_e=(0.9\pm0.1)\times10^{-9}$ yr.$^{-1}$, and a total half-period of $T=(0.45\pm0.05)\times10^9$ yr. for $K^{40}$. Then approximately 42 percent of the disintegrations of $K^{40}$ are by $\beta$-ray emission to the ground state of $Ca^{40}$; 4 percent by electron capture to a 1.5-Mev excited state in $A^{40}$, and 54 percent by electron capture to the ground state of $A^{40}$. It is shown that these revised disintegration constants lead to a sufficiently smaller thermal output by K early in the earth's history to satisfy Birch's calculations on the possibility of an early solid terrestrial crust, and to remove arguments relating to the origin of species through gene mutations caused by intense $K^{40}$ radiations early in the earth's history.

## INTRODUCTION

DIRECT observations of the $\beta$-rays, $\gamma$-rays, and x-rays associated with the decay of ${}_{19}K^{40}$ have shown that individual atoms of this isotope transform radioactively by either of two competing processes: $\beta$-ray emission to ${}_{20}Ca^{40}$, or electron capture to ${}_{18}A^{40}$. Some, if not all, of the electron capture transitions are accompanied by $\gamma$-ray emission. Thus:

$$ {}_{19}K^{40}\rightarrow{}_{20}Ca^{40}+\beta^-, \quad {}_{19}K^{40}+e^-\rightarrow{}_{18}A^{40}+h\nu. $$

Much of the recent literature has been summarized by Gleditsch and Gráf.[1] The more reliable experimental estimates of the decay constants, $\lambda_\beta$ for $\beta$-ray transitions, and $\lambda_e$ for electron capture transitions, vary sufficiently widely to lead to profound uncertainties in the geophysical significance of potassium.[2]

Extreme values of the half-period, $T$, of $K^{40}$ corresponding to the better direct measurements on its radioactive radiations range from $T=16\times10^8$ yr. obtained by Mühlhoff[3] to $T=2.4\times10^8$ yr. by Bleuler and Gabriel,[4] who report more than twice the absolute $\beta$-ray activity observed by Mühlhoff, and who, in addition, estimate from measurements of the x-rays that 1.9 atoms of $K^{40}$ transform to $A^{40}$ by electron capture for each atom of $K^{40}$ which transforms to $Ca^{40}$ by $\beta$-ray emission, i.e., $\lambda_e/\lambda_\beta=1.9$.

In their measurements with Geiger-Müller counters of the $\beta$-rays and x-rays of $K^{40}$, both of these authors used thin sources of potassium salts, mounted on the inside of a brass cylinder. Neither made any explicit estimate of the effects of back-scattered radiation,[5] which could introduce errors of as much as 50 percent in their calibrations. Mühlhoff used the mixed $\alpha$-rays and $\beta$-rays of uranium ($UI$, $UX_1$, $UX_2$, $UII$) for calibration, and may thus have obtained too high an apparent counter efficiency because of the high reflection factor for the very soft $\beta$-rays

* The work here reported was supported in part by the Office of Naval Research in conjunction with the Laboratory for Nuclear Science and Engineering.

[1] E. Gleditsch and T. Gráf, Phys. Rev. **72**, 640(L), 641(L) (1947).

[2] F. Birch, Phys. Rev. **72**, 1128(L) (1947).

[3] W. Mühlhoff, Ann d. Physik **7**, 205 (1930).

[4] E. Bleuler and M. Gabriel, Helv. Phys. Acta **20**, 67 (1947).

[5] S. Eklund, Arkiv Mate. Astron. Fysik **33A**, No. 14, 50 (1945).

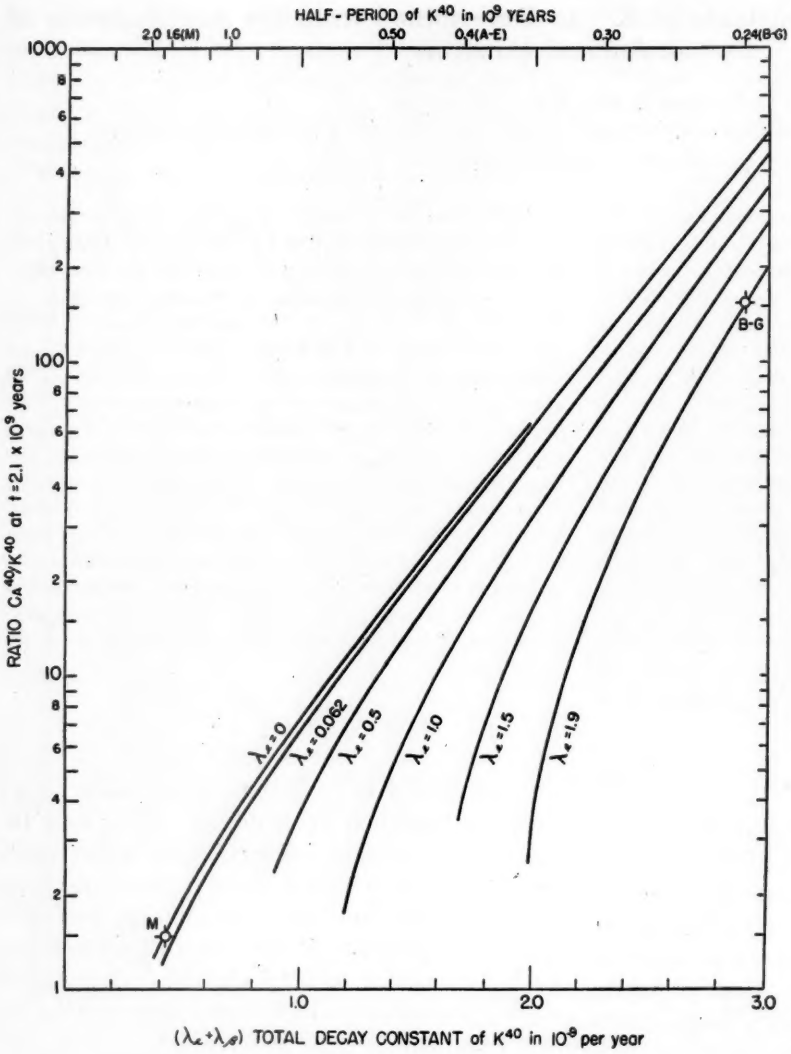


FIG. 1. Evaluation of Eq. (6) for the ratio of $Ca^{40}$ accumulated in $2.1\times10^9$ years to the residual $K^{40}$, as a function of the total decay constant $(\lambda_e+\lambda_\beta)$, and the partial decay constant $\lambda_e$ for electron capture. The numerical values of the half-period $T=0.693/(\lambda_e+\lambda_\beta)$ are shown at the top, corresponding to the scale of total decay constants. The predicted values of $Ca^{40}/K^{40}$, using Mühlhoff's data and using Bleuler and Gabriel's data, are shown by points marked *M* and *B-G*.

of $UX_1$. If so, this could account for the fact that more recent evidence suggests that Mühlhoff's absolute decay rates for both $K^{40}$ and for $Rb^{87}$ are too low.

On the other hand, Bleuler and Gabriel obtained their calibration purely by calculation, but completely neglected back scattering, or reflection, of $\beta$-rays and x-rays. The $K^{40}$ $\beta$-rays are thought[6–8] to have a maximum energy in the neighborhood of 1.3 Mev, and the back scattering from a thick brass source mounting may therefore add as much as 50 percent to the $\beta$-ray counting rate, as is the case[9] for the $\beta$-rays of $Na^{24}$ which have about the same maximum energy. Back scattering of the 3.0-kev x-rays of $A^{40}$ is difficult to estimate theoretically, but could be evaluated experimentally by studies on strong sources of other isotopes which decay by electron capture, such as $Fe^{55}$.

It seems qualitatively clear that Bleuler and Gabriel's decay constants $\lambda_\beta$ and $\lambda_e$ may both be appreciably too high and the corresponding half-period too short, because of neglect of back scattering from the source mounting. Calculations based on the fragmentary counting data included in Bleuler and Gabriel's paper, suggest that their net $\beta$-ray counting rates were about

[6] W. J. Henderson, Phys. Rev. **71**, 323(L) (1947).
[7] B. Dželepow, M. Kopjava, and E. Vorobjov, Phys. Rev. **69**, 538(L) (1946).
[8] O. Hirzel and H. Wäffler, Helv. Phys. Acta **19**, 216 (1946).
[9] W. C. Peacock, Thesis, Mass. Inst. of Tech. (1944).

180 counts per minute, while their estimate of $\lambda_e/\lambda_\beta = 1.9$ was based on a change of only about 3 counts per minute when argon and carbon tetrachloride mixtures were used to absorb the $A^{40}$ x-rays which follow electron capture in $K^{40}$. Clearly, their important experiment should be repeated, using enriched $K^{40}$, with counters which have been calibrated for both $\beta$-ray and $\gamma$-ray sensitivity through the use of isotopes whose decay schemes and absolute disintegration rates have been measured by other methods.*

Using amounts of $Co^{60}$ whose absolute decay rate has been determined by $\beta$-$\gamma$ coincidence methods, we[10] have compared the absolute rate of emission of $\gamma$-ray energy from $K^{40}$ with that of $Co^{60}$, by using copper screen cathode Geiger-Müller counters whose sensitivity is proportional to quantum energy and whose response is therefore proportional to $\gamma$-ray energy flux. It is found that 1 gram of ordinary (unenriched) potassium emits $4.9 \pm 0.1$ Mev of $\gamma$-rays per second. New measurements of the quantum energy in progress, but in the meantime we may use the current values[1,8] of about 1.5 Mev. Thus, we estimate $4.9/1.5 = 3.3$ quanta per second per gram of potassium, in substantial agreement with the value found by Gleditsch and Gráf.[1] If every electron capture transition of $K^{40}$ resulted in the emission of one photon, then the minimum decay constant of $K^{40}$ for electron capture would be:

$$\lambda_e = 0.062 \times 10^{-9} \text{ yr.}^{-1}. \quad (1)$$

For comparison, the $\beta$-ray counting results of Mühlhoff correspond to:

$$\lambda_\beta = 0.434 \times 10^{-9} \text{ yr.}^{-1},$$

and the $\beta$-ray and x-ray counting results of Bleuler and Gabriel correspond to:

$$\lambda_\beta = 1.0 \times 10^{-9} \text{ yr.}^{-1}, \quad \lambda_e = 1.9 \times 10^{-9} \text{ yr.}^{-1}.$$

Now that some potassium minerals are available whose measured geological age equals or exceeds the proposed range of values of the half-period of $K^{40}$, the opportunity has arisen to estimate the decay constants of $K^{40}$ by an experiment whose effective duration is of the order of $10^9$ years, instead of a few days or months. This involves, of course, observations of the accumulated $Ca^{40}$ and $A^{40}$, instead of short measurements of the radiations of $K^{40}$. If there were $N_0$ atoms of $K^{40}$ per gram of mineral at the time ($t = 0$) of formation of the mineral, then the number of $K^{40}$ atoms remaining at the present time, $t$, is:

$$N = N_0 \exp[-(\lambda_\beta + \lambda_e)t]. \quad (2)$$

The number of $Ca^{40}$ atoms formed will be:

$$Ca^{40} = (N_0 - N)\lambda_\beta/(\lambda_\beta + \lambda_e), \quad (3)$$

the number of $A^{40}$ atoms formed will be:

$$A^{40} = (N_0 - N)\lambda_e/(\lambda_\beta + \lambda_e) = Ca^{40}(\lambda_e/\lambda_\beta), \quad (4)$$

while the total amount of decay products formed is, of course, equal to the $K^{40}$ which has decayed, or:

$$Ca^{40} + A^{40} = N_0 - N = Ca^{40}(1 + \lambda_e/\lambda_\beta). \quad (5)$$

TABLE I. Calcium content (mean of 3 to 4 determinations on each sample) and geological age of 26 samples of lepidolite.

| No. | Locality | Percent Ca | Age ($\times 10^6$ yr.) |
|---|---|---|---|
| 1 | Falcon Island, Lake of the Woods, S.E. Manitoba | 0.019 | 2100 |
| 2 | Silver Leaf Mine, along Winnipeg River, S.E. Manitoba | 0.018 | 2100 |
| 3 | Silver Leaf Mine, along Winnipeg River, S.E. Manitoba | 0.032 | 2100 |
| 4 | Along Winnipeg River, S.E. Manitoba | 0.023 | 2100 |
| 5 | Pala, California | 0.0012 | 110 |
| 6 | Pala, California | 0.0023 | 110 |
| 7 | Buckfield, Maine | 0.008 | 270 |
| 8 | Newry, Maine | 0.016 | 270 |
| 9 | Norway, Maine | 0.014 | 270 |
| 10 | Topsham, Maine | 0.009 | 270 |
| 11 | Mt. Mica, Maine | 0.08 | 270 |
| 12 | Auburn, Maine | 0.01 | 270 |
| 13 | Haddam, Connecticut | 0.005 | 270 |
| 14 | Middleton, Connecticut | 0.02 | 270 |
| 15 | Portland, Connecticut | 0.011 | 270 |
| 16 | Dixon, New Mexico | 0.015 | ~850 |
| 17 | Brown Derby, Colorado | 0.008 | ~850 |
| 18 | Brown Derby, Colorado | 0.005 | ~850 |
| 19 | Black Hills, South Dakota | 0.006 | ~850 |
| 20 | Black Hills, South Dakota | 0.008 | ~850 |
| 21 | Black Hills, South Dakota | 0.015 | ~850 |
| 22 | Okongava Ost 72, Karibib, South West Africa | 0.013 | ~850 |
| 23 | Karibib, South West Africa | 0.008 | ~850 |
| 24 | Albrecht's Höhe, Karibib, South West Africa | 0.022 | ~850 |
| 25 | Warmbad, South West Africa | 0.0032 | ~850 |
| 26 | Omaruru, South West Africa | 0.006 | ~850 |

* *Note added in proof, 15 June 1948:* R. W. Stout, in an unpublished B.S. thesis under Prof. M. Deutsch at M. I. T., has just obtained a preliminary value of $30 \pm 6$ disintegrations per second per gram K for the absolute $\beta$-ray specific activity of normal unenriched K, by $\beta$-ray counting on KCl sources which have been internally standardized through the addition of known activities of $Na^{24}$, whose maximum $\beta$-ray energy is almost identical with that of $K^{40}$.

[10] R. D. Evans and R. O. Evans, Rev. Mod. Phys. **20**, 305 (1948).

Combining Eqs. (2) and (5), and writing $K^{40}$ for $N$, we have, for the $Ca^{40}/K^{40}$ ratio in a mineral of age, $t$:

$$Ca^{40}/K^{40}=[\lambda_\beta/(\lambda_e+\lambda_\beta)]\{\exp[(\lambda_e+\lambda_\beta)t]-1\}. \quad (6)$$

As described below, we have observed a $Ca^{40}/K^{40}$ ratio of about 11 in lepidolites of $2.1\times10^9$ years of age. Figure 1 is a plot of the $Ca^{40}/K^{40}$ ratio to be expected in a mineral of age $t=2.1\times10^9$ yr., for various values of the total decay constant $(\lambda_e+\lambda_\beta)$ and a series of particular values of the probability, $\lambda_e$, of electron capture transitions. The two points plotted on Fig. 1 show the $Ca^{40}/K^{40}$ ratios to be expected on a basis of Mühlhoff's decay constant for $K^{40}$ ($Ca^{40}/K^{40}=1.48$, marked *M*) and on a basis of Bleuler and Gabriel's decay constants ($Ca^{40}/K^{40}=152.$, marked *B–G*).

## CHOICE OF A SUITABLE POTASSIUM-RICH MINERAL

Some minerals of the mica group commonly contain only traces of calcium, in particular types like muscovite and lepidolite. Thus, chemical analyses of lepidolite invariably report calcium as either a trace or as absent; see, for example, analyses of lepidolite by Stevens.[11] An inspection of the spectra of 28 specimens of lepidolite and 2 of muscovite which had been recorded for making age determinations by the strontium-rubidium spectrochemical method,[12] showed that in general the intensities of the calcium lines were weak, and in most instances corresponded to about 0.01 percent in the magnitude of the calcium content. This magnitude is very small, and with reasonable fortune it should be possible to utilize lepidolite and probably also muscovite, for the determination of $Ca^{40}/K^{40}$ ratios, provided very ancient specimens of known age are obtainable.

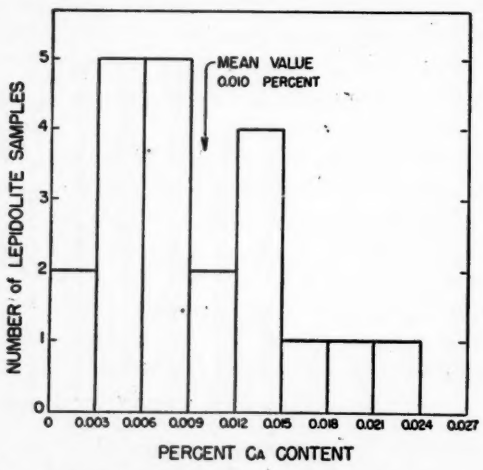


FIG. 2. Distribution histogram of the Ca content of 21 lepidolites, samples 5 to 10, and 12 to 26 of Table I. The oldest samples in this group have an age of $0.85\times10^9$ years, and should have accumulated only 0.001 percent $Ca^{40}$, using the decay constants $\lambda_e=1.0\times10^{-9}$ yr.$^{-1}$ and $\lambda_\beta=0.7\times10^{-9}$ yr.$^{-1}$.

[11] R. E. Stevens, Am. Min. **23**, 607 (1938).

Lepidolite usually contains about 10 percent $K_2O$ (8.3 percent K) and invariably the potassium content lies within ±5 percent (1/20) of this value; see for example, Stevens[11] analyses, which includes a sample from the Silver Leaf pagmatite (see Table I samples 2 and 3). According to Nier[13] 0.011 percent of potassium is $K^{40}$, and thus in lepidolite, 0.00091 percent K is $K^{40}$. The possible slight variation of ±5 percent in the $K_2O$ content of lepidolite is considered insignificant for the purpose of this investigation.

## AGE OF SOME ANCIENT LEPIDOLITE SPECIMENS

Several lepidolite specimens of pre-Cambrian age were available. Unless, however, extremely ancient specimens can be used, it is doubtful whether an investigation of this type could be employed with a reasonable chance of success. Thus, in specimens of middle pre-Cambrian age ($850\times10^6$ years), several of which were available, only about 0.001 to 0.003 percent $Ca^{40}$ would be generated, depending on the values assumed for the decay constants of $K^{40}$. These quantities are extremely small and, consequently, interference from common calcium will almost certainly be excessive. Recently, Ahrens[14] has been able to establish beyond reasonable doubt that the age of pegmatites from southeast Manitoba, Canada, is extremely great; using the available data (five $Sr^{87}/Rb^{87}$ age determinations and two $Pb^{207}/Pb^{206}$ age determinations), an age of $2100\times10^6$ years was assigned to these pegmatites. At this extreme age, sufficient quantities of $Ca^{40}$ would have been generated in leipdolite now containing 0.00091 percent $K^{40}$ to permit spectrochemical analysis.

[12] L. H. Ahrens, Bull. Geol. Soc. Am., in press (1948).
[13] A. O. Nier, Phys. Rev. **50**, 1041 (1936).
[14] L. H. Ahrens, Nature **160**, 874 (1947).

## ANALYTICAL

A spectrochemical procedure was employed for determining calcium quantitatively: a brief description of the procedure is as follows.

To avoid the use of synthetic standards, a specimen of lepidolite (Pala, California) was chosen, the calcium content of which was extremely low (~0.002 percent); CaO was added to this base material to provide standards containing up to 0.32 percent Ca. After admixture of each standard (1 part) with the purest carbon powder available (2 parts) each specimen was arced to completion, using d.c. arc anode excitation. From these spectra, a working curve was prepared, by means of which the calcium contents of the unknowns were determined after each had been prepared and arced as described before. Reproducibility was reasonably good, and the standard deviation was about ±10 percent per single determination. Unfortunately, below about 0.02–0.03 percent Ca, the blank error, due in part to the small amount of calcium in the Pala lepidolite and in the main to calcium impurity in the carbon, became serious; consequently, the limit of experimental error for specimens containing 0.01–0.03 percent Ca is considered to be about ±30 percent. Below 0.01 percent Ca, calcium determinations were made indirectly, using hydrofluoric acid residues (see Ahrens[12]) of lepidolite. By using some HF residues of lepidolite, which are relative rich in calcium and are of known calcium content, as secondary standards, calcium determinations could be made on specimens containing 0.001–0.01 percent Ca.

## ANALYTICAL RESULTS

In Table I, the calcium contents of 4 specimens of lepidolite from southeast Manitoba are given; in addition, quantitative data are also provided for 22 other specimens of lepidolite so as to obtain a reasonably accurate indication of the quantities of calcium likely to be found in lepidolite.

Excluding the s.e. Manitoba specimens and specimen No. 11, the high calcium content of which is quite exceptional, the mean calcium content of 21 specimens is 0.010 percent. Figure 2 is a frequency-distribution histogram of the Ca content of these 21 samples. In the 11 pre-Cambrian specimens (age = $850\times10^6$ years) which also average 0.010 percent Ca, the radiogenic calcium is probably 0.001 percent, and has a maximum value of 0.003 percent even if one uses Bleuler and Gabriel's decay constants. Consequently, the mean non-radiogenic calcium content in lepidolites is of the magnitude 0.008 to 0.010 percent.

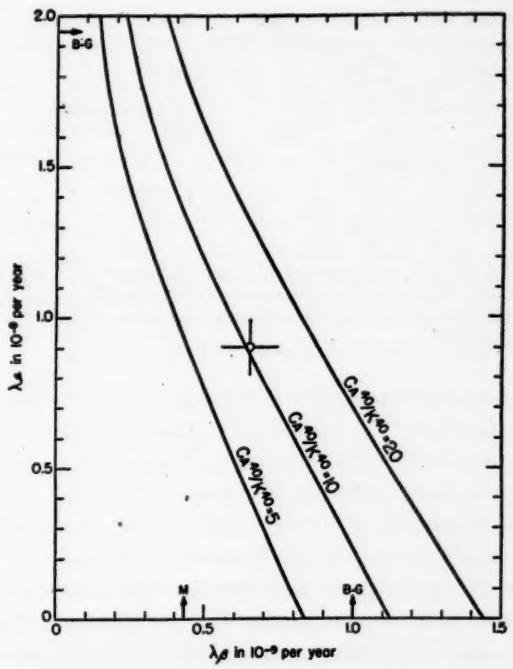


FIG. 3. The three curves show the simultaneous values of $\lambda_\epsilon$ and $\lambda_\beta$ of $K^{40}$ which in $2.1\times10^9$ years will give $Ca^{40}/K^{40}$ ratios of 5, 10, and 20. Measured values of $\lambda_\beta$ and $\lambda_\epsilon$ are shown by arrows marked *M* for Mühlhoff and *B-G* for Bleuler and Gabriel. Taking a value of $\lambda_\beta=(0.65\pm0.1)\times10^{-9}$ per year, and our observed ratio $Ca^{40}/K^{40}=11$, leads to $\lambda_\epsilon=(0.9\pm0.1)\times10^{-9}$, as shown by the single point near the middle of the graph.

All four specimens of lepidolite from s.e. Manitoba are characteristically high in calcium. Furthermore, the three specimens of lowest calcium content contain essentially the same amount of calcium (0.020 percent). This evidence strongly indicates that a significant portion of the total calcium in these 3 samples is radiogenic. It may be added further, that the high calcium content of these specimens provides the first direct indication of the formation of $Ca^{40}$ from the decay of $K^{40}$; it will be recalled that although $\beta$-activity of $K^{40}$ is well established and hence $Ca^{40}$ should be generated, no proof of the accumulation of $Ca^{40}$ in old, potassium-rich minerals has been made previously.

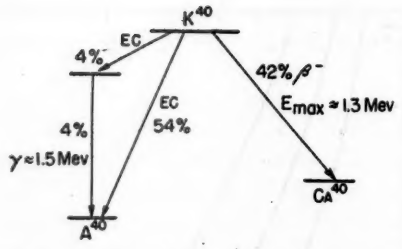


FIG. 4. Decay scheme of $K^{40}$, according to Eqs. (1), (7), and (8). Approximately 54 percent of the disintegrations of $K^{40}$ appear to be by electron capture to the ground state of $A^{40}$.

Arrangements have been made with Professor A. O. Nier to perform a mass-spectrometric analysis of Ca to be separated chemically from a new larger sample of ancient lepidolite from the Winnipeg River area. Professor Nier estimates that as little as 5 percent radiogenic $Ca^{40}$ can be successfully measured, when mixed with 95 percent non-radiogenic Ca, by measurements of the $Ca^{44}/Ca^{40}$ ratio. When available, these measurements will greatly reduce the uncertainties in our interpretation of the data of Table I. Also, Professor P. M. Hurley is collaborating in securing $A^{40}$ analyses of lepidolites and of other selected minerals. It is to be noted that the $A^{40}$ content would be of the order of 0.1 cc per gram in an ancient ($\sim 2\times 10^9$ yr.) lepidolite, and could not possibly have been retained quantitatively. Consequently, definitive studies of $A^{40}$ accumulation must be made either on very young lepidolites, or on minerals containing less potassium. It seemed unwise, however, to delay further the publication of the present results, both because of current general interest in the $K^{40}$ problem and because Dr. Ahrens is moving from the Massachusetts Institute of Technology to England.

We may reasonably assume that sample No. 3 of Table I contains a larger quantity of non-radiogenic Ca than the other three ancient samples, whose average Ca content is 0.020 percent. Deducting 0.010 percent as an average non-radiogenic Ca content of lepidolite (Fig. 2), we have an estimated excess Ca content of 0.010 percent for samples 1, 2, and 4, which is assumed to be $Ca^{40}$. It is to be noted that the maximum possible $Ca^{40}$ content of these 3 samples would be 0.020 percent if we made the unreasonable, but limiting, assumption that they contain no non-radiogenic Ca. Taking the K content of lepidolite as $8.5\pm 0.5$ percent, and hence the $K^{40}$ content as $0.00091\pm 0.00005$ percent, the most probable value of the $Ca^{40}/K^{40}$ ratio is $0.010/0.00091 = 11$. The maximum possible ratio, assuming that all the Ca is radiogenic $Ca^{40}$, and adding the reasonable geochemical assumption that no Ca is lost during geological time, is $0.020/0.0091 = 22$. This value could be raised further only by invoking our estimated limit of error of 30 percent in the Ca analysis.

### THE DECAY CONSTANTS OF $K^{40}$

The decay constants of $K^{40}$ reported by Bleuler and Gabriel predict a $Ca^{40}/K^{40}$ ratio of 152 for a mineral of $2.1\times 10^9$ years age. This is 7 times the maximum possible value obtained in our measurements, and 14 times our most probable value of $Ca^{40}/K^{40} = 11$. Reference to Fig. 1 shows that the observed $Ca^{40}/K^{40}$ ratio is consistent with a range of total decay constants $(\lambda_e+\lambda_\beta)$ between 1.2 and $2.2\times 10^{-9}$ per year with $\lambda_e$ between 0 and $1.9\times 10^{-9}$ per year.

In the introduction we pointed out that the omission of corrections for back scattering of $\beta$-rays from the brass source holders has the effect of making Mühlhoff's value of $\lambda_\beta = 0.434\times 10^{-9}$ per year too low, and also of making Bleuler and Gabriel's value of $\lambda_\beta = 1.0\times 10^{-9}$ per year too high. Thus the true value probably lies between these two limits, and may be close to $0.65\times 10^{-9}$ per year if we arbitrarily assign a 50 percent back-scattering error to each of these direct measurements.

Figure 3 shows three curves of constant $Ca^{40}/K^{40}$ ratios obtained from Eq. (6), and bracketing the values observed from the Manitoba lepidolites, plotted against $\lambda_\beta$ and $\lambda_e$ as independent variables, for $t = 2.1\times 10^9$ years. Taking:

$$\lambda_\beta' = (0.65\pm 0.1)\times 10^{-9} \text{ per year}, \quad (7)$$

and $Ca^{40}/K^{40} = 11$, leads to the value:

$$\lambda_e = (0.9\pm 0.1)\times 10^{-9} \text{ per year}, \quad (8)$$

or a total decay constant and half-period for $K^{40}$ of:

$$\lambda_e+\lambda_\beta = (1.55\pm 0.15)\times 10^{-9} \text{ per year}, \quad (9)$$

$$T = (0.45\pm 0.05)\times 10^9 \text{ years}. \quad (10)$$

These estimated probable errors have the usual significance of denoting even odds that the true

value lies within or outside the limits specified. Similarly, the "limit of error" would be given its usual value of 3 probable errors, and would specify a band having a 96 percent chance of containing the true value.

## DISCUSSION

The numerical values suggested in Eqs. (7) to (10) will, of course, be subjected to further improvement by independent measurements of $A^{40}$ accumulation in K minerals, and by new measurements of the x-rays and $\beta$-rays from samples of K enriched in $K^{40}$. As it may be a year or so before suitably enriched samples become available, it is worth noting that the disproof of Bleuler and Gabriel's decay constants requires also the modification of Birch's and of Gleditch and Gráf's conclusions.

The decay scheme of $K^{40}$, with revised branching ratios corresponding to Eqs. (1), (7), and (8), is shown in Fig. 4. The specific activity of ordinary potassium (0.011 percent $K^{40}$) would then be 34 $\beta$-rays per second per gram of potassium.

The total heat production per gram of ordinary potassium is then: 4.9 Mev/sec. for the $\gamma$-rays, plus approximately[15] $0.49\pm0.06$ Mev per $\beta$-ray or $34\times0.49=16.6$ Mev/sec. for the $\beta$-rays. This amounts to a total of about 22 Mev/sec., or $26\times10^{-6}$ cal. per year per gram of potassium. This estimate of the heat output should replace the early value of $5\times10^{-6}$ cal./yr. g by Evans and Goodman,[16] which was based on Mühlhoff's decay constant, Anderson and Neddermeyer's[17] $\beta$-ray energy, and Gray and Tarrant's[18] gamma-ray emission, all three of which were too low in the light of more recent measurements. This revised heat output also replaces Gleditch and Gráf's value of $38\times10^{-6}$ cal./yr. g, which uses Bleuler and Gabriel's decay constants. Birch[2] has pointed out that Bleuler and Gabriel's short half-period of $0.24\times10^{9}$ years, if accepted, would require re-evaluation of a number of important geophysical problems. In particular, the heat output[1] of potassium 1 to $1.5\times10^{9}$ years ago would have been too great to have permitted a permanent crust to exist on the earth. Our value of the half-period of $K^{40}$ is essentially twice that of Bleuler and Gabriel, and of course leads to very much lower values of the heat production at times comparable with the age of the earth. Illustrative numerical values are given in Table II, where it is seen, for example, that our estimate of the heat production by potassium $2\times10^{9}$ years ago is only about 5 percent as large as Gleditch and Gráf's value. Even if our smaller values are confirmed by further work on the radioactive properties of $K^{40}$, the heat production by radioactive decay $2\times10^{9}$ years ago would have been due mainly to $K^{40}$, which would then have exceeded the heat production by uranium and thorium[16,19] in all classes of igneous rocks.

TABLE II. Calculated heat production by the $K^{40}$ associated with 1 gram of $K^{39}$ and $K^{41}$, i.e., heat production per gram of *residual* potassium, as a function of geological time, $t$, measured backwards from the present, for two values of the half-period $T$, and of the present heat output $H_0$ per gram of potassium.

| | Time $t$ in $10^9$ years | | | | | |
|---|---|---|---|---|---|---|
| | 0 | 0.5 | 1.0 | 1.5 | 2.0 | 2.5 |
| $10^{-6}$ cal./yr. g K if $T=0.24\times10^9$ yr. and $H_0=38\times10^{-6}$ cal./yr. g K | 38. | 162. | 690. | 2920. | 12500. | 53200. |
| $10^{-6}$ cal./yr. g K if $T=0.45\times10^9$ yr. and $H_0=26\times10^{-6}$ cal./yr. g K | 26. | 57. | 122. | 388. | 577. | 1260. |

From the standpoint of the general theory of forbidden $\beta$-ray transformations, it was thought[20] some years ago that accurate knowledge of the $\beta$-ray energy and the half-period of $K^{40}$ would be crucial in deciding between the tensor and polar vector interactions, because it is known[21] that the nuclear angular momentum of $K^{40}$ is 4, while that of $Ca^{40}$ is probably zero. Marshak[22] has shown, however, that this is actually not the case, and that the shape of the $\beta$-ray spectrum, not its maximum energy, is destined to become the decisive evidence in settling the form of the interaction. Thus, the present results do not modify existing $\beta$-ray theory.

The average potassium content of mammalian tissues is about 0.11 percent, and varies in

[15] L. D. Marinelli, R. T. Brinckerhoff, and G. J. Hine, Rev. Mod. Phys. 19, 25 (1947).
[16] R. D. Evans and C. Goodman, Bull. Geol. Soc. Am. 52, 459 (1941).
[17] C. D. Anderson and S. H. Neddermeyer, Phys. Rev. 45, 653 (1934).
[18] L. H. Gray and G. T. P. Tarrant, Proc. Roy. Soc. 143A, 681 (1934).
[19] R. D. Evans, C. Goodman, and N. B. Keevil, Geol. Soc. Am., Sp. Paper No. 36, 269 (1942), edited by F. Birch.
[20] E. J. Konopinski, Rev. Mod. Phys. 15, 209 (1943).
[21] J. R. Zacharias, Phys. Rev. 61, 270 (1942).
[22] R. E. Marshak, Phys. Rev. 70, 980 (1946).

humans from 0.19 mg K/g of blood serum to 4.20 mg K/g red blood cells. The average potassium content of sea water is 0.39 mg/g of water. Because this is only about 2.6 percent of the K which has been released by the decomposition of crustal rocks, it is assumed that the remainder has been adsorbed and is to be found in sedimentary deposits. Thus, the K content of the oceans may be assumed to have been at substantially its present concentration for at least the major portion of the earth's history. Suggestions have reappeared[23] recently concerning the possible early importance of the radiations from $K^{40}$ on mutations and on the origin of species. Taking 4.9 Mev of $\gamma$-radiation plus 16.6 Mev of $\beta$-radiation per second per gram of potassium as the present rate of energy release, it can be shown from the ordinary principles of radiation dosage[24,25] that the K content of sea water now produces, on organisms whose dimensions are small compared with the range of the $\beta$-rays of $K^{40}$, a tissue dosage of only $1.4\times10^{-5}$ rep./day. Taking the half-period of $K^{40}$ as $0.45\times10^{9}$yr. and the K constant of ocean water as constant with respect to time, the corresponding tissue dosage $1.0\times10^{9}$ yr. ago would have been $0.066\times10^{-3}$ rep./day, while $2.0\times10^{9}$ yr. ago the dosage would have been $0.31\times10^{-3}$ rep./day. These are very small dosages, and can hardly be held accountable for any significant degree of mutation induced by radiation. By way of comparison, the cosmic radiation at sea level gives[24] a tissue dosage of $0.10\times10^{-3}$ rep./day. On the other hand, a total dosage of about 50 rep. per generation is required to double the natural mutation rate in lower organisms.

[23] F. Ellis, Brit. J. Radiology **21**, 1 (1948).

[24] R. D. Evans, Am. J. Roent. **58**, 754 (1947).
[25] R. D. Evans, Nucleonics **1**, No. 2, 32 (October 1947).

PHYSICAL REVIEW VOLUME 74, NUMBER 3 AUGUST 1, 1948

# Effect of Large Quadrupole Interactions on Nuclear Radiofrequency Spectra at Twice Larmor Frequency

NORMAN F. RAMSEY
*Harvard University,* Cambridge, Massachusetts*
(Received April 17, 1948)

The work of B. T. Feld and W. E. Lamb [Phys. Rev. **67**, 15 (1945)] on the effect of a nuclear electrical quadrupole moment on the radiofrequency absorption spectrum of a heteronuclear diatomic molecule in a magnetic field is extended to a special case not considered by them. This is a case in which the electrical quadrupole interaction energy is so large that even in magnetic fields of several thousand gauss the magnetic interaction energies are small compared to the electrical quadrupole interaction energy. In this case it is shown theoretically that for a spin of $\frac{3}{2}$ there are certain circumstances under which a maximum of absorption will occur at double the Larmor frequency instead of at the Larmor frequency and will have a field and molecule dependence similar in many ways to a resonance at the Larmor frequency. This result has the important implication that special care must be used in identifying the radiofrequency resonance absorption spectra or an error of a factor of two in the value of a nuclear magnetic moment can easily be made. The approximate shape and intensity of the radiofrequency absorption spectrum under these circumstances is calculated in order that a comparison of the theoretical shapes and intensities with the experimental ones can be used as a means of recognizing if an absorption is a double Larmor frequency one.

## I. INTRODUCTION

DETAILED consideration has been given by Feld and Lamb[1] to the effect of a nuclear electrical quadrupole moment on the radiofrequency absorption spectra of heteronuclear diatomic molecules in magnetic fields as such spectra are observed in the molecular beam resonance method.[2-4] Although Feld and Lamb[1]

* Part of this work was done at Columbia University.
[1] B. T. Feld and W. E. Lamb, Phys. Rev. **67**, 15 (1945).

[2] Rabi, Millman, Kusch, and Zacharias, Phys. Rev. **55**, 526 (1939).
[3] Kellogg, Rabi, Ramsey, and Zacharias, Phys. Rev. **56**, 728 (1939).
[4] Kellogg, Rabi, Ramsey, and Zacharias, Phys. Rev. **57**, 677 (1940).

in the third section of their paper consider the case in which the electrical quadrupole interaction energy is large compared with the magnetic interaction energy, they do so from the point of view of considering the magnetic field to be very weak. Consequently, they omit consideration of transitions for which there is no difference of quadrupole energy since in a very weak magnetic field the resonance absorption would occur at frequencies below those at which measurements are usually made. However, in the case of a very large quadrupole interaction energy of the order of several hundred megacycles (as found by Townes, Holden, Bardeen, and Merritt[5] in such molecules as BrCN) the limit of quadrupole interaction being large compared to the magnetic interaction can be achieved in magnetic fields of several thousand gauss, for which the resonance absorption will be at several megacycles even for transitions for which there is no difference in quadrupole energy.

The purpose of this paper is to consider such transitions in detail for the case of nuclear spin $\frac{3}{2}$ and heteronuclear diatomic molecules. Since the same terminology and symbolism will be used here as in Feld and Lamb,[1] the definitions of the various quantities will not be repeated.

A preliminary indication as to the nature of the results to be expected can be obtained by differencing the middle two equations of the group designated as III (18) by Feld and Lamb,[1] in which case to the first order and for negligibly small $g_J$.

$$W(+,m;-,m-1)=2\mu_0 g_I H(1-\tfrac{3}{4}z^2)^{\frac{1}{2}}. \quad (1)$$

Since $z$ can vary between $+1$ and $-1$ this means that transitions will occur at frequencies between

$$\nu=W(+,m;-,m-1)/h=\mu_0 g_I H/h \quad (2)$$

when $z=\pm 1$, and

$$\nu=2\mu_0 g_I H/h$$

when $z=0$. That is, transitions occur at all frequencies between the Larmor frequency and twice that frequency. A preliminary indication of the frequency at which the effect of the resonance absorption will be greatest can be obtained by calculating the density of transitions

$$D=1/(dW/dz)=-2(1-\tfrac{3}{4}z^2)^{\frac{1}{2}}/3\mu_0 g_I H z, \quad (3)$$

which becomes infinite for $z=0$. Since, as will be shown later, the transition probability is only a slowly varying function of $z$, the effect of the resonance absorption will be greatest when $z=0$, i.e., at twice the Larmor frequency.

Although this preliminary discussion is adequate to indicate partially the nature of the result, it is not adequate to determine the shape of the resonance curve, since the assumption of a very large quadrupole interaction of the order of several hundred megacycles invalidates the assumption made by Feld and Lamb that $J$ may be regarded essentially as infinite since the small added terms arising from the finiteness of $J$ are multiplied by a large factor determined by the quadrupole interaction so that the product of the two is quite comparable to the energy change in the transition considered.

## II. ENERGY VALUES

For quadrupole interactions much stronger than magnetic interactions with the external magnetic field, a representation in terms of a total angular momentum $\mathbf{F}=\mathbf{I}+\mathbf{J}$ may best be used as in Feld and Lamb (reference 1, page 24).

Calculation of the energy values for $I=\frac{3}{2}$ is complicated by the fact that the unperturbed (zero field) energy levels are degenerate to the extent to which $J$ may be taken as infinite. Although the finite value of $J$ removes this degeneracy in the case of a very large quadrupole interaction, it does so only by an amount comparable to or smaller than the magnitude of the magnetic interaction with the external field. Furthermore, there exist non-vanishing matrix elements of this magnetic interaction between the states $F=J+\frac{1}{2}$ and $F=J-\frac{1}{2}$. Consequently, these states are mixed by the application of the external magnetic field. The determination of the energy levels can be accomplished by solving the secular equation for a typical value of $m$ or of $z=m/J$ since the matrix is diagonal in $m$.

As in Casimir[6] and in Feld and Lamb (reference 1, pages 19 and 25), the Hamiltonian for

[5] Townes, Holden, Bardeen, and Merritt, Phys. Rev. 71, 644 (1947).

[6] H. B. G. Casimir, "On the interaction between atomic nuclei and electrons," Archives du Musée Teyler (III) 8, 201 (1936).

the relevant interactions is

$$\mathcal{H}=\mathcal{H}_Q+\mathcal{H}_M, \quad (4)$$

where

$$\mathcal{H}_Q=-[e^2q'Q/(2J+3)(2J-1)I(2I-1)] \times[3(\mathbf{I}\cdot\mathbf{J})^2+\tfrac{3}{2}(\mathbf{I}\cdot\mathbf{J})-I(I+1)J(J+1)] \quad (5)$$

and

$$\mathcal{H}_M=\mu_0 g_I H I_z, \quad (6)$$

where $g_J$ is taken as approximately equal to zero for simplification and the sign convention of Feld and Lamb is used in (6). Note that, in the above, $q$ which is used by Feld and Lamb[1] and which is dependent[7] on $J$ is replaced by $q'$ used by Nordsieck where

$$q=-[2J/(2J+3)]q',$$

since $q'$ is independent of $J$.[7] In two recent papers by Feld[8] and by Bardeen and Townes[9] alternative expressions for the interaction constant have been given. The relation of the $q'$ of the present paper to the $\partial^2V/\partial z^2$ of Feld[8] and the $q$ of Townes[9] is

$$q'=(1/2e)(\partial^2V/\partial z^2)=(1/2e)q.$$

The matrix elements $(F, m|\mathcal{H}|F', m)$ of $\mathcal{H}$ can be evaluated with the aid of Eqs. III (5) and III (11) of Feld and Lamb. The result after simplification is that for a single value of $m$ or $z$ all the non-zero matrix elements are one of the following:

$$\begin{aligned}
&(J+\tfrac{3}{2}, m|\mathcal{H}|J+\tfrac{3}{2}, m)=-a(1-\gamma)+\tfrac{3}{2}bz,\\
&(J+\tfrac{1}{2}, m|\mathcal{H}|J+\tfrac{1}{2}, m)=a(1+\gamma)+\tfrac{1}{2}bz,\\
&(J-\tfrac{1}{2}, m|\mathcal{H}|J-\tfrac{1}{2}, m)=a(1-\beta)-\tfrac{1}{2}bz,\\
&(J-\tfrac{3}{2}, m|\mathcal{H}|J-\tfrac{3}{2}, m)=-a(1+\beta)-\tfrac{3}{2}bz,\\
&(J+\tfrac{1}{2}, m|\mathcal{H}|J+\tfrac{3}{2}, m)=(J+\tfrac{3}{2}, m|\mathcal{H}|J+\tfrac{1}{2}, m)\\
&\qquad=(J-\tfrac{3}{2}, m|\mathcal{H}|J-\tfrac{1}{2}, m)\\
&\qquad=(J-\tfrac{1}{2}, m|\mathcal{H}|J-\tfrac{3}{2}, m)\\
&\qquad=\tfrac{1}{2}\sqrt{3}b(1-z^2)^{\frac{1}{2}},\\
&(J-\tfrac{1}{2}, m|\mathcal{H}|J+\tfrac{1}{2}, m)=(J+\tfrac{1}{2}, m|\mathcal{H}|J-\tfrac{1}{2}, m)\\
&\qquad=b(1-z^2)^{\frac{1}{2}},
\end{aligned} \quad (8)$$

where

$$a=e^2q'Q/4, \quad b=\mu_0 g_I H,$$
$$\gamma=3/(2J+3), \quad \beta=3/(2J-1).$$

Although in the above the effect of the finite size of $J$ is included in the large quadrupole interaction, $J$ is taken as essentially infinite in the much smaller magnetic interaction.

Since there are no matrix elements connecting the approximately degenerate states $J+\frac{3}{2}$ and $J-\frac{3}{2}$ and since $J\pm\frac{3}{2}$ is far from degenerate with $J\pm\frac{1}{2}$, the secular equation will approximately factor and the relevant factor for states involving $J\pm\frac{1}{2}$ is

$$(a+\gamma a+\tfrac{1}{2}bz-E)(a-\beta a-\tfrac{1}{2}bz-E) -b^2(1-z^2)=0, \quad (9)$$

whence

$$E=a[1+(\gamma-\beta)/2]\pm b[(1-\tfrac{3}{4}z^2) +\tfrac{1}{2}((\gamma+\beta)a/b)z+((\gamma+\beta)^2a^2/4b^2)]^{\frac{1}{2}}. \quad (10)$$

However, for large $J$ we have two terms of order $1/J$:

$$\begin{aligned}
&\gamma-\beta=-10/(2J+3)(2J-1)\approx-5/2J^2\approx0,\\
&\gamma+\beta=6(2J+1)/(2J+3)(2J-1)\approx3/J.
\end{aligned} \quad (11)$$

Hence, to this order

$$E(\pm, m)=a\pm b[(1-\tfrac{3}{4}z^2) +\tfrac{3}{2}(a/Jb)z+\tfrac{9}{4}(a/Jb)^2]^{\frac{1}{2}}. \quad (12)$$

Since in (12) $z$ is not multiplied by the large factor $a$ but only by the much smaller factors of the order of $b$ or $(a/J)$, $J$ may be considered to be sufficiently large that the change in $z=m/J$ for $\Delta m=\pm1$ may be neglected. In this case, with the notation of Feld and Lamb (reference 1, page 28)

$$W(+, m; -, m\pm1)=2b[(1-\tfrac{3}{4}z^2) +\tfrac{3}{2}(a/Jb)z+\tfrac{9}{4}(a/Jb)^2]^{\frac{1}{2}} \quad (13)$$

or, by rearrangement,

$$W(+, m; -, m\pm1)=2b \times[[1-\tfrac{3}{4}(z-(a/Jb)^2)]+3(a/Jb)^2]^{\frac{1}{2}}. \quad (14)$$

From (14), $z$ can be expressed in terms of $W\equiv W(+, M; -, M\pm1)$ as

$$z-(a/Jb)=\pm(2/\sqrt{3}) \times[1-(W/2b)^2+3(a/Jb)^2]^{\frac{1}{2}}. \quad (15)$$

Since $z$ must, by definition, be real and of absolute value less than one, $J$ and $W$ in this equation must be restricted to values such that this occurs. It may readily be seen from (15) that an absolute value of less than one is insured for $z$ provided

$$|a/Jb|<0.2 \quad \text{and} \quad |W/2b|>0.9, \quad (16)$$

[7] A. Nordsieck, Phys. Rev. **58**, 310 (1940).
[8] B. T. Feld, Phys. Rev. **72**, 1116 (1947).
[9] J. Bardeen and C. H. Townes, Phys. Rev. **73**, 97 (1948).

or provided

$$|a/Jb|<0.3 \quad \text{and} \quad |W/2b|>1.0. \quad (17)$$

These restrictions are not serious since the maximum of the resonance spectra, which is the part of interest, is at an energy consistent with these restrictions. The reality of $z$, which is a more pertinent restriction since the maximum occurs near $z=0$, is insured provided the $J$ contributing to any energy $W$ is restricted by

$$J\leqslant[3(a/b)^2/((W/2b)^2-1)]^{\frac{1}{2}}. \quad (18)$$

### III. THE SPECTRUM

For a single $J$, the "density of transitions" as defined by Feld and Lamb is

$$D=\tfrac{1}{2}[|dz/dW|_+ + |dz/dW|_-] = W/2b^2\sqrt{3}[1-(W/2b)^2+3(a/Jb)^2]^{\frac{1}{2}}, \quad (19)$$

where the subscripts + and − correspond to the two different signs in (15) and where the normalization is such that $DdW$ gives the probability that a molecule in rotational state $J$, with $F=+$, and with $m$ randomly selected will have a transition energy between $W$ and $W+dW$.

This density of transition must be multiplied by the transition probability, $p$. It may be readily confirmed that the transition $(+, m; -, m\pm1)$ is an allowed transition. This may be most easily done in the limit of infinite $J$ in which case the quantity $P$ of Feld and Lamb which is proportional to the transition probability for weak oscillating fields becomes

$$P(+, m; -, m-1) = \mu_0^2 g_I^2 H_x'^2 (+, m|I_x|-, m\pm1)^2. \quad (20)$$

The matrix element in (20) may readily be evaluated from Feld and Lamb's Eqs. III (16), III (17), and III (11). The resulting expression for (20) becomes

$$P(+, m; -, m\pm1) = \tfrac{1}{4}[1+(1/2(1-\tfrac{3}{4}z^2)^{\frac{1}{2}})]^2\mu_0^2 g_I^2 H_x'^2. \quad (21)$$

This is finite, varies by only a factor of two in the allowed range of $z$, and is comparable in magnitude to the values of $P$ of Feld and Lamb. Consequently, the transition is completely an allowed one. If the procedure of Feld and Lamb were followed, Eq. (19) would be multiplied by Eq. (21). However, in most of the relevant experiments Feld and Lamb's assumption of a weak oscillating field does not apply whence (21) does not give the actual transition probability. Instead, such a strong oscillating field is used that the net transition probability is of the order of one-third for non-forbidden transitions. Consequently, the transition probability at present will merely be taken as an approximately constant quantity $p$ which is less than one and of the order of one-third. Since the transitions from $m$ to both $m+1$ and $m-1$ occur, the effective probability as concerns the line intensity is $2p$.

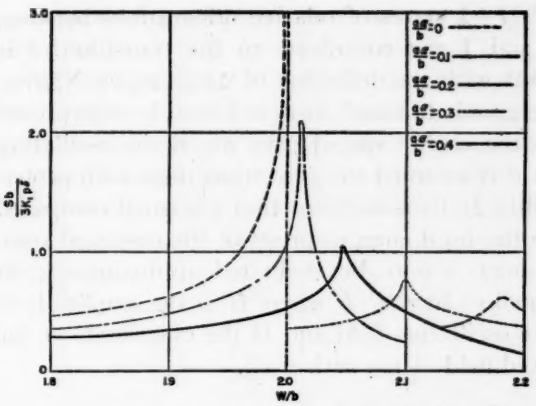


FIG. 1. $Sb/(3K_1p\delta)$ as a function of $W/b$ for different values of $a\alpha/b$.

The resonance line intensity contributed by a single molecule in rotational state $J$ with $F=+$ then would be $2pD$. For all the molecules, let $S$ be the ratio of the intensity of the resonance at frequency $W/h$ to the intensity of the entire beam. Then

$$S=\frac{\dfrac{2K_1\delta}{2I+1}\displaystyle\int_0^\infty 2pD2J\exp[-\alpha^2J^2]dJ}{\displaystyle\int_0^\infty 2J\exp[-\alpha^2J^2]dJ}, \quad (22)$$

where[10]

$$\alpha^2=h^2/8\pi^2I_0kT=(\pi/4)(1/(\bar{J})^2), \quad (23)$$

and $K_1$ is a factor introduced[10] to compensate for lack of complete deflecting power of the apparatus; $K_1$ is necessarily of a magnitude less than unity. $2/(2I+1)$ is introduced because only 2 out

[10] W. A. Nierenberg and N. F. Ramsey, Phys. Rev. **72**, 1075 (1947).

of $2I+1$ states of relative orientations between $\mathbf{I}$ and $\mathbf{J}$ can contribute to the transition. $\delta$ is $2h\Delta\bar{\nu}$ with the definition of $\Delta\bar{\nu}$ given by Nierenberg and Ramsey[10] so that $\delta$ may be interpreted as the energy spread over which the oscillating field is assumed to cause transitions with probability $2p$ (it is assumed that $\delta$ is small compared to the total energy spread of the observed resonance). $\delta$ may be evaluated approximately as equal to $2\Delta=H'/H$ where $H'$ is the amplitude of the oscillating field and $H$ the magnitude of the fixed field. Then with $I=\frac{3}{2}$,

$$S=K_1\delta\alpha^2 p(W/b^2\sqrt{3})\times\int_0^\infty \frac{J\exp[-\alpha^2J^2]dJ}{[1-(W/2b)^2+3(a/Jb)^2]^{\frac{1}{2}}}, \quad (24)$$

where the integration must be carried out consistent with conditions (16), (17), and (18).

For purposes of convenient integration, the function $J\exp[-\alpha J^2]$ in (24) may be replaced by a rectangular step function which affords the closest fit to the original function and which has the same area, that is, the function is replaced by

$$F(J)=1/2.8\alpha \quad \text{for} \quad 0.2/\alpha<J<1.6/\alpha$$
$$=0 \text{ elsewhere.} \quad (25)$$

With this approximation the integration in (24) can readily be carried out with the result that

$$Sb/3K_1p\delta=(1/7.28)[(W/2b)/(1-(W/2b)^2)]\times[[[1-(W/2b)^2]2.6+3(a\alpha/b)^2]^{\frac{1}{2}}-[[1-(W/2b)^2]0.04+3(a\alpha/b)^2]^{\frac{1}{2}}] \quad (26)$$

where the condition (18) is automatically satisfied if any imaginary square root in (26) is replaced by zero.

From (26), $Sb/3K_1p\delta$ can be numerically evaluated as a function of $W/2b$ for different assumed values of $a\alpha/b$ with the result that a rather general family of curves can be plotted. With this family, the predicted line shape for a specific set of values of $b$, $p$, $\delta$, $\alpha$, etc., can be obtained by suitable multiplications of the ordinates and abscissae. This family of curves is given in Fig. 1.

## IV. DISCUSSION

Since $W/b$ is equal the ratio of the observed frequency to the Larmor frequency, it can be seen that the spectral maximum (beam intensity minimum) is at approximately double the Larmor frequency as anticipated in the introduction.

It can also be seen that there are allowable combinations of nuclear and molecular constants for which this double frequency resonance is observable. If $3K_1p$ is taken as 1, if $\delta$ is taken as 0.02 which is reasonable for $H'/H$ and if $a\alpha/b<0.3$, then $S$, the line strength is greater than 1.4 percent which is easily observable. For $\alpha\approx0.2$, this implies

$$a<15b,$$

which is consistent with the requirement of $a\gg b$ in order for this coupling scheme to hold. As smaller intensity resonances are observable on a molecular beam apparatus than $S=1.4$ percent, a wider range of allowable ratios of $a/b$ is possible to obtain this effect. However, it is noteworthy that with high fixed magnetic fields the allowable range of $a/b$ consistent with both observable intensity and occurrence of the resonance near the double frequency is rather small. Consequently, although this phenomenon must be guarded against in magnetic moment measurements with diatomic molecules, its occurrence is rather unlikely at high fixed fields and weak oscillating fields. As $H'/H$ is increased the likelihood of observing this phenomenon is markedly increased.

It should be noted that the intensities predicted by Eq. (26) and Fig. 1 depend upon the assumption that the molecule is strictly a diatomic one. The intensities could be markedly different if the molecule concerned were an associated molecule such as $(LiBr)_n$ with $n>1$.

To a first approximation the position of the resonance maximum will shift in proportion to $H$ and will occur at approximately the same position in different molecules provided only that the quadrupole interaction is sufficiently similar for the assumed coupling to apply in both cases. These characteristics are particularly unfortunate since they provide the usual criteria for identifying the resonance as associated with the Larmor frequency of the common nucleus. However, a comparison of the experimental shape, intensity, and exact $H$ dependence of the resonance with the theoretical ones here pre-

sented provides a means of identification of whether the observed resonance is a double frequency one.

In a separate paper by Brody, Nierenberg, and Ramsey[11] the theory here presented is applied to identify the Br and Cl resonances. Consideration is now being given to generalizing this study to other odd integral spins since similar results would be expected in these cases since the $J+\frac{1}{2}$ and $J-\frac{1}{2}$ states will be approximately degenerate in these cases also. Further study of the case of intermediate coupling is also contemplated.

The author wishes to thank Professor I. I. Rabi for several helpful discussions in the course of this work.

[11] S. B. Brody, W. A. Nierenberg, and N. F. Ramsey, Phys. Rev. **72**, 258 (1947), and a full paper in course of preparation.

PHYSICAL REVIEW VOLUME 74, NUMBER 3 AUGUST 1, 1948

# Breakdown of a Gas at Microwave Frequencies*

MELVIN A. HERLIN AND SANBORN C. BROWN
*Research Laboratory of Electronics, Massachusetts Institute of Technology, Cambridge, Massachusetts*

(Received April 15, 1948)

An electric field of sufficiently high frequency applied to electrons in a gas may deliver energy to the electrons without imparting to them any continuous drift motion resulting from the field. The criterion for breakdown of a low pressure gas at microwave frequencies is therefore that ionization by collision of electrons with neutral gas molecules replace loss by diffusion to the walls of the discharge tube. The condition is mathematically expressed as a simple boundary value problem. This breakdown principle is applied to converting microwave breakdown measurements into measurements of ionization rates as a function of the electric field strength, pressure, and frequency. A new ionization coefficient is introduced appropriate to the high frequency discharge conditions, and its relation to the d.c. Townsend coefficient is explained. The energy transfer from the electric field to the electrons at a given $E/p$ is shown to be most efficient when the pressure is high enough or the frequency low enough to result in many collisions of electrons with gas molecules per cycle. This maximum efficiency is equal to the d.c. energy transfer efficiency. When the pressure is lower or the frequency is higher, the electrons have an out-of-phase component of motion and do not receive energy so efficiently, resulting in lower ionization rates observed experimentally.

## I. INTRODUCTION

THE Townsend theory for breakdown of a low pressure gas under the action of a d.c. electric field postulates two sources of electrons. Most of the electrons are generated in the volume of the gas through ionization by collision. The original source of electrons at the cathode results from secondary emission caused by positive ion or photon bombardment. Prediction of breakdown voltage requires numerical data on the efficiency of these processes. Thus attempts to determine ionization coefficients from breakdown data have been complicated by the operation of two electron generation processes.

Breakdown caused by a high frequency electric field is determined by the primary ionization process only; the electrons formed at the walls or in the gas by secondary emission have a negligible effect. It is therefore possible to predict the electric field for breakdown from a knowledge of the ionization coefficient only, or to measure the ionization coefficient from a breakdown experiment.

* This work has been supported in part by the Signal Corps, the Air Materiel Command, and O. N. R.

## II. MOTION OF ELECTRONS IN A HIGH FREQUENCY FIELD

Under the action of a d.c. electric field an electron is accelerated by the field until it collides with a gas molecule. The direction of motion is then reoriented almost randomly. Most of the kinetic energy gained during the acceleration period is kept during the scattering process, since the mass of the molecule is large compared to that of the electron. After collision, the electron is accelerated or decelerated by the field, depending on the direction of the electron velocity

relative to the field. The randomly directed velocity immediately after collision contributes nothing to the flow of electrons along the field direction. Only the component of velocity produced by acceleration in the field, which is destroyed on the average by random scattering at each collision, contributes to an electron current in the field direction. The kinetic energy of the electrons is built up through successive accelerations until the loss of energy by elastic and inelastic collisions and diffusion equals the gain of energy from the field. The motion consists of a large random and a small drift component. The energy transferred to the electrons is a function of $E/p$, where $E$ is the electric field strength and $p$ is the pressure. This quantity determines the energy gained between the collisions.

If an a.c. field whose radian frequency is small compared to the collision frequency is applied to electrons, their motion will be identical in most respects with that of electron motion in a d.c. field. The field-induced motion is interrupted by collisions, which occur often during an a.c. cycle. The drift current of the electrons oscillates in phase with the field and the energy transfer will be the same as that in a d.c. field, if the r.m.s. value of the a.c. field strength is used.

As the frequency is increased or the pressure decreased, collisions no longer occur frequently enough to keep the electron drift current in phase with the field. The inertia of the electrons causes an out-of-phase component. The transfer of energy from the electric field to the electrons becomes less efficient. As the pressure goes to zero or the frequency becomes infinite, the electrons merely oscillate out of phase with the field and no energy is transferred on the time average. The energy transfer efficiency may be taken into account through an effective field,[1]

$$E_e^2 = E^2[(v/l)^2/(v/l)^2+\omega^2],$$

where $E$ is the r.m.s. value of the applied field, $v$ is the electron velocity, $l$ is the mean free path, $v/l$ is the collision frequency, $\omega$ is the radian frequency of the field, and $E_e$ is the effective field which would produce the same energy transfer at zero frequency. The frequency variable may be introduced as the quantity $p\lambda$, where $p$ is the gas pressure and $\lambda$ is the free-space wave-length of the excitation energy.[2] This variable determines the ratio of the collision frequency to the field radian frequency for electrons of a given velocity.

The oscillatory drift current is not capable of transporting electrons from one point to another in the discharge tube. It cannot account for loss of electrons to the walls of the tube, which is a principal electron withdrawal mechanism in discharges. Electron losses to the walls must therefore be caused by diffusion, resulting from the large random motion. If the electric field is not uniform there may also be a flow of electrons resulting from an electron "temperature," or kinetic energy gradient. Both of these flow terms may be included in the expression,[3]

$$\Gamma = -\nabla(Dn), \tag{1}$$

where $D$ is the diffusion coefficient for electrons, $n$ the electron density, and $\Gamma$ the electron current density in electrons per second per unit area. The product may be differentiated to yield two terms; $-D\nabla n$ is the usual diffusion current density, and $-n\nabla D$ is the current density due to the kinetic energy gradient. The diffusion coefficient is proportional to the average velocity of the electrons.

Since the current density vector is given as the gradient of the scalar quantity $Dn$ in Eq. (1), this quantity may be referred to as the current density potential. It has nothing to do with energy, but is analogous to the velocity potential used in hydrodynamics. This potential,

$$\psi = Dn, \tag{2}$$

will be used in the diffusion computations for the breakdown condition.

## III. BREAKDOWN CRITERION: BALANCE OF IONIZATION AGAINST DIFFUSION

The breakdown condition will be developed for a region in a resonant cavity bounded by walls which absorb electrons. A radioactive

[1] H. Margenau, Phys. Rev. 60, 508 (1946).

[2] H. Margenau, Phys. Rev. 73, 326 (1948).

[3] The formula $\Gamma = -\nabla(Dn)$ may be obtained most directly from an extension of the work of P. M. Morse, W. P. Allis, and E. S. Lamar, Phys. Rev. 48, 412 (1935). See also E. H. Kennard, *Kinetic Theory of Gases* (McGraw-Hill Book Company, Inc., New York, 1938), pp. 204–205.

source near the discharge cavity provides a small amount of ionization in the cavity. The microwave field in the cavity is gradually increased until the gas suddenly begins to glow, becomes conducting, and the field drops to a much lower value. The field necessary to produce this phenomenon is called the breakdown field.

A detailed study of the build-up of the discharge is obtained from considering the continuity equation for electrons,

$$\partial n/\partial t = \nu n - \nabla \cdot \Gamma \tag{3}$$

where $\nu$ is the net production rate of electrons per electron. It may be represented as the difference,

$$\nu = \nu_i - \nu_a,$$

where $\nu_i$ is the ionization rate per electron and $\nu_a$ the attachment rate to neutral molecules per electron. At breakdown the electron density is low enough to neglect the effects of space charge and recombination of electrons with positive ions in the volume of the gas.[4] Using the current density given by Eq. (1) and putting Eq. (3) in terms of the potential $\psi$, we obtain for the continuity equation,

$$(1/D)(\partial\psi/\partial t) = \nabla^2\psi + (\nu/D)\psi.$$

The time factor may be separated by putting,

$$\psi = \psi_0(x, y, z) \exp(-t/\tau).$$

The resulting equation for $\psi_0$ is

$$\nabla^2\psi_0 + (\nu/D)\psi_0 + (1/D\tau)\psi_0 = 0. \tag{4}$$

The time constant $\tau$ is determined by the boundary conditions.

The boundary condition on $\psi$ is obtained by setting the diffusion current approaching the wall equal to the random current collected by the wall. This problem has been considered for neutron diffusion,[5] with the result that the extrapolated neutron density goes to zero at a distance of the order of a mean free path beyond the wall. For electrons the result should be modified to include the action of the image charge induced by the approaching electrons. Because diffusion theory holds only when the mean free path is small compared to the dimensions of the discharge tube, it is sufficiently accurate to apply the condition that the electron density, and therefore $\psi$, vanish at the walls.

The condition that $\psi$ is zero on the boundary results in a set of characteristic values for $1/\tau$, which are denoted by $1/\tau_a$, and in a corresponding set of orthogonal functions $\psi_a$. The function corresponding to the lowest of the $1/\tau_a$'s is positive everywhere, while the others all change sign at some point in the discharge tube. The background electron density at the instant the field is applied may be expanded in a series of the functions $\psi_a$. Each term thereafter rises or decays exponentially in time at its own characteristic rate, depending on whether $\tau_a$ is negative or positive. If the electric field is zero, $\nu$ is zero or negative, and all of the time constants are positive, because the discharge must decay without ionization. As the electric field is raised the $1/\tau_a$'s become smaller until the lowest goes through zero and the corresponding function builds up in time. The other terms do not build up, as their time constants are still positive. At this point the ionization rate produced by the field has reached the value where it is replacing diffusion losses. A slightly higher field then causes breakdown.

The breakdown field may now be defined as the field necessary to maintain a steady discharge in the limit of zero electron density. Although this field will not produce breakdown, any greater field will do so. It may be computed as the lowest characteristic value of the equation,

$$\nabla^2\psi + (\nu/D)(E)\psi = 0. \tag{5}$$

The ratio $\nu/D$ is indicated as a function of the electric field, which in turn is a function of the space coordinates. The field may be represented as

$$E = E_0 f(x, y, z),$$

where $E_0$ is the field at a reference point $P_0$, and $f$ is a space factor determined from Maxwell's equations. The value of $f$ at $P_0$ is unity. The electric field at any point may be specified by the field at the reference point and the function $f$. The characteristic value, obtained from

[4] L. M. Hartman, Phys. Rev. 73, 316 (1948), has computed breakdown for the case of an infinite medium in which diffusion losses are zero and recombination is the controlling loss mechanism. Such a case would be realized experimentally with very large tubes or high pressures, but is not within the range of the present experiments.

[5] G. Placzek and W. Seidel, Phys. Rev. 72, 550 (1947).

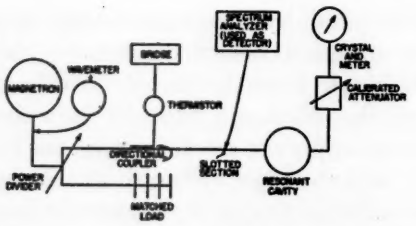


FIG. 1. Block diagram of experimental apparatus.

Eq. (5) and the boundary conditions, thus specifies the breakdown field in terms of $E_0$.

## IV. THE EFFECT OF SECONDARY PROCESSES

The effect of secondary emission of electrons from the walls of the discharge tube may be included by appropriate changes in the boundary conditions. These should be modified to make the diffusion current approaching the wall equal to the difference between the random current absorbed by the wall and the secondary emission current emitted from the wall. The secondary emission term is appreciable only when the number of secondary electrons per positive ion is of the order of unity, which is not the case.

In the d.c. discharge the electrons leave the cathode and multiply as they proceed toward the anode, but they cannot return to the cathode once they have lost energy through an inelastic collision. The discharge is therefore entirely dependent upon the emission properties of the cathode. On the other hand, the a.c. discharge may be maintained entirely from electrons obtained from ionization by collision in the gas. If an electron leaves the wall, one more electron must return to the wall to satisfy the continuity requirement. The only effect of this emission is to move the equivalent wall position slightly further from the center of the discharge, which reduces the breakdown field by an equally slight amount. This effect is entirely negligible because of the small emission probability.

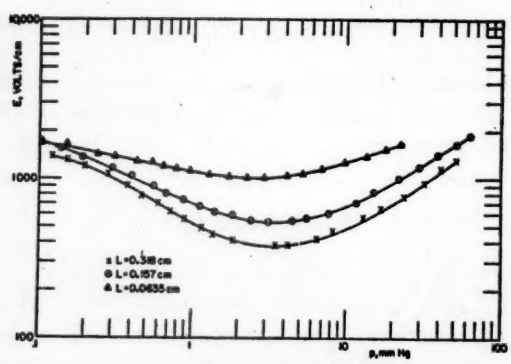


FIG. 2. Breakdown field (volts/cm) as a function of pressure (mm Hg) for three plate separation distances ($L$ cm). Cavity resonant wave-lengths were all near 9.6 cm.

## V. HIGH FREQUENCY IONIZATION COEFFICIENT

Equation (5) indicated that breakdown calculations depend on a knowledge of the ratio $\nu/D$ as a function of the gas used, the electric field, the pressure, and the frequency. This quantity is analogous to the Townsend coefficient $\alpha$. The number of ionizations per centimeter of electron drift is $\nu/\bar{v}$, where $\bar{v}$ is the drift velocity. A d.c. field produces a drift velocity much larger than that due to diffusion. Neglecting diffusion, $\bar{v}=\mu E$, where $\mu$ is the electron mobility. Then, $\alpha=\nu/\mu E$. The Townsend coefficient refers ionization to a drift motion produced by electron mobility, while $\nu/D$ refers it to a drift motion produced by diffusion.

The analogy is more apparent when the Townsend coefficient $\eta$ is compared with the corresponding high frequency coefficient. Since $\eta=\alpha/E$,

$$\eta=\nu/\mu E^2. \tag{6}$$

The units are 1/volt. The units of $\nu/D$ are 1/centimeter$^2$, which may be changed to 1/volt$^2$ by dividing by the square of the field:

$$\zeta=\nu/DE^2. \tag{7}$$

The coefficients are related by,

$$\zeta=\eta(\mu/D).$$

Putting the high frequency coefficient into the dimensions of volts has the advantage of making it a function of $E/p$ and $p\lambda$ for a given gas. Thus, if the function

$$\zeta=\zeta(E/p, p\lambda)$$

is known, breakdown may be computed using Eq. (5). The inverse problem of determining $\zeta$ from breakdown experiments will now be considered.

## VI. BREAKDOWN BETWEEN PARALLEL PLATES

Measurements of $\zeta$ from breakdown data were made using $TM_{010}$ mode cylindrical cavities. The end plate separations were small compared to the

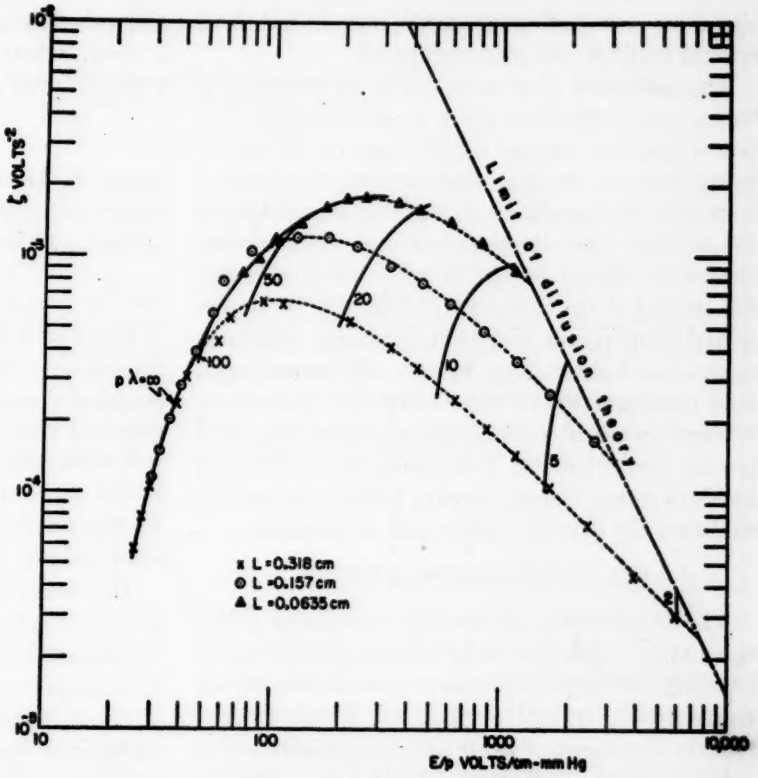


FIG. 3. High frequency ionization coefficient $\zeta=\nu/DE^2$ (ionizations/volt$^2$) as a function of $E/p$ (volts/cm-mm Hg) and $p\lambda$ (mm Hg-cm), determined from data shown in Fig. 2.

diameter of the region where the field is substantially uniform, in the vicinity of the center of the cavity. These cavities therefore approximated the conditions of infinite parallel plates with a uniform electric field. The solution of Eq. (5) for this case is

$$\psi=A\sin(z/\Lambda),$$

where $\Lambda=L/\pi$, $L$ is the plate separation distance, $z$ is the distance from one plate to an arbitrary point in the cavity, and $A$ is a constant. The breakdown condition is

$$\zeta=1/\Lambda^2E^2. \tag{8}$$

The electric field for breakdown may be measured as a function of pressure, frequency, and plate separation. From these data the ionization coefficient $\zeta$ may be computed.

### VII. EXPERIMENTAL APPARATUS

A block diagram of the apparatus used in the experiment is shown in Fig. 1. A continuous-wave tunable magnetron in the 10-cm wave-length region supplies up to one hundred fifty watts of power into a coaxial line connecting to the measurement equipment. A probe in the line samples a small signal for the cavity wavemeter. A power divider provides a means of varying the power. A known fraction of the incident wave is sampled by a directional coupler and sent to a thermistor element whose resistance change measured by a sensitive bridge provides a measure of the power incident on the cavity. A standing wave detector consisting of a slotted section of line and a movable probe is used to measure the standing wave ratio and position of minimum voltage in the line leading to the discharge cavity. The probe signal is carried through a flexible cable to a detector, which is equipped with a wave guide-beyond-cutoff type attenuator. With this arrangement one can measure the cavity input impedance and the fraction of incident power absorbed by the cavity.[6] The cavities are designed to resonate in the $TM_{010}$ mode at 10-cm wave-length. They are coupled to the input transmission line by a coupling loop. A second coupling loop provides a transmitted

[6] For details of experimental technique, reference should be made to such sources as: C. G. Montgomery, *Technique of Microwave Measurements* (McGraw-Hill Book Company, Inc., New York, 1947).

signal to a cut-off attenuator terminated in a crystal rectifier and microammeter.

The unloaded $Q$ of each cavity is determined by means of standing wave measurements. The power incident on the cavity and the standing wave ratio in the line provide the information necessary to determine the power dissipated in the cavity. The dissipated power with no discharge is related to the stored energy through the unloaded $Q$. The electric field can be determined from power and standing wave measurements, and from the known electromagnetic field configuration of the cavity. It proves convenient to use a transmission coupling loop and crystal current meter to measure field, after the incident power measurements have been used to calibrate the crystal, meter, and attenuator.

## VIII. EXPERIMENTAL RESULTS

The breakdown experiment consists of filling the cavity with gas at a certain pressure, increasing the magnetron power while watching the transmission crystal current until this current reaches a maximum value and drops suddenly to a lower value. This drop indicates that the gas has broken down, and the maximum crystal current indicates the breakdown field. This operation is repeated for a variety of experimental conditions.

Results of experiments on three thin parallel plate cavities are given in Fig. 2. The gas used was air from which impurities were removed by a liquid nitrogen trap. The r.m.s. breakdown field is plotted against pressure for each cavity. The field is lower for the larger cavities, because the diffusion losses are lower. For each curve there is a pressure at which the breakdown field is a minimum.

Figure 3 shows $\zeta$ plotted against $E/p$ for various values of constant $p\lambda$, as determined from Fig. 2. The dotted curves show the course of the data for a given cavity with variations of pressure. On the low $E/p$ side they come together to form a common envelope, but on the high side they depart from the envelope at various values of $E/p$, depending on the size of the cavity.

The dot-dash line sloping down to the right indicates the limit of validity of diffusion theory, where the mean free path is small compared to the tube dimensions. The line is drawn so that $l/\Lambda=1$, where $l$ is the mean free path. This relation, with Eqs. (5) and (7), results in

$$\zeta=P_c^2/(E/p)^2,$$

where $P_c$ is the collision probability per centimeter per millimeter of pressure ($l=1/P_c p$). $P_c$ is taken as 38 for air.

## IX. DISCUSSION

The ionization produced by a given value of $E/p$ is seen to be a maximum when $p\lambda$ is large. As $p\lambda$ decreases, the ionization drops, slowly at first and then more rapidly. A simple calculation will show that the experimental values of $p\lambda$ at which the ionization begins to drop correspond to the condition of the field radian frequency approaching the collision frequency.

The transition from the region of many oscillations per collision to many collisions per oscillation is marked also by the minimum breakdown voltage point in the field *versus* pressure curves. The breakdown voltage decreases as the pressure is lowered because the energy gained between collisions is increased and there is more ionization available to compensate for the increasing diffusion losses. When the transition region of $p\lambda$ is reached, the energy transfer is no longer at its maximum efficiency, and a higher field is required to replace the diffusion losses. The minimum is therefore not a Paschen minimum and would not be expected to follow the Paschen law.

The present paper has postulated a condition for breakdown which balances electron generation through ionization by collision against electron loss through diffusion. Application of the diffusion equation and boundary conditions provides a means of computing breakdown fields, if the high frequency ionization coefficient, which has been introduced, is known. The procedure has been reversed for the special case of parallel plate and uniform field breakdown, using breakdown data to infer the ionization coefficients. These data may then be used to compute breakdown fields for other geometries and field configurations. Thus parallel plate and uniform field breakdown curves constitute a basic set of data from which other cases may be treated. Although the experimental work has been performed for air, the method is generally applicable.

PHYSICAL REVIEW VOLUME 74, NUMBER 3 AUGUST 1, 1948

# The Disintegration of Scandium[46], Gold[198], and Tungsten[185, 187] *

CHARLES L. PEACOCK AND ROGER G. WILKINSON
*Indiana University, Bloomington, Indiana*

(Received April 16, 1948)

A survey of the nature and energies of the radiations of some radioactive isotopes of Sc, Au, and W has been made with a small 180° spectrometer of fair resolution. Samples were produced by neutron and deuteron activation.

The 85-day isotope of Sc is found to decay by the emission of two groups of beta-rays of maximum energies 0.36 and 1.49 Mev. The low energy group constitutes 98 percent of the total number of electrons. The residual $Ti^{46}$ nucleus returns to the ground state by the cascade emission of two gamma-rays with energies 0.89 and 1.12 Mev. The gamma-rays are converted with $K$ conversion coefficients of 0.0008 and 0.0004, respectively.

The decay scheme of $Au^{198}$ is found to be simple. The emission of a beta-ray of a single group, $E_{max}=0.97$ Mev, leads to an excited state of $Hg^{198}$ which returns to the ground state by the emission of a 0.408-Mev gamma-ray. The gamma-ray is converted with $\alpha_k=0.25$.

The radiations of 24-hour $W^{187}$ are complex. Two groups of beta-rays are present which have end points at 0.63 and 1.33 Mev. Five gamma-rays are noted with energies of 0.14, 0.21, 0.48, 0.62, and 0.69 Mev. The decay of the 77-day isotope, $W^{185}$, seems simple. A single beta-ray is found with an end point at 0.43 Mev.

## I. INTRODUCTION

THE energies of the radiations of $Sc^{46}$, $Au^{198}$, $W^{185}$, and $W^{187}$ have been reported by various workers with considerable variance in the results, not only in the energy values of the beta- and gamma-rays, but also in the number and nature of the components. This is particularly true of the early investigations carried out by absorption methods and with weak sources. More recent work tends towards consistency and, since the inception of this investigation, several workers have reported on some of the above-mentioned isotopes with results which are, in the main, in agreement with those of this paper.

The present work is concerned with a careful study of these disintegrations by means of a 180° spectrometer having a radius of 7.5 cm, used in a somewhat unconventional manner. The vacuum chamber is placed in the magnetic field so as to bring the outer electron paths into the fringing field. In this way the defocusing inherent in this type of instrument is reduced. The proper position of the chamber is determined experimentally by measuring known conversion lines and photoelectron lines for various settings of the chamber. An optimum half-width of 1.2 percent is found for conversion lines and 3.5 percent for photoelectron lines. In this way results have been obtained with fair resolution without sacrifice of transmission.

Both neutron and deuteron induced activities were used in the study. Strong neutron activated samples were obtained from the Oak Ridge pile; others were prepared by deuteron bombardment with the Indiana University cyclotron. In all cases careful attention was given to source preparation. Sources were chemically purified and were made as thin as was compatible with reasonable counting rates.

## II. SCANDIUM[46]

$Sc^{46}$ can be produced either by an $n-\gamma$ or $d-p$ reaction on the single stable isotope $Sc^{45}$. Initial studies by Walke[1] and his co-workers showed that the decay went by beta- and gamma-ray emission to $Ti^{46}$, with possibly some decay to $Ca^{46}$ by $K$-capture. The gamma-ray was reported as 1.25 Mev while the beta-rays were interpreted as being complex with two groups having energies of 0.26 and 1.5 Mev. Meitner[2] was unable to find the 1.5-Mev group and attributed Walke's result to scattering. More recently, Miller and Deutsch[3] have used spectrometer methods to obtain more accurate values of the energies. The results of their investigation indicate that the decay of $Sc^{46}$ goes by the emission of beta-rays of a single group of maximum energy of 0.36 Mev to $Ti^{46}$, which then returns to the ground state by the

* This research was supported by a grant from the Office of Naval Research.

[1] Walke, Williams, and Evans, Proc. Roy. Soc. **A171**, 360 (1939).
[2] L. Meitner, Arkiv f. Mat. Astr. och Fys. **A32**, No. 6.
[3] A. E. Miller and M. Deutsch, Phys. Rev. **72**, 527(A) (1947).

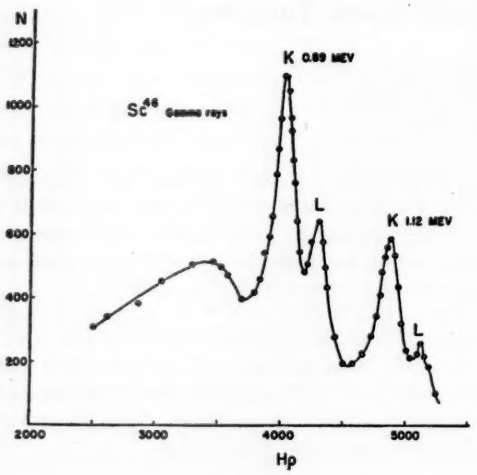


FIG. 1. Compton- and photoelectrons ejected from a 30-mg/cm² Pb radiator by the gamma-rays of $Sc^{46}$. The ordinate $N$ is the number of counts per minute. The values of the energy are for the gamma-ray, not the photoelectron line.

cascade emission of two gamma-rays of energies 1.12 and 0.90 Mev. These results are substantiated by Feister and Curtiss[4] and Mandeville and Scherb.[5] No evidence for $K$-capture was found by Deutsch.

The preliminary work of this investigation was done with deuteron activated $Sc_2O_3$. Chemical separation from the rare earths and other impurities generally associated with scandium was performed. Since the samples were weak in activity, sources were necessarily thick and the

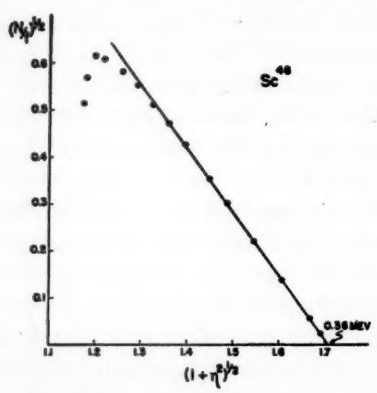


FIG. 2. Fermi plot of the low energy beta-ray group of $Sc^{46}$. The high energy component is too weak to be shown on this scale.

data as previously reported[6] is undecisive. These experiments indicate that there are two groups of beta-rays of maximum energies of 0.36 Mev and 1.49 Mev, as well as two gamma-rays having energies of 0.89 and 1.12 Mev. Coincidence studies carried out by Jurney and Ramsey in this laboratory show that each beta-ray of the 0.36-Mev group is followed by the cascade emission of the two gamma-rays. No beta-gamma coincidences could be found to substantiate the existence of the 1.49-Mev beta-ray group. However, the high energy component appears to be very low in intensity and negative coincidence results are not surprising.

Since the 1.49-Mev beta-ray group was not found by others,[2–5] the validity of the above determinations was subject to question. The presence of impurities, scattering inherent in the instrument, secondary electrons from the thick source, and low energy photoelectrons produced in the lead shielding at the detector might be supposed to account for the effect. To check this a series of careful determinations were made with high specific activity neutron induced $Sc^{46}$ from Oak Ridge. Following the procedure outlined by Noyes and Bray,[7] chemical purification of the samples was undertaken with special attention given to the removal of such elements as calcium, iron, yttrium, and other associated rare earths. Gamma-ray determinations were made by measuring the photoelectrons ejected from a lead radiator, 30 mg/cm² in thickness, placed over a $Sc_2O_3$ sample. Figure 1 shows the photoelectron spectrum. The photoelectrons corresponding to the two gamma-rays are clearly resolved into their $K$ and $L$ components and rise well above the accompanying Compton electrons, in accordance with good source geometry. The spectrometer was adjusted for low resolution to insure high counting rates so that the lines have the rather large half-width of 5 percent. The $K$ and $L$ photoelectron lines correspond to gamma-ray energies of $0.89 \pm 0.005$ and $1.12 \pm 0.005$ Mev.

For beta-ray measurements, care was taken to keep the sources thin. A very pure solution of

[4] I. Feister and L. F. Curtiss, J. Research Nat. Bur. Stand. **38**, 411 (1947).
[5] C. E. Mandeville and M. Scherb, Phys. Rev. **73**, 141 (1948).
[6] C. Peacock and R. G. Wilkinson, Phys. Rev. **72**, 251 (1947).
[7] A. Noyes and W. Bray, *Qualitative Analysis for the Rare Elements* (The Macmillan Company, New York, 1927), p. 210.

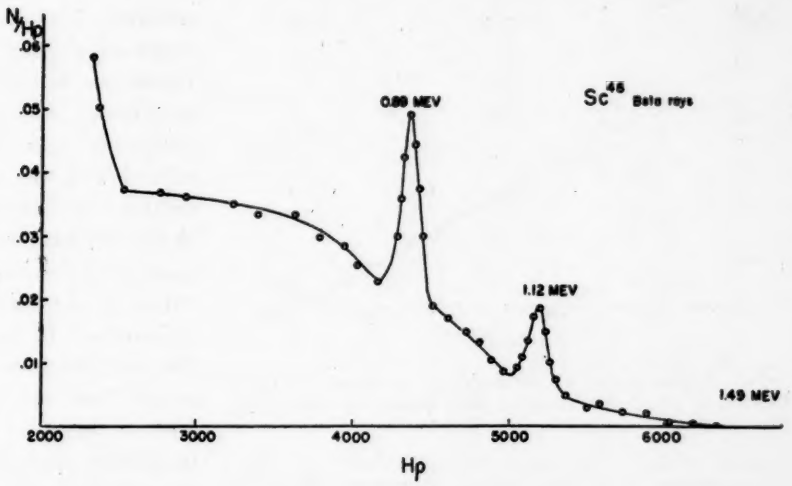


FIG. 3. High energy group of the beta-ray spectrum of $Sc^{46}$ plotted on an extended scale. The conversion lines have a half-width of about three percent. The energies given are those of the gamma-rays.

$ScCl_3$ was evaporated on a backing of Zapon film 0.04 mg/cm² thick. Source thicknesses ranged from 0.25 to 1.0 mg/cm² with an area of about 20×3 mm². As in earlier runs, the beta-ray spectrum consists of two components with end points at 0.36±0.005 and 1.49±0.01 Mev with the high energy group comprising about 2 percent of the total number of electrons, both groups decaying with the characteristic 85-day half-life. The Fermi plot of the 0.36-Mev group, shown in Fig. 2, is a straight line down to energy values corresponding to window cut-off. Since the high energy group is much the weaker, it appears as a barely discernible tail to the low energy group when the latter is plotted on an ordinary scale. A much expanded plot of this tail obtained by using a stronger source is given in Fig. 3. Two lines are superimposed on the beta-ray spectrum and have energies corresponding to the gamma-rays. Because of the narrowness of the lines, they must be ascribed to conversion of the gamma-rays and not to secondaries ejected from the source material or backing.

Auxiliary experiments were performed to make certain that the high energy tail was not due to secondary electrons. These electrons cannot be attributed to source thickness or scattering defects in the instrument. If the effect were to be due to secondaries associated with the gamma-rays owing to source thickness, one would expect to register no electrons with energies greater than the gamma-ray energies. However, electrons above this energy are present. While it is true that some of the electrons were found to be secondaries when thick sources were used, the tail persisted for sources as thin as 0.25 mg/cm² on negligible backing. It is unlikely that scattering defects of the instrument are responsible for the tail since other spectra of comparable end points show no such effect; e.g., that of $W^{185}$, which has an end point at 0.43 Mev. There remains the possibility of electrons being produced in the lead between the source and detector by the gamma-rays which might appear in the counter region. The effect of this might be to record low energy electrons at much higher $H$ values. To check this, copper absorbers of various thicknesses were placed over the counter window to shield out such radiation. With enough copper over the window to cut out 1.1-Mev electrons, the maximum energy to be expected, there was evidence of electrons above this energy entering

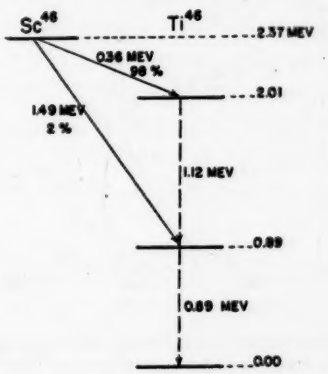


FIG. 4. Disintegration scheme of $Sc^{46}$.

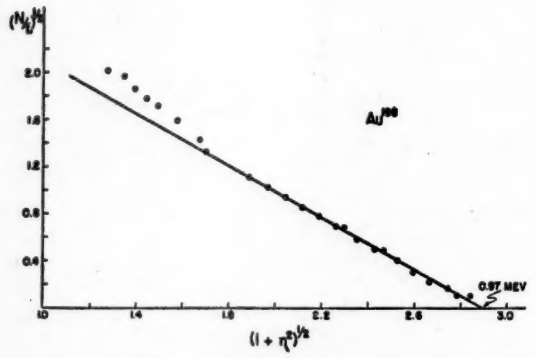


FIG. 5. Fermi plot of the beta-ray spectrum of $Au^{198}$. Deviation from the straight line begins at about 0.4 Mev.

the counter. It is concluded, therefore, that the 1.49-Mev group is real.

The results of these experiments and the coincidence experiments of Jurney and Ramsey lead conclusively to the disintegration scheme given in Fig. 4. About 98 percent of the disintegrations go by the emission of a beta-ray in the 0.36-Mev group to the 2.01-Mev level of $Ti^{46}$, which returns to the ground state by the cascade emission of the two gamma-rays. In the remaining 2 percent of the cases beta-emission leaves the $Ti^{46}$ in the 0.89-Mev excited level, which returns to stability by gamma-emission. The measured relative intensities of the gamma-rays are consistent with this picture. Estimates based on Gray's[8] empirical curve show that the gamma-rays have about the same intensity, the 0.89-Mev radiation being slightly more abundant. This is merely an indication of consistency, however, since the magnitude of the error involved does not make the difference significant. If the above scheme is assumed, the $K$-conversion coefficients of the gamma-rays can be computed from the data. These are found to be 0.0008 and 0.0004, respectively, for the 0.89- and the 1.12-Mev gamma-rays. Some idea of the spin change involved can be obtained by comparing these results with the theoretical values of $\alpha_k{}^l$ predicted by the Morrison-Dancoff formula. Best agreement between experimental and theoretical values is obtained for $l=4$, i.e., if the radiation is assumed to be electric multipole; or $l=3$ if the radiation is magnetic octapole. The low energy beta-ray group has a $ft$ value of $2\times10^6$ and is therefore first forbidden. On the other hand, the high energy group must be at least second forbidden since it has an ft value of $6.8\times10^9$. Since $Ti^{46}$ is an even-even nucleus, it may be supposed to have zero spin; hence the spin of the $Sc^{46}$ nucleus may have a large spin value.

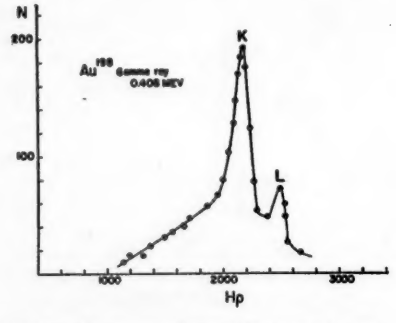


FIG. 6. Photoelectrons ejected from a 30-mg/cm² Pb radiator by the gamma-ray of $Au^{198}$.

[8] L. H. Gray, Proc. Camb. Phil. Soc. **27**, 103 (1931).

### III. GOLD[198]

Since the beginning of this study several papers have appeared concerning $Au^{198}$. The results of various recent investigations still seem to be somewhat at variance. Levy and Greuling[9] find conversion lines corresponding to three gamma-rays of energies 0.157, 0.208, and 0.408 Mev. From the non-linear Fermi plot which they obtain, they infer that the beta-ray spectrum has two components of energies 0.605 and 0.97 Mev. Their conclusions are supported by the coincidence studies of Mandeville[10] and Clark,[11] in which substantial gamma-gamma as well as beta-gamma coincidences are observed. On the other hand, Siegbahn[12] finds only one converted gamma-

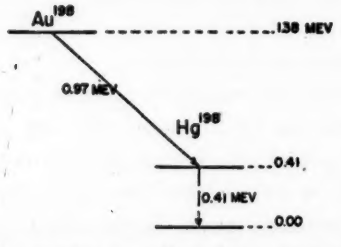


FIG. 7. Disintegration scheme of $Au^{198}$.

[9] P. Levy and E. Greuling, Phys. Rev. **73**, 83 (1948).
[10] C. E. Mandeville and M. V. Scherb, Phys. Rev. **73**, 634 (1948).
[11] A. Clark, Phys. Rev. **61**, 242 (1942).
[12] K. Siegbahn, Proc. Roy. Soc. **189**, 527 (1947).

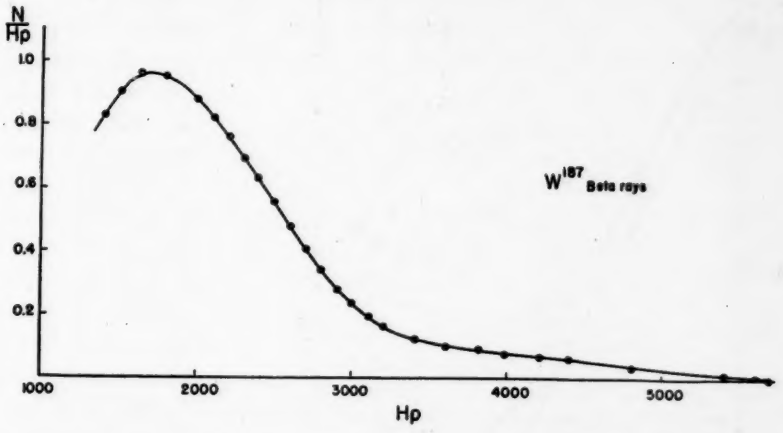


FIG. 8. Beta-ray spectrum of $W^{187}$ showing the presence of two groups.

ray at 0.403 Mev and a single beta-ray group of maximum energy 0.92 Mev. His results are in agreement with the coincidence studies of Norling[13] and Jurney[14] who reported beta-gamma coincidences but found no appreciable gamma-gamma coincidences. Moreover, Cork[15] reports the presence of only one conversion line at 0.4 Mev.

Our results were obtained by studying $Au^{198}$ prepared by deuteron activation. The material was chemically purified with special attention given to the separation from mercury. After adding mercury carrier, the gold was finally extracted from mercury with ethyl acetate. Sources were prepared by electro-plating the gold from a HCl solution on graphite strips approximately 28 mg/cm² thick. Sources ranging down to 5 mg/cm² in thickness were used. The use of the low $Z$ material compensated for the relatively heavy backing and the scattering was thus minimized. The Fermi plot of the beta-rays is shown in Fig. 5. The $K$ and $L$ conversion lines associated with a single gamma-ray were observed. These are omitted from the plot. Deviation from the straight line does not occur down to about 0.4 Mev. Presumably, thinner sources would cause the deviation to occur at even lower energies, owing to less degradation of electron energies in the source. We conclude from our data that there is a single group of beta-rays with an end point at 0.97±0.01 Mev. The photoelectron spectrum, obtained by using a 30-mg/cm² lead radiator, is shown in Fig. 6. Only one gamma-ray could be found in the region investigated, i.e., down to the counter window cut-off at 0.07 Mev. Measurements of the energy of the gamma-ray from the photoelectron lines and from the conversion line agree well and yield the value of 0.408±0.002 Mev.

Initial surveys were made with unseparated samples to check the nature of possible contaminants. Two conversion lines in the region of 0.15 Mev were observed which decayed with a 24-hour half-life. These were attributed to $Hg^{197}$ since the activity followed the chemistry of mercury. Accurate determinations could not be made of the gamma-ray energies, but they are estimated to be 0.17 and 0.23 Mev after adding the $K$ binding energy of Hg.

These results are in excellent agreement with Siegbahn's[12] and suggest the decay scheme shown in Fig. 7. On the basis of this scheme, the $K$ conversion coefficient of the gamma-ray is found to be 0.025. Our data suggests that the previously reported gamma-rays at 0.16 and 0.21 Mev[9] and the associated gamma-gamma coincidences might be due to mercury contamination. Consistent with this possibility is the fact that our Fermi plot rises above the straight line at a somewhat lower energy, although our sources were much thicker.

### IV. TUNGSTEN[187, 185]

The radiations of tungsten have been reinvestigated[16] using metallic tungsten activated

[13] F. Norling, Arkiv f. Mat. Astr. och Fys. **A27**, No. 27 (1941).
[14] E. Jurney and M. R. Keck, Bull. Am. Phys. Soc. **22**, No. 6, 6 (1947).
[15] J. M. Cork, Phys. Rev. **72**, 581 (1947).
[16] W. M. Schwarz and M. L. Pool, Phys. Rev. **71**, 122 (1947).

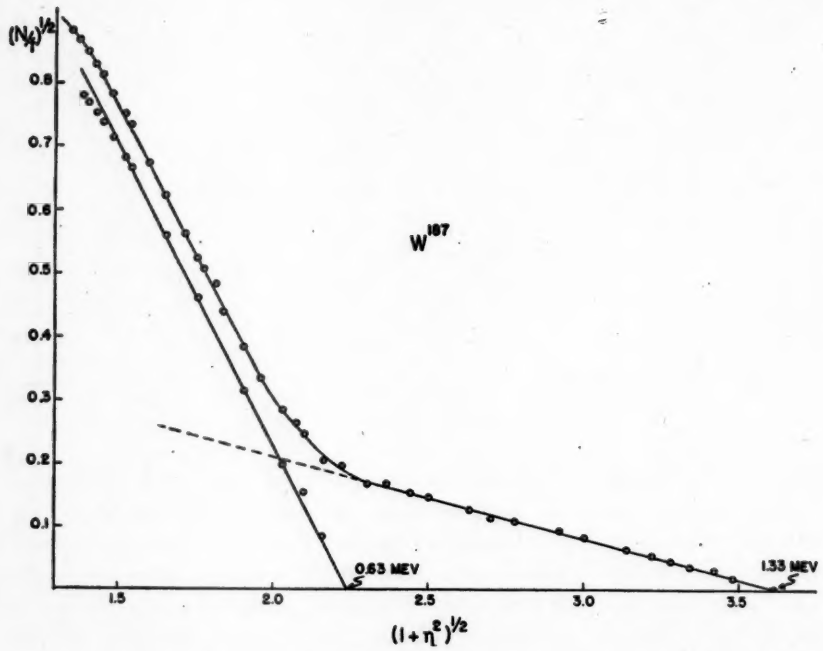


FIG. 9. Fermi plot of the beta-ray spectrum of $W^{187}$ showing the analysis into two groups.

by intense cyclotron probe bombardments. As in previous cases care was taken to purify the samples. Since the tungsten was silver-soldered to the copper probe, it was necessary to extract Ag, Cd, Cu, and Zn, as well as Re and Ta which might result from the bombardment of the tungsten itself. This was accomplished by a standard sulfide precipitation, and finally, repeated precipitation of tungsten from an acid solution. All purified samples showed the characteristic 24-hour half-life with no indication of impurity. Bombardments were not strong enough to produce the 77-day $W^{185}$. Beta-ray sources of pure $WO_3$ varied from 7 to 2 mg/cm² in thickness. In order to check the results and to study the 77-day activity, neutron activated samples were obtained from Oak Ridge. The results of both samples are essentially the same, although neutron activated sources were of higher specific activity and allowed the use of beta-ray sources less than one mg/cm² in thickness backed by Zapon films 0.08 mg/cm² thick.

The beta-ray spectrum shown in Fig. 8 is obviously complex. All parts of the spectrum

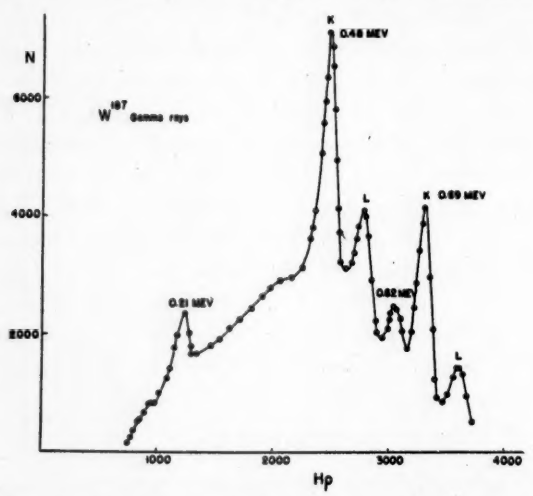


FIG. 10. Compton- and photoelectrons ejected from a 30-mg/cm² Pb radiator by the gamma-rays of $W^{187}$. The energy values are for the gamma-rays, not the photoelectron lines.

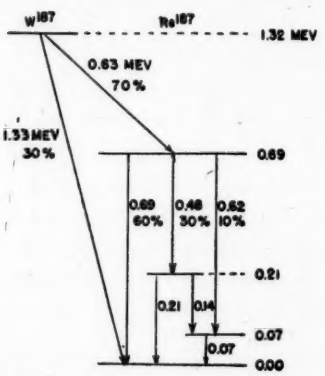


FIG. 11. A possible disintegration scheme of $W^{187}$. The 0.14- and 0.07-Mev gamma-rays are those reported by Valley.

decayed with the proper half-life. Figure 9 shows a Fermi analysis of the spectrum into two groups with end points at 0.63±0.01 and 1.33±0.01 Mev. The low energy group constitutes 70 percent of the total beta-rays; hence the inner end point is quite well determined. The outer end point is in fair agreement with absorption measurements of Fajans[17] and Clark.[11] The photoelectron spectrum resulting from the gamma-rays (Fig. 10) is also complex, with four gamma-rays definitely present at 0.21, 0.48, 0.62, and 0.69 Mev. In addition, there is evidence of a gamma-ray at 0.14 Mev as reported by Valley.[18] Counter window cut-off made it impossible to observe the two which he has reported at 0.1 and 0.086 Mev. No lines were found in any of the samples which did not decay with the 24-hour half-life. The predominant photoelectron lines are well resolved into their respective $K$ and $L$ components except for the one corresponding to the gamma-ray at 0.62 Mev. In this case the $L$ line is masked by the $K$ line of the 0.69-Mev gamma-ray. These results differ somewhat from those of Schwarz.[16] Apparently the gamma-rays which he reported at 0.57 and 0.79 Mev are to be ascribed to $L$ photoelectron lines since they are displaced from the 0.48- and 0.69-Mev lines by the binding energy of uranium which he used as a radiator. Other lines are probably due to contamination or poor statistics resulting from weak sources and high backgrounds.

Coincidence studies carried out by Jurney in this laboratory show that there are substantial beta-gamma coincidences in $W^{187}$. However, in spite of the complex gamma-ray spectrum, the gamma-gamma coincidence rate is quite low, though not zero. It must be concluded that the main components are not in cascade. The disintegration scheme is therefore complex and cannot be directly inferred from the data. The scheme shown in Fig. 11 is a tentative one, but it is probably the one most consistent with our data and the coincidence studies. The estimated relative intensities of the stronger lines, as well as Valley's results, support this picture.

[17] K. Fajans and W. H. Sullivan, Phys. Rev. **58**, 276 (1940).
[18] G. E. Valley, Phys. Rev. **59**, 686 (1941).

TABLE I.

| | Beta-ray energy Mev | Gamma-ray energy Mev | $K$ conversion coefficient |
|---|---|---|---|
| $Sc^{46}$ | 0.36±0.005 (98%)<br>1.49±0.01 (2%) | 0.89 ±0.005<br>1.12 ±0.005 | 0.0008<br>0.0004 |
| $Au^{198}$ | 0.97±0.01 | 0.408±0.002 | 0.0250 |
| $W^{187}$ | 0.63±0.01 (70%)<br>1.33±0.01 (30%) | ~0.14<br>0.21 ±0.005<br>0.48 ±0.005<br>0.62 ±0.005<br>0.69 ±0.005 | —<br>—<br>—<br>— |
| $W^{185}$ | 0.43±0.003 | — | — |

The mode of disintegration of $W^{185}$ is found to be simple. A simple beta-ray spectrum is obtained, with an end point at 0.43 Mev. No gamma-rays are found.

## V. SUMMARY

A summary of the energy values reported in this paper is given in Table I. The limits of error indicate the extent of consistency of successive measurements and do not take account of possible systematic errors. In most cases, however, the results are thought to be valid to one percent.

## VI. ACKNOWLEDGMENTS

We wish to thank Dr. Milo B. Sampson for his generous aid in this work. We are indebted to him for many cyclotron bombardments and for the preparation of the tungsten probes. We wish also to acknowledge the assistance of Mr. John Ricketts in connection with the chemistry. The frequent reference to the coincidence work of Mr. Edward T. Jurney is the result of many helpful conferences. His results will appear in a forthcoming paper.

# Use of an Electron Multiplier Tube as a New Technique in Disintegration Experiments

LETICIA DEL ROSARIO*
*Department of Physics, The University of Chicago, Chicago, Illinois*
(Received April 16, 1948)

An electron multiplier tube with 12 electrodes has been used as a detector in the bombardment of beryllium by protons of energy 239, 268, and 397 kv. The disintegration particles from the two possible reactions, $_4Be^9(p,\alpha)_3Li^6$ and $_4Be^9(p,d)_4Be^8$, were selected by an electrostatic analyzer which measured directly their energies. The results for each bombarding voltage are given as an energy distribution curve which shows a complete resolution of the various peaks. All the particles, except the unstable $_4^8$Be, were detected, an interesting feature being the detection of the recoil nucleus $_3^6$Li in its three states of ionization. The perfect resolution of the peaks is due to the fact that the target used was extremely thin and that no windows were used in the complete path of the particles from the target, through the analyzer and unto the detector, since the multiplier tube works in vacuum. Thus, no straggling was observed, and the width of the peaks coincide with the values predicted by the theory of the electrostatic analyzer for the slits used in these experiments. The ratios in which the three lithium ions appear are given and the problem of the probability for capture or loss of electrons by the ions is briefly discussed, on the basis of the ratio $\gamma$ of the electron orbital velocity to the velocity of the ion itself, as suggested by Bohr and used by Knipp, Teller, and Brunings in their treatment of heavy ions. The calculated values for $\gamma$ under our conditions are: for the process $Li^{+++} \rightleftarrows Li^{++}$, $\gamma=1.22$, and for $Li^{++} \rightleftarrows Li^{+}$, $\gamma=1.09$, which have a net effect of favoring the doubly ionized state of lithium. The actual counting rates observed indicate, in fact, that the $Li^{++}$ is the more abundant of the three ions.

## I. INTRODUCTION

IN detecting charged particles from nuclear disintegrations the instruments generally used, such as ionization chambers or counters, depend on the ionization produced by the particles in a gas, and hence windows are necessary to separate the detector from the vacuum system. In such devices the particle loses a certain amount of energy in traversing the window, and to be detected must still retain sufficient energy to produce an appreciable ionization. Therefore, the detection of particles of very low energy is extremely difficult since it is very hard to obtain thin windows of sufficiently small stopping power which at the same time will be strong enough to be vacuum tight and to hold the difference in pressure. Even if these conditions were satisfied, for the case of very slow particles, the pulses produced might be too small and would require a high external amplification.

Studies made by several people on the ejection of secondary electrons from metals when hit by photons or particles have resulted in the multiplier tube. After a careful study of the metals and of the shape of the electrodes, J. S. Allen[1] has developed an efficient electron multiplier tube of sturdy construction and great sensitivity. Since it works in vacuum no windows are required to separate it from the rest of the system, and it can thus be used as a detector of low energy particles.

This work is primarily concerned with the use of an electron multiplier tube as a new technique in the detection of disintegration particles and in the study of nuclear processes in general. The tube used in these experiments was first carefully studied in regard to its response to different kinds of particles (alpha-particles, protons, deuterons, and electrons) under various conditions, and was then used as the detecting device in counting the particles produced in the bombardment of beryllium by protons. An electrostatic analyzer served to select the particles and measure precisely their energy before entering the multiplier tube.

There are two possible reactions when beryllium is bombarded by low energy protons, namely:

$$_4Be^9+_1H^1 \rightarrow _3Li^6+_2He^4+Q_1, \quad (1)$$

$$_4Be^9+_1H^1 \rightarrow _4Be^8+_1H^2+Q_2. \quad (2)$$

These reactions were first suggested by Oliphant, Kempton, and Rutherford,[2] who identified the alpha-particles and the deuterons as the disinte-

* On leave of absence from the Physics Department, University of Puerto Rico. The work reported here was done in the Institute for Nuclear Studies of the University of Chicago.

[1] J. S. Allen, Phys. Rev. **55**, 336 (1939); **55**, 966 (1939).

[2] M. L. E. Oliphant, A. E. Kempton, and O. M. Rutherford, Proc. Roy. Soc. **A150**, 241 (1935).

gration particles of the two competing reactions. The alpha-particles from the first process were identified also in experiments described by Döpel,[3] Kirchner and Neuert,[4] and Zipprich.[5] Several other investigations have been subsequently made, such as those of Döpel,[6] and Kirchner and Neuert.[7] In regard to their yields there is the work of Allen,[8] who studied the range of 45- to 125-kv proton energy; Williams, Haxby, and Shepherd[9] up to 250 kv; and Hatch,[10] who extended the range to 400 kv. As for the energy release, the most precise values obtained so far are those measured by Allison[11–13] and his group of collaborators. These values, after correction,[14] are

$$Q_1 = 2.115 \pm 0.04 \text{ Mev}, \quad Q_2 = 0.547 \pm 0.006 \text{ Mev}.$$

However, in all the studies made so far it has been difficult to resolve completely the deuterons of reaction (2) from the alpha-particles of reaction (1). Allison *et al.*[12,13] were able to distinguish both particles at a bombarding voltage of 262 kv, and they measured accurately their energy from their energy limit, but the resolution was not complete.

This paper presents the successful resolution of the alpha-particles from the deuterons and the detection of the recoil nucleus $Li^6$ in its three stages of ionization. The energy releases $Q_1$ and $Q_2$ obtained in this investigation agree within the experimental error with the accepted values mentioned before. It will be suggested that from the ratios of the number of triply-charged lithium particles to the number of doubly- and singly-charged ions some information might be obtained in regard to the problem of capture and loss of electrons by ions.

[3] R. Döpel, Zeits. f. Physik **91**, 796 (1934).
[4] F. Kirchner and H. Neuert, Physik Zeits. **36**, 54 (1935).
[5] B. Zipprich, Zeits. f. Physik **96**, 337 (1935).
[6] R. Döpel, Physik. Zeits. **104**, 666 (1937).
[7] F. Kirchner and H. Neuert, Physik Zeits. **38**, 969 (1937).
[8] J. S. Allen, Phys. Rev. **51**, 182 (1937).
[9] J. H. Williams, R. O. Haxby, and W. G. Shepherd, Phys. Rev. **52**, 1031 (1937).
[10] G. T. Hatch, Phys. Rev. **54**, 165 (1938).
[11] S. K. Allison, L. S. Skaggs, and N. M. Smith, Jr., Phys. Rev. **54**, 171 (1938).
[12] S. K. Allison, E. R. Graves, L. S. Skaggs, and N. M. Smith, Jr., Phys. Rev. **55**, 107 (1939).
[13] L. S. Skaggs, Phys. Rev. **56**, 24 (1939).
[14] S. K. Allison, L. S. Skaggs, and N. M. Smith, Jr., Phys. Rev. **57**, 550 (1940).

## II. EXPERIMENTAL PROCEDURE

### Apparatus Used

#### *A. The Linear Accelerator*

The Cockroft-Walton voltage quadrupling circuit used before the war in this laboratory has been almost completely rebuilt. One of the main features of its reconstruction is the use of four sealed-off diodes with inverse peak rating of 250 kv instead of the older rectifiers which had to be continuously pumped. The new condensers used have larger capacities than the previous ones, and were distributed among the various stages of the circuit in such a way as to make the ripple and voltage lowering as small as possible. This 400-kv high potential source was used to accelerate protons produced by a low voltage capillary arc, which is described elsewhere.[15] Using a filament current of 24 amperes, an arc current of 0.5 amperes, and varying the probe voltage between 3000 and 6000 volts, beams as high as 80 microamperes at the target could be easily obtained. However, currents of only 10 to 20 microamperes were used in these experiments.

The accelerating voltage was measured by means of a resistance voltmeter consisting of a stack of resistor units. Each one of these units consists of 31 individual resistors of 10 megohms each, assembled helically in a frame of Lucite which insures good contacts, complete separation of each resistor, and prevents corona. A total of 21 of these units (each one of about $3.1 \times 10^8$ ohms) was screwed on top of each other and enclosed in a sealed glass cylinder with a dehydrating cap at its bottom. This high resistance stack was calibrated and found to be $6.83 \times 10^9$ ohms when 10 microamperes were passed through it. The variation of the resistance with the current was studied and the results showed, for instance, that at 30 $\mu$a the resistance dropped to $6.81 \times 10^9$ ohms, and at 55 $\mu$a it was $6.75 \times 10^9$ ohms. The current-resistance curve obtained was then used to determine the calibration curve for the high voltage.

#### *B. The Bombarding Chamber and Target*

This chamber consisted of a specially designed brass block which provided apertures for different

[15] S. K. Allison, Rev. Sci. Inst. **19**, 291 (1948).

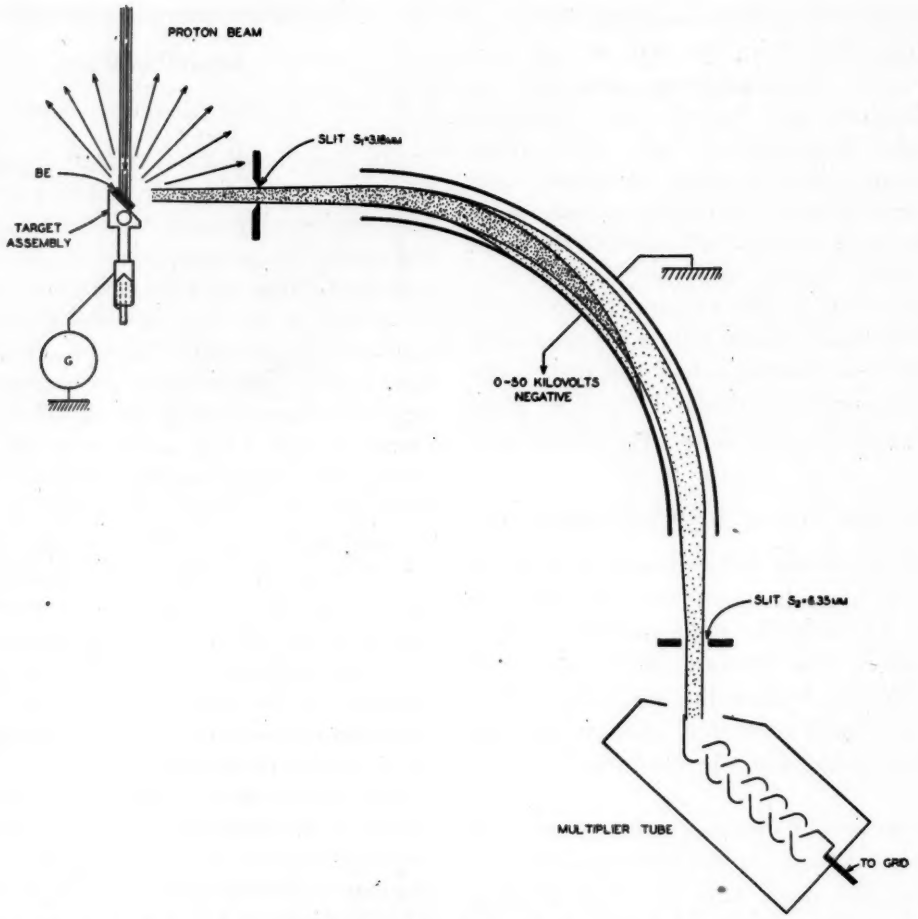


FIG. 1. Schematic arrangement of the target, electrostatic analyzer, and electron multiplier tube used as detector of disintegration particles.

target holders, namely, one for the beryllium target used in this work, one for a heavy ice target used in an investigation of the *D-D* reaction, and one for the polonium source mounted on a micrometer screw which was used in the initial study made of the multiplier tube. The beryllium target was prepared by evaporating the metal in vacuum onto a well polished nickel button. This was done by spot welding several pieces of beryllium on a tantalum wire which was then heated by a current in vacuum. Several nickel buttons were placed directly over this wire and the evaporated metal condensed on them. The first targets thus made were extremely thin. In fact, a test was made with two control buttons on both of which some polonium was deposited, but only one of them was placed with the other clean nickel buttons to receive the beryllium layer. The range *vs.* counting rate curve was then taken for the two polonium buttons to determine the stopping power of the beryllium layer, and it was found that the alphas from the polonium covered with Be had practically the same range as the alphas from the uncoated polonium. Thus the thickness of the beryllium layer was estimated to be equivalent to less than 1 mm of air.

This thin Be target was placed at 45° to the direction of the incoming protons and the disintegration particles entered the analyzer at 90° with the bombarding beam. To avoid the deposition of an oil film from the diffusion pumps on the target, this was heated by means of a platinum coil following the method described by Hatch.[10] The same thin target was used all throughout this investigation; it produced particles in sufficient intensities and its extreme

thinness caused no straggling, as will be shown later in the discussion of the results.

### C. The Electrostatic Analyzer

The description of this analyzer has appeared in previous literature,[11] and no fundamental changes have been made on the instrument. It consists of two concentric cylindrical plates made of aluminum which subtend an angle of 90° at their center of curvature. The radius of the outer plate is 25.717 cm and that of the inner one is 25.083 cm, the mean radius being 25.400 cm. The space between them is 0.635 cm and their height is 8.26 cm. Figure 1 shows the arrangement of the electrostatic analyzer, together with the bombarding chamber and the multiplier tube. The slit $S_1$, 0.318 cm wide, was placed at a distance of 8.90 cm from the entrance to the analyzer, which is the focal distance of the apparatus, and another slit $S_2$, 0.635 cm wide, was placed at the same distance from the exit. In the preliminary tests of the multiplier tube with a polonium source placed in the bombarding chamber, the slit $S_1$ was covered with a Nylon film 0.0002 inch thick, with a stopping power of about 0.9 cm of air. This was necessary in order to separate the vacuum system of the analyzer and multiplier tube from the air space in which the polonium alphas were slowed down. However, during the investigation of the beryllium-proton reaction there was no film on the slit $S_1$, the vacuum space being common for the accelerator tube, bombarding chamber, analyzer, and detector.

The voltage for the analyzer was supplied by a 50-kv source, the negative of which was connected to the inner plate of the deflector, the outer plate being grounded. This deflecting voltage was measured within 0.3 percent by an electrostatic voltmeter whose scale was calibrated and re-checked several times during the course of the experiments. For this electrostatic analyzer the relation giving the energy of a particle traveling along a circular orbit is

$$E = 20.00\,Vz, \tag{3}$$

in which $E$ represents the particle energy in electron volts, $z$ is its charge, and $V$ the deflecting potential on the analyzer in volts.

### D. The Electron Multiplier Detector

The multiplier tube used in this work was made in our laboratory according to a design by J. S. Allen, and under his personal guidance.** It consists of twelve multiplying stages made of

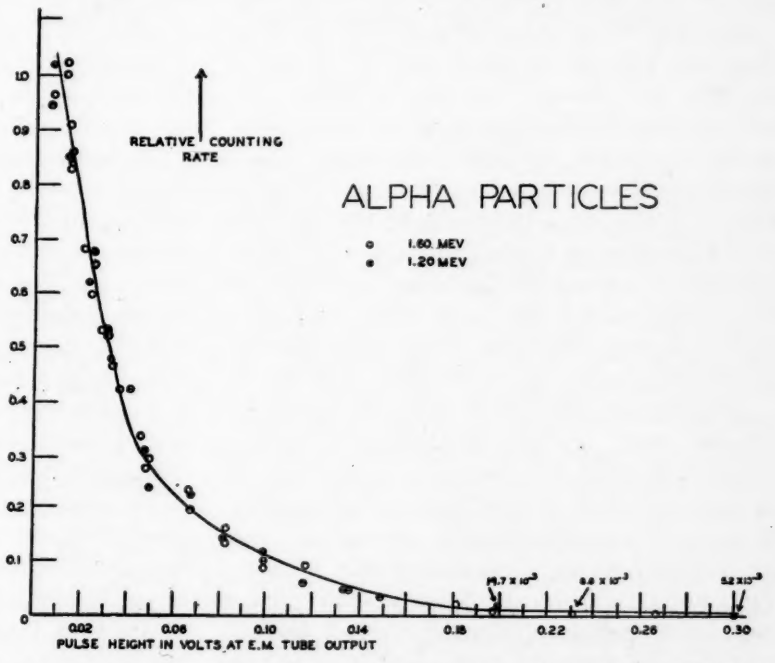


FIG. 2. Height distribution of pulses leaving the final plate of the electron multiplier tube when alpha-particles of 1.6 and 1.2 Mev are incident on the first plate.

** The preparation of these tubes was supported by the Office of Naval Research under Contract N6-ori-20, Task Order III.

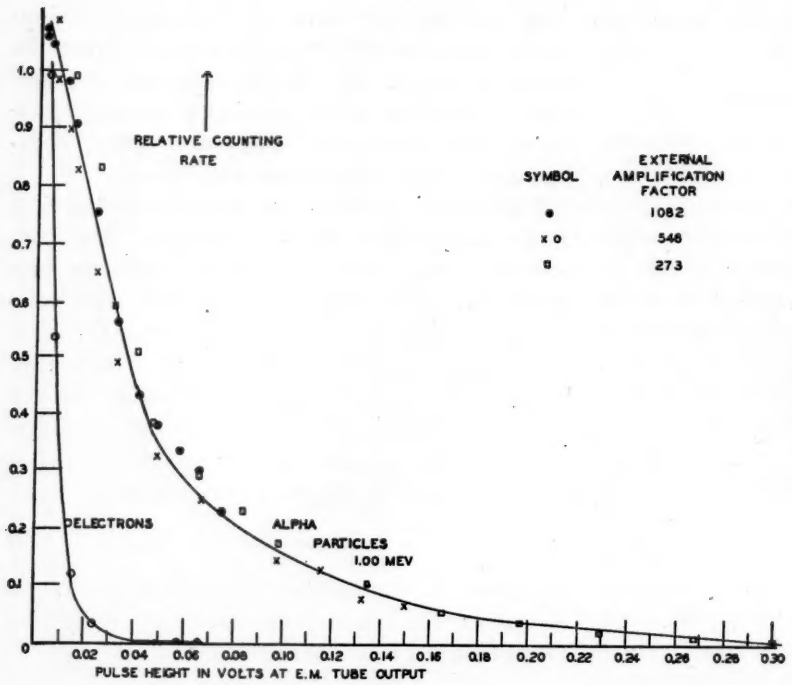


FIG. 3. Height distribution of pulses at the final plate of the electron multiplier tube due to 1-Mev alpha-particles and electrons of approximately 30 kv. The amplification of the external electronic circuit was varied in order to test the linearity of the discriminatory bias resistor on the scaling circuit.

beryllium copper. These electrodes were carefully polished and shaped by suitable presses, and held together by two Lavite plates. The whole assembly was baked in vacuum for activating the surfaces of the electrodes. It was then inserted in a tube about $7\frac{1}{2}$ inches long and 4 inches in diameter. The circular plate sealing one end of the tube had "Kovar" seal connections for the potential divider which provided the voltages between the stages. An 8000-volt supply whose output could be varied was used across the potential divider, and by studying the counting rate of the tube for Po alphas as a function of the voltage per stage, with a constant discriminator bias on the scaler, it was found that it attained a plateau at about 480 volts. We used 510 volts per stage safely during the subsequent experiments.

The first tests made showed that the multiplier required only an additional amplification of around 100. With this external gain we were able to detect alphas of less than 200-kv energy. However, it was thought to be convenient to use an amplifier giving a maximum gain of about 2160 which could be cut down in steps of one-half. The external amplification used all throughout this investigation was one-fourth of this value, i.e., 540, which proved to be sufficient and completely satisfactory. The multiplier was coupled to the amplifier through a cathode follower whose amplification was essentially equal to one. In a test made with electrons it was found that the multiplier had a multiplying factor of about $7\times10^5$.

The response of the tube to alphas of different energies, obtained by slowing them down in air before their admission to the electrostatic analyzer, was carefully studied. The bias curves obtained showed that the distribution of pulse heights was independent of the energy of the alphas, at least in the range studied (0.4 to 1.6 Mev), but it seemed to depend on the pressure. Figure 2 shows a curve for two different alpha-energies. For electrons it was found that the distribution was shifted toward the smaller pulse heights such that if the discriminator in the scaling circuit was set at a bias corresponding to a pulse of 0.04 volts from the multiplier tube, one could easily count alphas when electrons were present, for at this bias the number of electrons was practically zero. This is shown in Fig. 3 which gives the bias curves for electrons and for alphas of 1.0 Mev. Protons and deuterons coming from the accelerator tube and scattered by the target were also used to obtain bias curves, and the $Li^{++}$

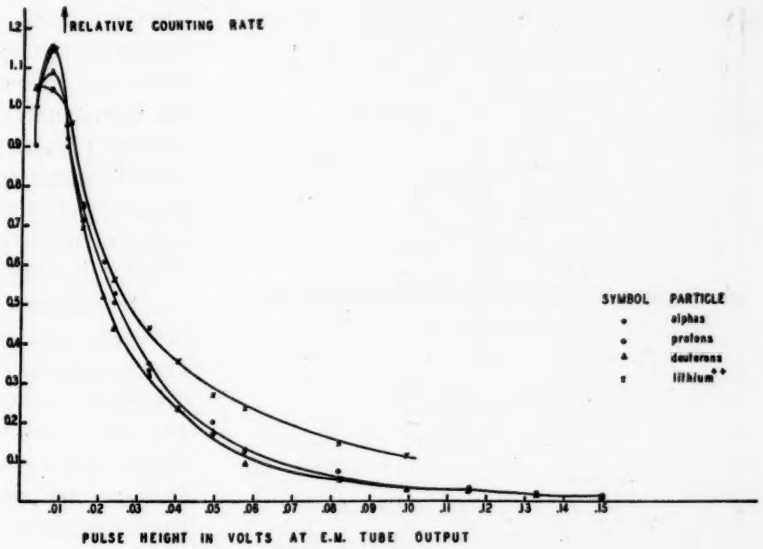


FIG. 4. Bias curves for different particles. Height distributions of pulses at the final plate of the electron multiplier tube due to various ions incident on the first plate. Their energies were 0.2 Mev for the alphas, 0.22 Mev for the protons, 0.230 Mev for the deuterons, and 0.9 Mev for the lithium ions.

ion from the Be-$p$ reaction was also selected and its bias curve obtained. Figure 4 shows these last results.

The background was also carefully studied, and it was found that it depended mainly on the following three factors: (a) the pressure in the tube, (b) oil from the diffusion pumps deposited on the insulators separating the plates in the electrostatic analyzer, which caused discharges when the deflecting voltage was increased, and (c) the high voltage on the analyzer when raised beyond 42 kv. The first factor was avoided by maintaining the pressure less than $5\times10^{-5}$ mm of Hg. The oil was avoided in great part by shutting off the analyzer from the main system overnight. A weak magnet was placed around the connection between the analyzer and multiplier to deflect any secondaries still produced by discharges. With these precautions the background, even at 48 kv on the analyzer, was only slightly greater than at the lower voltages. The counts were of about one or two per second, and in two of the main experiments done it was only about 0.5 count per second, while the intensities of the disintegration particles were of the order of 50 counts per second.

### III. METHOD OF TAKING OBSERVATIONS

The ion beam was magnetically analyzed before striking the target, and each peak was identified by considering the mass and charge of the ions that could be present in the beam, and the ratios of the magnet currents for the different peaks. The magnet current was then adjusted so as to select the proton beam. A second check was accomplished by adjusting the voltage $V$ on the electrostatic analyzer so that the protons scattered by the target were detected by the multiplier. This was done using Eq. (3) and knowing the energy $E_p$ of the bombarding protons. During a series of experiments the magnet current was readjusted either this way or by selecting one of the disintegration peaks on the analyzer, in order to insure a constant beam intensity during a given run.

The amplifier was set at an external gain of 540 and the discriminator of the scaler adjusted so that only pulses greater than 0.0124 volt, put out by the multiplier tube, could be registered. The pressure was never higher than $5\times10^{-5}$ mm of Hg. By varying the deflecting voltage $V$ on the electrostatic analyzer, readings were taken with a mechanical counter for 64 seconds, while the other quantities, namely, the bombarding voltage, the beam current intensity, and the magnet current, were kept as constant as possible. If discharges occurred either in the accelerating voltage or inside the analyzer, the readings were discarded and we waited until conditions were stabilized again. The data presented here is that obtained under almost perfectly steady conditions. As the analyzer voltage was increased in small steps, the counting rate showed the peaks caused by the various disintegration particles.

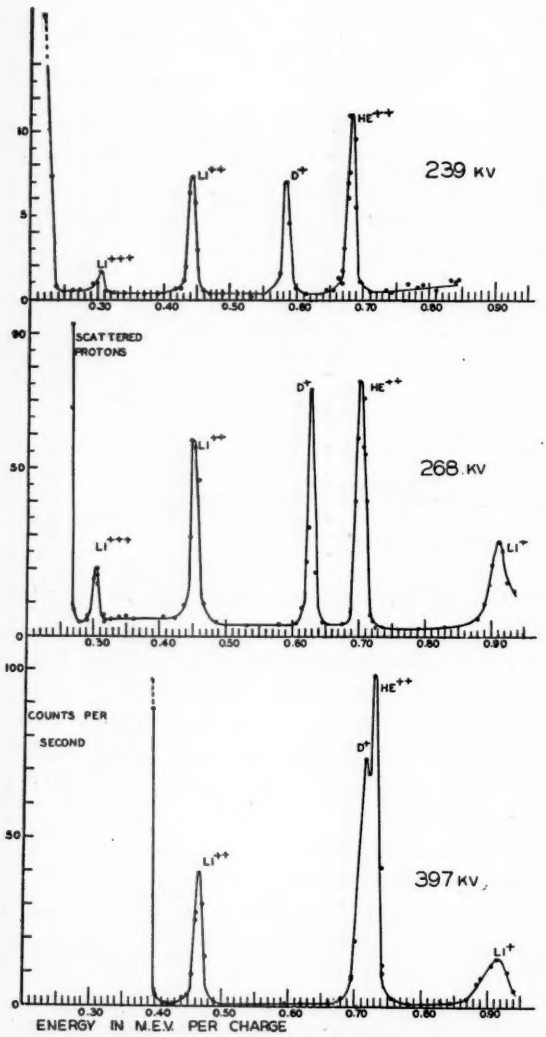


FIG. 5. Energy spectra of particles from the reactions of $_4Be^9(p,\alpha)_3Li^6$ and $_4Be^9(p,d)_4Be^8$ at various bombarding energies. The electrostatic analyzer selects groups of ions having the same energy to electronic charge ratio. The actual deflecting voltages in kilovolts may be obtained by multiplying the abscissae by 50.

## IV. RESULTS AND DISCUSSION

Three different bombarding energies were used: 239, 268, and 397 kv. Although the resistance voltmeter described in the previous section is intrinsically accurate enough to measure the high voltage on the accelerator tube, the electronic meter used to measure the current through the high resistance was later found to be unreliable. So, for these experiments we relied on the electrostatic analyzer for the measurement of the energy of the bombarding protons. This was done by selecting through the analyzer the protons scattered by the beryllium-nickel target, and the energy at the upper limit, as given by the analyzer, was corrected for the limit of resolution of the instrument (2.5 percent), for the increase in potential in entering the analyzer (~1 percent),[14] and, of course, for the loss of energy in scattering from nickel at 90°. In this way the bombarding energies turned out to be 239, 268, and 397 kv, as indicated above. The results for each one of these bombardments are shown in Fig. 5. The abscissae represent the energy of the particle in Mev per charge, obtained from Eq. (3), and the ordinates are the counting rates in counts per second. For the two lower bombarding energies, the resolution of the various peaks is complete. When the bombarding energy was increased to 397 kv the deuterons blend with the alphas, since the rate of energy increase of the particle with respect to the increase in proton energy is higher for the deuteron than for the alpha, as will be seen from the energy relations given below.

The detection of the recoil nucleus $Li^6$ is an interesting feature in these results. It was possible to detect this particle in its three ionized states for a proton energy of 268 kv. For the lower voltage of 239 kv the intensities were low and there was no reliable evidence of the $Li^+$ ion, although the $Li^{+++}$ and the $Li^{++}$ were present. For the higher proton energy, 397 kv, the $Li^{++}$ and the $Li^+$ were detected, but the $Li^{+++}$ was hidden by the screen of scattered protons. In other words, the energy of the lithium nucleus being about 0.921 Mev, we see from Eq. (3) that the analyzer voltage $V$ required to deflect the triply-charged ion would have been 15.4 kv, but since the upper limit of the energy of the scattered protons was around 0.390 Mev, they were detected in great intensities at $V$ less than 19.5 kv. Thus, these protons covered the $Li^{+++}$ ion, which therefore could not be detected.

From the three curves of Fig. 5 the energies of the various particles are obtained and summarized in Table I.

To obtain these energies the abscissa was read at each peak value, i.e., at the midpoint of the width at half-maximum in each case. This is justified by the fact that for our electrostatic analyzer the limit of resolution, set by the geometry of the instrument, is 2.5 percent, and from the curves we obtain, for instance, that for

the alpha-peak at $E_p=268$ kv, the half-width divided by the peak value is $0.036/1.392=2.58$ percent. Thus, the width of these peaks is very close to that expected from the theory of the analyzer for the slit widths used in these experiments. The energy $E$, read at the ordinate of the maximum point of each peak, was then corrected for the difference of potential between the grounded target and that of the calculated radius of the orbit through the electrostatic analyzer, the correction being taken approximately as $-0.01\ E$. The numbers in parentheses are not very accurate due to uncertainty in the position of the peaks because of low intensity, as in the case of $Li^{+++}$ at 239 kv, or because of increased background at the higher analyzer voltage needed to detect the $Li^{+}$ for 268 and 397 kv.

The perfect resolution is due to the fact that since there are no windows in the path of the particles from the instant of their emission to the time of their detection, and since the beryllium target is so thin, practically no straggling occurs, and hence the sharpness of the peaks.

The shifting of the various peaks as the bombarding energy is increased is also clearly seen in Fig. 5. This can be checked with the energy equations. Thus, for the beryllium-proton reactions the well-known relations from the conservation of momentum and energy for ejection at 90° reduce to

$$E_\alpha=0.5E_p+0.6Q_1, \quad (4)$$

$$E_{Li}=0.3E_p+0.4Q_1, \quad (5)$$

$$E_d=0.7E_p+0.8Q_2, \quad (6)$$

where the first two equations are for reaction (1) and the third for reaction (2).*** $E_\alpha$ is the energy of the alpha-particle, $E_p$ the energy of the bombarding protons, $E_{Li}$ the energy of the recoil lithium nucleus, $E_d$ the energy of the deuteron, and $Q_1$ and $Q_2$ the energy releases in the corresponding reactions. From Eqs. (4) and (6) we see, for instance, that the deuteron energy is more sensitive to the bombarding energy than the alpha-energy. Hence the overlapping of the deuterons with the alphas when the voltage was raised to 397 kv. The increase in energy for the alpha and for the deuteron as obtained from Eqs. (4) and (6) are:

$$\Delta E_\alpha/\Delta E_p=0.5,$$
$$\Delta E_d/\Delta E_p=0.7.$$

Thus, when the proton energy is increased from 239 kv to 397 kv, the deuterons should increase their energy by 110 kv, while the alphas receive an increase of only 79 kv. Experimentally, using the data in Table I we find, for the deuterons, an increase of 129 kv, and for the alphas, an increase of 88 kv for that change in proton energy.

TABLE I. Energies of the disintegration particles from $_4Be^9(p,\alpha)_3Li^6$ and $_4Be^9(p,d)_4Be^8$.

| Proton energy (kv) | Alpha-energy (Mev) | Lithium energy $Li^{+++}$ (Mev) | Lithium energy $Li^{++}$ (Mev) | Lithium energy $Li^{+}$ (Mev) | Deuteron energy (Mev) |
|---|---|---|---|---|---|
| 239 | 1.352 | (0.909) | 0.876 | | 0.579 |
| 268 | 1.392 | 0.900 | 0.895 | (0.903) | 0.621 |
| 397 | 1.440 | | 0.921 | (0.907) | 0.708 |

The energy releases $Q_1$ and $Q_2$ were calculated by substitution in Eqs. (4)–(6) and the data from Table I. Using the corrected energy of the alpha-particles to calculate $Q_1$, the values 2.056, 2.097, and 2.069 Mev result from the three values given. The best estimate from these results is $2.074\pm0.03$ Mev. On attempting to calculate the same $Q_1$ from the corrected energies of the $Li^{++}$ particles, one obtains 2.011, 2.039, and 2.005 Mev, a slightly lower value. The value deduced from the alpha-particles seems preferable, since the discrepancy could be accounted for by the loss of 20 kev by the relatively short range $Li^{++}$ particles in leaving the target.

Calculation of the energy release in the reaction $_4Be^9(p,d)_4Be^8$ from the corrected deuteron energies leads to the values 0.516, 0.543, and 0.539 Mev, of which the first seems definitely too low. Inspection of the curve in Fig. 5 for 239-kilovolts bombarding energy indicates that the actual deuteron peak was not located. Disregarding this low result we obtain $0.541\pm0.003$ Mev as the energy release.

As to the relative numbers of deuterons and alpha-particles, the curves are not inconsistent with the findings of other investigators that the cross sections for the two competing reactions are

*** Exact masses from Mattauch's Nuclear Physics Tables were first used, but the differences in the results for $Q_1$ and $Q_2$ were much too small compared to the experimental error in measuring the energies of the particles, hence mass numbers are used in these equations.

TABLE II. Relative numbers of $Li^+$, $Li^{++}$, and $Li^{+++}$ ions.

| Bombarding energy | $Li^{++}/Li^{+++}$ | $Li^{++}/Li^+$ |
|---|---|---|
| 239 kv | 5.9 | |
| 268 | 3.5 | 1.8 |
| 397 | | 2.9 |

approximately equal in this range of bombarding energies. It was difficult to hold the high voltages on the accelerating tube and on the electrostatic analyzer sufficiently steady to locate precisely the maximum ordinate of the sharp peaks.

For the same reason only rough estimates can be given, at the present stage of our experiments, for the relative numbers of lithium ions of various charges. The values of Table II are the maxima of the peaks of Fig. 5. It was shown by running bias curves on the $Li^{++}$ and $Li^{+++}$ peaks that there was no appreciable difference in pulse height distributions produced by the electron multiplier tube from these two ion beams of the same energy (see Fig. 4). In the estimation of the value of the $Li^{++}/Li^+$ ratio we have assumed, without the equivalent experiment having been performed, that the pulse height distributions for $Li^+$ are not widely different from those of $Li^{++}$ and $Li^{+++}$.

A theoretical attempt to explain these lithium ion ratios would be a part of the general problem of the capture and loss of electrons by moving ions. Knipp and Teller[16] have treated the problem for protons, alpha-particles, and intermediate and heavy ions produced in the fission process. They were primarily interested in considering the energy loss, which is due to collisions with electrons and with nuclei, the former being essentially determined by the ionic charge, which in turn depends on the ratio $\gamma$ of the velocity of the outermost electron $v_e$, within the ion, to the velocity $v_i$ of the ion itself. Bohr,[17] in considering the slowing down of a heavy ion, assumes that along its path the ion will lose those electrons whose orbital velocities are smaller than the velocity of the ion, while all the electrons for which $v_e > v_i$, the probability for loss is smaller than the probability for capture. There will be a value of $\gamma$, let us say $\gamma_0$, at which there will be equal probabilities for capture and loss, and $\gamma_0$ should be close to unity. Knipp and Teller have used the experimental data of Rüchardt,[18] Bartels,[19] and Rutherford[20] to estimate $\gamma_0$. They find that $\gamma_0 = 0.8 \pm 0.1$ for hydrogen-like ions, as follows:

for $H \rightleftarrows H^+$ $\gamma_0 = 0.7$ in $H_2$; 0.8 in $N_2$ and $O_2$,
$He^+ \rightleftarrows He^{++}$ $\gamma_0 = 0.8$ in mica.

In our experiments the process $Li^{+++} \rightleftarrows Li^{++}$ represents the capture or loss of a hydrogen-like electron, and might be expected to have a $\gamma_0$ of $0.8 \pm 0.1$.

The process $Li^{++} \rightleftarrows Li^+$ is not hydrogen-like, and there is less available evidence on which to predict $\gamma_0$. Knipp and Teller find that in the analogous process $He \rightleftarrows He^+$, the value of $\gamma_0$ is 1.6.

Calculations by Brunings, Knipp, and Teller[21] for the electron velocity $v_e$ have been used by them to give values of $\gamma_0$ for atomic number $Z = 6$ to $Z = 55$. It is indicated that $\gamma_0$ increases from 1.3 to 1.8 when $Z$ increases from 6 to 55, if the electron considered is the most easily removable one. However, if $v_e$ is to be taken as the velocity of the outermost electron, they calculate that $\gamma_0$ decreases from 0.6 to 0.35 as $Z$ increases through this range.

Since in our present case $Z$ is 3 for lithium, we cannot use their curves to determine $v_e$. We shall therefore estimate only roughly what the value $\gamma$ is, deriving the electron velocity from ionization potential data. Thus for the three lithium ions produced at $E_p = 268$ kv we see from Table I that their energy is about 0.900 Mev, and from Table II that their relative numbers are $Li^{++}/Li^{+++} = 3.53$ and $Li^{++}/Li^+ = 1.83$. We assume that the different ionized states are produced in traveling through the beryllium layer, since the space in the system is a vacuum. Consider the process $Li^{+++} \rightleftarrows Li^{++}$: the orbital velocity of the electron in $Li^{++}$, which is a hydrogen-like atom, is obtained from the energy:

$$E_e = \tfrac{1}{2} m_e v_e^2 = (9)\ (13.53)\ \text{ev},$$

[16] J. Knipp, and E. Teller, Phys. Rev. **59**, 659 (1941).
[17] N. Bohr, Phys. Rev. **58**, 654 (1940); Phys. Rev. **59**, 270 (1941).
[18] E. Rüchardt, Ann. d. Physik **71**, 377 (1923).
[19] H. Bartels, Ann. d. Physik **6**, 957 (1930); **13**, 373 (1932).
[20] E. Rutherford, Phil. Mag. **47**, 277 (1924).
[21] J. H. M. Brunings, J. K. Knipp, and E. Teller, Phys. Rev. **60**, 657 (1941).

while the ion energy is

$$E_i=\tfrac{1}{2}m_iv_i^2=0.900\times10^6 \text{ ev.}$$

Hence:

$$\frac{v_e^2}{v_i^2}=\frac{(121.77)(1840)(6)}{(0.900)(10^6)(1)},$$

$$\frac{v_e^2}{v_i^2}=1.49,$$

and

$$\gamma_1=\frac{v_e}{v_i}=1.22.$$

This value shows that, since $v_e>v_i$, the probability for $Li^{+++}$ to capture an electron and become $Li^{++}$ is greater than the reverse process, or that $Li^{++}$ tries to retain its electron rather than lose it. Hence the process $Li^{+++}\rightarrow Li^{++}$ is more probable than $Li^{++}\rightarrow Li^{+++}$. For the case $Li^{++}\rightleftarrows Li^{+}$, the orbital velocity of either electron is obtained by adding the second ionization potential for lithium, which is 75.28 ev to 121.77 ev of the hydrogen-like atom and dividing by 2. That is, if 75.28 ev is the energy required to remove either of the two electrons in $Li^+$ and 121.77 ev the energy needed to remove the remaining electron in $Li^{++}$, their sum, 197 ev, would represent the total energy of the original $Li^+$, which in absolute value is equal to the kinetic energy of both electrons in $Li^+$. Hence, for one electron only, its kinetic energy is $\frac{1}{2}$ (197) or 98.5 ev. Since the ion velocity is the same as in the preceding case, we have

$$\frac{v_e^2}{v_i^2}=\frac{(98.5)(1840)(6)}{(0.900)(10^6)(1)},$$

$$v_e^2/v_i^2=1.2,$$

and

$$\gamma_2=v_e/v_i=1.09.$$

If 1.6 is the value of $\gamma_0$ in this helium-like process, then for our conditions, where $\gamma_2=1.09$, the process $Li^+\rightarrow Li^{++}$ should be favored. These values of $\gamma_1$ and $\gamma_2$ seem to indicate that the net advantage is for the state $Li^{++}$. Hence the doubly ionized state should be more densely populated than either the singly- or the triply-ionized states. This is, in fact, verified by our data as given in Table II, the ratios $Li^{++}/Li^{+++}$ and $Li^{++}/Li^{+}$ indicating that the $Li^{++}$ ion is always favored.

These elementary considerations indicate that the ionic ratios of lithium should not depend on the bombarding energy as they apparently do in Table II. The variation in the kinetic energy of the lithium ions with proton energy, though observable because the experimental arrangement is adapted to energy rather than intensity measurements, is so small that no appreciable change in $\gamma$ should occur. Until more careful intensity measurements are made it cannot be said that the apparent effect is real.

The detection of the alpha-particles from the splitting of the recoil nucleus $Be^8$ was also attempted in this investigation without success. The first effort made was in connection with the characteristic bias curves for alphas and for protons obtained with the multiplier tube. Since the alphas from $Be^8$ have a very low energy, it was calculated that the deflecting voltage on the analyzer had to be lower than the voltage required to detect the scattered protons from the bombarding beam. However, the intensity of these protons was very high across a wide range of analyzer voltages, hence the first hope to detect the $Be^8$ alphas was based on a different distribution of pulses produced in the multiplier tube by the alphas as compared to that produced by the protons. Unfortunately, the bias curves obtained (see Fig. 4) showed that the distributions were the same, and therefore the protons could not be discriminated against in order to count only alphas.

The second attempt was made to see if any of the $Be^8$ disintegration products could be detected as singly-charge helium ions. It was hoped that the analyzer voltage $V$ required to detect such ions would be greater than that which selected the high energy edge of the scattered protons. In this experiment the analyzer voltage was lowered to a point beyond which the intensities of the disintegration particles would become too small. At 239 kv a careful investigation of the region between the proton limit and the $Li^{+++}$ peak was made, but no particles were detected. We may summarize the experiments by stating that no doubly-charged alpha-particles of energy greater than 480 kev, from the break-up of $Be^8$, could be

found, and no singly-charged helium ions appeared in the energy range above 240 kev.

## V. CONCLUSIONS

The results of this investigation show that the electron multiplier tube can be used successfully as an efficient and reliable detector of particles from nuclear disintegrations. Most of the disadvantages of other types of detectors are eliminated, such as the use of windows, the need of high amplification of pulses, and the troublesome microphonics present in devices like ionization chambers. It is most valuable for the detection of low energy particles and can be used to count either photons, betas, or heavier particles.

In regard to the detection of an atom in its different states of ionization, by using the multiplier tube in combination with the electrostatic analyzer, this investigation points out the possibility of studying the rather complicated problem of the capture and loss of electrons by ions, of which there is not as yet a well established theory. The results reported here, on the relative probabilities of the appearance of singly-, doubly-, and triply-charged ions in a beam of lithium nuclei of 0.900-Mev kinetic energy, support the view that the significant parameter is the ratio of the orbital electronic velocity to the ionic velocity. It is hoped that further experiments of this type will provide more reliable data on this capture and loss phenomenon.

## ACKNOWLEDGMENTS

I wish to thank Professor S. K. Allison, who suggested this problem and gave constant guidance during the progress of the work. My thanks are also due Dr. J. S. Allen for his generous and valuable help during the initial study of the electron multiplier tube and the various problems in electronics encountered during the investigation. I also wish to extend my appreciation to the other members of our laboratory group for their assistance during the course of these experiments: H. V. Argo, W. R. Arnold, H. A. Wilcox, and C. N. Yang.

# Gamma-Ray Spectrometer Measurements of Fluorine and Lithium under Proton Bombardment

R. L. WALKER AND B. D. MCDANIEL
*Cornell University, Ithaca, New York*

(Received April 16, 1948)

The spectra of the gamma-radiation emitted by lithium and fluorine under proton bombardment have been investigated with a spectrometer which measures the total energy of electron pairs produced in a thin radiator exposed to the gamma-radiation. A long-suspected 14.8-Mev gamma-ray line from the 440-kev resonance in lithium has been clearly resolved from the well-known sharp line at 17.6 Mev. The gamma-radiation from fluorine has been found to consist of two lines at 6.13±0.06 and 6.98±0.07 Mev, rather than a single line as previously believed. Possible variations in the positions and in the relative intensities of the two lines of each spectrum, with changes in the proton energy, have been investigated by using protons of energies approximately 0.45, 0.7, and 1.15 Mev from the Cornell cyclotron. The gamma-ray spectrometer used in these measurements is described, and a discussion given of the factors limiting its resolution. The resolution is such that the observed width at half-maximum of a sharp gamma-ray line is approximately 5.5 percent of its energy.

## I. INTRODUCTION

THE methods which have been used for the determination of gamma-ray energies in the region above 2 or 3 Mev are exemplified by the experiments which have been performed to measure the spectra of the gamma-radiation emitted by lithium and fluorine under proton bombardment. From early measurements of the absorption coefficient in different materials, McMillan[1] obtained a value 5.4 Mev for the quantum energy of the fluorine radiation; and Crane, Delsasso, Fowler, and Lauritsen[2] obtained values of 5.6 and 6.3 Mev for the fluorine and lithium gamma-rays, respectively.

In 1935, Crane, Delsasso, Fowler, and Lauritsen[3] reported at least eleven lines from lithium between 2 and 16 Mev, based on measurements of the spectrum of recoil electrons in a cloud chamber. By a similar method, Gaerttner and Crane[4] found large peaks at 11.5, 14.5, and 17 Mev, for lithium, and two lines for fluorine, at 4 and 5.7 Mev. In 1937, Delsasso, Fowler, and Lauritsen[5] pointed out sources of error in their previous work and gave results for the lithium spectrum, obtained by measuring the total energy of electron pairs ejected from a thin lead plate in a cloud chamber. Their curve shows a single peak with a maximum at 17.1 Mev. From a marked asymmetry in the peak, they conclude that in addition to the main line at 17.1±0.5 Mev, there are one or more additional lines near 14 Mev, but none between 2 and 10 Mev.

By the same method, Delsasso, Fowler, and Lauritsen[6] measured the fluorine spectrum and obtained a single symmetrical line at 6.0±0.2 Mev.

Magnetic spectrometers have been used by Dee, Curran, and Strothers[7] to measure the fluorine radiation, and by McDaniel, Von Dardel, and Walker[8] to measure the lithium spectrum, but thus far no improvements have been reported over the cloud-chamber results of Delsasso, Fowler, and Lauritsen.

The high energy gamma-rays from lithium are believed to arise from the reaction:

$$Li^7+H^1\rightarrow Be^{8*}\rightarrow Be^8+h\nu. \qquad (1)$$

The 17.6-Mev gamma-ray is emitted when the $Be^8$ nucleus is left in its ground level, whereas

[1] E. McMillan, Phys. Rev. **46**, 325, 868 (1934).
[2] H. R. Crane, L. A. Delsasso, W. A. Fowler, and C. C. Lauritsen, Phys. Rev. **46**, 531 (1934).
[3] H. R. Crane, L. A. Delsasso, W. A. Fowler, and C. C. Lauritsen, Phys. Rev. **48**, 125 (1935).
[4] E. R. Gaerttner and H. R. Crane, Phys. Rev. **52**, 582 (1937).
[5] L. A. Delsasso, W. A. Fowler, and C. C. Lauritsen, Phys. Rev. **51**, 391 (1937).
[6] L. A. Delsasso, W. A. Fowler, and C. C. Lauritsen, Phys. Rev. **51**, 527 (1937).
[7] P. I. Dee, S. C. Curran, and J. E. Strothers, Nature **143**, 759 (1939); S. C. Curran, P. I. Dee, and J. E. Strothers, Proc. Roy. Soc. **A174**, 546 (1940).
[8] B. D. McDaniel, Guy Von Dardel, and R. L. Walker, Phys. Rev. **72**, 985 (1947).

lower energy gamma-rays may be expected if the $Be^8$ is left in an excited state.[5]

Early measurements of the excitation curve for the lithium radiation showed resonances near 450 kev and 850 kev.[9–11] Hafstad, Heydenburg, and Tuve[12] showed that the 440-kev resonance is very narrow, with a width of about 11 kev. They did not confirm the existence of the higher energy resonance. In 1940, Hudson, Herb, and Plain[13] found that radiation from the higher resonance has an energy of only 459 kev, and interpreted it as arising from the excitation of the 455-kev level in $Li^7$ by inelastic scattering of the protons. They also found that above the sharp 440-kev resonance the yield of high energy gamma-rays from lithium does not drop to zero but to a small value which remains almost constant up to a proton energy of about 1.6 Mev. This result has been confirmed in a recent investigation of the excitation curve by Bonner and Evans.[14]

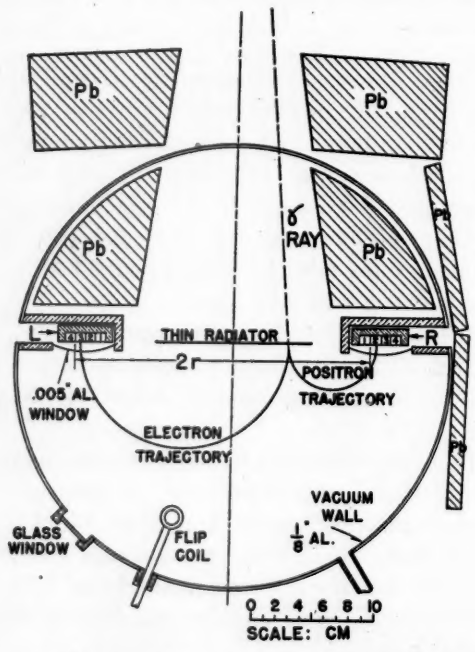


FIG. 1. Diagram of the spectrometer—a horizontal section through the gap of the large magnet which produces a magnetic field normal to the plane of the paper. The vertical height of the gap is 4 inches. Coincidences are observed between any one of the four Geiger counters at the left labeled *L* and any one of the four on the right labeled *R*. The gamma-ray source (cyclotron target) was 60 cm from the radiator in the present experiments.

In addition to the gamma-rays emitted by lithium under proton bombardment, alpha-particles of 8.4-cm range are produced by the reaction:[15,16]

$$Li^7+H^1\rightarrow Be^{8*}\rightarrow 2He^4. \qquad (2)$$

The excitation curve for these long-range alpha-particles shows a smooth Gamow type increase in alpha-particle yield with increasing proton energy,[12,15–19] with no sign of a resonance at 440 kev. As is well known, the sharpness of the 440-kev gamma-ray resonance is explained by the action of rigid selection rules preventing the disintegration of the $Be^{8*}$ "gamma-ray level" at 17.6 Mev into two alpha-particles.[5,12,20,21]

The origin of the gamma-radiation from fluorine has been the subject of much speculation, but the reaction is now believed to be:

$$F^{19}+H^1\rightarrow Ne^{20*}\rightarrow O^{16*}+He^4+Q,\quad O^{16*}\rightarrow O^{16}+h\nu. \qquad (3)$$

The simple capture reaction analogous to (1):

$$F^{19}+H^1\rightarrow Ne^{20*}\rightarrow Ne^{20}+h\nu \qquad (4)$$

was shown to be incorrect since no gamma-rays of the expected energy, 13 Mev, were observed.[1,4,6] Successive emission of two gamma-rays of about half the total energy was suggested by Burcham and Smith,[22] since they could not find the low energy alpha-particles expected from reaction (3). However, this was ruled out by Dee, Curran, and Strothers,[7] who measured coincidences between gamma-rays, and found less than 1 percent of the number expected if two suc-

[9] L. R. Hafstad and M. A. Tuve, Phys. Rev. **48**, 306 (1935).
[10] L. H. Rumbaugh and L. R. Hafstad, Phys. Rev. **50**, 681 (1936).
[11] R. G. Herb, D. W. Kerst, and J. L. McKibben, Phys. Rev. **51**, 691 (1937).
[12] L. R. Hafstad, N. P. Heydenburg, and M. A. Tuve, Phys. Rev. **50**, 504 (1936).
[13] C. M. Hudson, R. G. Herb, and G. J. Plain, Phys. Rev. **57**, 587 (1940).
[14] T. W. Bonner and J. E. Evans, Phys. Rev. **73**, 666 (1948).
[15] J. D. Cockcroft and E. T. S. Walton, Proc. Roy. Soc. **A137**, 229 (1932).
[16] M. L. E. Oliphant, B. B. Kinsey, and Lord Rutherford, Proc. Roy. Soc. **A141**, 722 (1933).
[17] M. C. Henderson, Phys. Rev. **43**, 98 (1933).
[18] R. G. Herb, D. B. Parkinson, and D. W. Kerst, Phys. Rev. **48**, 118 (1935).
[19] N. P. Heydenburg, C. T. Zahn, and L. P. D. King, Phys. Rev. **49**, 100 (1936).
[20] H. A. Bethe, Rev. Mod. Phys. **9**, 205, 211 (1937).
[21] F. Kalckar, J. R. Oppenheimer, and R. Serber, Phys. Rev. **52**, 279 (1937).
[22] W. E. Burcham and C. L. Smith, Proc. Roy. Soc. **A168**, 176 (1938).

cessive gamma-rays were emitted. They also obtained evidence against a reaction similar to (3):

$$F^{19}+H^1\rightarrow Ne^{20**}\rightarrow Ne^{20*}+h\nu,$$
$$Ne^{20*}\rightarrow O^{16}+He^4+Q, \quad (5)$$

by showing that the gamma-ray energy does not change with proton energy for protons of 330, 670, and 860 kev. This result was confirmed by Lauritsen, Lauritsen, and Fowler,[23] who concluded from cloud-chamber measurements that the gamma-radiation has the same average energy for protons of energy 334, 950, and 1400 kev on "semithick" targets.

The low energy alpha-particles expected from reaction (3) were found by Burcham and Smith,[24] and by McLean, Becker, Fowler, and Lauritsen.[25] Burcham and Devons[26] showed that the energy of these alpha-particles increases with proton energy by about the amount to be expected, and that their excitation function follows closely that of the gamma-rays, from 300 to 900 kev. A detailed study of these low energy alpha-particles at different proton energies was made by Becker, Fowler, and Lauritsen,[27] who obtained a value $Q=1.81\pm0.04$ Mev for reaction (3).

The excitation function for the gamma-rays emitted by fluorine under proton bombardment is a series of many sharp resonances, the lowest being at 334 kev.[14,28–30] The narrow widths of these resonances, most of them under 10 kev,[30,14] is again explained by selection rules which prohibit or retard the disintegration of the excited $Ne^{20}$ nucleus by long-range alpha-particle emission.[21,28,20]

The production of such alpha-particles of 6-cm range was observed by Henderson, Livingston, and Lawrence,[31] who obtained a smooth Gamow type excitation function for this reaction:

$$F^{19}+H^1\rightarrow Ne^{20*}\rightarrow O^{16}+He^4+Q. \quad (6)$$

Later, broad resonances were found in the thin target excitation curve for these long-range alpha-particles,[26,29] but these resonances are not correlated with those observed for the gamma-rays.

In addition to the long-range alpha-particles and gamma-rays emitted by fluorine under proton bombardment, electron pairs of total energy $5.9\pm0.5$ Mev were found by Fowler and Lauritsen[32] in 1939. The excitation function for these pairs[29,30,32] exhibits resonances which differ from the gamma-ray resonances, so that the pairs cannot be the result of ordinary pair internal conversion of the gamma-rays.[32] They are ascribed to the reaction:

$$F^{19}+H^1\rightarrow Ne^{20*}\rightarrow O_\pi^{16*}+He^4+Q,$$
$$O_\pi^{16*}\rightarrow O^{16}+\pi. \quad (7)$$

The oxygen pair level, $O_\pi^{16*}$, is assumed to have $J=0$, and to have no non-zero levels below it, so that the emission of a single quantum is forbidden.[32,33] The energy of the pairs has been measured with a magnetic spectrograph by

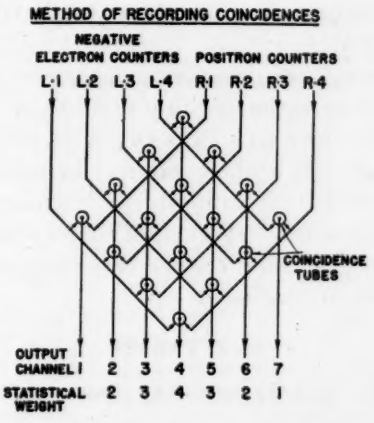
METHOD OF RECORDING COINCIDENCES
NEGATIVE ELECTRON COUNTERS
POSITRON COUNTERS
L-1 L-2 L-3 L-4 R-1 R-2 R-3 R-4
COINCIDENCE TUBES
OUTPUT CHANNEL 1 2 3 4 5 6 7
STATISTICAL WEIGHT 2 3 4 3 2 1

FIG. 2. Schematic diagram of the coincidence circuit. Coincidences from the sixteen possible combinations of one positron counter and one negative electron counter are grouped into seven different energy output channels according to the separation of the counters. The "statistical weight" of each channel is simply the number of individual counter pairs feeding it.

[23] T. Lauritsen, C. C. Lauritsen, and W. A. Fowler, Phys. Rev. **59**, 241 (1941).
[24] W. E. Burcham and C. L. Smith, Nature **143**, 795 (1939).
[25] W. B. McLean, R. A. Becker, W. A. Fowler, and C. C. Lauritsen, Phys. Rev. **55**, 796 (1939).
[26] W. E. Burcham and S. Devons, Proc. Roy. Soc. **A173**, 555 (1939).
[27] R. A. Becker, W. A. Fowler, and C. C. Lauritsen, Phys. Rev. **62**, 186 (1942).
[28] E. J. Bernet, R. G. Herb, and D. P. Parkinson, Phys. Rev. **54**, 398 (1938).
[29] J. F. Streib, W. A. Fowler, and C. C. Lauritsen, Phys. Rev. **59**, 253 (1941).
[30] W. E. Bennett, T. W. Bonner, C. E. Mandeville, and B. E. Watt, Phys. Rev. **70**, 882 (1946).
[31] M. C. Henderson, M. S. Livingston, and E. O. Lawrence, Phys. Rev. **46**, 38 (1934).
[32] W. A. Fowler and C. C. Lauritsen, Phys. Rev. **56**, 840 (1939).
[33] J. R. Oppenheimer and J. S. Schwinger, Phys. Rev. **56**, 1066 (1939).

Tomlinson,[34] who found a total energy of 6.0±0.2 Mev.

The results of the experiments to be described below confirm the essential features of the ideas outlined above as to the origin of the gamma-radiation from lithium and fluorine under proton bombardment. It will only be necessary to propose two gamma-ray levels of $O^{16}$ for reaction (3), in order to account for the two gamma-rays observed from fluorine.

## II. APPARATUS

### A. The Gamma-Ray Spectrometer

The spectrometer used in the present experiments is based upon the same principles as one used a year ago by McDaniel, Von Dardel, and Walker.[8] It performs a magnetic analysis of pairs produced by the gamma-rays in a thin radiator. A diagram of the apparatus is shown in Fig. 1, which is a horizontal cross section through the gap of a large magnet used to produce a magnetic field perpendicular to the plane of the paper.

Electron pairs are produced in the thin radiator by high energy gamma-rays from the cyclotron target or other source. The two particles of a pair are emitted in directions which do not deviate greatly from that of the incident gamma-ray, and follow circular paths in the magnetic field, as indicated schematically in Fig. 1. A fraction of the positrons produced will enter one of the four Geiger counters on the right labeled $R$ in the figure, and, similarly, a fraction of the negative electrons will have radii of curvature such as to enter one of the four Geiger counters on the left labeled $L$. Coincidences are observed between any one of the four positron counters and any one of the four electron counters, giving, in all, sixteen possible coincidence pairs. If an electron pair produces a coincidence between two counters whose separation is $2r$ (for example, counters $L3$ and $R2$ in Fig. 1), then the *sum* of the radii of curvature of the positron and that of the electron ($r_1$ and $r_2$) is known and is equal to $r$. From the well-known relation between the momentum of an electron and its radius of curvature in a magnetic field, the sum of the momenta of the positron and the electron is then

$$p_1+p_2=300H(r_1+r_2)=300Hr. \qquad (8)$$

If $H$ is in gauss and $r$ in cm, $p$ will be in electron volts.* The energy of the quantum which produced the pair will be equal to the total energy of the two particles, or

$$k=E_1+E_2=(p_1^2+\mu^2)^{\frac{1}{2}}+(p_2^2+\mu^2)^{\frac{1}{2}}.$$

If $p_1 \gg \mu$ and $p_2 \gg \mu$ then

$$k \approx 300Hr[1+(\mu^2/2p_1p_2)]. \qquad (9)$$

The "correction term," $\mu^2/2p_1p_2$, depends upon the individual momenta, $p_1$ and $p_2$, and thus depends upon the particular position along the radiator where the pair originated. However, if $k \gg \mu$, it is easily seen that this term is small, and that its dependence on the place of origin of the pair is actually very slight. This may be seen by calculating the correction term, using the approximation $p_1+p_2 \approx k$, for a pair produced at the center of the radiator, and for one produced at its edge. If a coincidence is observed for a pair produced at the center of the radiator, $(\mu^2/2p_1p_2)=(2\mu^2/k^2)$. If the pair were produced at the edge of the radiator, then for a radiator of the width actually used, $(\mu^2/2p_1p_2)=(8/3)(\mu^2/k^2)$. Using the average of these two results we may write

$$k=300Hr[1+(7/3)(\mu^2/k^2)], \qquad (10)$$

and the relative error caused by variations in the correction term for pairs originating at different places along the radiator will be less than $\frac{1}{3}(\mu^2/k^2)$. This is 0.9 percent for a 3-Mev gamma-ray, 0.2 percent for a 6-Mev gamma-ray, and much smaller for the 17.6-Mev gamma-ray from lithium.

The above considerations show that, for a given value of the magnetic field, all coincidences in a given pair of counters are produced by gamma-rays of essentially a single energy. Furthermore, all pairs of counters having the same separation are sensitive to gamma-rays of the same energy, and their data may be recorded together, as will be described later.

In the above discussion we have obviously neglected certain effects which will tend to reduce the resolving power of the spectrometer. Chief among these are the finite width of the Geiger

[34] E. P. Tomlinson, Phys. Rev. **60**, 159A (1941).

* We shall use energy units for both momentum and mass. The momentum of a light quantum is then equal to its energy and both will be denoted by $k$. Cf. Heitler, *Quantum Theory of Radiation* (Oxford University Press, London, 1936).

TABLE I. Effect of electron scattering in Al window.

| Electron energy (Mev) | $(\frac{1}{2}\langle\Theta^2\rangle_{Av})^{\frac{1}{2}}$ (radians) | $\delta$ (cm) | $\delta/w$ relative increase in effective counter width (%) |
|---|---|---|---|
| 10 | 0.17 | 0.14 | 17 |
| 5 | 0.34 | 0.26 | 32 |
| 2 | 0.9 | 0.9 | 110 |

TABLE II.

| Radiator | Thickness (g/cm²) | Thickness (radiation lengths)[36] | $\langle\Delta k/k\rangle_{Av}$ $k=17.6$ Mev (%) | $\langle\Delta k/k\rangle_{Av}$ $k=6.1$ Mev (%) |
|---|---|---|---|---|
| 0.003″ Al | 0.0211 | 0.00080 | 0.13 | 1.04 |
| 0.002″ Cu | 0.0466 | 0.0035 | 0.55 | 4.5 |
| 0.004″ Cu | 0.0888 | 0.0067 | 1.06 | 8.7 |
| 0.003″ Pb | 0.0846 | 0.0143 | 2.3 | — |

counters and the fact that the electrons are not emitted in a direction exactly normal to the surface of the radiator, but with a spread of angles from this normal. These and other effects will be investigated later in discussing the resolution obtainable, but it may be mentioned now that the 180-degree focusing utilized in the spectrometer is a powerful aid in reducing the effects of the spread in angles of emission of the electrons.

The Geiger counters used for measuring coincidences caused by pairs are of square cross section about 8 mm wide. Each row of four counters was constructed by milling four slots in a brass plate, separated by $\frac{1}{32}$-in. walls. The front face was then covered with 0.002-in. brass shim stock. Since the counters are 6 inches long, and the magnet gap only 4 inches high, the pole pieces are provided with slots to receive the counters. The pole pieces form the lids of a vacuum chamber whose $\frac{1}{8}$-in. aluminum walls are indicated in Fig. 1. The counters are not located within the vacuum itself, but are separated from it by a thin 0.005-in. aluminum window through which the electrons must pass. The height of this window, 8.3 cm, determines the useful length of the counters, and is sufficiently high to give a good counting rate even with weak gamma-ray intensities.

The area of the radiators used was $6.3\times12.8$ cm. The thickest radiator was of 0.004-in. copper and the thinnest of 0.003-in. aluminum. Two different radiators can be supported on rotating frames in the vacuum chamber in such a way that either one may be placed in position or removed from the gamma-ray beam, as desired, without breaking the vacuum.

The reason for evacuating the chamber of the spectrometer is not only to avoid scattering of the pair electrons by air, but also to avoid the production of pairs in the air. The latter effect would not always be entirely negligible since radiators as thin as 0.003-in. aluminum have been used and this is equivalent to only 25 cm of air for the production of pairs. Recoil electrons and pairs are produced in the front wall of the vacuum chamber, of course, but these are prevented from reaching the counters by the "clearing field" in front of the radiator.

The counters are shielded from direct gamma-rays from the source by the lead blocks shown in Fig. 1. There is also some lead shielding in the vertical direction, which is not shown, and which shields most of the top and bottom of the chamber from the direct gamma-rays. In addition, the $\frac{1}{2}$-inch lead plates shown in Fig. 1 were placed just outside the chamber by the side of the positron counters. This was found to cut down the "singles" counting rate of these counters by a large factor—presumably by preventing recoil electrons from the air and elsewhere outside the chamber from being deflected into the positron counters by the magnetic field.

It is obviously important that the magnetic field be uniform throughout the region which is traversed by the pair electrons. Since the gap height is rather large, the pole faces were supplied with "Rose shims"[35] to delay the falling off of the field near the edge of the magnet. A map of the field made with small search coils showed that the field was uniform within the accuracy of measurement, about 0.2 percent, from the center of the magnet out to a radius slightly larger than that given by the outside wall of the counters. In addition, the very local disturbances to the field caused by the slots in the pole pieces for holding the counters were measured to make sure they were negligible.

This description of the spectrometer may be concluded by giving an approximate value for its sensitivity in detecting gamma-rays. The counting efficiency has been calculated from the cross

[35] M. E. Rose, Phys. Rev. **53**, 715 (1938).

TABLE III. Summary of measurements.

| Figure | Target | Proton energy (Mev) | Energy range investigated (Mev) | Radiator (see Table II) |
|---|---|---|---|---|
| 3 | Thick Li | 1.15 | 3–19 | 0.002″ Cu |
| 4 | Thin Li (150 kev) | 0.46 | 12–19 | 0.002″ Cu |
| 4 | Thick Li | 0.75 | 10–19 | 0.002″ Cu |
| 4 | Thick Li | 1.15 | 10–19 | 0.002″ Cu |
| 5 | Thin Li (150 kev) | 0.46 | 11–19 | 0.004″ Cu |
| 5 | Thin Li (70 kev) | 1.15 | 11–19 | 0.004″ Cu |
| 6 | Thick $CaF_2$ | 1.15 | 3–18 | 0.002″ Cu |
| 7 | Thick $CaF_2$ | 1.15 | 4.8–7.8 | 0.003″ Al |
| 7 | Thick NaF | 1.15 | 4.8–7.8 | 0.003″ Al |
| 8 | Thick NaF | 0.45 | 4.8–7.8 | 0.002″ Cu |
| 8 | Thick NaF | 0.70 | 4.8–7.8 | 0.002″ Cu |
| 8 | Thick $CaF_2$ | 1.15 | 4.8–7.8 | 0.002″ Cu |

section for pair production in the radiator material and from the geometry of the apparatus. The result is that the peak counting rate per single counter pair, for 17.6-Mev gamma-rays and a 0.002-in. Cu radiator (0.0035 radiation lengths),[36] is approximately $10^{-7}$ times the rate of gamma-emission from the source. The source is assumed to be 60 cm from the radiator, as it was in the present experiments.

At lower gamma-ray energies the effective sensitivity decreases both because the cross section for pair production decreases, and because thinner radiators must be used to maintain the same resolution. At energies below 5 or 6 Mev the resolution becomes unavoidably worse than that attainable at higher energies, and below 3 Mev the spectrometer would not be very useful.

### B. Recording Equipment

Pulses from each of the eight Geiger counters in the spectrometer are given one stage of amplification, and then used to trigger a multivibrator which produces an approximately square, negative pulse about 1.5 microseconds long. This length determines the resolving time against accidental coincidences. The negative pulse from each counter channel is then fed into each of four Rossi cathode follower type coincidence tubes which measure coincidences between this counter and any one of the four on the opposite side of the spectrometer. This arrangement is shown by the schematic diagram of Fig. 2, as is also the manner of grouping the output pulses from the coincidence tubes into seven different channels according to the distance of separation of the two counters giving the coincidence. For a given magnetic field these seven channels count electron pairs in seven different energy intervals, according to the relation (10). The number of pulses in each of the seven output channels is counted by a scale of four, using the Higinbotham circuit[37] and a mechanical recorder.

The seven output channels have different statistical weights as shown in Fig. 2, according to the number of counter pairs having the appropriate separation. Thus only one counter pair ($L1+R1$) has the smallest separation, and coincidences from this pair are counted alone in the lowest energy channel, No. 1. On the other hand, four counter pairs ($L4+R1$, $L3+R2$, $L2+R3$, $L1+R4$) have the separation corresponding to the central channel, No. 4.

In addition to recording coincidences, the individual "singles" counting rates of one of the positron counters, and one of the negative electron counters, were measured in order to be able to calculate the accidental coincidence rate. The rate of accidental coincidences was 0.1 to 0.3 percent of the peak counting rate in typical cases, and no correction for it has been made in any of the data.

### C. Magnetic Field Measurement

The magnetic field in the spectrometer was measured by means of a flip coil and fluxmeter calibrated with a standard mutual inductance. A null method was used in order to obtain high sensitivity. This method is capable of high relative accuracy, but the absolute accuracy is limited by that of the mutual inductance and by possible uncertainties in the effective area of the flip coil. For this reason an independent absolute field calibration was obtained by a nuclear induction experiment in which the Larmor frequency of precession of protons in the magnetic field of the spectrometer was measured. From the accurately known value of the gyromagnetic ratio of the proton,[38] and the observed Larmor frequency, the field strength may be found.[39] From measure-

[36] See, for example, B. Rossi and K. Greisen, Rev. Mod. Phys. 13, 240 (1941).

[37] W. A. Higinbotham, J. Gallagher, and M. Sands, Rev. Sci. Inst. 18, 706 (1947).

[38] S. Millman and P. Kusch, Phys. Rev. 60, 91 (1941).

[39] F. Bloch, Phys. Rev. 70, 460 (1946); F. Bloch, W. W. Hansen, and M. Packard, Phys. Rev. 70, 474 (1946); E. M.

ments at magnetic fields of 1650, 2000, 2350, and 2820 gauss, it was found that the calibration of the flip coil equipment should be changed by only 0.5 percent. We are indebted to Mr. E. Sharp for making this absolute field calibration.

### D. Targets and Monitors

For the fluorine measurements, thick targets of $CaF_2$ and of NaF were used. These were prepared by mixing $CaF_2$ powder in distilled water, or disolving NaF, then pouring the mixture or solution into a recessed area in a brass target backing, and evaporating away the water. For some of the lithium measurements a thick target was used, which was made by melting pieces of lithium metal on a brass plate in a vacuum. Much more satisfactory were thin evaporated lithium targets used at proton energies of 0.46 and 1.15 Mev. These thin targets were made in a high vacuum by evaporating lithium metal from a steel crucible onto the brass target backing. Both thin targets used had about the same thickness, 0.36 mg/cm², as determined by weighing. This corresponds to about 70 kev for protons of 1.15 Mev and to about 150 kev for protons of 0.46 Mev.

In order to monitor the total gamma-ray intensity from the cyclotron target, two Geiger counters were placed in lead shields about 60 cm away from the target, one above, and one below. Two monitors were used merely to obtain a check on the constancy of one of them.

### E. Resolution

The various factors which may contribute to the resolution width of the spectrometer are the following:

#### (1) *The Finite Width of the Counters*

This is the most important contribution to the resolution width provided a sufficiently thin radiator is used to minimize multiple scattering of the electrons. Ideally, the effect of the counter width is to give a triangular resolution function. That is, the observed shape of a sharp gamma-ray line would be an isosceles triangle, with a base equal to the fraction $2w/2r$ of the energy of the line, where $w$ is the width of the counters and $2r$ their separation. This counter separation is somewhat different for each of the seven output channels of the coincidence circuit, as described above. However, by using the average value $\langle 2r\rangle_{Av}=24$ cm, and the geometrical width of the counters, $w=0.80$ cm, we obtain for the percentage width of a line at half-maximum, due to the finite size of the counters alone, $w/\langle 2r\rangle_{Av}=3.3$ percent.

#### (2) *Scattering of Electrons by the Counter Wall, or by the 0.005-in. Aluminum Window in Front of the Counters*

Because of this scattering the edge of a counter is not sharply defined as far as the electrons are concerned. If an electron enters the $\frac{1}{32}$-inch wall separating two adjacent counters, for example, it will almost certainly be scattered into one or the other of the counters, and thus be recorded. Moreover, an electron may sometimes be scattered in such a direction as to pass through two or more counter walls, and thus be recorded simultaneously in two or more of the seven different energy channels of the spectrometer. We believe that this effect is responsible for the low, broad "tail" which appears at the base of the observed gamma-ray lines. If so, this tail should be approximately symmetrical on the high and low energy sides.

The effect of scattering in the 0.005-in. Al window is to spread the electrons which would enter the counter row at a given point over an area of width approximately $2\delta$. This increases the counter width by something of the order of $\delta$,

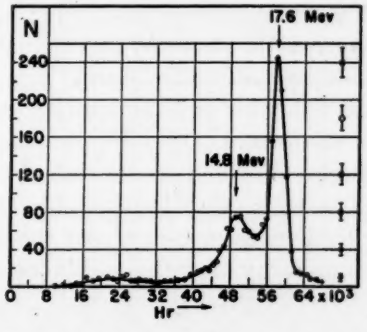


FIG. 3. Survey of the lithium gamma-ray spectrum between 3 and 19 Mev, obtained with a thick lithium target and protons of energy 1.15 Mev. The 0.002-in. Cu radiator was used in the spectrometer. The number of pair coincidences, $N$, obtained is plotted against $Hr$ in gauss cm, where $r$ is the *sum* of the radii of the two electrons of a pair. The standard statistical errors of each point, $(N)^{\frac{1}{2}}$, are indicated on the right of the curve.

Purcell, H. C. Torry, and R. V. Pound, Phys. Rev. 69, 37 (1946); A. Roberts, Rev. Sci. Inst. 18, 845 (1947).

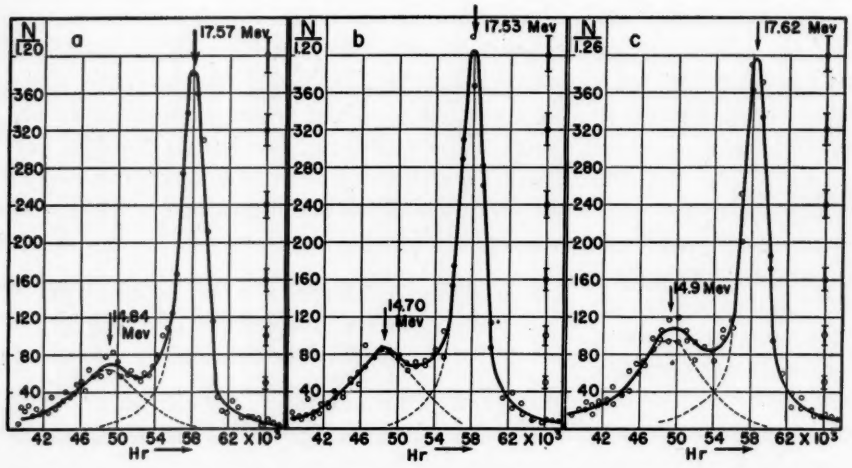


FIG. 4. Detail of the two gamma-ray lines from lithium bombarded with protons of three different energies: (a) Proton energy 0.46 Mev—target thickness approximately 150 kev; (b) proton energy 0.75 Mev—thick target; (c) proton energy 1.15 Mev—thick target. The 0.002-in. Cu radiator was used for all three curves.

in its effect on the resolution. Table I shows values of $\delta$ calculated for three different electron energies, from the distance between aluminum window and counters, and from the mean square angle of multiple scattering.[36]

$$\langle\Theta^2\rangle_{Av}=E_s^2t/p^2\beta^2, \qquad (11)$$

where $E_s=21$ Mev, and $t$ is the thickness in radiation lengths, of the material traversed by the electron.

### (3) *Multiple Scattering of Electrons in the Radiator*

If either electron of a pair is scattered in any direction from the normal to the radiator, it will appear to have too low an energy, because of the properties of 180-degree focusing. The result is to make the observed gamma-ray line asymmetrical, with a tail on the low energy side. The magnitude of this effect may be obtained by calculating the average lowering of the measured gamma-ray energy, $\langle\Delta k/k\rangle_{Av}$. This may be easily found with the help of the formula (11), and the assumption that all angles involved in the calculation are small. The result is tabulated in Table II for the 17.6-Mev lithium gamma-ray, and the 6.1-Mev fluorine gamma-ray, for the radiators actually used.

### (4) *Angular Divergence of the Electrons in the Pair Production Process*

This has, of course, the same effect as angular divergence caused by multiple scattering in the radiator.

The angular distribution of electrons in pair production is not known explicitly at small angles, but a characteristic angle of emission of an electron (or positron) of energy $E$ is $\theta_p\approx\mu/E$. Except for very thin radiators, this is smaller than the multiple scattering. It imposes, however, a fundamental lower limit on the angular divergence, and means that it is useless to employ a radiator so thin that the mean square scattering angle $\langle\Theta^2\rangle_{Av}$ is reduced below $\theta_p^2\approx\mu^2/E^2$. The two become equal for a radiator thickness $T=0.0011$ radiation lengths. This corresponds, for example, to 0.004-in. aluminum, so the effect of the angular divergence in pair production must be comparable to the effect of multiple scattering when the 0.003-in. aluminum radiator is used. It will be noted that this is independent of the electron energy since the energy dependence of the two angles is the same.

### (5) *Deviations from Normal Incidence upon the Radiator, of Gamma-Rays Striking the Radiator far from its Center*

The effect of the angular divergence arising from non-normal incidence of the gamma-rays on the radiator is small, and when calculated from the geometry of the apparatus, gives

$$\langle\Delta k/k\rangle_{Av}=0.37 \text{ percent.}$$

### (6) *Energy Loss of Electrons in the Radiator*

The angular divergence of electrons from the normal to the radiator tends to make the gamma-ray line asymmetrical rather than to shift the

position of the peak. Loss of energy by the electrons in the radiator will, however, cause the peak to shift toward lower energy by just the amount of the average energy loss. The shifts in the observed gamma-ray lines resulting from energy loss by inelastic collisions have been found[36] to have the following small values:

$\Delta k = 0.072$ Mev for the 17.6-Mev lithium gamma-ray and the 0.002-in. Cu radiator. $\Delta k/k = 0.4$ percent.

$\Delta k = 0.032$ Mev for the 6.1-Mev fluorine gamma-ray, and the 0.003-in. Al radiator. $\Delta k/k = 0.5$ percent.

In addition to shifting the position of the gamma-ray lines by the above amount, energy loss in the radiator also produces a small loss of resolution. This arises from the fact that pair electrons traverse thicknesses of the radiator varying from zero up to the full thickness. The resulting loss of resolution is indicated by $\Delta k/k$ above.

The effect of energy loss by radiation is considerably smaller, even for the high energy lithium radiation, which can produce electrons of sufficient energy that the average radiation loss is comparable with the collision loss in copper, and greater than the collision loss in lead.[40] This is because radiation of quanta of all energies up to the primary energy of the electron makes an appreciable contribution to the average radiation loss, whereas only processes in which the electron retains above 80 or 90 percent of its energy can affect the shape of an observed gamma-ray line. Losses greater than this merely produce a small background of low energy pairs.

### (7) *Fluctuations in the Magnetic Field*

Ripple in the magnetic field was measured to be less than 0.3 percent, and slow time variations were minimized by regulating the magnet current. The regulator used did not work perfectly, but the current was held constant to about 0.5 percent, or better.

### (8) *Secondary Radiation from the Lead Shielding*

The effect of secondary radiation from the lead shielding is difficult to estimate, but qualitatively it would be expected to contribute a small background of low energy pairs more or less evenly distributed below the energy of the primary gamma-radiation.

A somewhat related question is whether any of the pairs which cause coincidence can have been produced at places other than in the radiator. To find this out, the counting rate was observed without a radiator in the spectrometer. The background thus observed was of the order of 1 to 3 percent, showing that nearly all pairs observed actually come from the radiator.

The combined effect on the resolution of all the

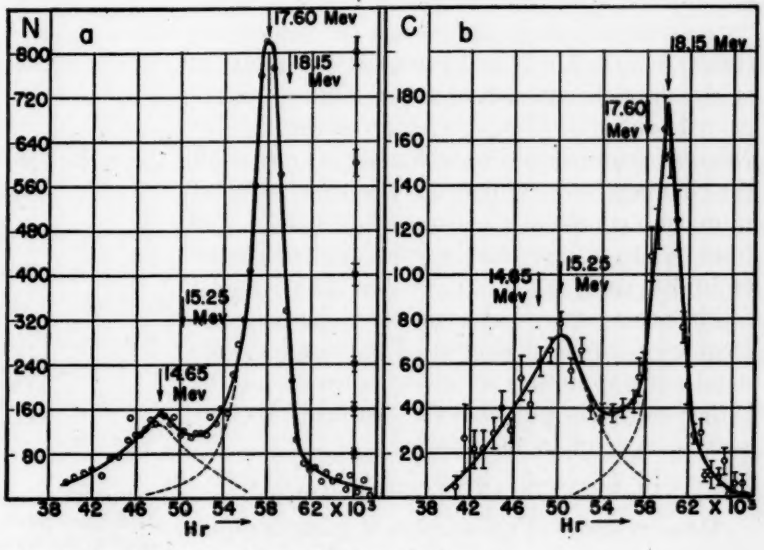


FIG. 5. Thin target lithium spectrum at two different proton energies, obtained with the 0.004-in. Cu radiator: (a) Proton energy 0.46 Mev—target thickness approximately 150 kev; (b) proton energy 1.15 Mev—target thickness approximately 70 kev. In curve (b) the relative coincidence rate $C$ is plotted rather than the number of coincidences $N$ obtained, since not all points were measured for the same number of monitor counts. A shift in energy of the two gamma-ray lines with increase in proton energy is apparent, as well as a marked increase in the relative intensity of the lower energy line with increasing proton energy.

[40] W. Heitler, *Quantum Theory of Radiation* (Oxford University Press, London, 1936).

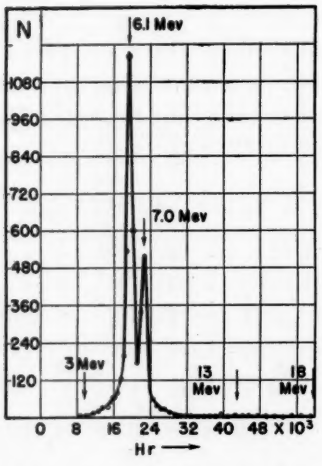


FIG. 6. Survey of the fluorine gamma-ray spectrum between 3 and 18 Mev obtained with a thick $CaF_2$ target, 1.15-Mev protons, and the 0.002-in. Cu radiator.

factors discussed above is best seen by looking at the measured gamma-ray lines in Figs. 4 and 7. It is probably safe to assume that the observed widths of the higher energy lithium line, and the 6.13-Mev fluorine line, for example, are entirely experimental. The widths of these lines at half-maximum are, respectively, 5.5 and 6.2 percent of the gamma-ray energy.

## III. PROCEDURE

Each measurement of a spectrum was made by recording the number of coincidences occurring per fixed number of monitor counts, in each of the seven different energy channels of the spectrometer, at a sequence of values of the magnetic field. Successive values of the magnetic field were chosen in such a way as to simplify the plotting of the data. Frequently a set of points was repeated with the same energies represented by different channels, in order to make sure that all the channels were equivalent. The time required to make a complete spectrum measurement was from five to fifteen hours, with a proton current of 50–100 $\mu$a.

The proton energy was varied by changing the frequency of the cyclotron. The energies were determined from the cyclotron frequency and the rather uncertain radius of the last orbit, so they may be in error by ten percent.

## IV. RESULTS AND CONCLUSIONS

Measurements of the spectra of gamma-radiation from lithium and fluorine under proton bombardment have been made under various conditions of proton energy, target thickness, and radiator thickness. The data are shown by the curves in Figs. 3–8, and a summary is given in Table III of the conditions under which each measurement was made.

The curves of Figs. 3–8 give the number of coincidences $N$ observed, as a function of $Hr$, which is approximately proportional to the gamma-ray energy. (Eq. (10).) The energies of all gamma-ray lines, as indicated by the arrows in these figures, have been corrected for the small energy loss of the pair electrons in the radiator.

In obtaining the ratio of intensities of two lines from the areas under the corresponding peaks, corrections have been made for two effects which tend to suppress the low energy end of the curves as plotted in Figs. 3–8. The first of these is simply that the cross section for pair production, and thus the sensitivity of the spectrometer, increases with the gamma-ray energy.[40] The second is that the resolution width due to the finite size of the counters increases directly with the gamma-ray energy. (The percentage width remains constant as shown above in discussing the resolution.) The probability that an electron pair be counted in a given pair of counters is independent of the energy of the gamma-ray producing the pair, provided the magnetic field has the appropriate value given by (10). However, the magnetic field interval throughout which gamma-rays of a given energy can be recorded in the given pair of

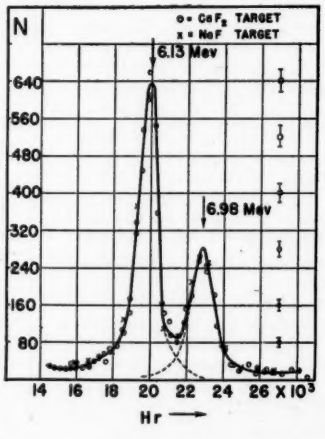


FIG. 7. Detail of the two fluorine lines observed with 1.15-Mev protons and the thin 0.003-in. Al radiator to obtain the best resolution. Data using thick targets of both $CaF_2$ and NaF are shown.

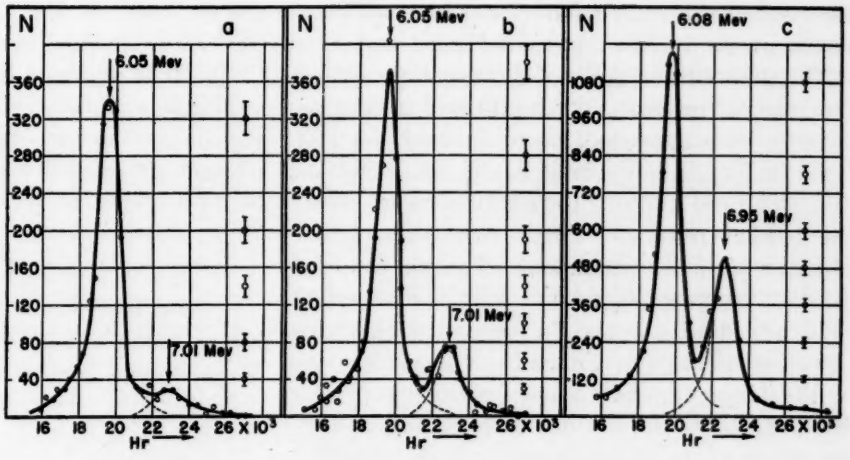


FIG. 8. The behavior of the two fluorine lines with change in proton energy. The 0.002-in. Cu radiator was used. (a) Proton energy 0.45 Mev—thick NaF target; (b) proton energy 0.70 Mev—thick NaF target; (c) proton energy 1.15 Mev—thick $CaF_2$ target. The relative intensity of the two lines changes with the proton energy. However, within the experimental accuracy, the energies of the two gamma-ray lines do not change.

counters is directly proportional to the magnetic field. Thus, for a gamma-ray line of given intensity, the area under the measured peak will be proportional to this resolution width, and thus to the gamma-ray energy.

### A. Lithium

A survey of the spectrum between 3 and 19 Mev for a thick lithium target bombarded with 1.15-Mev protons is shown in Fig. 3. No new gamma-ray lines were found, but the line at 14.8 Mev previously reported[5] is clearly resolved from the 17.6-Mev line.

A detailed study of the two lithium lines for a thick target** at three proton energies, 0.46, 0.75, and 1.15 Mev, is shown in Fig. 4. It will be noticed that the lower energy line is considerably broader than the experimental resolution width. This could indicate the presence of two or more unresolved lines, but it finds a natural explanation in the nuclear transition (1) believed to be responsible for the 14.8-Mev gamma-ray.

$$Li^7+H^1\rightarrow Be^{8*}\rightarrow Be^8+h\nu. \qquad (1)$$

The radiative transition giving the 14.8-Mev gamma-ray leaves the $Be^8$ nucleus in an excited level at 2.8 Mev, according to the difference in energy of the two gamma-ray lines. This energy agrees with that of a level in $Be^8$ which is known from other experiments[41,42] to be broad because of its short lifetime against decay into two alpha-particles. From experimental data of Oliphant, Kempton, and Rutherford[41] on the energy distribution of alpha-particles produced in the reaction:

$$B^{11}+H^1\rightarrow Be^{8**}+He^4+Q_1,$$
$$Be^{8**}\rightarrow 2He^4+Q_2, \qquad (12)$$

Bethe[43] obtains an approximate width of 0.8 Mev for the $Be^8$ level involved in this reaction, and an excitation energy of 2.8 Mev. One would like to identify this level with the one involved in reaction (1) above, and, further, with the lowest excited level of $Be^8$ obtained from the theoretical calculations of Feenberg and Wigner.[44] Theoretically, the first excited level of $Be^8$ is a $^1D$ level at about 2 Mev. The agreement between this energy and the experimental value 2.8 Mev is as good as could be expected from the rough approximations in the theory.

Although the 2.8-Mev levels of $Be^8$ involved in reactions (1) and (12) are probably the same, the agreement between the two experiments is not perfect. The width of the 14.8-Mev gamma-ray line appears to be considerably greater than 0.8 Mev, namely, of the order of 2.1 Mev. This is only a rough estimate, however, since it involves

** Although a thin evaporated Li target was used at proton energy 0.46 Mev a thick target can be expected to give the same result, since the yield of gamma-rays below the resonance energy of 0.440 Mev is very small.

[41] M. L. E. Oliphant, A. E. Kempton, and Lord Rutherford, Proc. Roy. Soc. **A150**, 241 (1935).
[42] J. D. Cockcroft and W. B. Lewis, Proc. Roy. Soc. **A154**, 246 (1936); P. I. Dee and C. W. Gilbert, Proc. Roy. Soc. **A154**, 279 (1936); C. L. Smith and E. B. M. Murrell, Proc. Camb. Phil. Soc. **35**, 298 (1939).
[43] H. A. Bethe, Rev. Mod. Phys. **9**, 217 (1937).
[44] E. Feenberg and E. Wigner, Phys. Rev. **51**, 95 (1937).

a somewhat arbitrary separation of the two lines shown by the broken curves of Figs. 4 and 5.

The three curves of Fig. 4 show a tendency for the relative intensity of the 14.8-Mev line to increase with increasing proton energy. Such a trend might be expected if the spectrum of radiation produced by protons at energies above the 440-kev resonance differs from that of the radiation from the resonance. Tangen (unpublished)*** and the Pasadena group[45] have reported that the radiation above the resonance is slightly less energetic, as determined from measurements of the absorption of secondary electrons.[46] To obtain further information on this point, and on the origin of the two gamma-ray lines, the data shown in Fig. 5 were taken. These two curves were obtained with thin targets at proton energies of 0.46 and 1.15 Mev. Thus the first curve shows essentially the gamma-ray spectrum produced by protons of the resonance energy, 440 kev, while the second curve shows the spectrum arising from that part of the gamma-ray excitation curve[13,14] considerably above the 440-kev resonance. It is immediately evident that the relative intensity of the lower energy line is considerably greater for 1.15-Mev protons than for 0.46-Mev protons, but it is also evident that both lines occur at both proton energies.

The ratio of intensities of the lower energy line to the higher energy line is found to be approximately 0.50 for 0.46-Mev protons; and 1.5 for 1.15-Mev protons.

Another interesting result may be seen by comparing the two curves of Fig. 5. This is a shift in the energy of the two peaks by just about the amount to be expected from the difference in energy of the protons: i.e., by $\frac{7}{8}$ the difference in proton energy.

The sharp, high energy line is produced by reaction (1) leaving the $Be^8$ nucleus in its ground level. The quantum energy of the gamma-ray will then be $h\nu = Q + \frac{7}{8}E_p$, where $Q$ is the energy available from the mass change, and $E_p$ is the proton energy. From the positions of the higher energy lines in Fig. 5, we obtain the value $Q = 17.2 \pm 0.2$ Mev, in agreement with the value $17.21 \pm 0.08$ obtained from the mass values.[47]

The best values for the energies of the two gamma-ray lines arising from the 440-kev lithium resonance are obtained from Figs. 4 and 5a: $14.8 \pm 0.3$ Mev, and $17.6 \pm 0.2$ Mev.

### B. Fluorine

A general survey of the gamma-ray spectrum from a thick $CaF_2$ target bombarded with 1.15-Mev protons is shown in Fig. 6. The gamma-radiation previously believed to consist of a single line near 6.3 Mev, is clearly resolved into two lines at 6.1 and 7.0 Mev. (Several lines between 5.4 and 7.2 Mev have been reported for high energy protons, 5 Mev, by Phillips and Kruger.[48]) No lines between 8 and 18 Mev exist having an intensity greater than one percent of the 6.1-Mev line. In particular, no radiation is observed near 13 Mev with an intensity greater than about 0.3 percent of that at the 6.1-Mev line, confirming the result of Delsasso, Fowler, and Lauritsen.[6] This is the energy to be expected for a gamma-ray arising from reaction (4).

A detailed investigation of the two fluorine lines is shown in Fig. 7, for a proton energy of 1.15 Mev, and thick fluoride targets. Both $CaF_2$ and NaF targets were used in order to confirm previous results[11] that the fluorine and not calcium is responsible for the radiation. Because of the use of thick targets, all resonances below 1.15 Mev in the gamma-ray excitation curve[14,29,30] contribute to the intensity of the lines. However, the resonances at proton energies 862 and 927 kev are much stronger than the others, and probably contribute a major fraction of the intensity. An extremely thin radiator of 0.003-in. aluminum was used in obtaining the data of Fig. 7, in order to achieve the best possible resolution. From the positions of the two peaks, we obtain for the quantum energies of the two fluorine gamma-rays: $6.13 \pm 0.06$ Mev, and $6.98 \pm 0.07$ Mev.

Using a somewhat thicker radiator of 0.002-in. Cu, the behavior of the thick target spectrum with changes in the bombarding proton energy

*** *Note added in proof:* Tangen's work is published: Roald Tangen, Kgl. Norske Vid. Sels. Skrifter (1946) NR1.

[45] W. F. Hornyak and T. Lauritsen, Rev. Mod. Phys. **20**, 191 (1948).

[46] W. A. Fowler, C. C. Lauritsen, and T. Lauritsen, Rev. Mod. Phys. **20**, 236 (1948).

[47] H. A. Bethe, *Elementary Nuclear Theory* (John Wiley and Sons, Inc., New York, 1947).

[48] J. A. Phillips and P. G. Kruger, Phys. Rev. **72**, 164 (1947).

was investigated. Measurements at proton energies of 0.45, 0.70, and 1.15 Mev are shown in the three curves of Fig. 8. A marked decrease in the relative intensity of the 7.0-Mev gamma-ray is noticed as the proton energy decreases. At 0.45-Mev proton energy this line has almost disappeared, and the radiation is nearly monochromatic. At this proton energy the resonance at 334 kev alone should contribute to the gamma-ray intensity. However, the proton energy is not very well known, so it is not impossible that the next fluorine resonance, at 479 kev, may have contributed something to the gamma-ray intensity in Fig. 8a.

From the data shown in Fig. 8, the ratio $R$ of intensities of the 6.1- to the 7,0-Mev lines has been calculated for the three different proton energies.

| Proton energy, $E_p$ | Ratio of intensities, $R=I(6.1)/I(7.0)$ |
|---|---|
| 0.45 Mev | 23 |
| 0.70 | 5.8 |
| 1.15 | 2.6 |

The three curves of Fig. 8 show that the energies of the two gamma-ray lines do not change with the bombarding proton energy, within the experimental accuracy. This is analogous to the results obtained by Dee, Curran, and Strothers,[7] and by Lauritsen, Lauritsen, and Fowler,[23] and used by them as an argument against reaction (5), and also against the emission of two successive quanta by the excited $Ne^{20}$ nucleus. However, the present result is more conclusive since the earlier experiments failed even to resolve the two gamma-ray lines.

The results of the present experiment thus substantiate the belief that reaction (3) is responsible for the origin of the fluorine gamma-rays.

$$F^{19}+H^1\rightarrow Ne^{20*}\rightarrow O^{16*}+He^4+Q,$$
$$O^{16*}\rightarrow O^{16}+h\nu. \qquad (3)$$

It is necessary, however, to assume two oxygen gamma-ray levels, $O^{16*}$ and $O^{16**}$, in order to account for the two gamma-rays, and two corresponding values of $Q$, $Q_1$, and $Q_2$. This means that there are at least three rather close lying levels of $O^{16}$ at 6–7 Mev. These are the "pair level" ($J=0$) of the reaction (7), at $6.0\pm0.2$ Mev, and the two "gamma-ray levels" at 6.1 and 7.0 Mev.***

The value $Q=1.81\pm0.04$ Mev for reaction (3) obtained by Becker, Fowler, and Lauritsen[27] corresponds to the lower energy gamma-ray, 6.13 Mev. Calling this $Q_1$, we obtain $Q_2=0.96\pm0.08$ Mev. (The alpha-particles preceding emission of the 6.98-Mev gamma-ray line may explain the small low energy alpha-particle peaks appearing in Figs. 5 and 6 of their paper.)

The sum of the gamma-ray energy 6.13 Mev and $Q_1=1.81$ Mev is $7.94\pm0.08$ Mev. This is to be compared with the energy available from the mass change,[47] $8.12\pm0.24$ Mev, and with the value $Q=7.95$ Mev obtained for the long-range alpha-particle reaction (6) by Burcham and Smith.[22]

The low energy of the alpha-particles preceding emission of the gamma-rays suggests that the observed decrease in relative intensity of the higher energy gamma-ray line with decrease in proton energy may be explained by the effect of the potential barrier on the relative probability of emission of the two alpha-particles. The higher energy gamma-ray follows the lower energy alpha-particle, which is suppressed more rapidly by the potential barrier as the proton energy decreases.


## ACKNOWLEDGMENTS

We are indebted to Dr. W. B. Jones and Bruce Dayton for help with the cyclotron, to Elmer Sharp for the absolute field calibration, and to Professor H. A. Bethe and Professor P. Morrison for valuable discussions.

This work was supported in part by the Office of Naval Research.


*** For a detailed discussion of the known energy levels in $O^{16}$, $Be^8$, and other light nuclei, see the review article by Hornyak and Lauritsen, reference (45).

# Relativistic Rankine-Hugoniot Equations

A. H. TAUB
*University of Illinois, Urbana, Illinois and Institute for Advanced Study, Princeton University, Princeton, New Jersey**

(Received April 13, 1948)

In Part I of this paper the stress energy tensor and the mean velocity vector of a simple gas are expressed in terms of the Maxwell-Boltzman distribution function. The rest density $\rho^0$, pressure, $p$, and internal energy per unit rest mass $\epsilon$ are defined in terms of invariants formed from these tensor quantities. It is shown that $\epsilon$ cannot be an arbitrary function of $p$ and $\rho^0$ but must satisfy a certain inequality. Thus $\epsilon=(1/\gamma-1)p/\rho^0$ for $\gamma>5/3$ is impossible. It is known that if $\epsilon$ is given by this relation and $\gamma>2$, then sound velocity in the medium may be greater than that of light in vacuum. This difficulty is now removed by the inequality mentioned above. In Part II of this paper the relativistic form of the Rankine-Hugoniot equations are derived and it is shown that as a consequence of the inequality mentioned earlier that the shock wave velocity is always less than that of light in vacuum for sufficiently strong shocks.

## PART I. SPECIFIC INTERNAL ENERGY

### 1. Introduction

MACROSCOPIC relativistic theories of fluid dynamics characterize the fluid by giving the internal energy per unit mass, $\epsilon$, measured by an observer at rest with respect to the element of the fluid as a function of the pressure, $p$ and the rest density $\rho^0$, and also by prescribing the viscosity and the heat conductivity of the fluid. For perfect fluids, for which the latter two quantities vanish, it follows from the work of Lamla[1] and Section 5 below that if

$$\epsilon=(1/\gamma-1)p/\rho^0 \tag{1.1}$$

and $\gamma$ is a constant greater than 2, then the velocity of sound in the fluid may be greater than the velocity of light in vacuum.

Thus, consistency of hydrodynamics with the special theory of relativity can only be achieved from the macroscopic viewpoint by restricting the allowed relations between specific internal energy, pressure, and density. This restriction applies to fluids with non-vanishing heat conductivity and viscosity as follows from the work of Eckart.[2] For it is evident from the equations Eckart gives for the flow of heat in a gas at rest (Eqs. (43) and (44)) that if $\epsilon$ is taken as given by (1.1) then the velocity of propagation is greater than the velocity of light in vacuum.

This functional restriction also enters in the discussion of the relativistic formulation of the Rankine-Hugoniot equations governing the propagation of shock waves, as follows from Part II of this paper.

It is our purpose in Part I of this paper to show how equations of the type of (1.1) are ruled out on the basis of the kinetic theory of gases when this theory is formulated relativistically. In Part II we derive the relativistic Rankine-Hugoniot equations and show that in view of the inequality that must hold on $\epsilon$ as a function of $p$ and $\rho^0$ the shock wave velocity is less than that of light in vacuum.

### 2. Derivation of the Hydrodynamical Equations

We shall now derive the equations governing the motion of the fluid considered a collection of a number of particles with rest mass $m$. Let

$$\xi^i=\frac{v^i}{(1-v^2/c^2)^{\frac{1}{2}}}, \quad v^i=\frac{\xi^i}{(1+\xi^2/c^2)^{\frac{1}{2}}} \tag{2.1}$$

where

$$v^2=\sum_{i=1}^{3}(v^i)^2, \quad \xi^2=\sum_{i=1}^{3}(\xi^i)^2$$

and $v^i$ are the components of the velocity of a particle. Let $f(x, t, \xi)$ be the number of particles in the region $x^i$ to $x^i+dx^i$ in space at time $t$ and with values of $\xi^i$ between $\xi^i$ and $\xi^i+d\xi^i$. Then the

* The major portion of this work was done while the author was a Guggenheim postservice Fellow in residence at the Institute for Advanced Study, on leave from the University of Washington.

[1] E. Lamla, "Über die Hydrodynamik des Relativitäts prinzips," Dissertation, Berlin (1912).

[2] C. Eckart, "The thermodynamics of irreversible processes. III. Relativistic theory of the simple fluid," Phys. Rev. 58, 919 (1940).

Boltzman equation for $f$ is

$$Df\equiv\frac{\partial f}{\partial t}+\frac{\xi^i}{(1+\xi^2/c^2)^{\frac{1}{2}}}\frac{\partial f}{\partial x^i}+F^i\frac{\partial f}{\partial \xi^i}=\Delta_e f, \quad (2.2)$$

where $F^i$ is the external force per unit mass and $\Delta_e f$ is the time rate of change in $f$ due to encounters between the particles.

An integration by parts shows that

$$\int \phi Df d_3\xi=\frac{\partial}{\partial t}(n\langle\varphi\rangle)+\frac{\partial}{\partial x^i}\left[n\left\langle\frac{\varphi\xi^i}{(1+\xi^2/c^2)^{\frac{1}{2}}}\right\rangle\right]-n\left\{\left\langle\frac{\partial\varphi}{\partial t}\right\rangle+\left\langle\frac{\xi^i}{(1+\xi^2/c^2)^{\frac{1}{2}}}\frac{\partial\varphi}{\partial x^i}\right\rangle+F^i\left\langle\frac{\partial\varphi}{\partial x^i}\right\rangle\right\} \quad (2.3)$$

where

$$n\langle h\rangle=\int h(\xi)f(\xi)d_3\xi, \quad n=\int f(\xi)d_3\xi,$$

and the integrations are carried out over the entire volume of the $\xi^1$, $\xi^2$, $\xi^3$ space. The notation $\int\cdots d_3\xi$ indicates such a volume integral.

The laws of conservation of mass, energy, and momentum follow from Eqs. (2.2) and (2.3) by observing that

$$\int \varphi^q\Delta_e f d_3\xi=0, \quad q=0, 1, \cdots, 4$$

where

$$\varphi^0=m, \quad \varphi^i=m\xi^i \qquad (i=1, 2, 3)$$

and

$$\varphi^4=m(1+\xi^2/c^2)^{\frac{1}{2}}.$$

Multiplying Eq. (2.2) by the various $\varphi^q$ in turn and integrating over all $\xi$'s we obtain five equations which may be written as

$$mU^\alpha{}_{,\alpha}=0, \quad (2.4)$$

$$T^{\alpha\beta}{}_{,\beta}=\rho^0F^\alpha, \quad \alpha,\beta=1, 2, 3, 4, \quad (2.5)$$

respectively, where the comma denotes differentiation the summation convention is used, and the quantities involved are defined as follows: $U^\alpha$ is the mass current four vector given by

$$U^\alpha=\int V^\alpha(\xi)f(\xi)\frac{d_3\xi}{(1+\xi^2/c^2)^{\frac{1}{2}}}\equiv\int V^\alpha(\xi)d\mu(\xi), \quad (2.6)$$

where

$$V^i=\xi^i/c, \quad V^4=(1+\xi^2/c^2)^{\frac{1}{2}};$$

hence

$$V^\alpha V^\beta g_{\alpha\beta}=V^\alpha V_\alpha=-1, \quad (2.7)$$

where now

$$g_{\alpha\beta}=0, \quad \alpha\neq\beta \quad \text{and} \quad g_{11}=g_{22}=g_{33}=-g_{44}=1.$$

That is,

$$U^4=\int f(\xi)d_3\xi\equiv\int(1+\xi^2/c^2)^{\frac{1}{2}}d\mu(\xi)=n,$$

$$U_i=\int\frac{\xi^i/c}{(1+\xi^2/c^2)^{\frac{1}{2}}}f(\xi)d_3\xi\equiv\int\xi^i/cd\mu(\xi)=n\left\langle\frac{\xi^i}{(1+\xi^2/c^2)^{\frac{1}{2}}}\right\rangle, \quad i=1, 2, 3.$$

$T^{\alpha\beta}$ is the stress energy tensor and it is defined as

$$T^{\alpha\beta}=mc^2\int V^\alpha(\xi)V^\beta(\xi)\frac{f(\xi)}{(1+\xi^2/c^2)^{\frac{1}{2}}}d_3\xi\equiv mc^2\int V^\alpha(\xi)V^\beta(\xi)d\mu(\xi). \quad (2.8)$$

$F^\alpha$ is the four-dimensional force vector:

$$F^4=F^iu^i/c,$$

$$u^i=\int\frac{\xi^i}{(1+\xi^2/c^2)^{\frac{1}{2}}}f(\xi)d_3\xi\Big/\int f(\xi)d_3\xi, \quad (2.9)$$

$$F^i=\frac{F^i}{(1-u^2/c^2)^{\frac{1}{2}}},$$

and $\rho^0$ is the rest density of the gas defined as

$$(\rho^0)^2=-m^2U^\alpha U_\alpha. \quad (2.10)$$

It follows from Eq. (2.7) that

$$T_\alpha{}^\alpha=-mc^2\int d\mu(\xi). \quad (2.11)$$

It is evident from Eq. (2.5) and the fact that $\rho^0F^\alpha$ is a four-dimensional vector that $T^{\alpha\beta}$ is a tensor. From Eq. (2.8) it then follows that $f(x, \xi)$ is a scalar function under Lorentz transformations since the Lorentz invariant volume measure in $\xi$ space is

$$\frac{d_3\xi}{(1+\xi^2/c^2)^{\frac{1}{2}}}.$$

### 3. Specific Internal Energy

We now define the function $\epsilon$ in terms of the components of $T^{\alpha\beta}$ and $U^{\alpha}$ as is done by Eckart.[3] We write

$$T^{\alpha\beta}=\frac{m^2w}{(\rho^0)^2}U^{\alpha}U^{\beta}+\frac{m}{\rho^0}U^{\alpha}W^{\beta}+\frac{m}{\rho^0}U^{\beta}W^{\alpha}+W^{\alpha\beta}, \quad (3.1)$$

where $W^{\alpha}$ is the heat flow vector and $W^{\alpha\beta}$ is the stress tensor. We require that

$$W^{\alpha}U_{\alpha}=0, \quad W^{\alpha\beta}U_{\beta}=0. \quad (3.2)$$

The scalar $w$ is the energy density as measured by some one instantaneously at rest with respect to an element of the fluid.

From Eq. (3.1) we have

$$T_{\alpha}{}^{\alpha}=3p-w, \quad (3.3)$$

where

$$W_{\alpha}{}^{\alpha}=3p$$

and $p$ is the hydrostatic pressure. It follows from (3.1), (3.2), and (2.10) that

$$w=m^2T_{\alpha\beta}\frac{U^{\alpha}U^{\beta}}{(\rho^0)^2}\equiv\rho^0(c^2+\epsilon). \quad (3.4)$$

The last of these equations will be regarded as our definition of $\epsilon$, the internal energy per unit rest mass of the fluid.

### 4. The Fundamental Inequality

We now propose to show that $\epsilon$ defined by Eq. (3.4) when considered as a function of $p$ and $\rho^0$ must satisfy an inequality which rules out functions of the type given by (1.1). Let us define

$$g(\xi')=\int V^{\alpha}(\xi')V_{\alpha}(\xi)d\mu(\xi)=V^{\alpha}(\xi')\int V_{\alpha}(\xi)d\mu(\xi). \quad (4.1)$$

It follows from Eq. (3.4) that

$$w=\frac{m^3c^2}{(\rho^0)^2}\int V_{\alpha}(\xi)V_{\beta}(\xi)d\mu(\xi)\times\int V^{\alpha}(\xi')d\mu(\xi')\int V^{\beta}(\xi'')d\mu(\xi'')$$
$$=\frac{m^3c^2}{(\rho^0)^2}\int\left(V_{\beta}(\xi)\int g(\xi)V^{\beta}(\xi')d\mu(\xi')\right)d\mu(\xi)=\frac{m^3c^2}{(\rho^0)^2}\int g^2(\xi)d\mu(\xi). \quad (4.2)$$

From Eq. (2.10) we have

$$-\left(\frac{\rho^0}{m}\right)^2=U^{\alpha}U_{\alpha}=\int V^{\alpha}(\xi)d\mu(\xi)\times\int V_{\alpha}(\xi')d\mu(\xi')=\int g(\xi)d\mu(\xi). \quad (4.3)$$

Now from Schwartz's inequality we have

$$\left(\int g(\xi)d\mu(\xi)\right)^2\leqslant\left(\int g^2(\xi)d\mu(\xi)\right)\left(\int d\mu(\xi)\right). \quad (4.4)$$

Substituting in (4.4) from (2.11), (4.3), and (4.2) we have

$$\frac{(\rho^0)^2}{m^4c^4}w(-T_{\alpha}{}^{\alpha})\geqslant\frac{(\rho^0)^4}{m^2}.$$

Using (3.3) we obtain

$$w(w-3p)\geqslant(\rho^0)^2c^4;$$

hence

$$w\geqslant\tfrac{3}{2}p+\rho^0c^2\left(1+\frac{9}{4}\left(\frac{p}{\rho^0c^2}\right)^2\right)^{\frac{1}{2}}$$

and

$$\epsilon\geqslant\tfrac{3}{2}p/\rho^0+c^2\left(\left(1+\frac{9}{4}\left(\frac{p}{\rho^0c^2}\right)^2\right)^{\frac{1}{2}}-1\right). \quad (4.5)$$

The existence of this inequality shows that the kinetic formulation of the theory of gases and the formalism of the special theory of relativity together are in contradiction with the macroscopic viewpoint which allows $\epsilon$ to be any function of $p$

[3] See reference 2, p. 921.

and $\rho^0$. In particular the functions of the type (1.1) with $\gamma \geqslant 5/3$ are not permitted. Thus the restrictions on the types of functions $\epsilon(p, \rho^0)$ have been shown to be furnished by kinetic theory and are not *ad hoc* ones.

## PART II. RANKINE-HUGONIOT EQUATIONS

### 5. One-Dimensional Motion of a Perfect Gas

The equations governing the motion of a perfect gas subject to no external forces are (2.4) and (2.5); these may be written as

$$(\rho^0 u^\alpha)_{,\alpha} = 0, \tag{5.1}$$

$$T_{,\beta}^{\alpha\beta} = 0, \tag{5.2}$$

where

$$u^\alpha = (m/\rho^0) U^\alpha \tag{5.3}$$

and

$$T^{\alpha\beta} = \rho^0(c^2 + \epsilon + p/\rho^0) u^\alpha u^\beta + p g^{\alpha\beta}, \tag{5.4}$$

since, for a perfect gas,

$$W^\alpha = 0 \tag{5.5}$$

and

$$W^{\alpha\beta} = p(g^{\alpha\beta} + u^\alpha u^\beta). \tag{5.6}$$

Substituting (5.4) into (5.2) and taking account of (5.1) we obtain

$$\rho^0 u^\beta (c^2 \mu u^\alpha)_{,\beta} + p_{,\beta} g^{\alpha\beta} = 0 \tag{5.7}$$

where

$$\mu = 1 + (1/c^2)(\epsilon + p/\rho^0). \tag{5.8}$$

Multiplying (5.7) by $-u_\alpha$ and summing we obtain the equation of conservation of energy

$$\rho^0(\epsilon + p/\rho^0)_{,\beta} u^\beta - p_{,\beta} u^\beta = \rho^0(\epsilon_{,\beta} u^\beta + p(1/\rho^0)_{,\beta} u^\beta) = 0. \tag{5.9}$$

Defining absolute temperature $\theta$ and specific entropy $S$ as measured by an observer at rest with respect to the gas from the equations

$$d\epsilon + p d(1/\rho^0) = \theta dS, \tag{5.9'}$$

where $\epsilon$ is a function of $p$ and $\rho^0$, Eqs. (5.9) may be written as

$$\rho^0 \theta S_{,\beta} u^\beta = 0. \tag{5.10}$$

Hence, the conservation of energy along the stream lines is equivalent to the statement that entropy is constant along a stream line. If all the gas is initially at the same entropy and the flow is continuous, then we shall have

$$S = \text{constant}. \tag{5.11}$$

This equation determines $p$ as a function of $\rho^0$. It is then sufficient to consider only three of the four Eqs. (5.7).

In the case of one-dimensional motion all quantities are assumed to be functions of $x^1 = x$ and $x^4 = ct$ and $u^2 = u^3 = 0$. Then we may write for $u^\alpha$

$$u^1 = \frac{u}{(1-u^2)^{\frac{1}{2}}}, \quad u^4 = \frac{1}{(1-u^2)^{\frac{1}{2}}}, \tag{5.12}$$

where $u$ is the velocity of the gas in units in which the velocity of light is one. Equations (5.1) and (5.7) with $\alpha = 1$ become

$$\frac{1}{c}\frac{\partial}{\partial t}\left(\frac{\rho^0}{(1-u^2)^{\frac{1}{2}}}\right) + \frac{\partial}{\partial x}\left(\frac{\rho^0 u}{(1-u^2)^{\frac{1}{2}}}\right) = 0, \tag{5.13}$$

$$\frac{1}{c}\frac{\partial}{\partial t}\left(\frac{c^2 \mu \rho^0 u}{1-u^2}\right) + \frac{\partial}{\partial x}\left(\frac{c^2 \mu \rho^0 u^2}{1-u^2} + p\right) = 0. \tag{5.14}$$

If we now introduce the two auxilliary quantities

$$\alpha = \frac{a}{c} = \left(\frac{\rho^0}{\mu}\frac{d\mu}{d\rho^0}\right)^{\frac{1}{2}}, \quad \varphi = \frac{1}{c}\int \frac{a}{\rho^0} d\rho^0, \tag{5.15}$$

Eqs. (5.13) and (5.14) may be written as

$$(1-u^2)\left(\frac{1}{c}\frac{\partial \varphi}{\partial t} + u\frac{\partial \varphi}{\partial x}\right) + \alpha\left(u\frac{1}{c}\frac{\partial u}{\partial t} + \frac{\partial u}{\partial x}\right) = 0,$$

$$\alpha(1-u^2)\left(u\frac{1}{c}\frac{\partial \varphi}{\partial t} + \frac{\partial \varphi}{\partial x}\right) + \frac{1}{c}\frac{\partial u}{\partial t} + u\frac{\partial u}{\partial x} = 0.$$

These in turn may be written as

$$D_+ u + (1-u^2) D_+ \varphi = 0,$$
$$D_- u - (1-u^2) D_- \varphi = 0,$$

where

$$D_+ f = (1+\alpha u)\frac{1}{c}\frac{\partial}{\partial t} f + (\alpha + u)\frac{\partial f}{\partial x},$$

$$D_- f = (1-\alpha u)\frac{1}{c}\frac{\partial}{\partial t} f - (\alpha - u)\frac{\partial f}{\partial x},$$

and hence

$$\frac{D_\pm u}{1-u^2} = D_\pm \log\left(\frac{1+u}{1-u}\right)^{\frac{1}{2}}.$$

Thus Eqs. (5.13) and (5.14) become

$$(1-u^2)D_+\left[\log\left(\frac{1+u}{1-u}\right)^{\frac{1}{2}}+\varphi\right]=0,$$

$$(1-u^2)D_-\left[\log\left(\frac{1+u}{1-u}\right)^{\frac{1}{2}}-\varphi\right]=0.$$

If we now define

$$r=\varphi+\log\left(\frac{1+u}{1-u}\right)^{\frac{1}{2}},$$
$$s=\varphi-\log\left(\frac{1+u}{1-u}\right)^{\frac{1}{2}}, \tag{5.16}$$

Eqs. (5.13) and (5.14) become equivalent to

$$\begin{aligned}(1+\alpha u)(1/c)(\partial r/\partial t)+(\alpha+u)(\partial r/\partial x)=0,\\ (1-\alpha u)(1/c)(\partial s/\partial t)-(\alpha-u)(\partial s/\partial x)=0.\end{aligned} \tag{5.17}$$

From these equations it is evident that $r$ and $s$ are the relativistic analogs of the Riemann functions which occur in the classical theory of propagation of one-dimensional waves of finite amplitude. In particular we have that

$r=$ constant along the curve $(dx/dt)$
$$=(\alpha+u/1+\alpha u),$$

$s=$ constant along the curve $(dx/dt)$
$$=-(\alpha-u/1-\alpha u).$$

The quantity $\alpha$ will be shown to be equal to the velocity of sound in units where the velocity of light is one. The expressions for $(dx/dt)$ are then the relativistic sum and difference of particle velocity and sound velocity.

## 6. Progressive Waves

A disturbance will be said to propagate as a progressive wave if either $r$ or $s$ is constant. Let us suppose

$$s=\varphi_0=\text{constant}.$$

Then from (5.16) we have

$$u=\tanh(\varphi-\varphi_0). \tag{6.1}$$

and the first of (5.17) becomes

$$(1/c)(\partial/\partial t)\varphi+\Gamma(\varphi)(\partial\varphi/\partial x)=0 \tag{6.2}$$

where

$$\Gamma(\varphi)=(\alpha+u/1+\alpha u) \tag{6.3}$$

and $\alpha$ is considered as a function of $\varphi$ determined by Eqs. (5.15).

The general solution of Eq. (6.2) is

$$f(\varphi)=x-\Gamma(\varphi)ct, \tag{6.4}$$

where $f(\varphi)$ is an arbitrary function. Equation (6.4) states that $\varphi$ is constant along the straight lines in the $x$, $ct$ plane of slope $\Gamma(\varphi)$, and hence $\Gamma(\varphi)$ is the velocity of propagation of $\varphi$. From Eq. (6.3) it is evident that for weak disturbances for which $u\to 0$, $\Gamma(\varphi)\to\alpha$, and hence $\alpha$ is the velocity of propagation of sound in units where the velocity of light is one.

If we define

$$\epsilon=(1/\gamma-1)p/\rho^0,$$

then Eqs. (5.9′) and (5.11) lead to

$$p/p_1=(\rho^0/\rho_1{}^0)^\gamma$$

as the equation for the adiabatics. It may then be verified that

$$\alpha=\left(\frac{\gamma p/c^2\rho^0}{1+\dfrac{\gamma}{\gamma-1}\dfrac{1}{c^2}p/\rho^0}\right)^{\frac{1}{2}}.$$

From this it follows that if a sound wave is progressing into a medium of high temperature, that is, if $p/c^2\rho^0$ is large, then

$$\alpha\to(\gamma-1)^{\frac{1}{2}}.$$

Hence for $\gamma>2$ sound waves propagate with velocity greater than that of light in vacuum. For gases the equation used for $\epsilon$ is not a possible one as follows from the argument given in the introduction.

## 7. Derivation of the Rankine-Hugoniot Equations

It follows from Eq. (6.4) that for certain functions $f(\varphi)$ which are determined by the boundary conditions the curves $\varphi=$constant in the $x$, $ct$ plane intersect. This is impossible physically and hence continuous one-dimensional motions are impossible under these conditions. From classical theory it is to be expected that shock waves form. We now derive the equations which must hold across these waves.

We first write the equations governing the motion in integral form. Thus Eqs. (5.1) and

(5.2) may be written as

$$\int (\rho^0 u^\alpha)_{,\alpha} d_4x = \int \rho^0 u^\alpha \lambda_\alpha d_3x = 0 \qquad (7.1)$$

and

$$\int T_{,\beta}{}^{\alpha\beta} d_4x = \int T^{\alpha\beta}\lambda_\beta d_3x = 0, \qquad (7.2)$$

where the integrals on the left of (7.1) and (7.2) are taken over a volume in space-time and the integrals on the right are taken over the three-dimensional hypersurface bounding this volume. $\lambda_\alpha$ are the covariant components of the outward drawn normal to the hypersurface.

Next we suppose that the three-dimensional volume is a shell of thickness $\epsilon$ enclosing a surface of discontinuity $\sum$ whose three-dimensional normal vector is $\Lambda_i$. If we choose our coordinate system so that the discontinuity is at rest, then since

$$\lambda_\alpha \lambda^\alpha = 1, \quad \sum_{i=1}^{3} \Lambda_i{}^2 = 1,$$

we have

$$\lambda_i = \Lambda_i \quad \text{and} \quad \lambda_4 = 0.$$

Hence Eqs. (7.1) and (7.2) become, as $\epsilon$ goes to zero,

$$[\rho^0 u^i \Lambda_i] = 0, \qquad (7.3)$$

$$[T^{\alpha i}\Lambda_i] = 0, \qquad (7.4)$$

where

$$[f] = f_+ - f_-$$

and represents the discontinuity in the function involved. That is $f_+$ represents the value of the function $f$ on one side of the surface $\sum$ and $f_-$ represents that on the other side. We shall take $f_+$ and $f_-$ as the values of the function $f$ on the side of the surface opposite to and in the direction of the outwardly drawn normal, respectively.

We may further restrict our coordinate system so that $\Lambda_i = \delta_i{}^1$, that is, the discontinuity is perpendicular to the $x$ axis. Then in view of Eqs. (5.4) and (5.12), Eqs. (7.3) and (7.4) may be written as

$$\frac{\rho_+{}^0 u_+}{(1-u_+{}^2)^{\frac{1}{2}}} = \frac{\rho_-{}^0 u_-}{(1-u_-{}^2)^{\frac{1}{2}}} = m \qquad (7.5)$$

and

$$\frac{mc^2\mu_+}{(1-u_+{}^2)^{\frac{1}{2}}} = \frac{mc^2\mu_-}{(1-u_-{}^2)^{\frac{1}{2}}},$$

$$\frac{mc^2\mu_+ u_+}{(1-u_+{}^2)^{\frac{1}{2}}} + p_+ = \frac{mc^2\mu_- u_-}{(1-u_-{}^2)^{\frac{1}{2}}} + p_-. \qquad (7.6)$$

The second of Eqs. (7.6) may be written as

$$m^2c^2\left(\frac{\mu_+}{\rho_+{}^0} - \frac{\mu_-}{\rho_-{}^0}\right) = p_- - p_+$$

or

$$m = \frac{1}{c}\left(\frac{p_+ - p_-}{\mu_-/\rho_-{}^0 - \mu_+/\rho_+{}^0}\right)^{\frac{1}{2}}. \qquad (7.7)$$

The second of Eqs. (7.6) may also be written as

$$m^2c^4\left(\frac{\mu_+{}^2 u_+{}^2}{1-u_+{}^2} - \frac{\mu_-{}^2 u_-{}^2}{1-u_-{}^2}\right) = (p_- - p_+)m^2c^2\left(\frac{\mu_+}{\rho_+{}^0} + \frac{\mu_-}{\rho_-{}^0}\right).$$

Subtracting this from the square of the first of (7.6) we obtain

$$m^2c^2(\mu_+{}^2 - \mu_-{}^2) = m^2(p_+ - p_-)\left(\frac{\mu_+}{\rho_+{}^0} + \frac{\mu_-}{\rho_-{}^0}\right). \qquad (7.8)$$

Equations (7.5), (7.7), and (7.8) are the relativistic Rankine-Hugoniot equations. It may readily be verified that if we neglect terms of order $p/c^2\rho^0$ compared to one, then these equations reduce to the classical ones. In the next section we investigate the effect of these terms when they are not negligible.

## 8. The Shock Velocity

Let us write

$$\xi = p_+/p_-, \quad \eta = \rho_+{}^0/\rho_-{}^0,$$

$$\epsilon_+ = \frac{1}{\gamma_+ - 1} p_+/\rho_+{}^0 = \frac{1}{\gamma_+ - 1}\xi/\eta \frac{p_-}{\rho_-{}^0} = \frac{\beta}{\gamma_+} c^2\xi/\eta,$$

$$\beta = \frac{\gamma_+}{\gamma_+ - 1}\frac{1}{c^2}\frac{p_-}{\rho_-{}^0}, \qquad (8.1)$$

$$\mu_+ = 1 + \beta\xi/\eta,$$

where $\gamma_+$ and hence $\beta$ may be functions of $p_+/\rho_+{}^0$. We shall assume that they are slowly varying functions and for the purposes of the discussion to follow $\gamma_+$ will be treated as a constant. From the inequality (4.5) and the requirement that $\epsilon \geqslant 0$, we have

$$1 < \gamma_+ \leqslant 5/3. \qquad (8.2)$$

Equation (7.8) may now be written as

$$(1+\beta\xi/\eta)^2-\mu_-{}^2=\frac{\gamma_+-1}{\gamma_+}\beta(\xi-1)\left(\frac{1}{\eta}+\frac{\beta\xi}{\eta^2}+\mu_-\right).$$

Treating $\gamma_+$ and $\beta$ as constants we obtain a quadratic equation for $1/\eta$ with one positive and one negative root. Since $\eta$ must be positive we have

$$\beta/\eta=\frac{R-[(\gamma_+ +1)\xi+\gamma_+-1]}{2\xi(\xi+\gamma_+-1)}, \tag{8.3}$$

where

$$R=[(\gamma_+-1)^2(\xi-1)^2+4\xi(\xi+\gamma_+-1)\times(\gamma_+\mu_-{}^2+\beta\mu_-(\gamma_+-1)(\xi-1))]^{\frac{1}{2}}. \tag{8.4}$$

Hence

$$\mu_+=\frac{R-(\gamma_+-1)(\xi-1)}{2(\xi+\gamma_+-1)}. \tag{8.5}$$

It follows from these equations that

$$\mu_--\frac{\mu_+}{\eta}=\mu_--\frac{\gamma_+\mu_-{}^2+\beta\mu_-(\gamma_+-1)(\xi-1)-\gamma_+\mu_+}{\beta(\xi+\gamma_+-1)}.$$

However, it is a consequence of (7.8) and the fact that $\mu_+$ and $\mu_-$ are positive that

$$\mu_+\geqslant\mu_-.$$

Hence we have

$$\mu_--\mu_+/\eta\geqslant\frac{\mu_-}{\beta(\xi+\gamma_+-1)}\times((\xi-1)\beta(2-\gamma_+)+\gamma_+(1+\beta-\mu_-)). \tag{8.6}$$

Now we may write

$$\mu_-=1+(\gamma_-/\gamma_--1)p/c^2\rho_-{}^0.$$

Then

$$1+\beta-\mu_-=(\gamma_--\gamma_+/\gamma_+(\gamma_--1))\beta,$$

and

$$\mu_--\mu_+/\eta\geqslant\frac{\mu_-}{\xi+\gamma_+-1}\times\left((\xi-1)(2-\gamma_+)+\frac{\gamma_--\gamma_+}{\gamma_--1}\right). \tag{8.7}$$

Since Eq. (7.7) may be written as

$$\frac{u_-}{(1-u_-{}^2)^{\frac{1}{2}}}=\left(\frac{(\gamma_+-1)\beta(\xi-1)}{\gamma_+(\mu_--\mu_+/\eta)}\right)^{\frac{1}{2}}, \tag{8.8}$$

we will have $u_-$ less than one whenever the right-hand side of the inequality (8.7) is positive. That is, in this case the velocity of the shock wave relative to the gas into which it is traveling will be less than that of light in vacuum. Now in view of the inequality (8.5) which must hold for both $\gamma_+$ and $\gamma_-$ it follows that for $\xi>3$ the right hand side of (8.7) is positive. Thus, for sufficiently strong shocks the shock velocity must be less than that of light in vacuum.

It is evident that if

$$\gamma_-\geqslant\gamma_+, \tag{8.9}$$

then this result holds for all values of $\xi$. The inequality (8.9) is satisfied for a monotonic gas as follows from the expression derived by Jüttner[4] for the internal energy of such a gas.

In case $\gamma_-=\gamma_+$ or in the general case for weak shocks where we may assume this equality because of the slowly varying nature of $\gamma$, it may be shown that as $\beta$ becomes large Eq. (8.8) becomes

$$u_-=\left(\frac{(\gamma-1)(\xi+\gamma-1)}{(\gamma-1)\xi+1}\right)^{\frac{1}{2}}.$$

It is evident from this that we must have $\gamma<2$ in order for $u_-$ to be less than one. The inequality (4.5) insures that $\gamma<2$.

[4] F. Jüttner, "Das Maxwellsche Gesetz der Geschwindigkeitsverteilung in der Relativtheorie," Ann. der Phys. **34**, 856–882 (1911).

# The Resonance Scattering of Slow Neutrons in Crystals

R. STERNHEIMER
*Department of Physics, The University of Chicago, Chicago, Illinois*
(Received April 19, 1948)

The theory of the diffraction of neutrons in single crystals is extended to the case in which the neutron energy lies in the region of a nuclear resonance. Equations (15a and b) describe the Laue-Bragg scattering. The isotropic background is given by Eq. (21).

THE resonance scattering of slow neutrons by nuclei has been demonstrated recently[1] for a number of elements. It appeared of interest to develop the theory of the interference effects which take place in a single crystal if the wavelength of resonance neutrons is comparable with the lattice spacing.* The present work is an extension of the theory which Goldberger and Seitz[2] and others[3] have developed for the scattering of neutrons by crystals.

We shall assume that the resonance is due to a single level of the compound nucleus and that the neutron width $\Gamma_n$ is small compared to the total width $\Gamma$ of the compound state. These conditions are satisfied for all resonances below 1 ev which have been investigated.[4]

Unless the bombarded nucleus has spin zero, the resonance scattering can take place either with or without a reversal of the direction of neutron spin. Only collisions of the latter type lead to coherent scattering** and contribute to the Laue spots. Neutrons which have undergone spin reversal emerge from the crystal as an isotropic component in the approximation in which $\Gamma_n/\Gamma \ll 1$. The slight departures from isotropicity will be explained below.

We shall now calculate the intensity of Laue spots for an ideal single crystal*** on which is incident a well collimated, monochromatic beam of neutrons. Our treatment is based on the method of the pseudopotential.[2,5] For a lattice of nuclei with identical scattering properties, the wave function satisfies the equation

$$-(\hbar^2/2m)\Delta\psi + V\psi = E\psi, \tag{1}$$

with

$$V(\mathbf{r}) = -(2\pi\hbar^2/mk)\eta \sum_j \delta(\mathbf{r}-\mathbf{r}_j). \tag{2}$$

$V$ is the pseudopotential, $m$ and $E$ are the mass and the energy of the neutron, respectively; $k$ is its wave number outside the crystal; $\mathbf{r}$ and $\mathbf{r}_j$ are the position vectors of the neutron and of the $j$th nucleus, respectively. $\delta$ is the delta-function. The summation extends over all nuclei. The phase shift $\eta$ is the constant which appears in the asymptotic expression of the wave scattered by a single nucleus,

$$\frac{\text{const.}}{|\mathbf{r}-\mathbf{r}_j|}(\exp(-ik|\mathbf{r}-\mathbf{r}_j|) - \exp(2i\eta + ik|\mathbf{r}-\mathbf{r}_j|)). \tag{3}$$

As will be seen below, the phase shift in the resonance region depends on the magnetic quantum number of the bombarded nucleus. It will be assumed that nuclei with different magnetic quantum numbers are distributed at random over the lattice. This situation leads to an isotropic component[6] which is added to the isotropic background resulting from incoherent processes. It can be shown[6] that the intensity of Laue spots is the same as if the lattice were made of identical scatterers whose phase shift $\bar{\eta}$ is given by

$$\bar{\eta} = (1/2j+1)\sum_m \eta_{m\mu}, \tag{4}$$

$\eta_{m\mu}$ is the phase shift for coherent scattering of a

[1] A. S. Langsdorf, Jr. and W. Arnold, Phys. Rev. **72**, 167 (1947); S. P. Harris, A. S. Langsdorf, Jr., and F. G. P. Seidl, Phys. Rev. **72**, 866 (1947).

* It will be assumed that the electrons in the lattice do not contribute to the scattering.

[2] M. L. Goldberger and F. Seitz, Phys. Rev. **71**, 294 (1947).

[3] For references to the earlier literature, see Goldberger and Seitz, reference 2.

[4] W. Sturm and S. Turkel, Phys. Rev. **70**, 103 (1946).

** This was pointed out by O. Halpern and M. H. Johnson, Phys. Rev. **55**, 898 (1939).

*** We assume that the lattice contains only the one kind of nucleus whose resonance scattering we wish to investigate. The extension to the case of several isotopes will be made later.

[5] E. Fermi, Ricerca Scient. **7**, Part 2, 13 (1936).

[6] G. C. Wick, Physik. Zeits. **38**, 689 (1937). I. Pomeranchuk, Physik. Zeits. Sowjetunion **13**, 65 (1938).

neutron of spin component $\mu\hbar$ by a nucleus of magnetic quantum number $m$ and spin $j$. The sum extends over all $m$ such that $-J\leqq m+\mu\leqq J$, $J$ being the spin of the compound nucleus. Thus the potential (2) can be used, if we write $\bar{\eta}$ in place of $\eta$.

We wish to comment on the validity of the representation by a pseudopotential. As was shown by Goldberger, Seitz, and Wigner,[2] a discussion of this point should be given in terms of an alternative approach in which an inhomogeneity in the wave equation takes the place of the potential. This procedure leads to the same results as the pseudopotential, but requires a lesser number of assumptions; in fact, the only condition for its validity is that the phase shift be small compared to $2\pi$. $\bar{\eta}$ is of the order of $\Gamma_n/\Gamma$, so that we are justified in using a pseudopotential.

In order to obtain $\eta_{m\mu}$ we consider the superposition $\psi_{m\mu}$ of the incident $s$ wave with the $s$ wave† which is scattered from an isolated nucleus of magnetic quantum number $m$.[7] The asymptotic expression for $\psi_{m\mu}$ is

$$\psi_{m\mu}\underset{r}{\overset{a}{\longrightarrow}}\Big[\exp(-ikr)-\Big(1-\frac{i\Gamma_n|C_{jm\mu}{}^J|^2}{E-E_0+\frac{1}{2}i\Gamma}\Big)\exp(2i\eta_p+ikr)\Big]. \quad (5)$$

$a$ is a normalization constant, $r$ is the distance from the nucleus to the neutron, $\eta_p$ is the phase shift for potential scattering, $E_0$ is the neutron energy at exact resonance, $C_{jm\mu}{}^J$ is a coefficient[8] in the expansion of the eigenfunction for angular momentum $J$ in terms of products of eigenfunctions for $j$ and $\frac{1}{2}$.

In view of (2), we find, to the first order in $\Gamma_n/\Gamma$,

$$\eta_{m\mu}=\eta_p-\frac{1}{2}\frac{|C_{jm\mu}{}^J|^2\Gamma_n(E-E_0)}{(E-E_0)^2+\frac{1}{4}\Gamma^2}+\frac{i}{4}\frac{|C_{jm\mu}{}^J|^2\Gamma_n\Gamma}{(E-E_0)^2+\frac{1}{4}\Gamma^2}. \quad (6)$$

Finally,

$$\bar{\eta}=\eta_p-\frac{2J+1}{4(2j+1)}\frac{\Gamma_n(E-E_0)}{(E-E_0)^2+\frac{1}{4}\Gamma^2}+i\frac{2J+1}{8(2j+1)}\frac{\Gamma_n\Gamma}{(E-E_0)^2+\frac{1}{4}\Gamma^2}. \quad (7)$$

The imaginary part of $\bar{\eta}$ corresponds to the average absorption cross section of the isolated nucleus which we shall denote by $\sigma_{abs}$,

$$\sigma_{abs}=\frac{\pi}{k^2}(1-|\exp(2i\bar{\eta})|^2)\sim\frac{4\pi}{k^2}Im\,\bar{\eta}=\frac{2J+1}{2(2j+1)}\frac{\pi}{k^2}\frac{\Gamma_n\Gamma}{(E-E_0)^2+\frac{1}{4}\Gamma^2}, \quad (8)$$

where $Im$ means "imaginary part of."

When several isotopes are present, we have[6]

$$\bar{\eta}=\sum_\lambda f_\lambda\eta_{p\lambda}-\frac{(2J+1)f_0}{4(2j+1)}\frac{(E-E_0)\Gamma_n}{(E-E_0)^2+\frac{1}{4}\Gamma^2}+i\frac{(2J+1)f_0}{8(2j+1)}\frac{\Gamma_n\Gamma}{(E-E_0)^2+\frac{1}{4}\Gamma^2}. \quad (7a)$$

$f_\lambda$ is the relative abundance of the $\lambda$th isotope, $\eta_{p\lambda}$ is the corresponding phase shift for potential scattering. $\lambda=0$ pertains to the active isotope.

The potential $V$ (Eq. (2)) is now determined and can be introduced into (1). In accordance with the derivation of $\bar{\eta}$, the isotropic background will not appear in $\psi$.

In solving (1) we shall follow the same procedure as Goldberger and Seitz.[2] $\psi$ and $V$ are expanded in Fourier series involving the vectors $K$ of the reciprocal lattice. Thus

$$\psi=\exp(-i\mathbf{k}'\cdot\mathbf{r})\sum_{\mathbf{K}}\psi_{\mathbf{K}}\exp(-i\mathbf{K}\cdot\mathbf{r}), \quad (9)$$

$$V=\sum_{\mathbf{K}}V_{\mathbf{K}}\exp(-i\mathbf{K}\cdot\mathbf{r}), \quad (10)$$

$\psi_{\mathbf{K}}$ and $V_{\mathbf{K}}$ are constants, $\mathbf{k}'$ is an unknown vector which is determined in the course of the solution of (1). The sums extend over all vectors of the reciprocal lattice. $V_{\mathbf{K}}$ can be found from (2) by means of the usual inversion formula. We have††

$$V_{\mathbf{K}}=\Big(-\frac{\hbar^2}{2m}\Big)\frac{4\pi n_0\bar{\eta}}{k}\sum_{j\text{cell}}\exp(i\mathbf{K}\cdot\mathbf{r}_j), \quad (11)$$

† At the energies in which we are interested, only the $s$ wave is scattered appreciably.

[7] H. A. Bethe, Rev. Mod. Phys. 9, 101 (1937).

[8] E. U. Condon and G. H. Shortley, *The Theory of Atomic Spectra* (Cambridge University Press, Teddington, England, 1935), p. 76.

†† If the lattice contains a second chemical element, its phase shift replaces at the appropriate site in the lattice cell.

where $n_0$ is the number of unit cells per unit volume and the summation is to be taken over the nuclei in one cell. To save writing, we introduce a set of quantities $a_{\mathbf{K}}$ as follows,

$$a_{\mathbf{K}} = -(2m/\hbar^2) V_{\mathbf{K}}. \tag{12}$$

Upon inserting (9), (10) and (12) into (1), we obtain the following family of equations:

$$[(\mathbf{K}+\mathbf{k}')^2 - \mathbf{k}'^2]\psi_{\mathbf{K}} = \sum_{\mathbf{K}'} a_{\mathbf{K}-\mathbf{K}'}\psi_{\mathbf{K}'}. \tag{13}$$

As was pointed out by Goldberger and Seitz[2] the equations (13) are identical with the equations of the dynamical theory of diffraction of x-rays in crystals. We shall avail ourselves of the results obtained by this theory. Let us first determine which situations are of interest in the present problem.

Because of the absorption which accompanies the resonance scattering, the intensity at a given Laue position depends strongly on the path length inside the crystal of those neutrons which reach the Laue spot. Reflections for which the neutron has to cross the entire thickness $t$ of the crystal are connected with a reduction of the intensity by a factor of the order of $\exp(t/\Lambda_{\text{abs}})$, where $\Lambda_{\text{abs}}$ is the absorption mean free path at exact resonance. The situation is different when the neutron enters and emerges through the same surface of the crystal. Here the reduction of intensity as compared to zero absorption is of the order of 2 and is independent of $t$ (if $t/\Lambda_{\text{abs}} \gg 1$). Hence we are not restricted to the use of very thin crystals. The discussion will be confined to reflections of the latter type. For simplicity, we shall consider only the case in which the reflecting planes are parallel to the surface which the beam traverses (symmetrical Bragg reflection). For $t/\Lambda_{\text{abs}} \gg 1$, we find[9]

$$|\psi_{\mathbf{K}}/\psi_0|^2 = |w + (w^2-1)^{\frac{1}{2}}|^2, \tag{14}$$

with

$$w = \frac{2(k-k_\theta)k_\theta \cos^2\theta}{(a_{\mathbf{K}}a_{-\mathbf{K}})^{\frac{1}{2}}} - \frac{a_0}{(a_{\mathbf{K}}a_{-\mathbf{K}})^{\frac{1}{2}}}. \tag{14a}$$

$|\psi_{\mathbf{K}}/\psi_0|^2$ gives the probability that a neutron with wave number $k$ which makes an angle $\theta$ with the normal to the crystal surface be reflected from the set of crystallographic planes associated with $\mathbf{K}$. $k_\theta$ is that wave number which would be required by the Bragg condition. In (14) the sign of the square root is determined by the condition that $|\psi_{\mathbf{K}}/\psi_0|^2$ shall be less than unity.

In the neighborhood of the resonance $a_0$, $a_{\mathbf{K}}$ and $a_{-\mathbf{K}}$ have imaginary parts which cannot be neglected. If $a_0$, $a_{\mathbf{K}}$ and $a_{-\mathbf{K}}$ are all different, the equations are very cumbersome. In order to bring out the essential features we assume that a set of primitive translations can be introduced such that $a_0 = a_{\mathbf{K}} = a_{-\mathbf{K}}$. This condition is realized in body-centered and face-centered cubic lattices. $|\psi_{\mathbf{K}}/\psi_0|^2$ is appreciable only when $|w|$ is not much larger than 1, i.e., within a certain range of wave numbers of the order of

$$\Delta k = (|a_0|/k_\theta \cos^2\theta).$$

$\Delta k$ corresponds to an energy range which, for resonances below 1 ev and $\Gamma_n/\Gamma \sim 1/100$, is of the order of $10^{-5}$ ev. On the other hand, $\Gamma$ is about 0.1 ev. Hence $\bar{\eta}$ varies very little in the region $\Delta k$ and will be regarded as a constant in the integration which follows.

The total intensity at a Laue spot can be obtained from the integrated reflecting power

$$R_{\mathbf{K}} = \int_0^\infty \left|\frac{\psi_{\mathbf{K}}}{\psi_0}\right|^2 dk. \tag{15}$$

$R_K$ is the ratio of the number of reflected neutrons to the number of incident neutrons per unit wave number interval. We find

$$R_{\mathbf{K}} = \frac{4|a_0|}{3k_\theta \cos^2\theta} g(\rho), \tag{15a}$$

with

$$\rho \equiv Im\,\bar{\eta}/|\bar{\eta}| = Im\,a_0/|a_0|. \tag{15b}$$

$g(\rho)$ is a uniformly decreasing function of $\rho$. The following estimates have been made which are accurate to 2 percent: $g(0.2)=0.71$; $g(0.4)=0.57$; $g(0.6)=0.47$; $g(0.8)=0.41$; $g(1.0)=0.36$.

We have written $R_{\mathbf{K}}$ in this particular way in order to separate as much as possible the effects on which it depends when $E \sim E_0$. For a given intensity of neutrons which impinge on a nucleus, the scattering is enhanced by the resonance. At the same time the resonance introduces strong absorption. Finally, a neutron may be reflected back and forth between the incident wave and

[9] See, for example, M. V. Laue, *Roentgenstrahlinterferenzen*, (Becker and Erler, Leipzig, 1941), p. 270, Eq. (28.18).

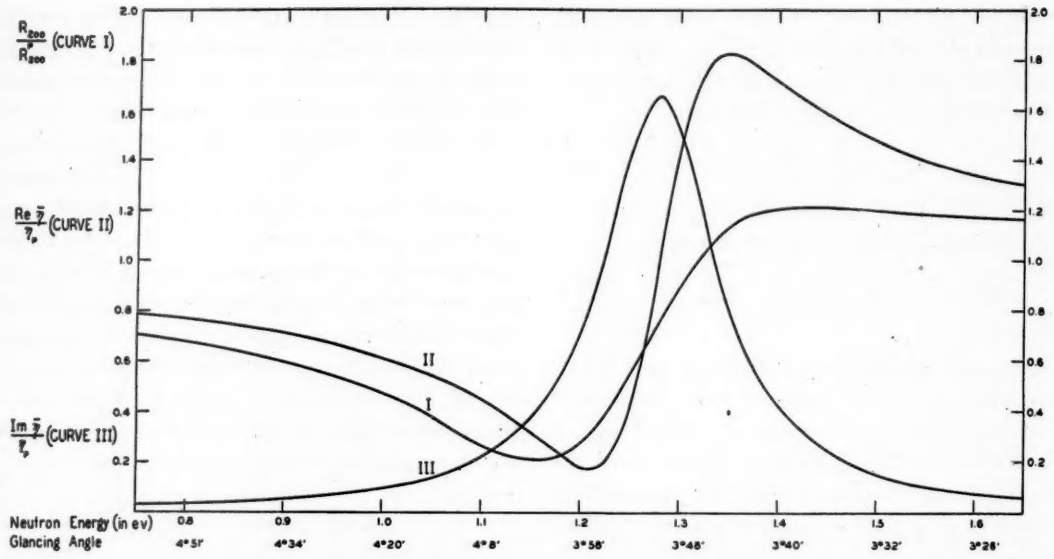


FIG. 1. Resonance scattering from a rhodium crystal (200 reflection).

the diffracted wave inside the crystal. The last effect is relatively unimportant because of the large absorption. In order to separate the other two factors we make use of the wave kinematical theory of interferences which neglects the absorption as well as the complicated interaction between the incident and the diffracted waves. According to this theory, the intensity of a Laue spot is proportional to $\sigma_{int}$, where

$$\sigma_{int} \equiv 4\pi|\bar{\eta}|^2/k^2. \tag{16}$$

Thus the scattering depends essentially on the absolute value of $\bar{\eta}$, while absorption effects are proportional to $Im\,\bar{\eta}$ (Eq. (8)).

The product which precedes $g(\rho)$ in (15a) is the intensity from a lattice of hypothetical nuclei which scatter with a real phase shift of magnitude $|\bar{\eta}|$. Hence this product measures the scattering. $g(\rho)$ represents primarily the absorption of neutrons before and after they have been scattered. The strength of this absorption could have been predicted. For this purpose we compare $\Lambda_{abs}$ with the mean path length $\Lambda_{dif}$, which neutrons would cover inside the hypothetical non-absorbing crystal. From the theory of x-ray diffraction, $\Lambda_{dif}$ is of the order of $k/|a_0|$. Also, we have

$$\Lambda_{abs} = 1/n_0\sigma_{abs} = k/Im\,a_0. \tag{17}$$

Since $Im\,\bar{\eta}$ and $|\bar{\eta}|$ are of the same order of magnitude for $E \sim E_0$, we find that $\Lambda_{abs}$ and $\Lambda_{dif}$ are comparable. The absorption may be expected to reduce the intensity by a factor of the order $e$. This result is in agreement with the values obtained for $g(\rho)$.

Curve I in Fig. 1 shows $R_K/R^p_K$ for the 200††† reflection in rhodium for neutrons whose energy lies in the neighborhood of the resonance at 1.28 ev.[4] $R^p_K = 7.76\times10^4$ cm$^{-1}$ is the reflectivity at 1.28 ev which would be obtained in the absence of a resonance. The appropriate glancing angle is indicated below each neutron energy. Curves II and III represent the real ($Re\,\bar{\eta}$) and the imaginary part of $\bar{\eta}$, respectively, expressed in terms of the phase shift for potential scattering at exact resonance, $\eta_p = -1.73\times10^{-3}$.

We took $\Gamma_n = 0.8\times10^{-3}$ ev, $\Gamma = 0.14$ ev, $(2J+1)/2(2j+1) = \frac{1}{2}$. The magnitude of $\eta_p$ was obtained from the approximate relation, $|\eta_p| = k_0R$, where $k_0$ is the wave number at exact resonance and $R$ is an appropriate nuclear radius. The variation of this phase shift over the resonance region was neglected. In the absence of information, we took the negative sign for $\eta_p$, which is by far the more common case. If $\eta_p$ were positive, curve I would have to be reflected with respect to a vertical axis passing through $E = 1.28$ ev.

††† The Miller indices refer to the usual basis for a face-centered lattice in which there are 4 atoms per unit cell.

If we have a well collimated beam containing neutrons of all energies, for which the number of neutrons per unit wave number interval is constant in the neighborhood of 1.28 ev, then curve I gives the variation of the intensity as the angular setting of the scatterer is varied. The intensity changes reflect the dependence of $\bar{\eta}$ on $E$, in particular of the real part of $\bar{\eta}$. The latter is small on that side of the resonance where the first two terms of (7) tend to cancel one another (interference between potential scattering and resonance scattering). An experiment along these lines is difficult. The effect for rhodium is crowded into a small angular region, because the wave-length at 1.28 ev is small compared to the lattice spacing. Unfortunately, there does not seem to exist an element with a resonance much below 1 ev of which sufficient quantities are available to grow a single crystal. In addition, the relative abundance of the active isotope must be appreciable (Eq. (7a)). Cadmium is excluded for this reason.

An estimate will now be given of the intensity of the isotropic background. On the basis of the wave kinematical theory and for the case of zero absorption, Wick[6] has shown that the isotropic scattering is the same as if every nucleus in the lattice had a fixed cross section, which we shall denote by $\sigma_{\text{iso}}$. If the potential scattering is negligible, we have

$$\sigma_{\text{iso}}=f_0\sigma_{\text{sca}}-\sigma_{\text{int}}, \tag{18}$$

where $\sigma_{\text{sca}}$ is the scattering cross section of the active isotope and $f_0$ is its relative abundance. We have

$$\sigma_{\text{sca}}=\frac{2J+1}{2(2j+1)}\frac{\pi}{k^2}\frac{\Gamma_n^2}{(E-E_0)^2+\frac{1}{4}\Gamma^2}, \tag{19}$$

$$\sigma_{\text{int}}=\left(\frac{2J+1}{2(2j+1)}\right)^2\frac{\pi f_0^2}{k^2}\frac{\Gamma_n^2}{(E-E_0)^2+\frac{1}{4}\Gamma^2}. \tag{20}$$

Thus

$$\sigma_{\text{iso}}=f_0\sigma_{\text{sca}}\left(1-\frac{(2J+1)f_0}{2(2j+1)}\right). \tag{21}$$

In order to complete the estimate, we consider the attenuation of the incident wave which is due to absorption and diffraction. If the condition for Bragg reflection is satisfied, the mean path length of neutrons inside the crystal is somewhat smaller than either $\Lambda_{\text{abs}}$ or $\Lambda_{\text{dif}}$, but of the same order of magnitude, because $\Lambda_{\text{abs}}$ and $\Lambda_{\text{dif}}$ are comparable. If Bragg reflection cannot take place, the mean path length is again of the order of $\Lambda_{\text{abs}}$. In either case, the fraction of incident neutrons which is scattered isotropically is of the order of $\sigma_{\text{iso}}/\sigma_{\text{abs}}\sim\Gamma_n/\Gamma$.

In the preceding treatment of the ideal crystal, we were able to divide the problem into two parts: the Laue-Bragg scattering and the isotropic background. We note that this separation led us to disregard two effects:

1. The intensity outside the Laue spots is not rigorously isotropic, because a neutron which has been incoherently scattered out of the incident beam may suffer further scattering by the lattice. The multiple scattering takes place with particular intensity when the first scattering is along a direction for which Bragg reflection is possible. It can be shown that the contribution of this effect is of the order of $\Gamma_n/\Gamma$ of the isotropic background.

2. If our treatment were exact, $Im\,\bar{\eta}$ would account for the disappearance of all neutrons which can no longer participate in the Laue-Bragg scattering after the incident beam has passed by a given nucleus. We have seen (Eq. (8)) that $Im\,\bar{\eta}$ leads to $\sigma_{\text{abs}}$. It does not include the loss resulting from isotropic scattering.

Thus our separation of the scattering into two parts is implicitly based on the assumption that $\Gamma_n/\Gamma\ll 1$.

We shall briefly consider the influence of the mosaic structure. Mosaic structure is always present, but we may disregard it if the incident beam penetrates only one microcrystal or if the alignment of the microcrystals is unusually good. When the mosaic structure is relevant, several cases are to be distinguished. A treatment of these cases can be developed on the basis of the theory given by Zachariasen[10] with the help of the expressions for $\bar{\eta}$ and $\sigma_{\text{int}}$. Here we shall merely write down the expression for the Laue intensity $\mathfrak{R}_{\text{K}}$ when both primary and secondary extinction are negligible (ideally imperfect crystal),

$$\mathfrak{R}_{\text{K}}=(\pi^2 n_0\sigma_{\text{int}}/2k^2\cos^2\theta\sigma_{\text{abs}}). \tag{22}$$

[10] W. H. Zachariasen, *Theory of X-Ray Diffraction in Crystals* (John Wiley and Sons, Inc., New York, 1945), Sections 2 and 3, Chapter IV.

The assumption was made that the unit cell contains only one atom. $\mathcal{R}_{\mathbf{K}}$ is of the same order of magnitude as the reflectivity from an ideal crystal, $R_{\mathbf{K}}$. Thus,

$$(\mathcal{R}_{\mathbf{K}}/R_{\mathbf{K}}) = (3\pi|\bar{\eta}|/32g(\rho)Im\,\bar{\eta}) \qquad (23)$$

is of the order unity. On the other hand, when the neutron energy is not in the neighborhood of a resonance, the mosaic structure may enhance the intensity by as much as a factor of 100.[2] These results can be explained in the following way: The introduction of a spread in the angular orientation of microcrystals decreases the probability that a given neutron will be diffracted along a given distance. Far from resonances, the absorption is small and an upper limit on the reflectivity is set by the attenuation of the incident wave caused by diffraction. Hence the mosaic structure enhances the scattered intensity. In the neighborhood of the resonance this effect cannot take place, because in this region absorption is as important a factor as diffraction in attenuating the incident wave.

It can be shown that the influence of atomic oscillation,[11] which we have disregarded, does not affect our results in a significant way.

The author wishes to express his sincere thanks to Professor E. Teller, who suggested this problem, for helpful advice, and to Mr. M. L. Goldberger for many valuable discussions. He is also indebted to Mrs. D. Kurath for help in the computations.

---

[11] R. Weinstock, Phys. Rev. **65**, 1 (1944).

# Production of Neutrons by the Capture of Cosmic-Ray Mesons at Sea Level*

GERHART GROETZINGER AND GORDON W. MCCLURE
*Institute for Nuclear Studies, University of Chicago, Chicago, Illinois*
(Received June 14, 1948)

SEVERAL cases of nuclear disintegrations caused by the capture of mesons have been observed in photographic emulsions exposed to cosmic radiation at altitudes of approximately 3500 meters. One to five heavy, charged particles are emitted in this process. Mesons responsible for these events have been designated as $\sigma$- (or negative $\pi$-) mesons and are believed to have masses of approximately 300 electron masses. At the same altitude more than ten times as many mesons reach the end of their range in the emulsion without producing visible secondary tracks. The latter mesons are designated as $\rho$- (or positive and negative $\mu$-) mesons and are supposed to be identical with the mesons of mass 200 which predominate at sea level.[1] No disintegrations caused by the capture of cosmic-ray mesons have been found at sea level in photographic emulsions. Several cases of negative mesons reaching the end of their range in the gas of a cloud chamber or in thin iron or lead foils inside the chamber have been observed at sea level. In no case were heavy particles observed starting at the end of the meson track.[2]

Experiments using G-M counters indicate that the capture of light cosmic-ray mesons is not accompanied by the emission of photons with energies above 30 Mev.[3]

In the investigation to be described, an attempt was made to obtain information concerning the capture of mesons at sea level by making a search for neutrons emitted during this process. This constitutes a new approach to the problem of meson-induced nuclear disintegrations through observing the emission of one or more neutrons which are not accompanied by charged heavy particles. By using materials of high atomic weight, fission induced by slow mesons could be detected in this way.[4]

Our apparatus consists of a fourfold coincidence counter telescope in which the incident mesons are deflected in magnetized iron plates. The arrangement distinguishes between positive and negative mesons but is not sufficiently selective to distinguish between particles of 200 and 300 electron masses. All mesons traversing the telescope impinge at a glancing angle upon a 1-cm lead stopping plate surrounded by a *V*-shaped bank of G-M counters allowing the entrance of the mesons on top. Below the *V* bank and interposed between two 8-cm-thick slabs of paraffin were located four $BF_3$ proportional counters containing boron of a 96 percent concentration of $B^{10}$.[5] Each time the telescope is tripped, a 20-microsecond oscillograph sweep is triggered and photographed. The *V* bank of G-M counters and the $BF_3$ counters produce separate and distinguishable pulses on the oscillograph trace, so that if either or both is tripped with the 20-microsecond interval, this information along with the corresponding time delays is recorded on the photograph.

Any fourfold coincidence followed by a neutron counter pulse and not accompanied by a *V*-bank pulse corresponds to stoppage of a meson in the lead plate with the resulting ejection of a neutron. Two types of processes besides neutrons produced in the capture of a meson could cause a "neutron" pulse to appear on the sweep; namely, cosmic-ray showers containing neutrons,[6] or showers containing a density of charged particles sufficient to trigger the $BF_3$ proportional counters. Both processes are recognizable since

* A portion of this work was supported by the Office of Naval Research. Contract N6ori-20, T.O.III.

[1] C. M. G. Lattes, G. P. S. Occhialini, and C. F. Powell, Nature **160**, 453 (1947), and **160**, 458 (1947).

[2] T. H. Johnson and R. P. Shutt, Phys. Rev. **61**, 380 (1942); W. Y. Chang, Bull. Am. Phys. Soc. **23**, 42 (1948).

[3] O. P. Piccioni, Phys. Rev. **73**, 411 (1948); Bull. Am. Phys. Soc. **23**, 42 (1948).

[4] It was predicted by J. A. Wheeler (Bull. Am. Phys. Soc. **23**, 20 (1948)) that slow ordinary negative mesons could probably produce fission in uranium and with reasonable probability in heavier elements where the energy available exceeds with greater certainty the threshold for fission.

[5] The concentrated $B^{10}$ was secured through the isotope branch of the Atomic Energy Commission at Oak Ridge, Tennessee.

[6] Vanna Tongiorgi, Phys. Rev. **73**, 923 (1948).

in either case at least one of the *V*-bank counters would be tripped simultaneously with the telescope. In the first case the neutron pulse would be delayed a few microseconds because of the slowing down of the neutron in the paraffin.

Out of 1167 negative mesons stopped in the lead plate, four were accompanied by neutron counter pulses having time delays of 1.6, 1.8, 5.6, and 8.2 microseconds after the telescope was traversed. No neutron pulses were observed during the stoppage of 688 positive mesons nor in the stoppage of 148 negative mesons where in the latter case the neutron counters were shielded by 1 mm of cadmium between paraffin and counters. In the course of the investigation 20 neutron counter pulses appeared which were accompanied by the discharge of at least one of the G-M counters of the *V*-bank. These neutron pulses were not delayed and their statistics were unaffected by the polarity of the magnetic telescope or the presence of cadmium surrounding the neutron counters.

The efficiency of the neutron counter arrangement for registering neutrons of several Mev created at the position of the stopping plate was determined by placing a Ra-Be neutron source of known intensity at this position. If, furthermore, account is taken of the fact that we register only those neutrons leaving the paraffin within 20 microseconds after the capture of the meson, while the mean transit time of the neutrons through the paraffin is of the order of 100 microseconds,[7] it follows that approximately two neutrons are produced per negative meson captured in lead. This number would be even higher if the neutrons are produced with energies exceeding ten Mev. Whether they are accompanied by heavy charged particles cannot be determined from our experiments. If one assumes that the appearance of neutrons indicates nuclear disruptions leading to the emission of several charged particles and say an average of four neutrons, approximately two meson captures would lead to one disintegration. Because of the poor statistics and other uncertainties, these numbers represent only the order of magnitude for this process. Since the number of heavy mesons at sea level is negligible, the produced neutrons are due to the capture of the light mesons. The appearance of neutrons might, on the other hand, indicate the fission of the lead nucleus as a result of the capture of light mesons rather than a disintegration resulting in the emission of several heavy particles. An attempt will be made to settle this question by using materials of different atomic weights for stopping the mesons.

[7] J. Rainwater and W. W. Havens, Jr., Phys. Rev. **70**, 136 (1946).

# Letters to the Editor

*PUBLICATION of brief reports of important discoveries in physics may be secured by addressing them to this department. The closing date for this department is five weeks prior to the date of issue. No proof will be sent to the authors. The Board of Editors does not hold itself responsible for the opinions expressed by the correspondents. Communications should not exceed 600 words in length.*

## Clustering Phenomena in Solid Solution

A. OPINSKY AND R. SMOLUCHOWSKI
*Metals Research Laboratory, Carnegie Institute of Technology Pittsburgh, Pennsylvania*
June 17, 1948

WHEN a binary solid solution decomposes on cooling and a precipitate forms, the new phase has a definite crystallographic orientation with respect to the matrix as well as habit plane which separates the matrix from the new phase. In many cases in which this habit plane and orientation have been observed, both can be explained in terms of mechanism of transformation or in terms of lattice coherency. The coherency requirement takes into account the fact that the atoms on the boundary tend to be least disturbed. In the case of silver-copper alloys, however, these two factors obviously do not play a significant role because on both ends of the equilibrium system—that is, for copper precipitating out of silver and silver precipitating out of copper—the orientation relationship between the two phases is identical; but on the silver-rich end of the system the habit plane is the (111) plane, while at the other end it is the (100) plane.

This difference can be explained as a result of the structure of the solid solution. A random solution, even in condition of perfect randomness, has a number of areas in which, because of statistical fluctuation, the concentration of the solute atoms is particularly high. Let us consider three solute atoms which tend to make as many nearest neighbors among themselves as possible and which are larger than the atoms of the matrix. It is possible, using fairly simple assumptions, to estimate the energy of elastic deformation of the matrix surrounding the three atoms as a function of the index of the crystallographic plane determined by these atoms. It turns out that the elastic energy is greatest for the (111) plane, somewhat smaller for the (100), and still less for the (110) plane. The same sequence of planes can be obtained using a treatment similar to that of Nabarro[1] which he used in the case of an isotropic medium. On the (111) plane the three atoms form three nearest neighbors, on the (100) plane two neighbors, and on the (110) plane only one nearest neighbor. Thus, the (111) plane, although most favorable from the point of view of bond formation, is less favorable from the point of view of elastic energy. Since the absolute values of the two types of energy are difficult to estimate, we can only conclude that in a copper-rich alloy on the (100) plane the balance of the two energies is optimum. With lower bond energies or higher deformation energies one might expect the habit plane to be the (110) plane. On the silver-rich end of the system, on the other hand, where the precipitate atoms are smaller than the matrix atoms, this elastic energy functions to a much lesser extent because the matrix is less deformed and also the binding of the copper atoms is stronger than that of the silver atoms as evidenced in various atomic and metallic properties. Thus, here the (111) plane is most favorable.

Nabarro's work indicates that crystals of atoms which do not fit into the lattice prefer to form disks or plate-like shapes rather than spherical agglomerates or needles. The treatment here discussed indicates that these plates prefer to be oriented with respect to the crystal lattice. Many other phenomena can be explained on a similar basis. Among them is the influence of silicon on the mechanism of the deformation of alpha-iron, which indicates that silicon preferentially blocks planes (211) and (123) so that a slip can occur only on the (110) planes. Further such effects as the (210) habit plane in the precipitation of $Fe_4N$ from alpha-iron can be explained. A more complete treatment will be published later.

[1] N. F. R. Nabarro, Proc. Phys. Soc. **52**, 90 (1940); Proc. Roy. Soc. **175**, 519 (1940).

## On the Isotopic Composition of Meteoritic and Terrestrial Gallium

MARK G. INGHRAM AND DAVID C. HESS, JR.
*Argonne National Laboratory, Chicago, Illinois*
AND
HARRISON S. BROWN AND EDWARD GOLDBERG
*Institute for Nuclear Studies, University of Chicago, Chicago, Illinois*
June 11, 1948

CONTINUING our comparisons of the isotopic composition of elements occurring in meteorites with those occurring in the earth's crust,[1] the isotopic composition of gallium has been studied. A sample of commercial gallium, converted to the nitrate, was used as the terrestrial standard. Several milligrams of meteoritic gallium were isolated from the Canyon Diablo meteorite for comparison. The Canyon Diablo meteorite, having as its major constituent the element iron, contains on the average 38 ppm of gallium.[2] A kilogram of the meteorite was dissolved in concentrated HCl, the acidity was adjusted to $6M$, and the solution was ether-extracted. Under such conditions gallium is ether-soluble. The major portion of the iron is in the ferrous stage and is not ether-soluble, although some of the iron is unavoidably oxidized by air and accompanies the gallium in the ether layer. The ether solution of gallium, containing some iron, was extracted into water, the iron was reduced to the ferrous stage, and the solution was again ether-extracted. The gallium was finally precipitated as gallium 8-hydroxy quinoline, following which it was converted to the nitrate.

The mass-spectrometer technique used in the analysis of these samples was that described by some of us in connection with studies of lanthanum and cerium.[3] Aliquots of the samples were pipetted onto the filament of a surface ionization type source as a nitric acid solution. Gentle heating served to convert the nitrate to an adherent oxide coat. Emission of $Ga^+$ ions began at approximately 650°C. No compound gallium ions were observed throughout the course of the experiment. The results obtained, along with the results of Sampson and Bleakney,[4] are given in Table I.

TABLE I. Abundance ratio of $Ga^{69}/Ga^{71}$ from terrestrial and meteoritic sources.

| Investigator | Source | $Ga^{69}/Ga^{71}$ ratio |
|---|---|---|
| Sampson and Bleakney[4] | Terrestrial | 1.58 |
| This work | Terrestrial | 1.510 |
| This work | Meteoritic | 1.509 |

The samples were four times introduced, each for purposes of precision in the comparison of the isotopic ratios. Evaluation of errors shows that the isotopic ratios of the terrestrial and meteoritic samples are the same to within two-tenths of one percent. The absolute ratios given in Table I are the average values of 250 individual results. As a result of possible fractionations and discriminations they are good to three-fourths of one percent. It is apparent, however, that our value is not compatible with that of Sampson and Bleakney. This may be due to voltage effects in the Sampson and Bleakney measurements which were avoided in our observations.

[1] H. Brown and M. G. Inghram, Phys. Rev. **72**, 347 (1947).
[2] H. Brown and E. Goldberg (work to be published).
[3] M. G. Inghram, R. J. Hayden, and D. C. Hess, Jr., Phys. Rev. **72**, 967 (1947).
[4] M. B. Sampson and W. Bleakney, Phys. Rev. **50**, 456 (1936).

## Long-Lived Tc Activities Produced by Deuteron Bombardment of Separated Mo Isotopes*

E. E. Motta and G. E. Boyd
*Oak Ridge National Laboratory, Oak Ridge, Tennessee*
June 10, 1948

IN two earlier letters (April 30, 1948 and May 26, 1948) a preliminary report was given on a group of Tc activities (element 43) produced by irradiation of the separated Mo isotopes with ~16-Mev deuterons. It is now possible to report confirmatory evidence on the mass assignment of several of the known long-lived Tc activities, based on the results of bombardments of the various separated Mo isotopes with *ca.* 22-Mev deuterons from the Berkeley 60-inch cyclotron.

*4.2-day* Tc. This Tc activity[1,2] was produced in greatest yield from the deuteron bombardment of Mo enriched in $Mo^{96}$ and decayed with a half-life of 4.2±0.1 days (Fig. 1). This result serves to confirm the assignment of the 4.2-day Tc to $Tc^{96}$. Gamma-rays of 0.8±0.1-Mev energy as well as 17–18-kev x-rays were observed. Charged particles of 0.64-Mev energy[2] were not found, however.

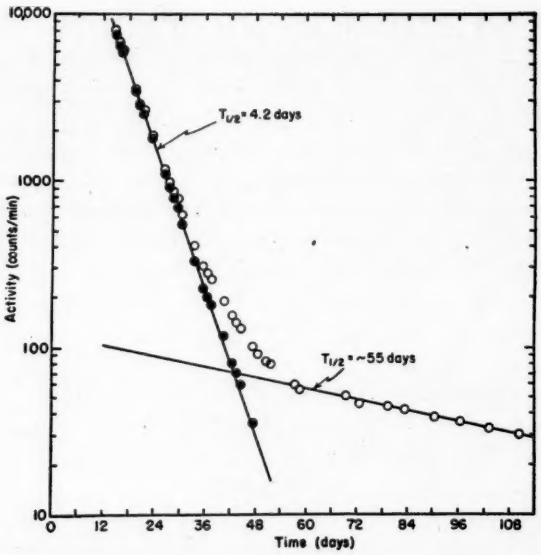


FIG. 1. Decay curve of the 4.2-day Tc activity produced by deuteron bombardment of Mo enriched in $Mo^{96}$.

*50–60-day* Tc. The previously studied 50–60-day $Tc^{2-4}$ was produced in greatest yield from the deuteron bombardment of Mo enriched in $Mo^{95}$. The decay curve (Fig. 2A) gave an apparent half-life of 59 days. This value will be reduced slightly by the subtraction of a 90-day component which is almost certainly present. The radiations found associated with this period were a 0.8±0.1-Mev γ-ray, a 0.24±0.05-Mev γ-ray, and x-rays characteristic of the

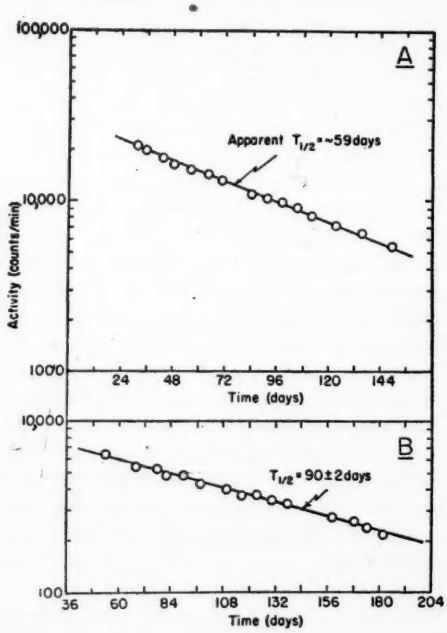


FIG. 2. A. Decay curve of the 50–60-day Tc activity produced by deuteron bombardment of Mo enriched in $Mo^{95}$. B. Decay curve of the 90-day Tc activity produced by deuteron bombardment of Mo enriched in $Mo^{97}$

Mo-Tc region. The $\gamma$-ray of lower energy was twice as abundant as that of higher energy in agreement with Huber *et al.*[4] In addition, conversion electrons of ~180-kev energy were observed (visual range 40 mg Al/cm²). The predominantly greater yield of this 50–60-day Tc activity from Mo enriched in $Mo^{95}$ supports its assignment to $Tc^{95}$.

*90-day* Tc. Our earlier work[5] on the approximately 90-day Tc had indicated its assignment to mass 97. It was to be expected, then, that a $d,2n$ reaction would give the greatest yield of $Tc^{97}$ when carried out on Mo enriched in $Mo^{97}$. This result was actually found and confirms the assignment of the 90-day Tc. Soft electrons of ~85-kev energy ($\tau\frac{1}{2}$=1.5 mg Al/cm²), and 17–18-kev x-rays were again found associated with this period. The yield of any unconverted soft gamma-radiation (~97 kev) was so small that its presence was doubtful. The decay curve (Fig. 2B) gave a 90±2-day half-life.

* This document is based on work performed under Contract No. W-7405-eng.-26 for the Atomic Energy Project at Oak Ridge National Laboratory.

[1] Ewing, Perry, and McCreary, Phys. Rev. 55, 1136 (1939).
[2] J. E. Edwards and M. L. Pool, Phys. Rev. 72, 384 (1947).
[3] E. N. Cacciapuoti and E. Segrè, Phys. Rev. 55, 110 (1939).
[4] Huber, Medicus, Preiswerk, and Steffen, Phys. Rev. 73, 1211 (1948).
[5] Motta, Boyd, and Brosi, Phys. Rev. 71, 210 (1947).

## Increase in Vapor Pressure of Liquid Helium Due to $He^3$ in Solution*

HENRY A. FAIRBANK, CHARLES A. REYNOLDS, AND C. T. LANE
*Sloane Physics Laboratory, Yale University,** New Haven, Connecticut*
AND
B. B. MCINTEER, L. T. ALDRICH, AND ALFRED O. NIER
*Department of Physics, University of Minnesota,** Minneapolis, Minnesota*
June 16, 1948

WITH a thermal diffusion column[1] we have recently produced about 100 standard cm³ of helium gas containing approximately 0.16 percent $He^3$. This sample, therefore, contains about ten thousand times more $He^3$ than ordinary gas well-helium. It seemed, therefore, worth while to attempt to measure differences in the vapor pressure between this enriched gas and the normal well-helium, the latter being practically pure $He^4$.

The apparatus consisted of two identical thin-walled copper vessels, each of volume approximately 0.16 cm³, the two being silver-soldered together. A pair of thin-walled stainless steel tubes ran from each vessel out of the cryostat to the respective legs of an oil manometer, the latter containing low vapor pressure diffusion pump oil (Octoil-S). The two levels in the manometer were read with a cathetometer, and with this apparatus vapor pressure differences of the order of $10^{-3}$ mm Hg could be detected. The two copper vessels were surrounded by a bath of liquefied well-helium whose temperature could be controlled by pumping in the usual way. Corresponding absolute temperatures were computed from the vapor pressure of this bath using the Leiden 1937 tables.

The results of the measurement are shown in Fig. 1. As

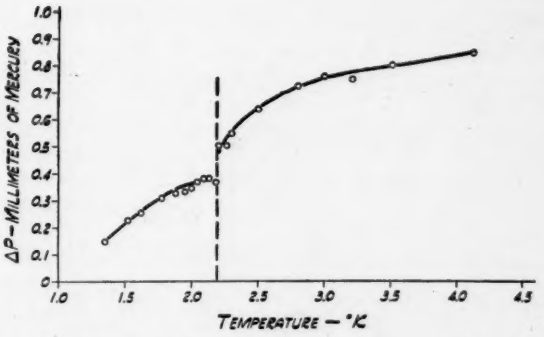


FIG. 1. The difference in vapor pressure ($\Delta P$) between helium containing 0.16 percent $He^3$ and well-helium as a function of temperature. The vertical broken line passes through the $\lambda$-point.

was expected, the $He^3$-enriched material showed a higher vapor pressure than the $He^4$ at all temperatures. In order to check the reliability of our apparatus we performed a blank experiment using well-helium in both copper vessels. Under these conditions, the vapor-pressure difference was less than the least count of our manometer (~$10^{-2}$ mm Hg) at all temperatures in the range shown in Fig. 1. In view of this it seems unlikely that the discontinuity at the $\lambda$-point shown in Fig. 1 is due to small-temperature inhomogeneities in the bath when it is in the He I region. Further, the results were quite reproducible.

The possibility that the $\lambda$-point discontinuity is due to a secondary effect connected with the creeping film is being investigated. One possibility is that the evaporated film on recondensing produces a downward heat flush in the liquid in the copper bulb disturbing the isotope distribution.[2]

If one assumes that this solution of $He^3$ in $He^4$ is ideal, that is, obeys Raoult's and Henry's laws, then it can be shown that the following relations hold:

$$\Delta P = C_L[(C_V/C_L)-1]\pi_4, \quad (1)$$

$$\Delta P = C_L(\pi_3-\pi_4). \quad (2)$$

Here the $\pi$'s represent the saturated vapor pressures of the two pure isotopes, and $C_V$, $C_L$ are, respectively, the $He^3$ to $He^4$ concentrations in the vapor and liquid. Previously values of $C_V/C_L$ as a function of temperature in the He I region for very dilute solutions have been measured by us.[3] If we suppose that the much more concentrated (by about $10^3$) solution we have here obeys the same relationship, then $C_L$ as a function of temperature may be computed from this and the balance of mass and composition equations. This is tantamount to supposing Henry's law to be valid in this concentration range. Since now all quantities on the right of Eq. (1) are known, $\Delta P$ may be computed as a function of temperature in the He I region. The results of this give only order-of-magnitude agreement, the computed values being around 40 percent lower than the measured values, but the calculation nevertheless suggests that, in the He I region, the solution is not far removed from an ideal classical solution. Similarly, from Eq. (2) a rough estimate may be made of the vapor-pressure curve[4] for $He^3$. A plot of $\log\pi_3$ *versus* $1/T$ made from the above data gives a

straight line, from which the normal boiling point is approximately 2.9°K.

* A short report of this measurement was given by one of us (C.T.L.) at the Shelter Island Conference on Low Temperature Physics on June 1, 1948.

** The work at Yale University was assisted by the Office of Naval Research under Contract N6ori-44, Task Order 3. That at the University of Minnesota was aided by Contract N5ori-147, Task Order 3; the Graduate School; and the University of Minnesota Technical Research Fund.

[1] B. B. McInteer, L. T. Aldrich, and A. O. Nier, Phys. Rev. 72, 510 (1947). A manuscript giving a complete description of this column is in preparation.

[2] C. T. Lane, H. A. Fairbank, L. T. Aldrich, and A. O. Nier, Phys. Rev. 73, 256 (1948).

[3] H. A. Fairbank, C. T. Lane, L. T. Aldrich, and A. O. Nier, Phys. Rev. 73, 729 (1948); 71, 911 (1947).

[4] It is possible that pure $He^3$ would not exist as a saturated liquid at any temperature down to absolute zero. In this connection see F. London, Phys. Rev. 73, 1188 (1948).

## Nuclear Paramagnetism at Low Temperatures

B. V. Rollin and J. Hatton
*Clarendon Laboratory, Oxford, England*
June 10, 1948

FURTHER measurements on nuclear paramagnetism at low temperatures have been made using the magnetic resonance absorption method.[1,2]

Experiments have been made on single crystals of calcium fluoride in order to determine the effect of temperature, magnetic field strength, and paramagnetic impurities on the spin-lattice equilibrium time of the fluorine nuclei. The results of measurements at a frequency of 5.3 mcs/sec. on two specimens of natural fluorite are given in Table I. Crystal *A* was colorless and *B* was a greenish-blue color.

The remarkable difference between *A* and *B* is probably due to the presence of paramagnetic rare earth impurities or *F*-centers in specimen *B*; but as the line width was only about 8 gauss in both specimens, the concentration of paramagnetic impurity could not have greatly exceeded 1 in 10.[4]

In order to investigate the effect of *F*-centers,[3] specimen *A* was irradiated with x-rays at liquid air temperature for a time sufficient to give a blue coloration. As a result of the irradiation, the relaxation times at 4.2°K and 1.2°K were reduced to about half of the previous values.

These results suggest that impurities or *F*-centers play a predominant part in the relaxation process and that even concentrations as low as 1 in $10^6$ may have an appreciable effect.

The dependence of $T_1$ on magnetic field strength has been investigated by making measurements on specimen *A* at a frequency of 2.05 mc/sec. The values of $T_1$ obtained at this frequency were about half those obtained at 5.3 mc/sec.

TABLE I. Relaxation time of two specimens of calcium fluoride crystals.

| Specimen | Temperature T°K | Relaxation time $T_1$ (sec.) |
|---|---|---|
| *A* | 20.0° | 17.0 |
| | 4.2° | 67.0 |
| | 1.2° | 280.0 |
| *B* | 20.0° | 0.1 |
| | 4.2° | 0.46 |
| | 1.2° | 1.0 |

It is not possible at the present time to give a complete explanation of these results, but the approximate proportionality between $1/T_1$ and T°K suggests that only those Debye waves which are fully excited at 1°K are effective in the relaxation process, the nuclear transition probability being proportional to the energy in these waves. The increase of $T_1$ with increase of magnetic field strength cannot be accounted for by a mechanism of direct interaction between nuclear spins and lattice waves, and suggests that the relaxation process may be associated with magnetic field fluctuations caused by change of direction of the electron spins in the paramagnetic impurities or *F*-centers.

By making use of the long relaxation time of specimen *A* we have carried out a nuclear demagnetization experiment. At a temperature of 1.2°K, the specimen was maintained in a field of 4000 gauss for 12 minutes. On reducing the field to 500 gauss, the nuclear spin temperature was observed to fall to 0.17°K and then subsequently to rise to the lattice temperature of 1.2°K with a relaxation time of 1 minute.

Previous experiments on solid hydrogen[2] have been extended to lower temperatures, using an improved design of apparatus. It is found that at 1.3°K, in addition to the main resonance, a subsidiary peak appears on either side of the main peak at a distance of 18 gauss. On reducing the temperature to 1.1°K, the intensity of the side peaks increases while that of the central peak diminishes. The measurements were made on a polycrystalline specimen. This splitting of the resonance is presumably associated with the increase in the state of order of the molecular rotation which occurs in this temperature region.

In order to determine the relaxation time of the nuclei in a metal, experiments have recently been made on a specimen of aluminum in the form of a spiral of thin foil. Using a frequency of 2.45 mc/sec. the value of $T_1$ at 1.1°K and 4.2°K was found to be approximately one second which is in agreement, as regards order of magnitude, with the theoretical estimate of Heitler and Teller.[4] The width of the resonance was about 10 gauss.

[1] B. V. Rollin and J. Hatton, Nature 159, 201 (1947).

[2] B. V. Rollin, J. Hatton, A. H. Cooke, and R. J. Benzie, Nature 160, 436 (1947).

[3] The possible effect of *F*-centers on nuclear relaxation was suggested by H. Fröhlich at a colloquium in Oxford early in 1947.

[4] W. Heitler and E. Teller, Proc. Roy. Soc. London A155, 629 (1936).

## The Isotopic Effect of the Potential Function of Molecular States

J. G. Valatin
*Institut Henri Poincaré, Paris, France*
June 9, 1948

BESIDES the known isotopic effects in the band constants, a difference of 350 $cm^{-1}$ in the energy distance of the minimum of the potential function from the asymp-

totic value in the $X^2\pi$ ground states of the CH and CD doublet spectra has been observed by Gerö and the effect is shown by numerous limiting curves of predissociation.[1,2] The greater bond energy of the CD potential function is connected with a somewhat shorter observed equilibrium internuclear distance. The dependence of the potential function on the isotopic mass should be a quite general effect in all the diatomic hydrid and deuterid spectra.

For the observed rotational constants $B$, one has

$$B=(h^2/8\pi^2\mu)\int\bar{\phi}(1/r^2)\phi d\tau,$$

with $\mu=M_1M_2/(M_1+M_2)$, and in first approximation

$$B(CD)/B(CH)=\rho^2=\mu(CH)/\mu(CD).$$

Some effects causing slight deviations from this isotopic ratio of the rotational constants are dealt with in Van Vleck's review.[3] According to the observation of Gerö and Schmid, however, the rotational constants of diatomic hydrid and deuterid spectra show, in general, a deviation from this rule larger in order of magnitude than the effects given in Van Vleck's paper. One should also mention the remark of Sandeman,[4] who concluded from an analysis of the band constants of the $D_2$, DH, and $H_2$ spectra, that these three molecules have three different potential curves.

In order to obtain a suitable description of the interaction of the particles in a diatomic molecule, instead of the coordinates $x_i''$ of the electrons and $X_1''$, $X_2''$ of the nuclei one must introduce the relative coordinates $x_i'=x_i''-X_1''$, $X_r'=X_2''-X_1''$ of the particles related to one of the nuclei, besides the coordinates of the center of gravity, $X=(m\Sigma x_i''+M_1X_1''+M_2X_2'')/M$.[5] The total kinetic energy of the particles,

$$\frac{h^2}{8\pi^2}\left\{\frac{1}{M}\Delta+\frac{1}{\mu}\Delta_r'+\frac{1}{m}\Sigma\Delta_i'+\frac{1}{M_1}\left(\left(\Sigma\frac{\partial}{\partial x_i'}\right)^2+\left(\Sigma\frac{\partial}{\partial y_i'}\right)^2+\left(\Sigma\frac{\partial}{\partial z_i'}\right)^2\right)+\frac{2}{M_1}\left(\frac{\partial}{\partial X_r'}\Sigma\frac{\partial}{\partial x_i'}+\frac{\partial}{\partial Y_r'}\Sigma\frac{\partial}{\partial y_i'}+\frac{\partial}{\partial Z_r'}\Sigma\frac{\partial}{\partial z_i'}\right)\right\},\quad(1)$$

contains besides the first three terms corresponding to the kinetic energy of the center of gravity, of the relative nuclear motion and of the electrons, the last two small correction terms. Though these correction terms are not the most important ones from the point of view of isotopic effects, it is worth while to stress, for instance, in the case of CH and CD, that in taking the H or D nucleus as reference particle, their effect corresponds to terms explicitly containing the different masses $M_1$, whereas with the carbon nucleus as reference particle this part of the isotopic effect is already included in the molecular wave functions.

As pointed out in a previous paper,[6] owing to the influence of the nuclear motion on the electronic motions, clear distinction is to be made between the corresponding part of the potential function of an unperturbed electronic state,

$$V_1(r)=\int\bar{\phi}_e^{(\Omega)}(x_i,r)(T_e+U)\phi_e^{(\Omega)}(x_i,r)dx_i,\quad(2)$$

and the energy eigenvalue function of the fixed nuclei problem. The influence of the nuclear motion, represented by the second term in expression (1), on the wave function factor $\phi_e^{(\Omega)}(x_i,r)$ characterizing an unperturbed electronic state, may be considerable. Thus one can understand the observed isotopic effects which cannot be understood on the ground of the correction terms in a model in which this wave function factor is identified with an eigenfunction of the fixed nuclei problem.

[1] L. Gerö and R. Schmid, Zeits. f. Physik 118, 210 (1941).
[2] L. Gerö and R. Schmid, Zeits. f. Physik 118, 250 (1941).
[3] J. H. Van Vleck, J. Chem. Phys. 4, 327 (1936).
[4] I. Sandeman, Proc. Roy. Soc. Edinburgh 59, 130 (1939).
[5] J. G. Valatin, Hungarica Acta Phys. 1, 23 (1947).
[6] J. G. Valatin, Proc. Phys. Soc. 58, 695 (1946).

## Products of High Energy Deuteron and Helium Ion Bombardments of Copper

D. R. Miller, R. C. Thompson,[1] and B. B. Cunningham
*Department of Chemistry and Radiation Laboratory, University of California, Berkeley, California*
June 17, 1948

THIS communication summarizes the preliminary observations made when natural copper (stable mass numbers 63 and 65) was bombarded with 190-Mev deuterons and 380-Mev helium ions produced by the 184-inch frequency-modulated cyclotron.[2] After a 10- to 40-minute bombardment with a beam of about 0.5 microamperes for the deuterons or of unknown intensity for the helium ions, the spectrographically pure metallic copper target was dissolved in acid, inactive carrier elements added, and chemical separations performed until pure elemental fractions were isolated. Aliquots of these fractions were evaporated on platinum foil disks and the rate of decay carefully followed with a thin-window (*ca.* 3 mg/cm² mica) Geiger-Müller counter. Identification of radioactive product isotopes was made by these half-life determinations supplemented in most cases by at least one of the following methods: (a) observation of parent-daughter relationships when possible; (b) observation of the sign of the radiation by counting through a magnetic field; (c) rough energy determinations by counting through aluminum, beryllium, or lead absorbers; and (d) differential counting through different absorbers. The results of the deuteron bombardments are summarized in Table I.

Two previously unreported isotopes were found. Freshly precipitated zinc fractions showed a growth corresponding to *ca.* 11 minutes half-life, followed by a 9.5-hour decay. Removal of copper from the zinc fractions yielded in the copper fractions a pure 11-minute activity which was identified as $Cu^{62}$; the 9.5-hour activity was therefore assigned to $Zn^{62}$. The number of counts per minute of the 11-minute copper activity removed from the zinc fraction (extrapolated back to the time of separation) was the same within ±10 percent as the number of counts per minute of the 9.5-hour activity in the zinc-copper mixture immediately before copper-zinc separation. Since $Zn^{62}$ was thus apparently detected only by virtue of the activity of its daughter, it is presumed to decay by orbital electron

TABLE I. Isotopes observed as products of the bombardment of natural copper with 190-Mev deuterons.

| Isotope | Type of radiation[a] | Half-life Literature[b] | Half-life Observed | Yield[c] relative to $Cu^{61}$ | Change in $A$ and $Z$ from $Cu^{65}$ $A$ | $Z$ |
|---|---|---|---|---|---|---|
| $_{30}Zn^{62}$ | $(K)$ | — | 9.5 h. | 0.035 | −3 | +1 |
| $Zn^{63}$ | $(\beta^+)$ | 38 m. | 36 m. | 0.05 | −2 | +1 |
| $_{29}Cu^{60}$ | $(\beta^+)$ | 24.5 m.[d] | *ca.* 25 m. | 0.3 | −5 | 0 |
| $Cu^{61}$ | $\beta^+$, $(K)$ | 3.4 h. | 3.3 h. | 1.0 | −4 | 0 |
| $Cu^{62}$ | $\beta^+$ | 10.5 m. | *ca.* 11 m. | 2.3 | −3 | 0 |
| $Cu^{64}$ | $(\beta^+, \beta^-, K)$ | 12.8 h. | 13 h. | 0.6 | −1 | 0 |
| $_{28}Ni^{57}$ | $\beta^+$ | 36 h. | 37 h. | 0.04 | −8 | −1 |
| $Ni^{65}$ | $\beta^-$ | 2.6 h.[e] | 2.5 h. | 0.04 | 0 | −1 |
| $_{27}Co^{55}$ | $\beta^+$ | 18.2 h. | 17 h. | 0.04 | −10 | −2 |
| $Co^{61}$ | $\beta^-$ | 1.8 h.[f] | 1.7 h. | 0.14 | −4 | −2 |
| $_{26}Fe^{52}$ | $\beta^+$ | — | 7.8 h. | 0.003 | −13 | −3 |
| $Fe^{53}$ | $(\beta^+)$ | 8.9 m. | 9 m. | 0.07 | −12 | −3 |
| $Fe^{59}$ | $\beta^-$ | 47 d. | 49 d. | 0.07 | −6 | −3 |
| $_{25}Mn^{51}$ | $(\beta^+)$ | 46 m. | 45 m. | 0.04[g] | −14 | −4 |
| $Mn^{52}$ | $\beta^+$, $(K)$ | 6.5 d. | 6 d. | 0.1 | −13 | −4 |
| $Mn^{56}$ | $\beta^-$ | 2.59 h. | 2.5 h. | 0.15 | −9 | −4 |
| $_{24}Cr^{49}$ | $\beta^+$ | 41.9 m. | 41 m. | 0.01 | −16 | −5 |
| $Cr^{51}$ | $(K)$ | 26.5 d. | 27 d. | *ca.* 0.02[g,h] | −14 | −5 |
| $_{23}V^{48}$ | $\beta^+$, $(K)$ | 16 d. | 16 d. | 0.05[g] | −17 | −6 |
| $_{17}Cl^{38}$ | $\beta^-$ | 37 m. | 38 m. | 0.0005 | −27 | −12 |
| $_{15}P^{32}$ | $(\beta^-)$ | 14.30 d. | 15 d. | 0.0005[g] | −33 | −14 |

[a] Parentheses indicate that the sign of the radiation has not been directly observed in these investigations.
[b] Unless otherwise noted the reference is to Seaborg, Table of Isotopes, Rev. Mod. Phys. 16, 1–32 (1944).
[c] A rough estimate indicates that a relative yield of one is equivalent to a cross section of the order of $10^{-35}$ cm².
[d] Leith, Bratenahl, and Moyer, Phys. Rev. **72**, 732 (1947).
[e] Conn, Brosi, Swartout, Cameron, Carter, and Hill, Phys. Rev. **70**, 768 (1946).
[f] Parmley and Moyer, Phys. Rev. **72**, 82 (1947).
[g] Results of only one bombardment. All other figures represent best values or averages resulting from two to seven bombardments.
[h] Corrected for amount formed by $Mn^{51}$ decay.

capture; decay by a positron of energy too small to have been detected efficiently by our Geiger-Müller tubes is not ruled out, however. A 7.8-hour activity was noted in the iron fractions and was shown by iron-manganese separations to give growth to a 21-minute manganese daughter activity. An aluminum absorption curve of the parent-daughter equilibrium mixture showed, in addition to a component of *ca.* 2.3 Mev attributable to the 21-minute $Mn^{52}$, a component of *ca.* 0.55-Mev maximum energy presumably as a result of the 7.8-hour parent, assigned to $Fe^{52}$.

The yields for the radio-isotopes of any one element increase as the difference between the mass number of the product isotope and mass number of maximum stability for that element decreases; it seems probable that the total yield of stable isotopes is of the same order of magnitude as the total yield of radio-isotopes. In the most extensively investigated region, from chromium through zinc, practically all known radio-isotopes which could have been observed in view of half-life and experimental time considerations were identified. Intermittent deuteron bombardment of one target over a period of several months, in which the total bombardment was about 20 times that of the usual shorter bombardment, resulted in observation of long-lived activities (>70 d.), which have not been positively identified, in the zinc, cobalt, manganese, and titanium fractions. Assuming that the activities in the zinc, manganese, and titanium fractions are due solely to $Zn^{65}$(250 d. $\beta^+$, $K$), $Mn^{54}$(310 d. $K$), and $Ti^{51}$(72 d. $\beta^-$), the maximum relative yields are calculated to be 0.007, 0.12, and 0.0005, respectively. Since three or four isotopes are probably contributing to the long-lived activity in the cobalt fraction, a relative yield figure is of no significance. It is noteworthy that little or no positron activity was found in the chlorine fraction; the yield of $Cl^{34}$(33 m. $\beta^+$) is $\leqslant 0.00005$.

One bombardment with approximately 380-Mev helium ions (contaminated with about 20 percent deuterons) was conducted. The yields of the radio-isotopes in the fractions investigated (copper, iron, manganese, chromium, and chlorine) were in all cases except one within the range of the yields obtained from the several deuteron bombardments (within a factor of about 2). The exception was $Cl^{38}$, which was produced with a yield six times as great as that from deuteron bombardments.

We wish to express our gratitude to Professor G. T. Seaborg for his advice and help in planning the experiments, and to the 184-inch cyclotron crew under the direction of Dr. D. C. Sewell and Mr. J. T. Vale for their cooperation in conducting the bombardments. The interest of Professor E. O. Lawrence and members of the Radiation Laboratory is gratefully acknowledged.

This paper is based on work performed under Contract No. W-7405-eng-48 with the Atomic Energy Commission in connection with the Radiation Laboratory, University of California.

[1] Present address: Department of Chemistry, University of Texas, Austin, Texas.
[2] Broebeck, Lawrence, MacKenzie, McMillan, Serber, Sewell, Simpson, and Thornton, Phys. Rev. **71**, 449 (1947).

## Notes on the Beta-Ray Spectra from Copper 64

W. E. MEYERHOF AND M. GOLDHABER
*Department of Physics, University of Illinois, Urbana, Illinois*
June 16, 1948

IN the investigation of beta-ray spectra one may meet with two possible sources of extraneous electrons: homogeneous internal conversion electrons, which are usually easily recognized as such, and electrons from internal pair production, which have a continuous distribution in energy. If pair electrons are present, and are not recognized as such, they may distort the experimentally obtained beta-ray distributions. This possibility is, therefore, worth excluding before experimentally obtained beta-ray spectra are compared with theoretical predictions.

Cook and Langer[1] have recently investigated the negatron and positron spectra from $Cu^{64}$ by means of a high resolution spectrometer[2] as a test of the Fermi theory of beta-decay.[3] They found in the case of the negatrons a total excess of 6 percent slow negatrons (i.e., below app. 200 kev); and in the case of the positrons a total excess of 9 percent slow positrons (i.e., below app. 250 kev) above the numbers predicted by the Fermi theory. On a Kurie plot[4] these deviations show up in the low energy region as positive deviations from the expected straight-line graph, already found by other investigators.[5]

If one assumes the decay scheme of $Cu^{64}$, as shown in Fig. 1,[6] one can easily calculate that the percentage excess of slow negatrons found by Cook and Langer represents

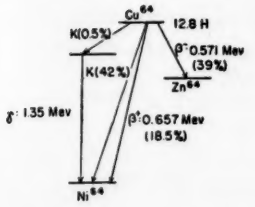


FIG. 1. Decay scheme of $Cu^{64}$.

2.5 percent of the total number of transitions and the excess of slow positrons 1.8 percent of all transitions. It seemed, therefore, worth while to investigate in this case the possibility that this excess might be caused by internal pairs, perhaps formed by a high internal-pair conversion of the 1.35-Mev gamma-ray. This would give rise to pairs of approximately 330-kev total energy, which is not far from the energy at which the excess of slow beta-particles becomes noticeable.

We have looked for pairs from $Cu^{64}$ (obtained through the Atomic Energy Commission from Oak Ridge) in a pair spectrometer of approximately 10 percent resolution for total pair energy. The total pair energy range covered was 100 to 400 kev. Our results show that in this range the number of pairs, if they exist, must be less than 0.2 percent of the total number of transitions, which is about 10 times too small to explain the effect noticed by Cook and Langer.

Incidentally, we have also looked for internal conversion electrons of the 1.35-Mev gamma-ray, using a conventional 180° type magnetic spectrometer of approximately 5 percent resolution. Since there is some question as to the exact energy of this gamma-ray, we have covered an electron range of 1.15 to 1.55 Mev. According to our results the internal conversion coefficient of the 1.35-Mev gamma-ray must be less than $5 \cdot 10^{-3}$.

This research was supported in part by contract N6-ori-71 between the University of Illinois and the Office of Naval Research.

[1] C. S. Cook and L. M. Langer, Phys. Rev. **73**, 601 (1948).
[2] L. M. Langer and C. S. Cook, Rev. Sci. Inst. **19**, 257 (1948).
[3] E. Fermi, Zeits. f. Physik **88**, 161 (1934).
[4] F. N. D. Kurie, J. R. Richardson, and H. C. Paxton, Phys. Rev. **49**, 368 (1936).
[5] See reference 1 for other investigators.
[6] H. Bradt *et al.*, Helv. Phys. Acta **19**, 219 (1946); M. Deutsch, Phys. Rev. **72**, 729 (1947).

## Diffraction by Circular Disks and Apertures

R. D. SPENCE
*Department of Physics, Michigan State College, East Lansing, Michigan*
AND
A. LEITNER
*Institute for Mathematics and Mechanics New York University, New York, New York*
June 14, 1948

IN a recent Letter to the Editor, Storruste and Wergeland[1] have reported the acoustical cross sections for scattering and transmission by circular disks and apertures. These results appear to be in fairly good agreement with those previously reported by one of us.[2] At the time we reported these results Professor Zernike pointed out that Bouwkamp[3] had previously reached essentially the same conclusions. It is interesting to note that although all the above calculations have been made with the oblate spheroidal wave functions, Levine and Schwinger[4] have obtained the same results by variational methods.

Calculations for the electromagnetic case have been completed by the authors. The electromagnetic cross sections for scattering and transmission by circular disks and apertures have a wave-length dependence similar to that of the scattering cross section of a circular disk in a sound field. These calculations are for a normally incident plane wave. An expansion obtained by one of us (A. L.) makes possible discussion of the problem at any incidence. Details of these calculations will be reported soon.

[1] A. Storruste and H. Wergeland, Phys. Rev. **73**, 1396 (1948).
[2] R. D. Spence, Bull. Am. Phys. Soc. **23**, No. 2, 40 (1948); see also J. Acous. Soc. Am. **20**, 380 (1948).
[3] C. J. Bouwkamp, *Diss. Groningen* (1941).
[4] H. Levine and J. Schwinger, Bull. Am. Phys. Soc. **23**, No. 3, 15 (1948).

## Mean Life of Negative Mesons in Carbon

C. W. KISSINGER AND D. COOPER
*Department of Physics, University of Maryland, College Park, Maryland*
June 7, 1948

LAST year Conversi, Pancini, and Piccioni[1] found that negative mesons decay in carbon, but not in iron. These results, which are important in the evaluation of the interaction of mesons and nucleons, have been confirmed and extended by other investigators.

In the present experiment, measurements are being made of the separate lifetimes of negative and positive mesons in graphite. The experimental arrangement is shown in Fig. 1. The mesons enter through the solid angle determined by counters $A$ and $B$. Coincidences $AB$ are formed with a resolving time of less than $\frac{1}{4}$ microsecond by using suitable pulse-forming preamplifiers ($P$) and a crystal diode coincidence circuit. Slow mesons are separated with respect to sign and deflected into their respective absorbing blocks ($G$'s) by the magnetic field ($F$), which was about 5000 gauss in iron. $AB$–$E$ triggers the 8-microsecond sweep of the servoscope. A pulse from $C$ or $D$ during the sweep unblanks the scope, and the horizontal position of the pulse on the scope gives the life of the meson. The data are recorded by continuous photography of the face of the scope. Decays

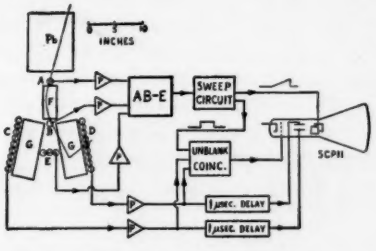


FIG. 1. Schematic of the experimental set-up for meson life measurements.

UNIVERSITY OF MICHIGAN LIBRARIES

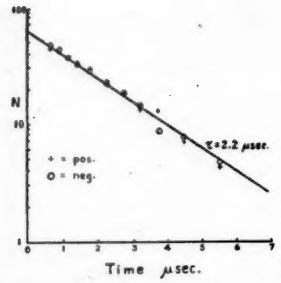


FIG. 2. Integral decay curve for positive and negative mesons in carbon.

are observed at the rate of about one every three hours. Argon-alcohol counters 1 in. in diameter and 16 in. long were used.

Seventy-one positive decays and 62 negative decays in carbon have been observed, of which about six of each sign are caused by accidentals. Figure 2 shows the corrected data plotted as an integral decay curve. (The ordinates were adjusted to an equal total number of positive and negative decays.) Calculations of the average decay time yielded 2.16 and 2.25±0.20 microseconds for the mean life of the positive and the negative mesons, respectively. These mean lives are consistent with the accepted value[2] of about 2.2 microseconds for the decay of positive mesons in all materials.

The effectiveness of the magnetic field in the separation of the positive and negative mesons was determined by replacing the graphite blocks with lead blocks of equivalent thickness, the decay electron range. (Negative mesons do not disintegrate in lead.[3]) Twenty-eight positive and 4 negative decays were recorded, after correction for accidentals.

These lifetime and yield results for carbon indicate that few, if any, of the negative mesons undergo nuclear capture in this element. Valley[4] has obtained similar results for Be. Ticho and Schein[5] observed a mean life of 1.33±0.14 microsecond for the decay of negative mesons in NaF, and Valley and Rossi[6] observed 0.74±0.17 microsecond for Al. Following Wheeler,[7] the above data should be related by the expression

$$\tau_0/\tau = 1+(Z/Z_0)^s = 1/f.$$

$\tau_0$ and $\tau$ are the mean lives of negative mesons in free space and in a material of atomic number $Z$, respectively. $Z_0$ is the atomic number for which decay and capture are equally probable, and $f$ is the fraction of decays which send out decay electrons. If the mean lives in Al and NaF are substituted into this equation, the constants are found to be $Z_0=11$ to 12 and $s\approx 4$ (in agreement with Wheeler's predictions). By this equation, a difference of 6 percent is to be expected in the mean lives and relative yields of positive and negative mesons in carbon. This difference is within the probable errors of the experimental values.

[1] M. Conversi, E. Pancini, and O. Piccioni, Phys. Rev. 71, 209 (1947).
[2] N. Nereson and B. Rossi, Phys. Rev. 64, 199 (1943).
[3] J. G. Retallack, Phys. Rev. 73, 921 (1948).
[4] G. E. Valley, Phys. Rev. 73, 1251 (1948).
[5] H. K. Ticho and M. Schein, Phys. Rev. 73, 81 (1948).
[6] G. E. Valley and B. Rossi, Phys. Rev. 73, 177 (1948).
[7] J. A. Wheeler, Phys. Rev. 71, 320 (1947).

## On the Dissociation Energy of Carbon Monoxide and the Heat of Sublimation of Carbon

J. G. VALATIN
*Institut Henri Poincaré, Paris, France*
June 9, 1948

AN attempt to interpret the observed effects in the spectrum of CO on the base of $D(CO)=9.61$ ev has been made recently by Hagstrum.[1] This coordination leaves, however, a number of observed effects without direct interpretation, among these, predissociation effects at 8.87 ev and 11.11 ev. Besides, the convergence of the $^1\Sigma^-$ levels[2] to about 82,000 cm$^{-1}$ cannot be reconciled in any way with this dissociation scheme.

The dissociation scheme given by Schmid and Gerö[3,4] results in $D(CO)=6.90$ ev, by identifying the energy height of the predissociation limit observed at 77,497±44 cm$^{-1}$ ~9.61 with the height of the atomic term combination $C(^1S)+O(^3P_0)$, and explains a great variety of observed spectroscopical effects. As to the results of electron-impact experiments, the interpretation of the appearance potential at 20.9±0.2 ev of $C^+$ and $O^-$ ions observed by Hagstrum and Tate[5] seems to need a more thorough knowledge about the $O^-$ ion. With respect to the difference of 0.45 ev between the appearance potential of $C^+$ ions at 22.8±0.2 ev and the nearest term combination $C^+(^2P)+O(^1S)$ in the dissociation scheme of Schmid and Gerö, it can be noted that also in the experiments in $O_2$—the spectroscopical dissociation energy of which is generally accepted—there is a difference of 0.5 ev between the observed appearance potential of $O^+$ ions at 19.2±0.2 ev and the height of the term combination $O(^3P)+O^+(^4S)$, interpreted by Hagstrum and Tate by means of a potential curve with maximum. The interpretation of the divergences between the results of spectroscopy and electron-impact experiments seems to need, in general, further investigation.

As to the conclusion of Kenty, Aicher, Noel, Paritsky, and Paolino,[6] who argue in favor of a lower limit of 9.4 ev of the dissociation energy of CO on the ground of observations on some bands in the green, it should be noted that, from the supposed failure of dissociation of CO molecules by collision with metastable Xe atoms with an excitation energy of 9.4 ev, no conclusion can be drawn as to a lower limit of $D(CO)$. The dissociation by collision is also a function of transition probability, and the failure of decomposition by collision does not yield a lower limit of dissociation energy, in the same way as the failure of photochemical decomposition of CO by the 1470A Xe line does not give such a limit.[7]

The fact that the value ~33,800 cm$^{-1}$ of the excitation energy of the $^5S$ state of carbon deduced from the CO spectrum had represented the best one of the proposed values[8] until the recent determination of Shenstone[9] resulting in 33,735.2 cm$^{-1}$, gives further support to the CO dissociation scheme of Schmid and Gerö. The secondary processes of the sublimation of carbon need still further investigations, but the deduced value of $L_2=169.73$ kcal./mole at 0°K for the heat of sublimation of graphite into $^5S$ carbon atoms gives full account of the thermochemical facts and enables the calculation of bond energies.[10] For

the energy required to remove a hydrogen atom from methane there results, according to the calculations of Gerö, 100.76 kcal./mole at 0°K, whereas the measurements of Andersen, Kistiakowsky, and Van Artsdalen[11] give 100.8 kcal./mole. The energy required to rupture ethane into two methyl radicals results in 82.78 kcal./mole, while the cycle proposed by Van Artsdalen[12] gives 82.9 kcal./mole at 0°K.

[1] H. D. Hagstrum, Phys. Rev. **71**, 736 (1947); *ibid.* **72**, 947 (1947).
[2] R. Schmid and L. Gerö, Zeits. f. Physik **106**, 205 (1937). See especially Fig. 5.
[3] R. Schmid and L. Gerö, Zeits. f. physik. Chemie (B), **36**, 105 (1937).
[4] R. Schmid and L. Gerö, Physik. Zeits. **39**, 460 (1938).
[5] H. D. Hagstrum and J. T. Tate, Phys. Rev. **59**, 354 (1941).
[6] C. Kenty, J. O. Aicher, E. B. Noel, A. Paritsky, and V. Paolino, Phys. Rev. **69**, 36 (1946).
[7] R. F. Schmid and L. Gerö, Proc. Phys. Soc. **58**, 701 (1946); see also J. G. Valatin, Proc. Phys. Soc. **59**, 502 (1947).
[8] See L. H. Long and R. G. W. Norrish, Nature **157**, 486 (1946); **158**, 237 (1946); J. G. Valatin, *ibid.*, 237 (1946); B. Edlen, *ibid.*, 129 (1947); S. Goudsmit, *ibid.*, 742 (1947).
[9] A. G. Shenstone, Phys. Rev. **72**, 411 (1947).
[10] Papers of L. Gerö and of J. G. Valatin in the course of publication.
[11] H. C. Andersen and G. B. Kistiakowsky, J. Chem. Phys. **11**, 10 (1943), G. B. Kistiakowsky and E. R. Van Artsdalen, *ibid.*, **12**, 469 (1944).
[12] E. R. Van Artsdalen, J. Chem. Phys. **10**, 653 (1942).

## Rotation Vibration Levels of the $Fe^{57}$ and $Ni^{59}$ Nuclei

H. A. Wilson
*Rice Institute, Houston, Texas*
May 3, 1948

THE resonances for neutron scattering with Fe and Ni reported by Barschall, Bockelman, and Seagondollar[1] appear to be rotation vibration levels analogous to those[2] of $Si^{28}$ and $Al^{28}$.

Table I gives values of $15+5(j(j+1)-\frac{3}{4})$ and of the observed resonances in Fe.

The graph showing the variation of the cross section with the neutron energy falls steeply from a value about 8 barns at 15 kev to 2 barns at 25 kev but there are no values given below 15 kev. The level at 15 kev is therefore doubtful. The shape of the graph between 30 kev and 70 kev suggests that there may be a low level at about 55 kev. There is no indication of a level at 255 kev but there is a doubtful level about 280 kev.

The moment of inertia of the Fe nucleus is given by

TABLE I. Values of $15+5(j(j+1)-\frac{3}{4})$ and of the observed resonances in Fe.

| $j$ | $15+5(j(j+1)-\frac{3}{4})$ | Observed resonances kev |
|---|---|---|
| $\frac{1}{2}$ | 15 | 15? |
| $1\frac{1}{2}$ | 30 | 30 |
| $2\frac{1}{2}$ | 55 | — |
| $3\frac{1}{2}$ | 90 | 90 |
| $4\frac{1}{2}$ | 135 | 150 |
| $5\frac{1}{2}$ | 190 | 195 |
| $6\frac{1}{2}$ | 255 | 280? |
| $7\frac{1}{2}$ | 330 | 325 |

TABLE II. Values of $15+4.1(j(j+1)-\frac{3}{4})$ and the values of the resonances found with Ni.

| $j$ | $15+4.1(j(j+1)-\frac{3}{4})$ | Resonances observed kev |
|---|---|---|
| $\frac{1}{2}$ | 15 | 15 |
| $1\frac{1}{2}$ | 27 | — |
| $2\frac{1}{2}$ | 48 | — |
| $3\frac{1}{2}$ | 77 | 70 |
| $4\frac{1}{2}$ | 113 | — |
| $5\frac{1}{2}$ | 159 | 160 |
| $6\frac{1}{2}$ | 212 | 210<br>245? |
| $7\frac{1}{2}$ | 273 | 280? |

$h^2/8\pi^2K=5\times1.6\times10^{-9}\times56/57$, which gives $K=7.1\times10^{-47}$. Putting $K=2Mr^2/3$ we get $r=10.6\times10^{-13}$ cm.

The spherical shell formula[3] $\Delta E=h(Ze/4\pi r)(Amr)^{-\frac{1}{2}}$ with $\Delta E=0.387$ Mev gives $r=4.65\times10^{-13}(Z^2/A)^{\frac{1}{3}}$ which gives $r=10.6\times10^{-13}$ cm for $Fe^{57}$ agreeing with the value got from the resonance levels.

Resonances with Fe were also found at 405 kev and at 800 kev, with doubtful resonances at 445 and 475 kev.

According to the spherical shell model[3] the excitation levels of a nucleus are equal to $\Delta E((n-1)(n+2))^{\frac{1}{2}}+(h^2/8\pi^2K)j(j+1)$. The second term is the rotational energy and $\Delta E$ is found to be 0.387 Mev for nuclei with $A>25$.

The energy of the reaction $Fe^{56}+n\rightarrow Fe^{57}$ is about 10.2 Mev, which is near to the value of $0.387((n-1)(n+2))^{\frac{1}{2}}$ with $n=26$ which is 10.23 Mev. We should therefore expect a resonance with small neutron energy and we may assume this to be the resonance at 15 kev with $j=\frac{1}{2}$.

There should then be excitation levels of the $Fe^{57}$ nucleus with spacings 0.387 Mev and corresponding neutron resonances with spacings $0.387\times57/56=0.394$ Mev. There should therefore be resonances at $15+394=409$ kev and at $15+2\times394=803$ kev which agree well with the observed resonances at 405 and 800 kev.

The resonances at 445 and 475 may be rotation resonances with $j=2\frac{1}{2}$ and $3\frac{1}{2}$ which are equal to $394+55=449$ and $394+90=484$, respectively.

Table II gives values of $15+4.1(j(j+1)-\frac{3}{4})$ and the values of the resonances found with Ni.

The resonance at 15 kev extends to about 50 kev and so prevents resonances at 28 and 48 being observed. There is a doubtful indication of a resonance at about 45 kev. There is also a doubtful indication of a resonance between 100 and 130 kev.

The moment of inertia of the Ni nucleus is given by $h^2/8\pi^2K=4.1\times1.6\times10^{-9}\times58/59$, which gives $K=8.6\times10^{-47}$. Putting $K=2Mr^2/3$ we get $r=11.3\times10^{-13}$ cm. The equation $r=4.65\times10^{-13}(Z^2/A)^{\frac{1}{3}}$ gives $r=11.0\times10^{-13}$ for $Ni^{59}$.

There is also a resonance at 430 kev. This may correspond to unresolved resonances 409, 422, and 442 analogous to those found with Fe. No resonance near 800 kev was observed.

[1] Barschall, Beckelman, and Seagondollar, Phys. Rev. **73**, 659 (1948).
[2] H. A. Wilson, Phys. Rev. **73**, 350 (1948).
[3] H. A. Wilson, Phys. Rev. **69**, 538 (1946).

UNIVERSITY OF MICHIGAN LIBRARIES

## Rotation Vibration Levels of the $Si^{28}$ and $Al^{28}$ Nuclei

H. A. WILSON
*Rice Institute, Houston, Texas*
March 25, 1948

SEVERAL of the $Al^{27}(p,\gamma)Si^{28}$ resonance levels measured by Brostrom, Huns, and Tangen[1] can be explained as belonging to rotation vibration levels of the product nucleus.

The following table gives values of $986+16.15j(j+1)$ and of observed levels. The last column gives the counts per microcoulomb observed with thick targets.

The following table gives values of $994+16.15j(j+1)$ and observed values.

The level 1192 is complex and probably has three components: 1189, 1192, and 1195.

The constant 16.15 kev or $16.15\times1.6\times10^{-9}$ ergs should be equal to $(28/27)\hbar^2/8\pi^2K$ where $K$ is the moment of inertia of the $Si^{28}$ nucleus. This gives $K=2.23\times10^{-47}$. Putting $K=\frac{2}{3}Mr^2$ for a spherical shell nucleus gives $r=8.4\times10^{-13}$ cm. Putting $K=\frac{2}{5}Mr^2$ for a sphere of uniform density gives $r=10.9\times10^{-13}$.

The spherical shell nuclear model suggested by the writer gives nearly equally spaced levels with separations $\Delta E=\hbar(Ze/4\pi r)(Amr)^{-\frac{1}{2}}$. With $\Delta E=0.387$ Mev this gives $r=8.9\times10^{-13}$ cm for silicon, which is nearly equal to the value got from the rotation vibration levels for a spherical shell nucleus.

Some of the $Al^{27}(n,\gamma)Al^{28}$ resonances measured by Seagondollar and Barschall[3] appear to be rotation vibration levels of the $Al^{28}$ nucleus.

The following table gives values of $45+21j(j+1)$ and of the observed levels.

The observed values probably have possible errors of several kev so that the observed and calculated values agree as well as could be expected. The value $21\times1.6\times10^{-9}$ erg for the constant gives $7.4\times10^{-13}$ for the radius of the $Al^{28}$ nucleus with $K=\frac{2}{3}Mr^2$. This is rather smaller than the radius of $Si^{28}$, as would be expected.

The last column in the table gives the orbital angular momentum quantum number for the incident neutrons

TABLE I. Values of $986+16.15j(j+1)$ and of observed levels.

| $j$ | Calculated | Observed kev | Counts per $\mu$C |
|---|---|---|---|
| 0 | 986 | 986 | 47.0 |
| 1 | 1018.3 | 1018 | 7.2 |
| 2 | 1082.9 | 1083 | 1.5 |
| 3 | 1179.8 | 1176 | 6.5 |
| 4 | 1309.0 | 1309 | 14.0 |

TABLE II. Values of $994+16.15j(j+1)$ and observed values.

| $j$ | Calculated | Observed kev | Counts per $\mu$C |
|---|---|---|---|
| 0 | 994 | 994 | 2.0 |
| 1 | 1026.3 | — | — |
| 2 | 1090.9 | 1091 | 0.8 |
| 3 | 1187.8 | 1192 | — |
| 4 | 1317.0 | 1320 | 10.5 |

TABLE III. Values of $45+21j(j+1)$ and of the observed levels.

| $j$ | Calculated | Observed kev | Cross section barns | $l$ |
|---|---|---|---|---|
| 0 | 45 | 45 | 5.5 | 2 or 3 |
| 1 | 86 | 95 | 7.2 | 1 or 2 |
| 2 | 168 | 160 | 9.0 | 0 or 1 |
| 3 | 291 | 290 | 5.1 | 1 or 0 |

The cross section would probably be expected to increase as $l$ gets smaller.

[1] Broström, Huus, and Tangen, Phys. Rev. 71, 661 (1947).
[2] H. A. Wilson, Phys. Rev. 69, 538 (1946).
[3] L. W. Seagondollar and H. H. Barschall, Rev. Mod. Phys. 19, 271 (1947).

## Spectroscopic Evidence for Ammonia in the Earth's Atmosphere

ORREN C. MOHLER, LEO GOLDBERG, AND ROBERT R. MCMATH
*McMath-Hulbert Observatory of the University of Michigan, Lake Angelus, Pontiac, Michigan*
June 15, 1948

A SERIES of tracings of the infra-red solar spectrum in the 2-m$\mu$ region, made at the McMath-Hulbert Observatory with the McGregor infra-red recording spectrometer, exhibits many coincidences with individual lines in the band spectrum of ammonia. The lines originate in the earth's atmosphere, for they appear most strongly developed when the sun is near the horizon. Agreement in wave-length within the limits $\pm0.05$ cm$^{-1}$ has been established between eight intense lines in the ammonia spectrum, and features in the spectrum of the sun.

The coincidences were verified by comparing spectra obtained using the sun as a source, and spectra produced by a tungsten filament lamp and an absorption cell 25 cm long, filled with air and a trace of ammonia at atmospheric pressure. The McGregor infra-red spectrometer was used to record both the solar and tungsten lamp spectra. We were able to select persistent lines of ammonia by observing the effect of successive reductions in the quantity of ammonia in the absorption cell. The persistent lines that remain after nearly all of the ammonia has been washed out of the cell with an air stream are the ones that appear in the solar spectrum. With the sun at maximum altitude, the lines are of weak-to-medium strength.

A direct comparison, using a laboratory light source and absorption cell, was required because there are large variations in the intensities of ammonia lines as the quantity of ammonia in the path is diminished. All of the published data refer to large amounts of ammonia and cannot be used for direct comparison with the solar spectrum. The new laboratory spectra have been recorded on a scale not possible before the introduction of the Cashman lead-sulfide cell. They reveal new structure and contain much information about the curve of growth for individual lines of ammonia.

The small residual quantity of ammonia that produced a laboratory spectrum most nearly matching the line intensities in the spectrum of the sun was not measured, but the

quantity is certainly very minute. Ammonia in the earth's atmosphere probably is present in trace amounts only. Spectroscopic evidence for methane and ammonia and the measurement of the amounts of these gases in the earth's atmosphere is important because of possible implications in connection with the tremendous abundance of the two gases in the atmospheres of Jupiter and Saturn.

A complete report on the evidence for ammonia in the earth's atmosphere will appear in the Astrophysical Journal.

## Atmospheric Absorption of Microwaves

H. R. L. LAMONT
*Research Laboratories of the General Electric Company, Limited, Wembley, England*
June 17, 1948

THE absorption by oxygen molecules of electromagnetic radiation in a wave-length region arouhd 5 mm has been predicted theoretically by Van Vleck[1] and measured in the laboratory by Beringer.[2] We* have used a field method in which the attenuation is derived from measurement of the variation of field strength with distance in the open air.

The transmitter was mounted on the control tower of an aerodrome and the receiver on the roof of a vehicle, measurements of signal strength being made at a number of fixed positions on the runways. The transmitter consists of a velocity modulation oscillator, operating at twice the required wave-length, whose output passes into a germanium crystal distorter from which second harmonic power is extracted and fed to a high gain aerial. The receiver has a local oscillator operating at half the signal frequency, and a germanium crystal mixer. Ten wave-lengths between 6.34 mm and 4.48 mm were used, and the distances varied from 0.12 km to 2.2 km.

TABLE I. Summary of experimental results.

| Wave-length mm | Mean attenuation db/km | Probable error |
|---|---|---|
| 6.34 | 0.05 | ±0.15 |
| 5.76 | 1.0 | 0.1 |
| 5.60 | 1.8 | 0.2 |
| 5.28 | 10.2 | 0.1 |
| 5.19 | 12.7 | 0.05 |
| 5.13 | 15.7 | 0.2 |
| 5.10 | 13.9 | 0.1 |
| 5.04 | 14.5 | 0.15 |
| 4.96 | 14.7 | 0.1 |
| 4.48 | 0.4 | 0.1 |

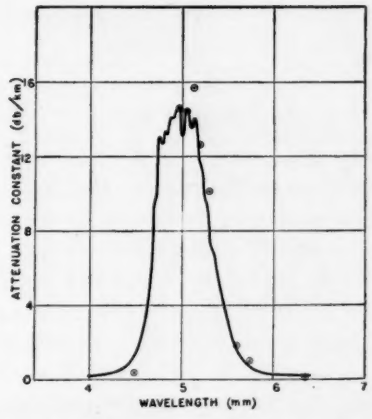


FIG. 1. Theoretical and experimental values of atmospheric attenuation (293°K, 760 mm Hg, 21 percent $O_2$).

In calculating the attenuation, constant free-space propagation was assumed. With the small aerial beam-width used this proved justified for distances up to 1 km; beyond this distance some interference from the ray reflected by the ground was experienced.[3] From each measured attenuation was subtracted an amount appropriate to the attenuation caused by the water vapor in the air, and the remainder was corrected for temperature and pressure to 293°K and 760 mm Hg. Finally a correction for oxygen concentration was made to give the results in terms of an atmosphere of 21 percent $O_2$ molecules.

The mean corrected values, which for each wave-length are calculated from some 20 to 30 readings, are given in Table I, together with their probable errors. Figure 1 shows these values in relation to Van Vleck's theoretical curve for a line-breadth constant $\Delta\nu/c$ of 0.02 $cm^{-1}$, with which they are obviously in good agreement. The value of 15.7 for $\alpha$ obtained at 5.13-cm wave-length shows a marked deviation from the curve, but seems as reliable as the other points; it may indicate a line-breadth constant rather less than 0.02 $cm^{-1}$. On the whole the points suggest that the curve should be moved slightly in the direction of increasing wave-length, but there would appear to be no warrant for this on a theoretical basis.

We are indebted to the Chief of the Royal Naval Scientific Service, on whose behalf the work was done, for permission to publish this note.

* The experimental work was carried out by G. J. Benwell, E. M. Hickin, H. R. L. Lamont, R. G. Robertshaw, and J. R. Tew.

[1] J. H. Van Vleck, Phys. Rev. 71, 413 (1947).
[2] R. Beringer, Phys. Rev. 70, 53 (1946).
[3] Cf. this effect over sea, H. R. L. Lamont and A. G. D. Watson, Nature 158, 943 (1946).

UNIVERSITY OF MICHIGAN LIBRARIES

# Proceedings of the American Physical Society

## Minutes of the Meeting of the New England Section at Harvard University, Cambridge, Massachusetts, on May 29, 1948

THE thirtieth meeting of the New England Section of the American Physical Society was held at the Physics Laboratories, Harvard University, Cambridge, Massachusetts, on Saturday, May 29, 1948. Ninety-nine members of the Section registered. The programme included four invited papers, three of which formed a symposium on cosmic rays. There follow the titles of the invited papers and the abstracts of the ten-minute contributed papers relating to research. Abstracts of the ten-minute contributed papers relating to the teaching of physics will appear in the American Journal of Physics.

GORDON F. HULL, JR.
*Secretary-Treasurer*

### *Invited Papers*

**The Physics Laboratories, and Researches in Progress at Harvard University,** R. W. HICKMAN AND E. L. CHAFFE, *Harvard University.*

### *Symposium on Cosmic Rays*

**Interpretation of Cosmic Ray Phenomena,** BRUNO ROSSI, *Massachusetts Institute of Technology.*

**Cosmic-Ray Showers at Low Altitudes,** C. G. MONTGOMERY, *Yale University.*

**Application of Crystal Counters to Cosmic Ray-Studies,** J. C. STREET, *Harvard University.*

### *Contributed Papers*

**Interaction of Nuclear Quadrupole Moments with Molecular Rotation in Slightly Asymmetric Rotor Molecules.** G. KNIGHT AND B. T. FELD, *Massachusetts Institute of Technology.* The interaction energy of a nuclear quadrupole moment with the electric field in a molecule depends on the molecular symmetry only through the factor $[(3\cos^2\theta-1/r^3)]_{\text{av}}$. Bragg* has shown that for any asymmetric top molecule this parameter depends on the transformation which diagonalizes the rotational energy and on the molecular constants $\partial^2V/\partial z^2$ and $(\partial^2V/\partial x^2)-(\partial^2V/\partial y^2)$, where $x$, $y$, and $z$ are the principle axes of the molecule and $V$ is the electrostatic potential at the interacting nucleus. However, his method does not lead to an explicit expression for the general case. We have obtained an explicit formula for the desired average in the case of slightly asymmetric rotors by approximating the asymmetric rotor wave functions by a sum of symmetric rotor wave functions involving a parameter of asymmetry, $b=(A-B)/[2C-(A+B)]$ where $A$, $B$, and $C$ are the reciprocal principle moments of inertia of the molecule. The result for $K\neq\pm1$, (Including only terms to the first order in $b$), is:

$$[(3\cos^2\theta-1/r^3)]_{\text{av}}=(J/2J+3)\{[3K^2/J(J+1)]-1\}\times\partial^2V/\partial z^2-b[G(J,K)+G(J,-K)](\partial^2V/\partial x^2-\partial^2V/\partial y^2)$$

where

$$G(J,K)=[(J+K+1)(J+K+2)(J-K-1)(J-K)/8(K+1)(J+1)(2J+3)].$$

The expression for $K=\pm1$ is similar in form to the above, but differs because of the degeneracy of these states.

* J. K. Bragg, Bull. Am. Phys. Soc. **23**, No. 2, G10 (1948).

**The Detection of Beta Radiation by Photographic Film,** JOCK COBB AND A. K. SOLOMON, *Harvard University Medical School.* The effect of beta-radiation from $C^{14}$ has been examined on nineteen different films. The method employed uses a "radiator," a set of eight radiating sources of different intensities, to replace the stable light source and absorbing wedge common in spectral photometry. With this device sensitivity and contrast of the nineteen films have been measured. Based upon these results and a microscopic estimation of the grain size, recommendations are made for the most desirable film for use in radioautography and detection of radioactivity. Of the films examined, Eastman No-screen x-ray film appears best for the detection of the beta-rays; and Ansco Reprolith, and Eastman Type M x-ray stripping films appear to be most desirable for work with radioautographs.

**Effects of Absorption and Scattering of Mesons on Coincidence-Anticoincidence Counts.** ALMA ROSENBAUM AND ROGERS D. RUSK, *Mount Holyoke College.* Absorption and scattering effects caused by iron, lead and paraffin on the penetrating component of cosmic rays have been studied using a quadruple coincidence-anticoincidence counter. The effects of the position of the various absorbing layers, and combinations of different absorbing layers, were studied and the effects due to paraffin were compared with those due to the heavier elements.

The increase in counting rate obtained with the heavier materials above the anticoincidence tube can be explained at least in part by scattering as was done by Rossi and others* in their experiment concerned with possible incident neutral rays. In addition to scattering in the present arrangement, however, there is also the possibility of some of the increase being due to neutral particles produced in the heavy absorber. This is considered in the light of recent investigations indicating absorption of negative mesons by heavier elements.

* B. Rossi, L. Janossy, G. D. Rochester, and M. Bound, Phys. Rev. **58**, 761 (1940).